Supporting Information

Heterocyclic Hemithioindigos: Highly Advantageous Properties as Molecular Photoswitches

V. Josef, F. Hampel, H. Dube*

Table of Contents

Materials and General Methods

General. All reactions with the participation of oxygen- or moisture-sensitive compounds were carried out in dry reaction vessels under an inert atmosphere of argon using anhydrous solvents and standard Schlenk techniques. All oxygen- and moisture-sensitive liquids and anhydrous solvents were transferred *via* a syringe.

Solvents and reagents. Reagents were purchased at reagent grade from commercial suppliers (*ABCR*, *Acros*, *BLD Pharmatech*, *Merck*, *Sigma-Aldrich* or *TCI*) and used without further purification. Na_2SO_4 was used as the drying agent after aqueous workup.

Thin-layer chromatography (TLC). Analytical TLC analysis was performed on aluminum plates coated with 0.20 mm silica gel containing a fluorescent indicator (Macherey-Nagel, ALUGRAM®, SIL G/UV$_{254}$) or on aluminum plates coated with 0.20 mm aluminum oxide containing a fluorescent indicator (Macherey-Nagel, ALUGRAM®, ALOX N/UV$_{254}$). Detection was visualized by exposure to ultraviolet light (254 nm or 366 nm).

Mass spectrometry. Mass spectra were measured on a MircoTOF II (Bruker, HR, ESI and APPI) mass spectrometer at the Institute of Organic Chemistry, University of Erlangen-Nürnberg.

^{1}H NMR and ^{13}C NMR spectra were measured on a *Bruker Avance Neo HD 400* (400 MHz), *Bruker Avance Neo HD 500* (500 MHz) and a *Bruker Avance Neo HD 600* (600 MHz) spectrometer. Chemical shifts (δ) are stated in ppm and were referenced to the residual solvent signal as an internal reference ($CDCl_3$: 7.26 ppm for ^{1}H and 77.16 for ^{13}C, CD_2Cl_2: 5.32 ppm for ^{1}H and 54.00 ppm for ^{13}C, $(CD_3)_2SO$: 2.50 ppm for ^{1}H and 39.52 ppm for ^{13}C, toluene-*d$_8$*: 2.09 ppm for ^{1}H and 20.43 ppm for ^{13}C, CD_3OD: 3.31 ppm for ^{1}H and 49.00 ppm for ^{13}C, C_6D_6: 7.16 ppm for ^{1}H and 128.06 ppm for ^{13}C, CD_3CN: 1.94 ppm for ^{1}H and 1.32 ppm for ^{13}C, THF-*d$_8$*: 3.58 ppm for ^{1}H and 67.21 ppm for ^{13}C). Coupling constants (*J*) are given in Hz as observed and the apparent resonance multiplicity is reported as s (singlet), d (doublet), t (triplet), q (quartet), quint (quintet) or m (multiplet). Signal assignments are given in the experimental part with the arbitrary numbering indicated.

Melting points (Mp) were obtained on a Büchi M560 melting point apparatur in open capillaries.

IR spectra were determined on a 660-IR (Varian, ATR mode) spectrometer and characteristic IR absorptions were reported in cm^{-1} and labeled as strong (s), medium (m) and weak (w).

UV/Vis spectra measurements were acquired on a Cary 500 UV-Vis NIR (Varian) spectrophotometer and Cary 60 UV-Vis (Agilent Technologies). Spectra were recorded in a

quartz cuvette (1 cm) at 22 °C. The absorption maxima (λ) are reported in nm with the extinction coefficient (ε) L·mol^{-1}·cm^{-1}.

Photoisomerization experiments were performed using *Roithner Lasertechnik GmbH* LEDs (405 nm, 420 nm, 430 nm, 450 nm, 470 nm, 490 nm, 505 nm, 530 nm, 554 nm, 565 nm) to determine the corresponding isomer compositions in the PSS by continuous irradiation of the solutions.

X-ray diffraction of a single crystals was performed on a *SuperNova Atlas* diffractometer using Cu-Kα-radiation.

Synthesis of Compounds

The precursor benzothiophenone **17** was synthesized based on an earlier established method.[1] Het-HTIs **1**–**16** were synthesized by a simple condensation reaction following published protocols.[1,2,3] Scheme S1 shows the synthesis of Het-HTIs **1**–**16**.
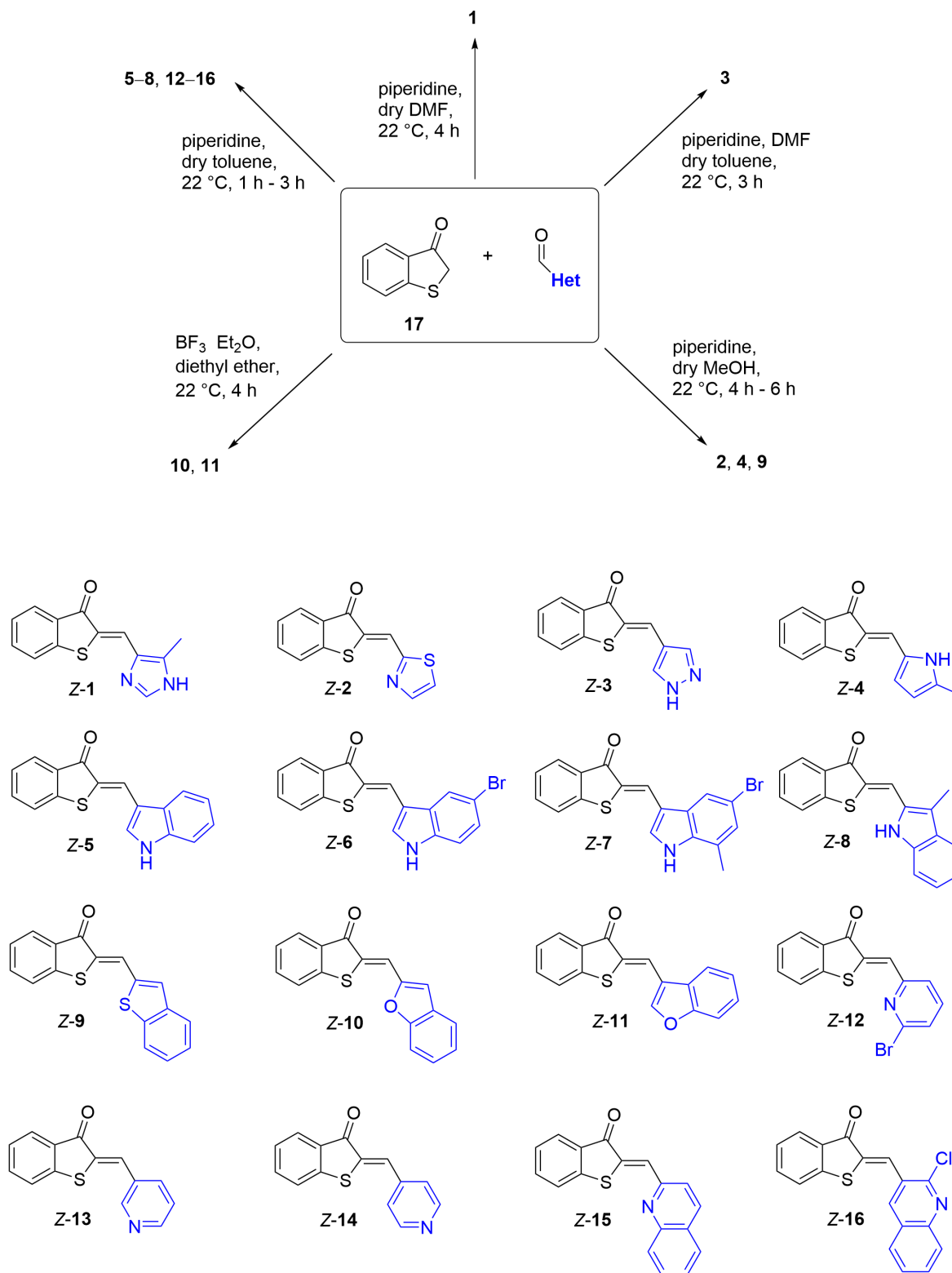
Scheme 1: General scheme for the synthesis of Het-HTIs **1-16**.

Benzo[*b*]thiophen-3(2*H*)-one (17)

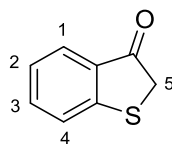To a dry Schlenk flask under argon atmosphere thiophenoxy acetic acid (2.50 g, 15.0 mmol, 1.00 eq.) was dissolved dry 1,2-dichlorethane (22.0 mL, 0.66 M) and TfOH (6,60 mL, 75,0 mmol, 5,00 eq.) was added carefully and the reaction was heated at 40 °C for 5 h. After that the reaction mixture was cooled to room temperature and ice/water (300 mL) was added. The aqueous phase was extracted with CH_2Cl_2 (3 x 100 mL). The combined organic phases were washed with sat. aq. $NaHCO_3$ (100 mL) and brine (100 mL). The combined organic layers were dried over Na_2SO_4, filtered and the solvent was removed under reduced pressure. The crude yellow benzo[*b*]thiophen-3(2*H*)-one solid (1.86 g, 12.4 mmol, 83%) was obtained and need to be stored under N_2 atmosphere at −25 °C.
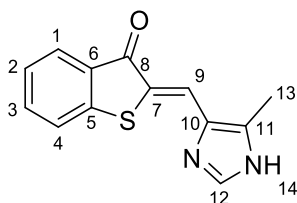
R$_f$ (SiO$_2$, i-Hex/EtOAc 1:1) = 0.26.

^{1}H-NMR (400 Hz, CDCl$_3$) δ (ppm) = 7.68 (dd, 1H), 7.45 (ddd, 1H), 7.33 (d, 1H), 7.25 − 7.15 (m, 1H), 3.66 (s, 2H).

^{13}C NMR (126 MHz, CDCl$_3$) δ (ppm) = 200.2, 154.5, 135.8, 131.3, 126.8, 125.0, 124.8, 39.5.

HR-MS (APPI) for $C_8H_7OS^+$, $[M+H]^+$, 151.0173, found 151.0175.

M.p.: 63 °C − 65 °C.

2-((4-methyl-1*H*-imidazol-5-yl)methylene)benzo[*b*]thiophen-3(2*H*)-one (1)

Benzo[*b*]thiophen-3(2*H*)-one (369 mg, 2.46 mmol, 1.25 eq) and 4-methyl-1*H*-imidazol-5-carbaldehyde (213 mg, 1.93 mmol, 1.00 eq.) were dissolved in dry DMF (6.0 mL, 0.33 M) under argon atmosphere in a flame dried flask. Piperidine (0.04 mL, 0.425 mmol, 0.20 eq.) was added and the reaction mixture was stirred at 23 °C. After 4 h the reaction mixture was diluted with CH_2Cl_2 (100 mL) and was washed with a sat. aq. NH$_4$Cl solution (50 mL) and water (50 mL). The combined aqueous phases were extracted with CH_2Cl_2 (3 x 50 mL) and the combined organic layers were dried over Na$_2$SO$_4$, filtered and concentrated. The crude product was recrystallized from methanol, filtered and washed with cold methanol to afford 2-((4-methyl-

1*H*-imidazol-5-yl)methylene)benzo[*b*]thiophen-3(2*H*)-one (496 mg, 2.05 mmol, 83%) as an orange solid.

R$_f$ (SiO$_2$, i-Hex/EtOAc 1:1) = 0.2.

^{1}H NMR (500 MHz, DMSO-*d$_6$*) δ (ppm) = 12.57 (s, 1H, H-N(14)), 7.83 (s, 1H, H-C(12)), 7.80 (s, 1H, H-C(9)), 7.81 – 7.78 (m, 1H, H-C(1)), 7.68 (dt, *J* = 7.8, 1.0 Hz, 1H, H-C(4)), 7.65 – 7.62 (m, 1H, H-C(3)), 7.31 (ddd, *J* = 7.9, 7.0, 1.2 Hz, 1H, H-C(2)), 2.42 (s, 3H, H-C(13)).

^{13}C NMR (126 MHz, DMSO-*d$_6$*) δ (ppm) = 187.4 (C(8)), 148.0 (C(5)), 136.6 (C(12)), 135.0 (C(10), 134.8 (C(3)), 132.8 (C(11)), 130.8 (C(6)), 125.8 (C(1)), 125.3 (C(7)), 125.0 (C(2)), 124.3 (C(9)), 124.2 (C(4)), 9.4 (C(13)).

HR-MS (APPI) for C$_{13}$H$_{11}$N$_2$OS$^+$, [M+H]$^+$, 243.0587, found 243.0593.

IR: $\tilde{v}$/cm^{-1} = 3180 (m), 3097 (m), 2979 (m), 2914 (m), 1658 (s), 1587 (s), 1574 (s), 1545 (s), 1533 (s), 1504 (s), 1444 (s), 1427 (s), 1392 (s), 1315 (s), 1281 (s), 1244 (s), 1211 (s), 1136 (s), 1113 (s), 1092 (m), 1072 (s), 1051 (s), 1016 (s), 943 (s), 903 (s), 883 (s), 814 (m), 787 (s), 775 (vs), 739 (vs), 704 (s), 690 (s), 675 (s), 625 (vs), 542 (s), 498 (s), 486 (s), 459 (s), 432 (s), 409 (s).

M.p.: 263 °C – 264 °C.

2-((thiazol-2-yl)methylene)benzo[*b*]thiophen-3(2*H*)-one (2)
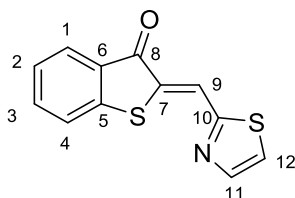
The benzo[*b*]thiophen-3(2H)-one (255 mg, 1.70 mmol, 1.25 eq.) and thiazole-2-carbaldehyde (181 mg, 1.60 mmol, 1.00 eq.) were dissolved in methanol (4.80 mL, 0.33 M) in a dry Schlenk flask under an argon atmosphere. Then piperidine (0.03 mL, 0.32 mmol, 0.20 eq.) was added and the mixture was stirred for 4 h at 23 °C. The reaction was diluted with CH$_2$Cl$_2$ and washed with a sat. aq. NH$_4$Cl solution (50 mL) and water (50 mL). The aqueous phases were extracted with CH$_2$Cl$_2$ (2 x 50 mL). The combined organic phases were washed with sat. aq. NaCl solution (100 mL) and dried over Na$_2$SO$_4$ and filtered. The solvent was removed under reduced pressure and the crude product was recrystallized from methanol. The product was obtained as a dark green solid (335 mg, 1.36 mmol, 85%).

R$_f$ (SiO$_2$, i-Hex/EtOAc 8:2) = 0.07.

¹H NMR (500 MHz, DMSO-d_6) δ (ppm) = 8.21 (d, J = 3.1 Hz, 1H, H-C(12)), 8.10 (s, 1H, H-C(9)), 8.10 (d, J = 3.1 Hz, 1H, H-C(11)), 7.86 (d, J = 7.3 Hz, 1H, H-C(1)), 7.78 (d, J = 7.6 Hz, 1H, H-C(4)), 7.74 (dd, J = 6.9, 1.3 Hz, 1H, H-C(3)), 7.40 (td, J = 7.4, 1.3 Hz, 1H, H-C(2)).

¹³C NMR (126 MHz, DMSO-d_6) δ (ppm) = 187.9 (C(8)), 161.5 (C(10)), 147.2 (C(5)), 145.3 (C(12)), 133.4 (C(7)), 129.6 (C(6)), 126.4 (C(2)), 126.2 (C(1)), 125.4 (C(11)), 124.7 (C(4)), 121.9 (C(9)).

HR-MS (APPI) for $C_{12}H_8S_2NO^+$, $[M+H]^+$, 246.0042, found 246.0042.

IR: $\tilde{v}$/cm^{-1} = 3093 (m), 3066 (m), 1672 (s), 1583 (s), 1566 (s), 1462 (m), 1448 (s), 1282 (s), 1255 (m), 1217 (m), 1147 (m), 1119 (m), 1109 (m), 1063 (s), 1049 (s), 1018 (s), 876 (m), 773 (m), 739 (vs), 731 (vs), 698 (m), 677 (s), 665 (s), 634 (s), 619 (m), 602 (m), 580 (s), 530 (s), 490 (m), 482 (s), 442 (m), 418 (s).

M.p.: 194 °C – 195 °C.

2-((1*H*-pyrazol-4-yl)methylene)benzo[*b*]thiophen-3(2*H*)-one (3)
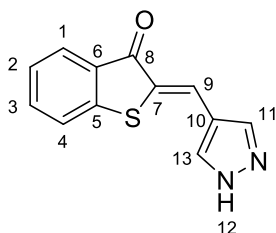
Benzo[*b*]thiophen-3(2*H*)-one (300 mg, 2.00 mmol, 1.25 eq) and 1*H*-pyrazol-4-carbaldehyde (154 mg, 1.60 mmol, 1.00 eq.) were dissolved in dry toluene (4.1 mL, 0.33 M) under an argon atmosphere in a flame dried flask. Piperidine (0.03 mL, 0.32 mmol, 0.20 eq.) and DMF (2.00 mL, 0.27 mmol, 0.20 eq.) were added and the reaction mixture was stirred at 23 °C. After 3 h the reaction mixture was diluted with CH_2Cl_2 (100 mL) and was washed with a sat. aq. NH_4Cl solution (50 mL) and water (50 mL). The combined aqueous phases were extracted with CH_2Cl_2 (3 x 50 mL) and the combined organic layers were dried over Na_2SO_4, filtered and concentrated. The crude product was recrystallized from methanol, filtered and washed with cold methanol to afford 2-((1*H*-pyrazol-4-yl)methylene)benzo[*b*]thiophen-3(2*H*)-one (214 mg, 0.940 mmol, 59%) as a yellow solid.

R$_f$ (SiO$_2$, i-Hex/EtOAc 8:2) = 0.07.

¹H NMR (500 MHz, DMSO-d_6) δ (ppm) = 13.57 (s, 1H, H-N(12)), 7.95 (s, 1H, H-C(9)), 7.86 – 7.82 (m, 1H, H-C(1)), 7.78 (d, J = 7.8 Hz, 1H, H-C(4)), 7.74 – 7.70 (m, 1H, H-C(3)), 7.39 (d, J = 6.8 Hz, 1H, H-C(2)).

8.33 (s, 1H), 7.97 (s, 1H) cannot be unambiguously assigned to H(11) or H(13).

¹³C NMR (126 MHz, DMSO-d_6) δ (ppm) = 187.4 (C(8)), 144.9 (C(5)), 136.1 (C(3)), 131.1 (C(6)), 127.0 (C(1)), 126.8 (C(2)), 126.0 (C(4)).

132.6, 126.9, 125.0, 117.0 cannot be unambiguously assigned to C(7), C(10), C(11) or C(13).

HR-MS (APPI) for $C_{12}H_9N_2SO^+$, $[M+H]^+$, 229.0430, found 229.0432.

IR: $\tilde{v}$/cm⁻¹ = 3165 (m), 3103 (m), 3022 (m), 2960 (m), 1649 (s), 1577 (s), 1554 (s), 1448 (s), 1350 (s), 1259 (s), 1196 (s), 1157 (s), 1076 (vs), 999 (vs), 926 (s), 910 (s), 872 (s), 791 (s), 779 (vs), 746 (s), 733 (vs), 679 (s), 654 (vs), 619 (vs), 538 (s), 496 (s), 486 (s), 465 (s), 424 (s), 409 (s).

M.p.: 258 °C – 259 °C.

2-((5-methyl-1*H*-pyrrole-2-yl)methylene)benzo[*b*]thiophen-3(2*H*)-one (4)
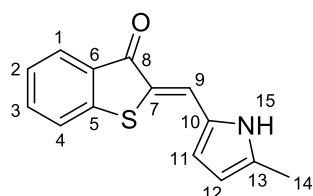
5-Methyl-1*H*-pyrrole-2-carbaldeyde (200 mg, 1.85 mmol, 1.00 eq.) and benzo[*b*]thiophen-3(2*H*)-one (369 mg, 2.46 mmol, 1.25 eq) were added to a flame-dried flask under argon atmosphere and dissolved in dry methanol (7.50 mL, 0.33 M). Under stirring, piperidine (0.04 mL, 0.425 mmol, 0.20 eq.) was added. The reaction mixture was stirred at 23 °C for 6 h before CH₂Cl₂ (100 mL) was added. The organic phase was washed with a sat. aq. NH₄Cl solution (50 mL) and water (50 mL). The combined aqueous phases were extracted with CH₂Cl₂ (3 x 50 mL) and the combined organic phases were then dried over Na₂SO₄, filtered and the solvent was removed under reduced pressure. The crude product was recrystallized from heptane/CH₂Cl₂, filtered and washed with cold heptane. The product (358 mg, 1.48 mmol, 80%) was obtained as red solid.

R$_f$ (SiO₂, i-Hex/EtOAc 8:2) = 0.18.

¹H NMR (500 MHz, DMSO-d_6) δ (ppm) = 11.66 (s, 1H, H-N(15)), 7.78 (dd, *J* = 8.0, 1.7 Hz, 1H, H-C(1)), 7.76 (s, 1H, H-C(9)), 7.74 (d, *J* = 7.9 Hz, 1H, H-C(4)), 7.67 – 7.62 (m, 1H, H-C(3)), 7.35 (td, *J* = 7.3, 1.0 Hz, 1H, H-C(2)), 6.69 (d, *J* = 3.8 Hz, 1H, H-C(11)), 6.18 (d, *J* = 3.7 Hz, 1H, H-C(12)), 2.29 (s, 3H, H-C(14)).

¹³C NMR (126 MHz, DMSO-d_6) δ (ppm) = 186.2 (C(8)), 144.0 (C(5)), 136.5 (C(13)), 134.7 (C(3)), 131.2 (C(6)), 127.2 (C(10)), 125.8 (C(1)), 125.6 (C(2)), 124.4 (C(4)), 123.3 (C(9)), 121.1 (C(7)), 116.5 (C(11)), 112.0 (C(12)), 13.0 (C(14)).

HR-MS (APPI) for $C_{14}H_{11}NOS^+$, $[M+H]^+$, 242.0639, found 242.0634.

IR: $\tilde{v}$/cm^{-1} = 3259 (s), 3143 (m), 3057 (m), 2976 (m), 2895 (m), 1647 (s), 1599 (m), 1577 (s), 1560 (s), 1473 (m), 1466 (m), 1444 (s), 1414 (m), 1398 (s), 1375 (m), 1325 (s), 1311 (m), 1296 (s), 1282 (s), 1205 (s), 1092 (s), 1065 (m), 1049 (s), 1016 (m), 997 (s), 899 (m), 885 (s), 760 (vs), 731 (vs), 710 (s), 675 (s), 638 (m), 607 (s), 542 (s), 498 (s), 486 (s), 424 (m), 407 (m).

M.p.: 233 °C – 235 °C.

2-((1*H*-indol-3-yl)methylene)benzo[*b*]thiophen-3(2*H*)-one (5)
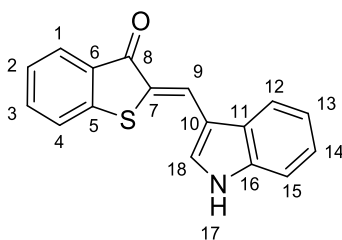
Benzo[*b*]thiophen-3(2*H*)-one (180 mg, 1.20 mmol, 1.25 eq) and 1*H*-indol-3-carbaldehyde (140 mg, 0.958 mmol, 1.00 eq.) were dissolved in dry toluene (3.0 mL, 0.33 M) in a dry Schlenk flask under argon atmosphere. Piperidine (0.02 mL, 0.192 mmol, 0.20 eq.) was added and the reaction was stirred for 2 h at 90 °C. The reaction was cooled to 23 °C and diluted with CH$_2$Cl$_2$ (100 mL) and washed with a sat. aq. NH$_4$Cl$_4$ solution (50 mL) and water (50 mL). The combined aqueous phases were extracted with CH$_2$Cl$_2$ (3 x 50 mL) and the combined organic phases were dried over Na$_2$SO$_4$, filtered and the solvent was removed under reduced pressure. The crude product was recrystallized from heptane/CH$_2$Cl$_2$, filtered and washed with cold heptane. The product (176 mg, 0.630 mmol, 66%) was received as red solid.

R$_f$ (SiO$_2$, i-Hex/EtOAc 8:2) = 0.2.

^{1}H NMR (400 MHz, DMSO-*d$_6$*) δ (ppm) = 12.26 (s, 1H, H-N(17)), 8.27 (s, 1H, H-C(9)), 8.00 (s, 1H, H-C(18)), 7.97 (d, *J* = 7.1 Hz, 1H, H-C(12)), 7.86 (d, *J* = 7.4 Hz, 1H, H-C(1)), 7.79 (d, *J* = 7.9 Hz, 1H, H-C(4)), 7.71 (s, 1H, H-C(3)), 7.54 (d, *J* = 7.1 Hz, 1H, H-C(15)), 7.43 – 7.37 (m, 1H, H-C(2)), 7.30 – 7.26 (m, 1H, H-C(14)), 7.25 – 7.21 (m, 1H, H-C(13)).

^{13}C NMR (101 MHz, DMSO-*d$_6$*) δ (ppm) = 186.4 (C(8)), 144.0 (C(5)), 136.4 (C(16)), 135.1 (C(3)), 131.1 (C(6)), 130.0 (C(18)), 127.2 (C(11)), 126.1 (C(1)), 125.8 (C(2)), 125.7 (C(9)), 124.4 (C(4)), 123.9 (C(7)), 123.3 (C(14)), 121.3 (C(13)), 118.5 (C(12)), 112.6 (C(15)), 111.6 (C(10)).

HR-MS (APPI) for C$_{17}$H$_{11}$NOS$^+$, [M+H]$^+$, 278.0634, found 278.0640.

IR: $\tilde{v}$/cm^{-1} = 3111 (m), 3059 (m), 3041 (m), 3020 (m), 2924 (m), 2871 (m), 1593 (m), 1535 (s), 1508 (s), 1489 (s), 1456 (s), 1441 (s), 1414 (s), 1352 (m), 1342 (s), 1331 (s), 1313 (s), 1286 (s), 1279 (s), 1250 (s), 1213 (s), 1171 (s), 1142 (s), 1122 (s), 1101 (s), 1090 (s), 1066 (s), 1049

(s), 1020 (s), 1011 (s), 980 (s), 958 (m), 945 (m), 914 (s), 872 (s), 833 (m), 779 (m), 748 (s), 739 (s), 723 (vs), 683 (s), 673 (s), 648 (s), 619 (s), 604 (s), 577 (s), 565 (s), 546 (s), 536 (s), 488 (vs), 465 (s), 451 (s), 413 (vs).

M. p.: 267 °C – 268 °C.

2-((5-bromo-1*H*-indol-3-yl)methylene)benzo[*b*]thiophen-3(2*H*)-one (6)
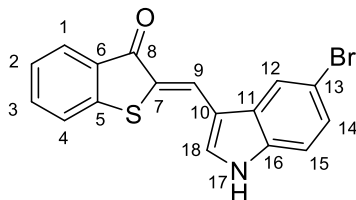
Benzo[*b*]thiophen-3(2*H*)-one (419 mg, 2.79 mmol, 1.25 eq.) and 5-bromo-1*H*-indole-3-carbaldehyde (500 mg, 2.23 mmol, 1.00 eq.) were dissolved in dry toluene (6.8 mL, 0.33 M) under argon atmosphere in a flame dried flask. Piperidine (0.09 mL, 0.446 mmol, 0.20 eq.) was added and the reaction mixture was stirred at 90 °C. After 3 h the reaction mixture was cooled to 23 °C, diluted with CH_2Cl_2 (100 mL), and washed with a sat. aq. NH_4Cl solution (50 mL) and water (50 mL). The combined aqueous phases were extracted with CH_2Cl_2 (3 x 50 mL) and the combined organic phases were dried over Na_2SO_4, filtered and concentrated. The crude product was recrystallized from methanol, filtered and washed with cold methanol to afford the product (756 mg, 2.12 mmol, 95%) as a red solid.

R$_f$ (SiO$_2$, i-Hex/EtOAc 8:2) = 0.15.

¹H NMR (500 MHz, DMSO-*d₆*) δ (ppm) = 12.32 (s, 1H, H-N(17)), 8.26 (d, *J* = 0.4 Hz, 1H, H-C(9)), 8.23 (d, *J* = 1.9 Hz, 1H, H-C(12)), 8.03 (s, 1H, H-C(18)), 7.86 (m, 1H, H-C(1)), 7.79 (m, 1H, H-C(4)), 7.74 – 7.68 (m, 1H, H-C(3)), 7.50 (d, *J* = 8.6 Hz, 1H, H-C(15)), 7.41 – 7.38 (m, 1H, H-C(14)), 7.37 ((dd, *J* = 8.7, 1H, H-C(2)).

¹³C NMR (126 MHz, DMSO-*d₆*) δ (ppm) = 186.5 (C(8)), 144.0 (C(5)), 135.3 (C(3)), 135.2 (C(16)), 131.0 (C(18)), 131.0 (C(6)), 126.2 (C(1)), 125.9 (C(14)), 125.9 (C(9)), 125.4 (C(2)), 124.5 (C(4)), 121.3 (C(12)).

129.0, 114.6, 114.0, 111.3 cannot be unambiguously assigned to C(7), C(10), C(11) or C(13).

HR-MS (APPI) for $C_{17}H_{10}NOSBr^+$, [M+H]$^+$, 355.9739, found 355.9748.

IR: ṽ/cm^{-1} = 3109 (m), 3033 (m), 2920 (m), 2893 (m), 1637 (m), 1593 (s), 1537 (s), 1508 (s), 1471 (s), 1446 (s), 1348 (m), 1300 (s), 1292 (s), 1255 (s), 1217 (vs), 1147 (s), 1130 (s), 1107 (s), 1092 (s), 1063 (s), 1053 (s), 1022 (s), 918 (m), 901 (m), 877 (s), 854 (s), 796 (m), 785 (s), 777 (s), 746 (s), 733 (vs), 673 (s), 613 (vs), 565 (m), 540 (vs), 490 (s), 463 (s), 417 (vs), 409 (s).

M.p.: 311 °C – 312 °C.

2-((5-bromo-7-methyl-1*H*-indol-3-yl)methylene)benzo[*b*]thiophen-3(2*H*)-one (7)
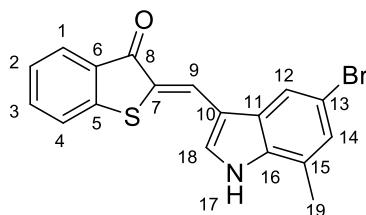
Benzo[*b*]thiophen-3(2*H*)-one (197 mg, 1.31 mmol, 1.25 eq.) and 5-bromo-7-methyl-1*H*-indol-2-carbaldehyde (250 mg, 1.05 mmol, 1.00 eq.) were dissolved in dry toluene (3.0 mL, 0.33 M) in a dry Schlenk flask under argon atmosphere. Piperidine (0.02 mL, 0.210 mmol, 0.20 eq.) was added and the reaction was stirred for 3 h at 90 °C. Then, the reaction mixture was cooled to 23 °C, diluted with CH_2Cl_2 (100 mL), and washed with a sat. aq. NH_4Cl_4 solution (50 mL) and water (50 mL). The combined aqueous phases were extracted with CH_2Cl_2 (3 x 50 mL) and the combined organic layers were dried over Na_2SO_4, filtered and the solvent was removed under reduced pressure. The crude product was recrystallized from heptane/CH_2Cl_2, filtered and washed with cold heptane. The product (270 mg, 0.730 mmol, 69%) was received as red solid.

R$_f$ (SiO$_2$, i-Hex/EtOAc 8:2) = 0.2.

^{1}H NMR (400 MHz, DMSO-d_6) δ (ppm) = 12.46 (s, 1H, H-N(17)), 8.23 (s, 1H, H-C(9)), 8.04 (d, *J* = 2.1 Hz, 1H, H-C(12)), 7.94 (d, *J* = 2.2 Hz, 1H, H-C(18)), 7.86 (dd, *J* = 7.7, 1.7 Hz, 1H, H-C(1)), 7.79 (d, *J* = 7.8 Hz, 1H, H-C(4)), 7.72 (dd, *J* = 7.1, 1.2 Hz, 1H, H-C(3)), 7.40 (td, *J* = 7.4, 1.0 Hz, 1H, H-C(2)), 7.25 – 7.22 (m, 1H, H-C(14)), 2.52 (s, 3H, H-C(19)).

^{13}C NMR (101 MHz, DMSO-d_6) δ (ppm) = 186.5 (C(8)), 143.9 (C(5)), 135.2 (C(3)), 134.8 (C(16)), 131.0 (C(6)), 130.3 (C(18)), 128.6 (C(11)), 126.1 (C(1)), 126.1 (C(14)), 125.9 (C(2)), 125.4 (C(9)), 124.5 (C(4)), 118.7 (C(12)), 111.7 (C(10)), 16.3 (C(19))

124.6, 124.6, 114.0 cannot be unambiguously assigned to C(7), C(13) or C(15).

HR-MS (APPI) for $C_{17}H_{10}NOSBr^+$, [M+H]$^+$, 369.9896, found 369.9902.

IR: $\tilde{v}$/cm^{-1} = 3222 (m), 3157 (m), 3070 (m), 3047 (m), 2900 (m), 1653 (m), 1591 (m), 1577 (m), 1543 (s), 1510 (s), 1466 (s), 1442 (s), 1379 (m), 1344 (s), 1309 (s), 1279 (s), 1250 (s), 1215 (s), 1146 (s), 1126 (s), 1065 (s), 1018 (s), 1009 (s), 982 (m), 960 (m), 945 (m), 904 (s), 868 (s), 847 (vs), 812 (m), 777 (s), 739 (vs), 731 (vs), 702 (s), 675 (vs), 665 (s), 613 (vs), 586 (s), 573 (s), 542 (s), 528 (s), 507 (s), 492 (s), 480 (s), 467 (s), 413 (s).

M.p.: 223 °C – 225 °C.

2-((3-methyl-1*H*-indol-2-yl)methylene)benzo[*b*]thiophen-3(2*H*)-one (8)
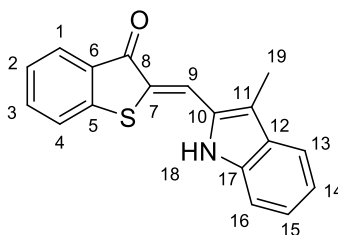
3-Methyl-1*H*-indol-2-carbaldeyde (458 mg, 1.57 mmol, 1.00 eq.) and benzo[*b*]thiophen-3(2*H*)-one (295 mg, 1.97 mmol, 1.25 eq.) were added to a flame-dried flask under argon atmosphere and dissolved in dry toluene (4.8 mL, 0.33 M). Under stirring piperidine (0.05 mL, 0.315 mmol, 0.20 eq.) was added. The reaction was stirred at 90 °C for 4 h and subsequently cooled to 23 °C before CH_2Cl_2 (100 mL) was added. The organic phase was washed with a sat. aq. NH_4Cl solution (50 mL) and water (50 mL). The combined aqueous phases were extracted with CH_2Cl_2 (3 x 50 mL) and the combined organic phases were dried over Na_2SO_4, filtered and concentrated. The crude product was recrystallized from heptane/CH_2Cl_2, filtered and washed with cold heptane. The product (381 mg, 1.30 mmol, 83%) was obtained as red solid.

R$_f$ (SiO$_2$, i-Hex/EtOAc 8:2) = 0.48.

^{1}H NMR (500 MHz, DMSO-d_6) δ (ppm) = 10.78 (s, 1H, H-N(18)), 7.99 (s, 1H, H-C(9)), 7.90 (ddd, *J* = 7.6, 1.4, 0.7 Hz, 1H, H-C(1)), 7.82 (dt, *J* = 7.9, 0.9 Hz, 1H, H-C(4)), 7.76 – 7.72 (m, 1H, H-C(3)), 7.64 (dt, *J* = 8.1, 1.1 Hz, 1H, H-C(13)), 7.56 (dt, *J* = 8.3, 1.0 Hz, 1H, H-C(16)), 7.42 (ddd, *J* = 7.9, 7.2, 1.0 Hz, 1H, H-C(2)), 7.29 – 7.26 (m, 1H, H-C(14)), 7.11 – 7.07 (m, 1H, H-C(15)), 2.49 (s, 3H, H-C(19)).

^{13}C NMR (126 MHz, DMSO-d_6) δ (ppm) = 186.7 (C(8)), 144.8 (C(5)), 139.6 (C(17)), 135.5 (C(3)), 130.2 (C(6)), 128.3 (C(17)), 126.5 (C(1)), 125.9 (C(2)), 124.4 (C(14)), 124.4 (C(4)), 121.4 (C(9)), 120.0 (C(15)), 119.8 (C(16)), 112.8 (C(13)), 9.2 (C(19)).

129.7, 125.9z, 122.3 cannot be unambiguously assigned to (C(7)), (C(10)) or (C(11)).

HR-MS (APPI) for $C_{18}H_{14}NOS^+$, $[M+H]^+$, 292.0791, found 292.0791.

IR: $\tilde{v}$/cm^{-1} = 3386 (m), 3059 (m), 2914 (m), 1655 (w), 1641 (m), 1587 (s), 1527 (s), 1446 (s), 1309 (s), 1277 (s), 1234 (s), 1219 (s), 1130 (m), 1111 (s), 1074 (s), 1012 (s), 941 (s), 893 (s), 762 (s), 737 (vs), 704 (s), 694 (s), 661 (s), 640 (s), 526 (s), 488 (s), 459 (s), 424 (s).

M.p.: 209 °C – 210 °C.

2-(benzo[*b*]thiophen-2-ylmethylene)benzo[*b*]thiophen-3(2*H*)-one (9)
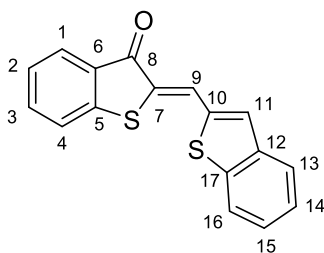
Benzo[*b*]thiophene-3(2*H*)-one (300 mg, 2.00 mmol, 1.25 eq.) and benzo[*b*]thiophene-2-carbaldehyde (260 mg, 1.60 mmol, 1.00 eq.) were dissolved in dry methanol (4.80 mL, 0.33 M) in a flame dried Schlenk flask. Piperidine (0.03 mL, 0.32 mmol, 0.2 eq.) was added and the reaction mixture was stirred for 4 h at 23 °C. The reaction mixture was then diluted with CH_2Cl_2 and washed with sat. aq. NH_4Cl solution (50 mL) and water (50 mL). The combined aqueous phases were extracted with CH_2Cl_2 (2 x 50 mL). The combined organic phases were washed with sat. aq. NaCl solution (100 mL) and dried over Na_2SO_4. The solvent was removed under reduced pressure. The crude product was recrystallized from methanol, filtered, and washed with cold methanol. The product was obtained as a yellow solid (280.4 mg, 0.95 mmol, 59%).

R$_f$ (SiO$_2$, i-Hex/EtOAc 9:1) = 0.41.

^{1}H NMR (500 MHz, DMSO-d_6) δ (ppm) = 8.34 (s, 1H, H-C(11)), 8.22 (s, 1H, H-C(9)), 8.18 (dd, J = 7.1, 1.2 Hz, 1H, H-C(16)), 8.12 (dt, J = 7.9, 1.0 Hz, 1H, H-C(13)), 7.91 (ddd, J = 7.6, 1.4, 0.6 Hz, 1H, H-C(1)), 7.83 (dt, J = 7.9, 0.9 Hz, 1H, H-C(4)), 7.78 – 7.74 (m, 1H, H-C(3)), 7.57 – 7.53 (m, 1H, H-C(15)), 7.53 – 7.49 (m, 1H, H-C(14)), 7.43 (ddd, J = 7.9, 7.2, 1.0 Hz, 1H, H-C(2)).

^{13}C NMR (126 MHz, DMSO-d_6) δ (ppm) = 187.2 (C(8)), 144.6 (C(6)), 139.2 (C(12)), 138.0 (C(17)), 136.1 (C(3)), 131.9 (C(11)), 130.0 (C(5)), 126.6 (C(1)), 126.4 (C(2)), 125.6 (C(14)), 125.3 (C(15)), 124.7 (C(4)), 123.2 (C(13)), 122.5 (C(9)), 121.7 (C(16)).

131.0, 129.9 cannot be unambiguously assigned to C(7) or C(10).

HR-MS (APPI) for $C_{17}H_{11}S_2O^+$, [M+H]$^+$, 294.0168, found 294.0168.

IR: $\tilde{v}$/cm^{-1} = 3101 (w), 3059 (w), 2962 (w), 1672 (s), 1581 (s), 1550 (s), 1491 (m), 1446 (s), 1419 (m), 1350 (m), 1313 (m), 1279 (s), 1246 (m), 1215 (m), 1097 (m), 1090 (m), 1065 (s), 1032 (s), 1016 (s), 916 (s), 860 (m), 735 (vs), 721 (vs), 685 (s), 675 (s), 652 (m), 609 (m), 575 (s), 534 (s), 499 (m), 482 (s), 413 (s).

M.p.: 180 °C – 181 °C.

2-(benzofuran-2-ylmethylene)benzo[*b*]thiophen-3(2*H*)-one (10)
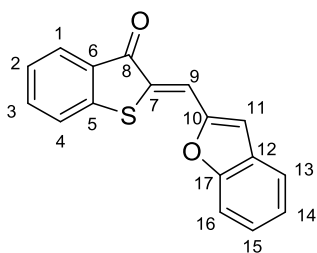
Benzofuran-2-carbaldeyde (0.2 mL, 1.50 mmol, 1.00 eq.) and benzo[*b*]thiophen-3(2*H*)-one (225 mg, 1.50 mmol, 1.00 eq.) were added to a flame-dried flask under argon atmosphere and dissolved in dry diethyl ether (4.5 mL, 0.33 M). Under stirring $BF_3 \cdot Et_2O$ (0.38 mL, 3.00 mmol, 2.00 eq.) was added. The reaction was stirred at 23 °C for 4 h. The reaction was stopped by addition of a sat. aq. $NaHCO_3$ solution and the aqueous phase was extracted with CH_2Cl_2 (3 x 50 mL). The combined organic phases were dried over Na_2SO_4, filtered and the solvent was removed under reduced pressure. The crude product was recrystallized from methanol, filtered and washed with cold methanol. The 2-(benzofuran-2-ylmethylene)benzo[*b*]thiophen-3(2*H*)-one (271 mg, 0.970 mmol, 65%) was obtained as orange solid.

R_f (SiO_2, i-Hex/EtOAc 9:1) = 0.43.

^{1}H NMR (400 MHz, DMSO-d_6) δ (ppm) = 7.92 (d, *J* = 0.6 Hz, 1H, H-C(9)), 7.88 (dt, *J* = 7.6, 1.3, 0.6 Hz, 1H, H-C(1)), 7.84 (dt, *J* = 8.0, 0.9 Hz, 1H, H-C(4)), 7.80 (dt, *J* = 7.8, 1.3, 0.8 Hz, 1H, H-C(16)), 7.79 – 7.71 (td, 1H, H-C(3)), 7.70 (dd, *J* = 8.3, 0.9 Hz, 1H, H-C(13)), 7.64 (s, 1H, H-C(11)), 7.49 (td, *J* = 8.5, 7.2, 1.3 Hz, 1H, H-C(15)), 7.42 (td, *J* = 7.9, 7.1, 1.1 Hz, 1H, H-C(2)), 7.35 (td, *J* = 8.0, 7.3, 1.0 Hz, 1H, H-C(14aa)).

^{13}C NMR (101 MHz, DMSO-d_6) δ (ppm) = 187.3 (C(8)), 155.5 (C(17)), 151.9 (C(5)), 145.6 (C(6)), 136.1 (C(2)), 130.4 (C(7)), 129.7 (C(12)), 128.2 (C(10)), 127.4 (C(13)), 126.5 (C(4)), 126.1 (C(14)), 124.6 (C(16)), 124.1 (C(3)), 122.6 (C(15)), 119.4 (C(1)), 115.3 (C(9)), 111.5 (C(11)).

HR-MS (APPI) for $C_{17}H_{11}O_2S^+$, [M+H]$^+$, 279.0474, found 279.0477.

IR: $\tilde{v}$/cm^{-1} = 3022 (m), 2920 (m), 2850 (m), 1668 (s), 1593 (s), 1583 (s), 1523 (m), 1446 (m), 1346 (m), 1281 (s), 1066 (m), 1053 (m), 1005 (m), 947 (s), 812 (s), 741 (s), 729 (vs), 706 (s), 687 (s), 631 (s), 611 (m), 515 (m), 494 (m), 482 (m), 471 (s), 428 (m), 411 (s), 403 (s).

M.p.: 188 °C – 189 °C.

2-(benzofuran-3-ylmethylene)benzo[*b*]thiophen-3(2*H*)-one (11)
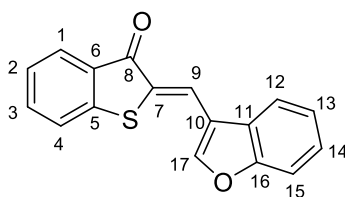
Benzofuran-3-carbaldeyde (0.2 mL, 1.50 mmol, 1.00 eq.) and benzo[*b*]thiophen-3(2*H*)-one (225 mg, 1.50 mmol, 1.25 eq.) were added to a flame-dried flask under argon atmosphere and dissolved in dry diethyl ether (4.5 mL, 0.33 M). Under stirring $BF_3 \cdot Et_2O$ (0.38 mL, 3.00 mmol, 2.00 eq.) was added. The reaction mixture was stirred at 23 °C for 4 h. The reaction was stopped by adding a sat. aq. $NaHCO_3$ solution and the aqueous phase was extracted with CH_2Cl_2 (3 x 50 mL). The combined organic phases were dried over Na_2SO_4, filtered, and the solvent was removed under reduced pressure. The crude product was recrystallized from methanol, filtered and washed with cold methanol. The product (215 mg, 0.724 mmol, 48%) was obtained as orange solid.

R_f (SiO_2, i-Hex/EtOAc 8:2) = 0.63.

^{1}H NMR (601 MHz, DMSO-d_6) δ (ppm) = 8.56 (s, 1H, H-C(17)), 8.11 – 8.09 (m, 1H, H-C(15)), 8.09 (s, 1H, H-C(9)), 7.90 (dt, *J* = 7.6, 1.0 Hz, 1H, H-C(1)), 7.82 (dt, *J* = 7.9, 0.9 Hz, 1H, H-C(4)), 7.78 – 7.75 (m, 1H, H-C(3)), 7.73 (dt, *J* = 8.2, 1.0 Hz, 1H, H-C(12)), 7.49 – 7.46 (m, 1H, H-C(13)), 7.45 – 7.43 (m, 1H, H-C(2)), 7.43 – 7.41 (m, 1H, H-C(14)).

^{13}C NMR (151 MHz, DMSO-d_6) δ (ppm) = 187.4 (C(8)), 155.1 (C(11)), 148.2 (C(17)), 144.5 (C(5)), 136.7 (C(3)), 131.4 (C(10)), 130.6 (C(6)), 127.1 (C(1)), 126.9 (C(2)), 126.5 (C(13)), 126.2 (C(16)), 125.1 (C(4)), 124.5 (C(14)), 121.5 (C(9)), 120.8 (C(15)), 117.5 (C(7)), 112.3f (C(12)).

HR-MS (APPI) for $C_{17}H_{11}O_2S^+$, [M+H]$^+$, 279.0474, found 279.0476.

IR: $\tilde{v}$/cm^{-1} = 3018 (m), 2900 (m), 2858 (m), 1663 (s), 1595 (s), 1569 (s), 1525 (m), 1446 (m), 1339 (m), 1281 (s), 1184 (s), 1066 (m), 1033 (m), 1005 (m), 947 (s), 812 (s), 741 (s), 729 (vs), 706 (s), 687 (s), 683 (s), 659 (s), 631 (s), 610 (m), 532 (m), 510 (m), 496 (m), 483 (m), 471 (s), 449 (m), 425 (m), 416 (s), 401 (s).

M.p.: 191 °C – 192 °C.

2-((6-bromopyridin-2-yl)methylene)benzo[*b*]thiophen-3(2*H*)-one (12)
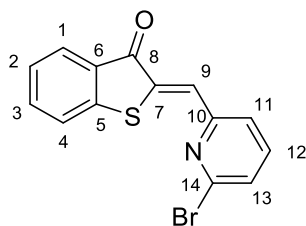
Benzo[*b*]thiophen-3(2H)-one (300 mg, 2.00 mmol, 1.25 eq.) and 6-bromopicoline aldehyde (260 mg, 1.60 mmol, 1.00 eq.) were dissolved in dry toluene (4.80 mL, 0.33 M) in a dry Schlenk flask under an argon atmosphere. While stirring, a drop of piperidine was added and the reaction mixture was stirred for 1 h at 90 °C. After cooling to 23 °C, the reaction mixture was diluted with CH_2Cl_2 and washed with a sat. aq. $NaHCO_3$ solution (50 mL) and water (50 mL). The aqueous phases were extracted with CH_2Cl_2 (2 x 50 mL). The combined organic phases were washed with sat. aq. NaCl solution (100 mL) and dried over Na_2SO_4, filtered and concentrated. The crude product was recrystallized from methanol, filtered and washed with cold methanol. The product was obtained as a yellow solid (341 mg, 1.07 mmol, 67%).

R$_f$ (SiO$_2$, i-Hex/EtOAc 9:1) = 0.27.

^{1}H NMR (400 MHz, DMSO-*d$_6$*) δ (ppm) = 7.96 (dd, *J* = 7.6, 1.0 Hz, 1H, H-C(11)), 7.91 (d, *J* = 1.4 Hz, 1H, H-C(9)), 7.89 (s, 1H, H-C(13)), 7.86 (dt, *J* = 7.8, 1.1 Hz, 1H, H-C(1)), 7.81 (d, *J* = 7.8 Hz, 1H, H-C(4)), 7.72 (td, *J* = 7.6, 1.3 Hz, 1H, H-C(3)), 7.68 (dd, *J* = 7.9, 1.0 Hz, 1H, H-C(12)), 7.38 (td, *J* = 7.3, 1.1 Hz, 1H, H-C(2)).

^{13}C NMR (101 MHz, DMSO-*d$_6$*) δ (ppm) = 188.5 (C(8)), 153.3 (C(10)), 148.3 (C(5)), 140.4 (C(13)), 136.4 (C(3)), 135.0 (C(6)), 129.3 (C(14)), 129.0 (C(7)), 128.1 (C(12)), 127.8 (C(9)), 127.4 (C(11)), 126.4 (C(1)), 126.1 (C(2)), 124.7 (C(4)).

HR-MS (APPI) for $C_{14}H_9SNBrO^+$, $[M+H]^+$, 317.9583, found 317.9584.

IR: $\tilde{v}$/cm^{-1} = 3070 (w), 3033 (w), 2962 (m), 1680 (s), 1603 (m), 1591 (m), 1568 (s), 1539 (m), 1448 (m), 1435 (s), 1406 (s), 1309 (w), 1281 (m), 1257 (s), 1225 (m), 1163 (m), 1122 (s), 1086 (s), 1057 (s), 1012 (vs), 984 (s), 935 (s), 912 (s), 887 (m), 843 (m), 793 (vs), 737 (s), 725 (vs), 673 (vs), 621 (m), 600 (m), 569 (s), 496 (s), 484 (m), 440 (m),

M.p.: 172 °C – 174 °C.

2-(pyridin-3-yl)methylenebenzo[*b*]thiophen-3(2*H*)-one (13)
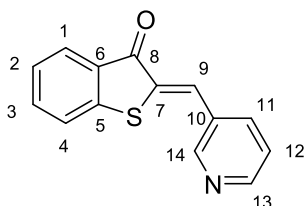
Under argon atmosphere in a flame dried flask, benzo[*b*]thiophen-3(2H)-one (300 mg, 2.00 mmol, 1.25 eq.) and nicotinic aldehyde (0.15 mL, 1.60 mmol, 1.00 eq.) were dissolved in dry toluene (4.80 mL, 0.33 M). A drop of piperidine was added and the reaction mixture was heated to 90 °C for 1 h. Then the reation mixture was cooled to 23 °C. diluted with CH_2Cl_2 (50 mL), and washed with sat. aq. $NaHCO_3$ solution (50 mL) and water (50 mL). The aqueous phases were extracted with CH_2Cl_2 and the combined organic phases were washed with a sat. aq. NaCl solution (50 mL), dried over Na_2SO_4, filtered, and the solvent was removed under reduced pressure. The crude product was recrystallized from methanol, filtered and washed with cold methanol. The product (242 mg, 1.01 mmol, 63%) was obtained as a yellow solid.

R$_f$ (SiO$_2$, i-Hex/EtOAc 8:2) = 0.26.

¹H NMR (400 MHz, DMSO-*d$_6$*) δ (ppm) = 9.01 (dt, *J* = 2.5, 0.8 Hz, 1H, H-C(14)), 8.66 (dd, *J* = 4.8, 1.6 Hz, 1H, H-C(13)), 8.22 – 8.14 (m, 1H, H-C(11)), 8.00 (s, 1H, H-C(9)), 7.94 – 7.91 (m, 1H, H-C(1)), 7.86 – 7.83 (m, 1H, H-C(4)), 7.80 – 7.76 (m, 1H, H-C(3)), 7.63 (ddd, *J* = 8.4, 4.7, 0.9 Hz, 1H, H-C(12)), 7.47 – 7.43 (m, 1H, H-C(2)).

¹³C NMR (101 MHz, DMSO-*d$_6$*) δ (ppm) = 187.4 (C(8)), 152.0 (C(14)), 150.6 (C(13)), 146.9 (C(7)), 144.8 (C(5)), 136.7 (C(11)), 136.4 (C(3)), 129.9 (C(6)), 129.6 (C(9)), 129.3 (C(10)), 126.8 (C(1)), 126.5 (C(2)), 124.7 (C(4)), 124.2 (C(12)).

HR-MS (APPI) for $C_{14}H_{10}SNO^+$, [M+H]$^+$, 240.0478, found 240.0481.

IR: $\tilde{v}$/cm^{-1} = 3030 (w), 3006 (w), 1680 (s), 1599 (m), 1583 (s), 1558 (m), 1471 (m), 1448 (m), 1421 (m), 1406 (m), 1284 (s), 1261 (m), 1068 (s), 1039 (s), 1020 (s), 800 (m), 777 (m), 735 (vs), 723 (s), 700 (s), 675 (s), 660 (s), 617 (m), 571 (m), 534 (m), 525 (m), 484 (m), 418 (m).

M.p.: 152 °C – 154 °C.

2-(pyridin-4-yl)methylenebenzo[*b*]thiophen-3(2*H*)-one (14)
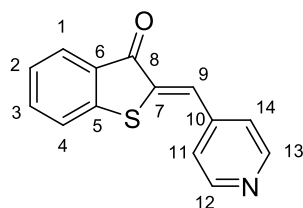
Benzo[*b*]thiophen-3(2*H*)-one (300 mg, 2.00 mmol, 1.25 eq.) and isonicotin aldehyde (0.17 mL, 1.60 mmol, 1.00 eq.) were dissolved in dry toluene (4.8 mL, 0.33 M) in a dry Schlenk flask under argon atmosphere. A drop of piperidine was added and the reaction mixture was stirred for 3 h at 90 °C. Then the reaction was cooled to 23 °C, diluted with CH_2Cl_2 (100 mL), and washed with a sat. aq. $NaHCO_3$ solution (50 mL) and water (50 mL). The combined aqueous phases were extracted with CH_2Cl_2 (3 x 50 mL) and the combined organic phases were washed with a sat. aq. NaCl solution, dried over Na_2SO_4, filtered and the solvent was removed under reduced pressure. The crude product was recrystallized from methanol, filtered and washed with cold heptane. The product (299 mg, 1.25 mmol, 78%) was received as yellow solid.

R_f (SiO_2, i-Hex/EtOAc 8:2) = 0.30.

^{1}H NMR (500 MHz, DMSO-d_6) δ (ppm) = 8.79 – 8.74 (m, 2H, H-C(12, 13)), 7.91 (dt, *J* = 7.8, 1.3 Hz, 1H, H-C(1)), 7.89 (s, 1H, H-C(9)), 7.84 (dt, *J* = 8.0, 1.0 Hz, 1H, H-C(4)), 7.79 (dd, *J* = 7.1, 1.3 Hz, 1H, H-C(3)), 7.73 – 7.69 (m, 2H, H-C(11, 14)), 7.45 (ddd, *J* = 8.0, 7.0, 1.1 Hz, 1H, H-C(2)).

^{13}C NMR (126 MHz, DMSO-d_6) δ (ppm) = 187.6 (C(8)), 150.6 (C(12, 13), 144.8 (C(5)), 140.7 (C(3)), 134.2 (C(6)), 129.7 (C(9)), 129.0 (C(7)), 126.9 (C(1)), 126.6 (C(2)), 124.8 (C(4)), 124.0 (C(11, 14)).

HR-MS (APPI) for $C_{14}H_{10}SNO^+$, [M+H]$^+$, 240.0478, found 240.0485.

IR: $\tilde{v}$/cm^{-1} = 3072 (w), 3043 (w), 1685 (m), 1599 (m), 1587 (s), 1572 (m), 1450 (m), 1437 (m), 1412 (m), 1284 (s), 1259 (s), 1217 (m), 1065 (s), 1045 (vs), 1016 (vs), 1009 (vs), 993 (s), 918 (m), 893 (m), 868 (m), 795 (vs), 775 (vs), 742 (vs), 729 (s), 677 (s), 667 (s), 638 (s), 555 (m), 534 (s), 484 (s).

M.p.: 181 °C – 183 °C.

2-(quinolin-2-ylmethylene)benzo[*b*]thiophen-3(2*H*)-one (15)
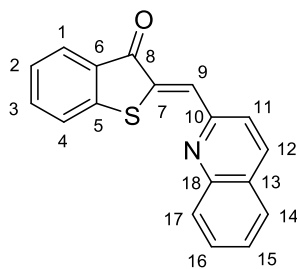
Under argon atmosphere in a flame dried flask, benzo[*b*]thiophen-3(2H)-one (300 mg, 2.00 mmol, 1.25 eq.) and quinolin-2-aldehyde (252 mg, 1.60 mmol, 1.00 eq.) were dissolved in dry toluene (4.80 mL, 0.33 M). A drop of piperidine was added and the reaction mixture was heated to 90 °C for 1 h. Then the reaction was cooled to 23 °C, diluted with CH_2Cl_2 (50 mL), and washed with a sat. aq. $NaHCO_3$ solution (50 mL) and water (50 mL). The aqueous phases were extracted with CH_2Cl_2 and the combined organic phases were washed with a sat. aq. NaCl solution, dried over Na_2SO_4, filtered, and the solvent was removed under reduced pressure. The crude product was recrystallized from methanol, filtered, and washed with cold methanol. The product (299 mg, 1.25 mmol, 78%) was obtained as a yellow solid.

R_f (SiO_2, i-Hex/EtOAc 9:1) = 0.34.

¹H NMR (500 MHz, DMSO-*d₆*) δ (ppm) = 8.48 (dd, *J* = 8.4, 1.0 Hz, 1H, H-C(12)), 8.19 – 8.16 (m, 1H, H-C(17)), 8.11 (s, 1H, H-C(9)), 8.03 (dd, *J* = 8.1, 1.7 Hz, 1H, H-C(14)), 8.00 (d, *J* = 8.6 Hz, 1H, H-C(11)), 7.91 – 7.88 (m, 1H, H-C(1)), 7.88 – 7.84 (m, 1H, H-C(16)), 7.81 (dd, *J* = 7.8, 0.8 Hz, 1H, H-C(4)), 7.76 – 7.72 (m, 1H, H-C(3)), 7.69 (ddd, *J* = 8.1, 6.8, 1.3 Hz, 1H, H-C(15)), 7.42 – 7.37 (m, 1H, H-C(2)).

¹³C NMR (126 MHz, DMSO-*d₆*) δ (ppm) = 188.6 (C(8)), 152.6 (C(10)), 149.2 (C(5)), 147.2 (C(5)), 137.0 (C(12)), 136.2 (C(3)), 135.5 (C(13)), 130.5 (C(17)), 129.5 (C(6)), 129.0 (C(9)), 128.6 (C(14)), 128.0 (C(7)), 127.7 (C(15)), 127.1 (C(16)), 126.4 (C(1)), 126.0 (C(2)), 125.0 (C(11)), 124.6 (C(4)).

HR-MS (APPI) for $C_{18}H_{12}SNO^+$, [M+H]⁺, 290.0634, found 290.0636.

IR: $\tilde{v}$/cm⁻¹ = 3062 (w), 3053 (w), 2962 (w), 1676 (s), 1599 (m), 1581 (s), 1570 (s), 1498 (m), 1448 (s), 1279 (s), 1261 (m), 1215 (s), 1196 (m), 1117 (m), 1097 (m), 1072 (s), 1055 (s), 1020 (s), 1014 (s), 881 (s), 860 (m), 825 (s), 800 (m), 789 (m), 779 (s), 735 (vs), 708 (m), 687 (s), 671 (s), 650 (m), 609 (s), 534 (m), 496 (m), 480 (m), 449 (m), 432 (m).

M.p.: 200 °C – 201 °C.

2-((2-chloroquinolin-3-yl)methylene)benzo[*b*]thiophen-3(2*H*)-one (16)
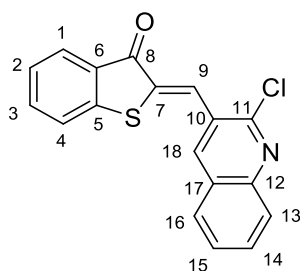
Under argon atmosphere in a flame dried flask, benzo[*b*]thiophen-3(2*H*)-one (300 mg, 2.00 mmol, 1.25 eq.) and 2-chloroquinoline-3-carbaldehyde (307 mg, 1.60 mmol, 1.00 eq.) were dissolved in dry toluene (4.80 mL, 0.33 M) and a drop of piperidine was added. The reaction mixture was heated to 90 °C for 1 h. After cooling to 23 °C the mixture was diluted with CH_2Cl_2 (50 mL) and washed with a sat. aq. $NaHCO_3$ solution (50 mL) and water (50 mL). The aqueous phases were extracted with CH_2Cl_2 (3 x 50 mL) and the combined organic phases were washed with a sat. aq. NaCl solution (50 mL), dried over Na_2SO_4, filtered and concentrated. The crude product was recrystallized from methanol, filtered and washed with cold methanol. The product (316 mg, 0.980 mmol, 61%) was obtained as a yellow solid.

R$_f$ (SiO$_2$, i-Hex/EtOAc 9:1) = 0.39.

^{1}H NMR (400 MHz, DMSO-d_6) δ (ppm) = 8.80 (s, 1H, H-C(18)), 8.28 – 8.24 (m, 1H, H-C(16)), 8.16 (s, 1H, H-C(9)), 8.02 (d, *J* = 1.3 Hz, 1H, H-C(13)), 7.97 – 7.91 (m, 2H, H-C(1, 14)), 7.86 (dt, *J* = 7.9, 1.0 Hz, 1H, H-C(4)), 7.82 – 7.74 (m, 2H, (3, 15)), 7.47 (ddd, *J* = 8.0, 7.1, 1.1 Hz, 1H, H-C(2)).

^{13}C NMR (101 MHz, DMSO-d_6) δ (ppm) = 185.3 (C(8)), 150.7 (C(10)), 149.2 (C(11)), 146.5 (C(12)), 144.9 (C(5)), 138.9 (C(18)), 136.7 (C(3)), 134.4 (C(7)), 132.5 (C(14)), 129.3 (C(6)), 129.0 (C(16)), 128.3 (C(15)), 127.8 (C(13)), 127.0 (C(1)), 126.7 (C(17)), 126.4 (C(9)), 124.8 (C(4)).

HR-MS (APPI) for $C_{18}H_{11}SNClO^+$, $[M+H]^+$, 324.0244, found 324.0245.

IR: $\tilde{v}$/cm^{-1} = 3059 (w), 3033 (w), 1678 (m), 1591 (m), 1577 (m), 1562 (s), 1485 (m), 1446 (s), 1371 (m), 1338 (m), 1279 (s), 1219 (m), 1203 (m), 1188 (m), 1142 (m), 1130 (m), 1072 (m), 1045 (vs), 1016 (s), 958 (m), 930 (m), 897 (m), 883 (m), 854 (m), 779 (m), 773 (m), 735 (vs), 714 (m), 692 (m), 671 (s), 648 (s), 594 (m), 536 (m), 499 (m), 484 (s), 471 (s), 418 (s).

M.p.: 224 °C – 225 °C.

UV/Vis Spectroscopic Measurements

Photoisomerization at UV/Vis Concentrations in Different Solvents

To determine the photostationary states PSS in different solvents (toluene, benzene, tetrahydrofuran, acetonitrile, DMSO or methanol) and at different wavelengths of irradiation, stock solutions of **1-11** and **15** and **16** ($3.85 \cdot 10^{-5} - 5.46 \cdot 10^{-5}$ mol/L) were prepared. A UV/Vis cuvette (1 cm) was prepared with 2.5 mL spectroscopic solvent and a defined volume of stock solution was added to obtain a concentration of $1.57 \cdot 10^{-5} - 2.72 \cdot 10^{-5}$ mol/L in the cuvette.

An absorption spectrum was recorded and subsequently the solution in the cuvette was irradiated with an LED of a specific wavelength (385 nm, 405 nm, 410 nm, 420 nm, 430 nm, 450 nm, 470 nm, 490 nm, 505 nm, 515 nm, 530 nm, 554 nm, 565 nm, 590 nm) and the absorption spectrum was measured.

Calculation of UV/Vis Spectra of Pure *Z* and *E* Isomers

UV/Vis absorption spectra of the pure *E/Z* isomer were determined by subtracting one absorption spectrum of a *E/Z* mixture with known isomeric composition from a second spectrum of a different *E/Z* mixture containing again a known isomeric composition.[4] The isomeric compositions were established concomitantly based on the integration of suitable signals in the corresponding ^{1}H NMR spectra, which were recorded immediately after measuring the absorption spectra of the *E/Z* mixtures as explained below.

A deuterated solvent stock solution ($4.16 \cdot 10^{-3} - 8.76 \cdot 10^{-3}$ mol/L) toluene-d_8, DMSO-d_6, benzene-d_6, acetonitrile-d_3 or THF-d_8 was prepared. 0.8 mL of the stock solution was transferred to the NMR tube and a UV/Vis cuvette (1 cm) was also filled with spectroscopic solvent (2.5 mL) and mixed with 10 µL of the stock solution. A ^{1}H NMR and an absorption spectrum were simultaneously measured. For further measurements, the NMR tube was irradiated at 405 nm, 420 nm, 430 nm or 450 nm and a new isomer ratio was established, quantified again by simultaneous measurement of a ^{1}H NMR and absorption spectrum. For this purpose, 10 µL of the irradiated NMR solution was transferred to the UV/Vis cuvette and diluted with 2.5 mL of spectroscopic solvent.

The following conditions must be fulfilled for all measurements:

- o There must be no by-products, except for double-bond isomerization. Otherwise, no clear isosbestic points can be obtained.
- o The concentration in the UV/Vis cuvette must be the exact same in all measurements. Otherwise, no clear isosbestic points are obtained.
- o The *E/Z* mixed spectrum is the result of the addition of pure *E* and *Z* spectra (no spectroscopic cross-talk between isomers in the mixture).

The pure *E* and *Z* isomer absorption spectra are defined as:

$$S(E) = S(X_{E(1,2,3,...)};\ Y_{E(1,2,3,...)}) \qquad \text{(eq.1)}$$

$$S(Z) = S(X_{Z(1,2,3,...)};\ Y_{Z(1,2,3,...)}) \qquad \text{(eq.2)}$$

with the wavelength X_Z and X_E and the absorption Y_Z and Y_E, leading to the full absorption spectrum $S(Z)$ or $S(E)$. The absorption spectra of an *E/Z* mixture, where one isomer is enriched (*Z+* and *E+*) can be described as addition of pure *Z* and *E* spectra with different weighting factors for each isomer:

$$S_{mix}(E +) = S(E) \cdot z_1 + S(Z) \cdot z_2 \qquad \text{(eq.3)}$$

$$S_{mix}(Z +) = S(E) \cdot z_3 + S(Z) \cdot z_4 \qquad \text{(eq.4)}$$

The weighting factors z_1, z_2, z_3 and z_4, determined by integrating the corresponding signals of the *E* and *Z* isomer in the ^{1}H NMR spectrum, correspond to the concentration of each isomer in the enriched spectrum.

	E isomer	*Z* isomer
E enriched spectrum (S(*E*+))	z_1	z_2
Z enriched spectrum (S(*Z*+))	z_3	z_4

The pure S(*Z*) and S(*E*) can then be calculated from the spectra of the mixtures as:

$$S(Z) = \frac{S_{mix}(Z+) \cdot z_1 - S_{mix}(E+) \cdot z_3}{z_1 \cdot z_4 - z_2 \cdot z_3} \qquad \text{(eq.5)}$$

$$S(E) = \frac{S_{mix}(Z+) \cdot z_4 - S_{mix}(E+) \cdot z_2}{z_2 \cdot z_3 - z_1 \cdot z_4} \qquad \text{(eq.6)}$$

by solving linear equations eq.3 and eq.4.

Based on the calculated absorption spectrum of pure *E* and *Z* isomer and the known concentration in the UV/Vis cuvette, the molar extinction coefficients can be determined. For this purpose, the *Lambert Beer Law* is applied:

$$A = \varepsilon \cdot c \cdot d \qquad \text{(eq.7)}$$

with the absorption *A*, the concentration *c*, the path length of the cuvette *d* and the molar extinction coefficient ε.

Photobleaching experiment

Fifteen switching cycles were performed to determine the photochemical stability of the photoswitches. For this purpose, a sample was prepared with UV/Vis concentration in a spectroscopic solvent. The sample was then irradiated alternately with 420 nm, 430 nm, 450 nm (accumulation of the *E* isomer) or 490 nm, 505 nm, and 530 nm (accumulation of the *Z* isomer) and switched between the *E* and *Z* isomer. It is essential to reach the pss and immediately record a UV/Vis spectrum of this condition. For evaluation of the experiment, the absorbance of the two isomers at a particular wavelength and the absorbance at the isosbestic point are compared for each cycle.
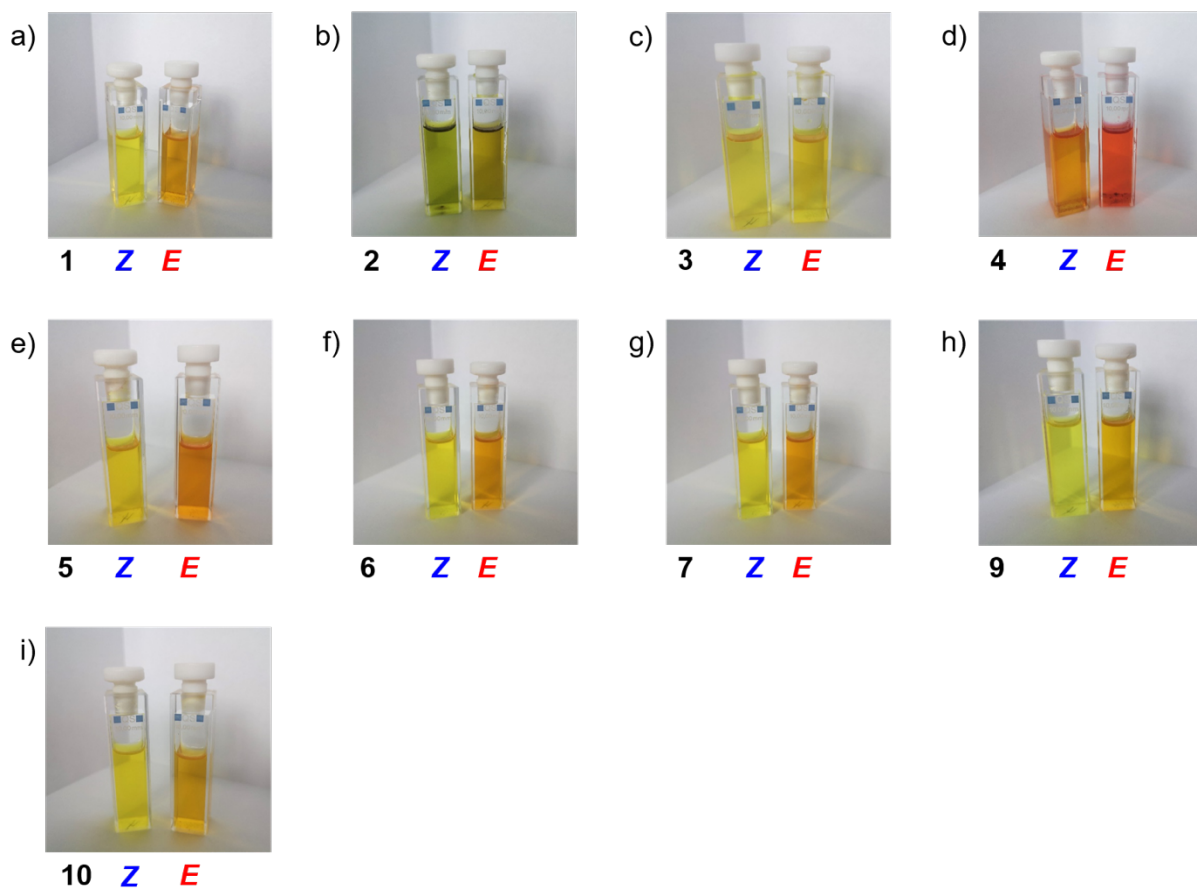
Figure S 1: Irradiation of Het-HTIs in DMSO with light of different wavelengths results in a visible color change; a) compound **1**; b) compound **2**; c) compound **3**, here no color change visible to the naked eye; d) compound **4**; e) compound **5**; f) compound **6**; g) compound **7**; h) compound **9**; i) compound **10**.
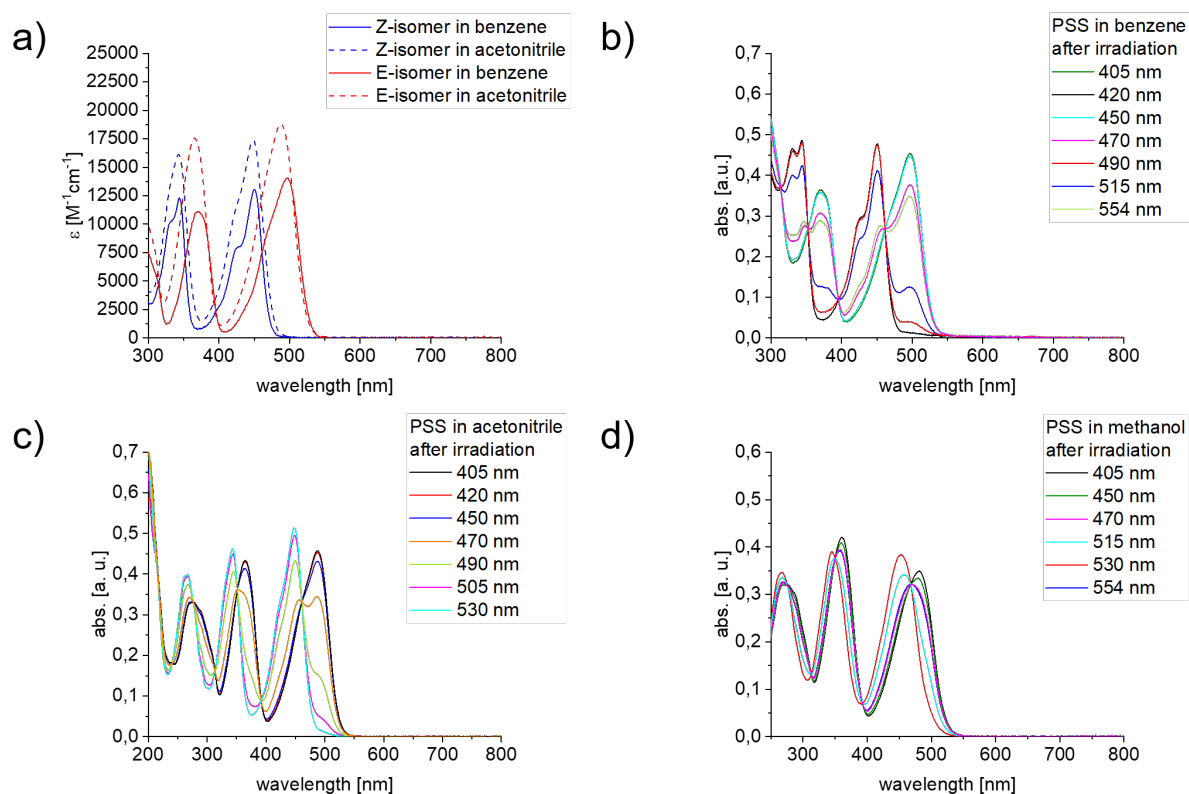
Figure S 2: a) Molar extinction coefficients of pure *Z* (blue) and *E* (red) isomer of compound **1** in benzene (solid line) and acetonitrile (dashed line); b) UV/Vis absorption spectra of *Z* and *E* isomer measured in benzene at 23 °C after irradiation with various wavelengths; c) UV/Vis absorpt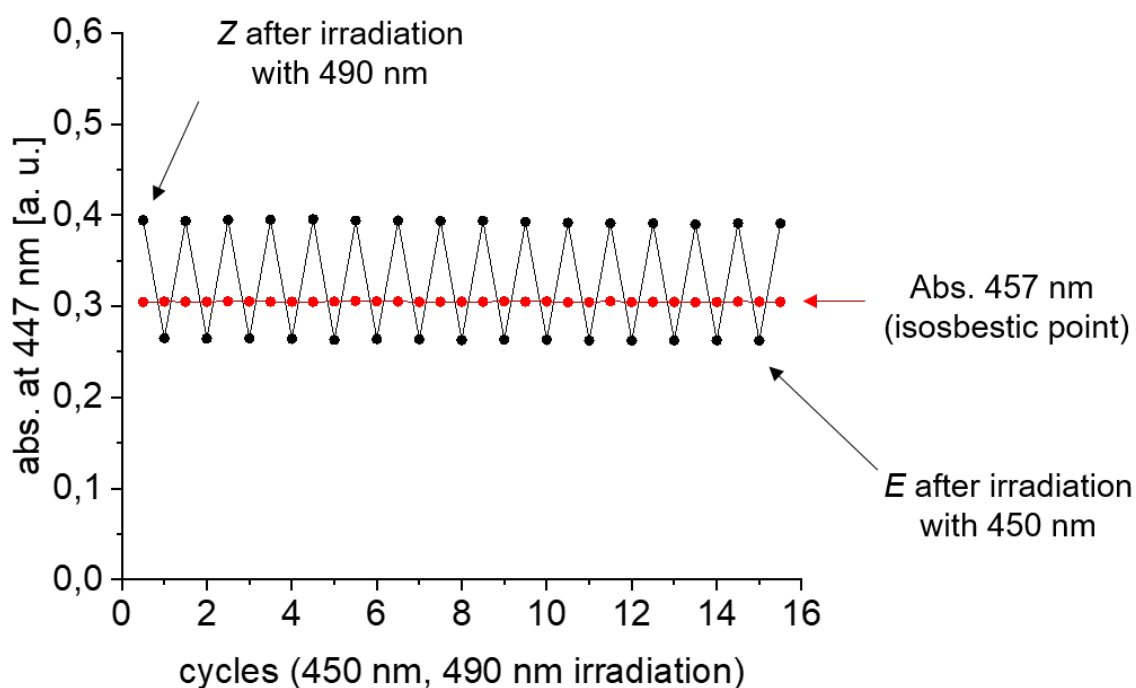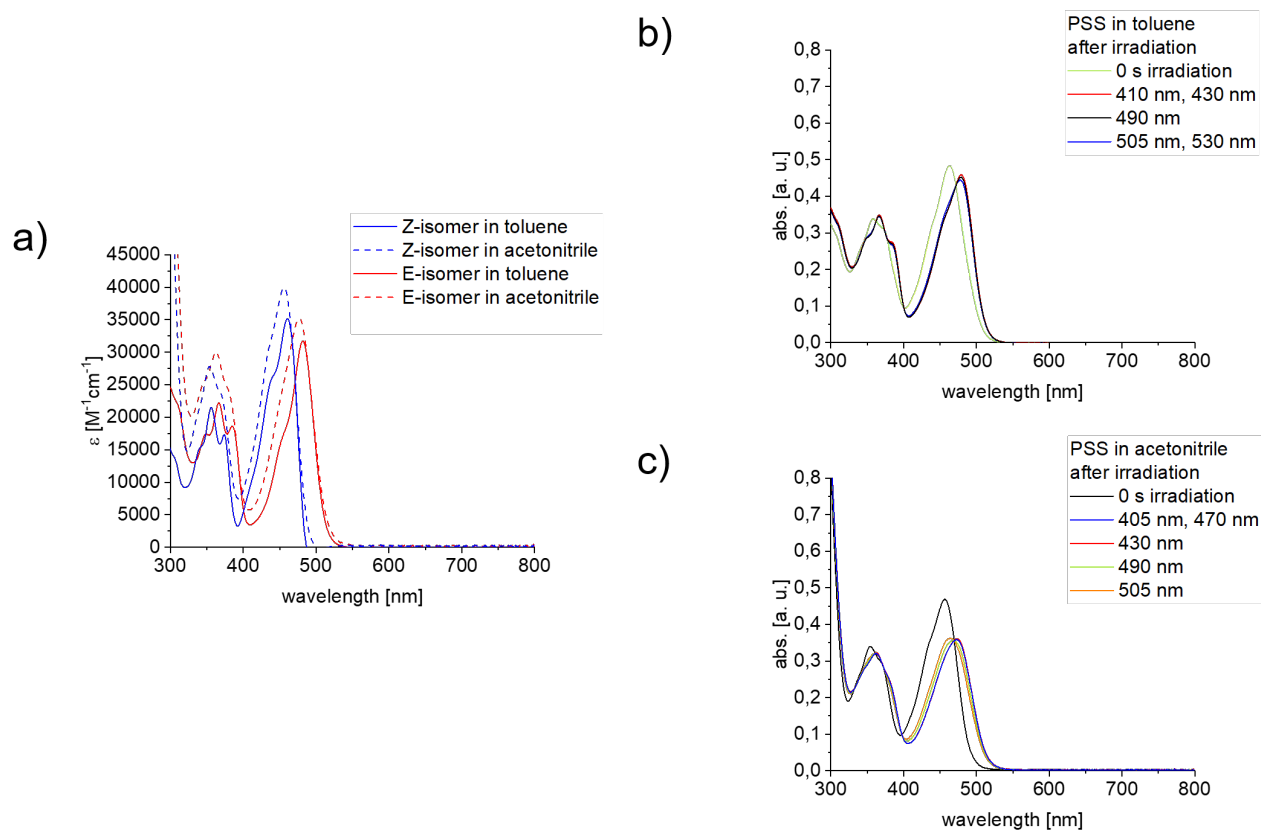ion spectra of *Z* and *E* isomer measured in acet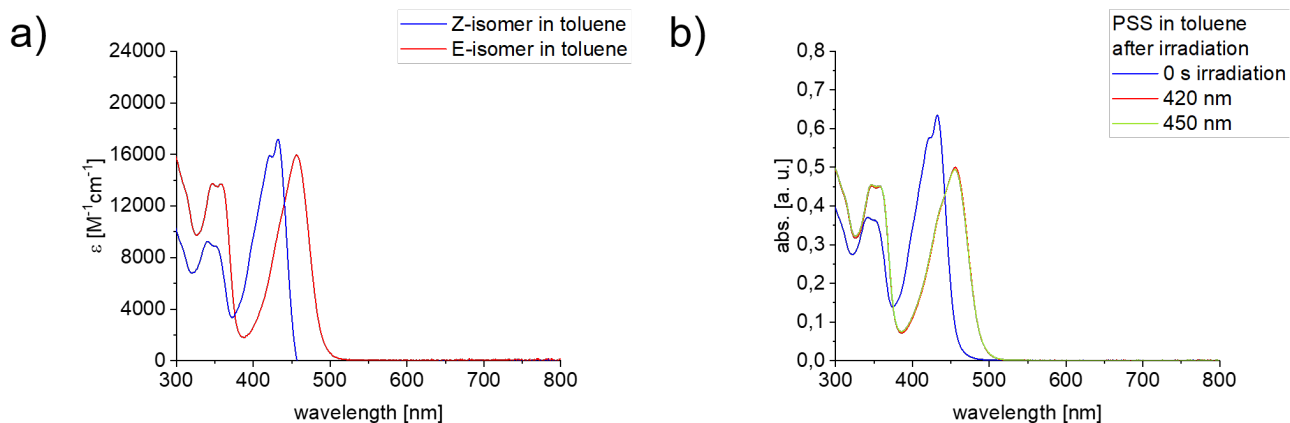onitrile at 23 °C after irradiation with various wavelengths; d) UV/Vis absorption spectra of *Z* and *E* isomer measured in methanol at 23 °C after irradiation with various wavelengths.
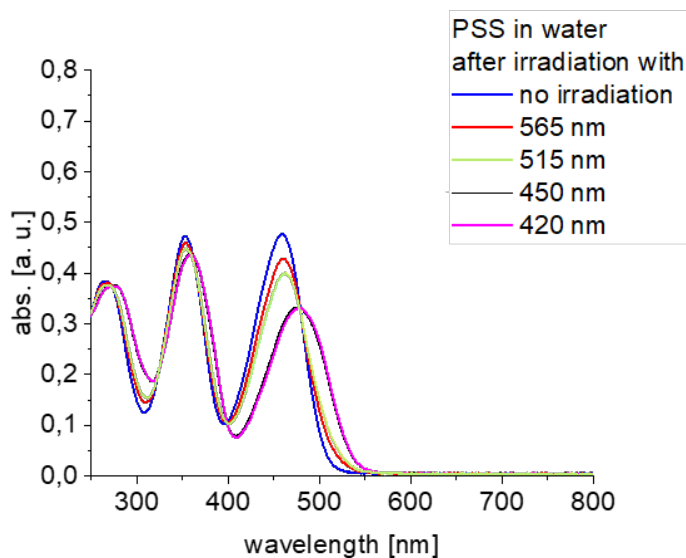
**Figure S 3:** UV/Vis absorption spectra of *Z* and *E* isomer of compound **1** obtained in water (3,00 mL and 40,0 µL DMSO for improved solubility) at 23 °C after irradiation with different wavelengths.
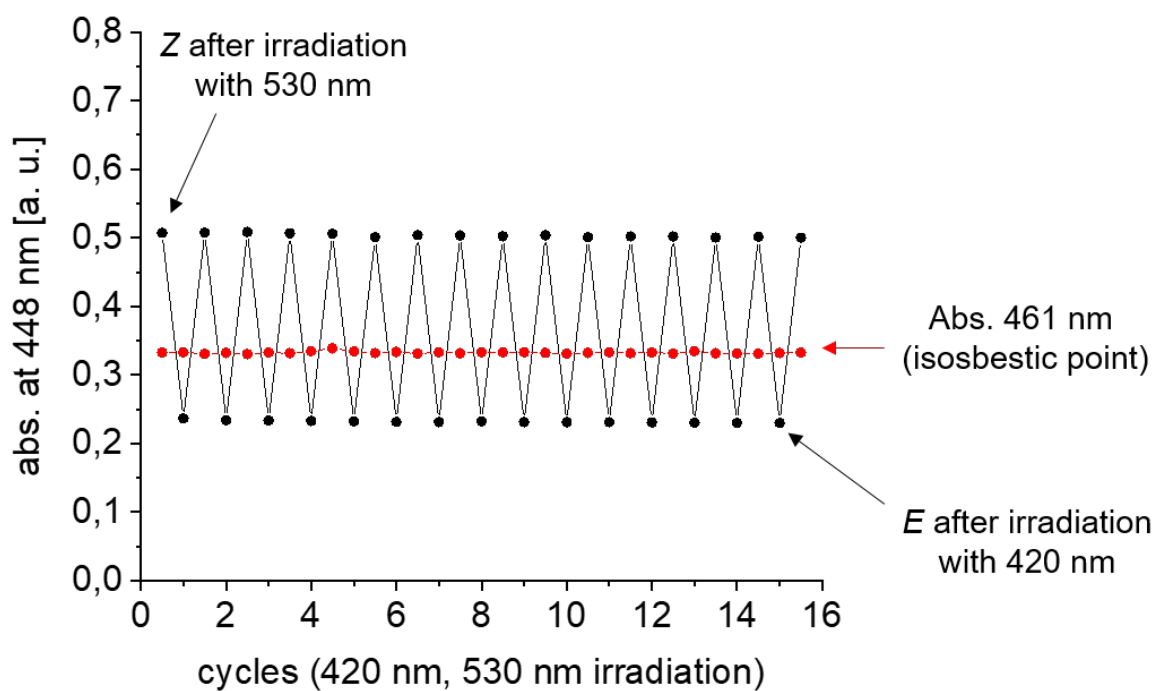
Figure S 4: Photochemical stability measurement of compound **1** in acetonitrile. The *Z* isomer was enriched at 530 nm and the *E* isomer at 420 nm. The absorbance at 448 nm and 461 nm (isosbestic point) were compared for each cycle.
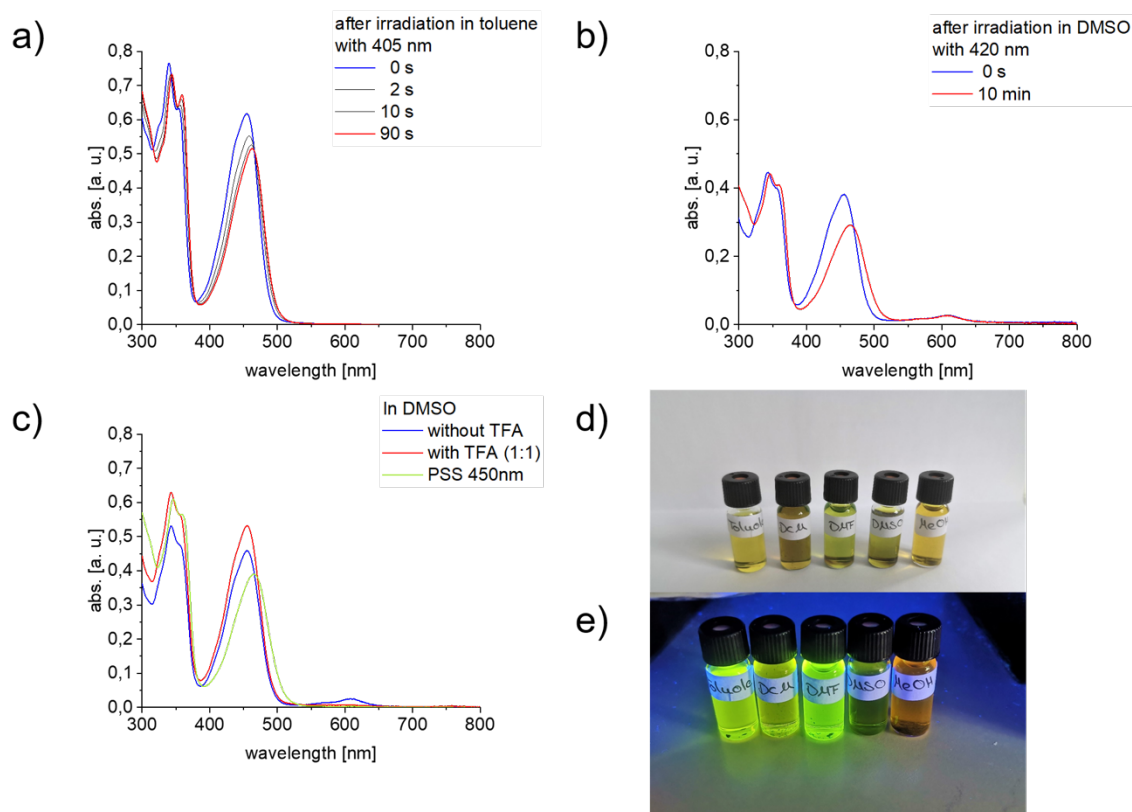
Figure S 5: a) UV/Vis absorption spectra of pure *Z* (blue line) and a mixture of *Z* and *E* isomer (red line) of compound **2** measured in toluene at 23 °C after irradiation with 405 nm; b) UV/Vis absorption spectra of pure *Z* (blue line) and a mixture of *Z* and *E* isomer (red line) measured in DMSO at 23 °C after irradiation with 420 nm; c) UV/Vis absorption spectra of pure *Z* (blue and red line) and a mixture of *Z* and *E* isomer (green line) measured in DMSO at 23 °C after protonation with TFA (1:1) and irradiation with 450 nm; d) Compound **2** dissolved in different solvents (from left to right: toluene, CH_2Cl_2, DMF, DMSO, methanol); e) Compound **2** dissolved in different solvents and irradiated with 366 nm (from left to right: toluene, CH_2Cl_2, DMF, DMSO, methanol).
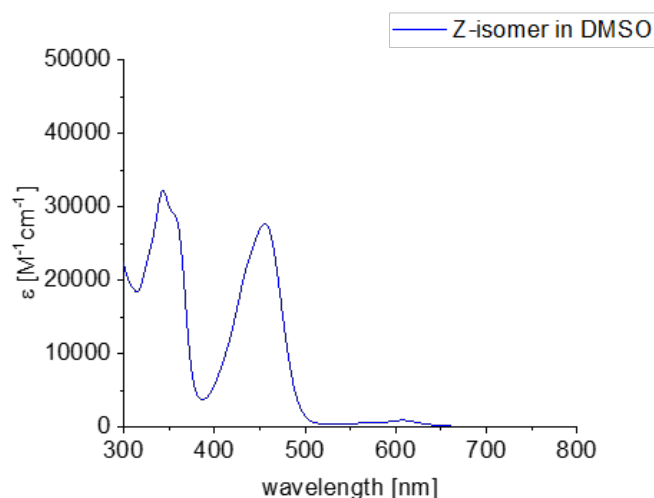
Figure S 6: Molar extinction coefficients of pure *Z* isomer of compound **2** in DMSO.
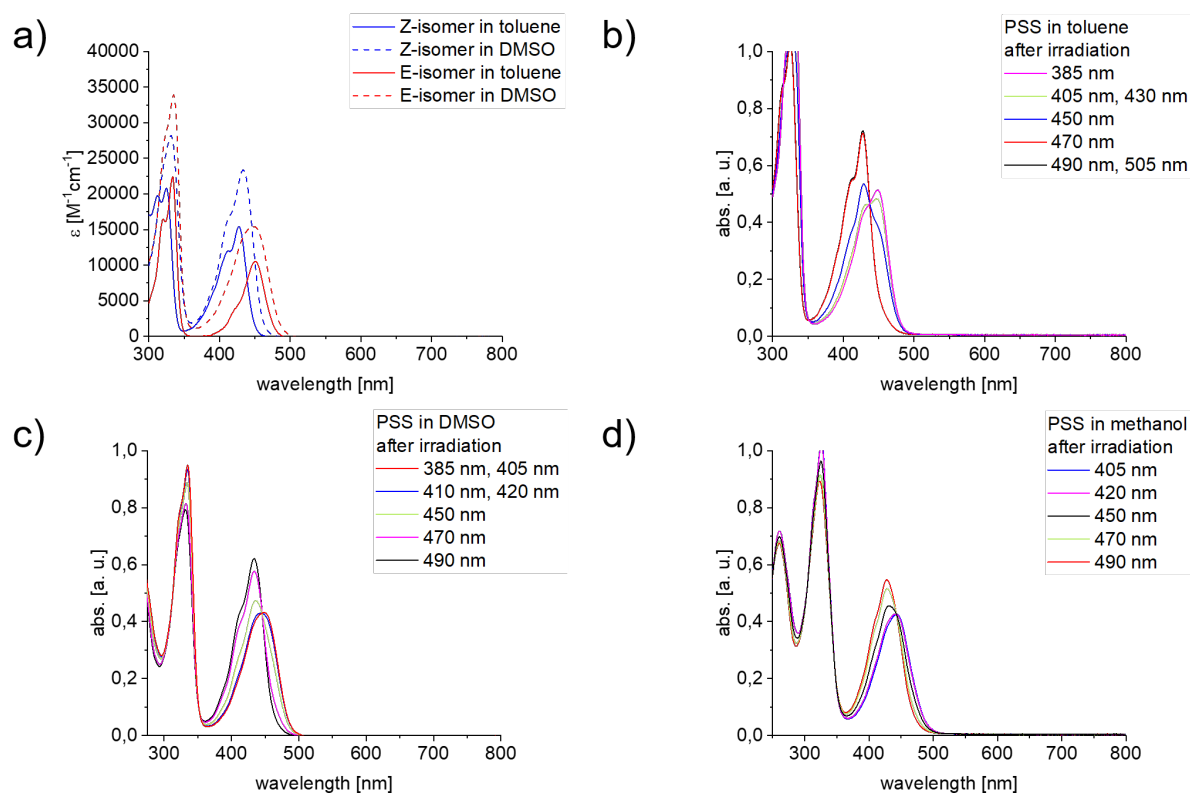
Figure S 7: a) Molar extinction coefficients of pure *Z* (blue) and *E* (red) isomer of compound **3** in toluene (solid line) and DMSO (dashed line); b) UV/Vis absorption spectra of *Z* and *E* isomer measured in benzene at 23 °C after irradiation with various wavelengths; c) UV/Vis absorption spectra of *Z* and *E* isomer measured in acetonitrile at 23 °C after irradiation with various wavelengths; d) UV/Vis absorption spectra of *Z* and *E* isomer measured in methanol at 23 °C after irradiation with various wavelengths.
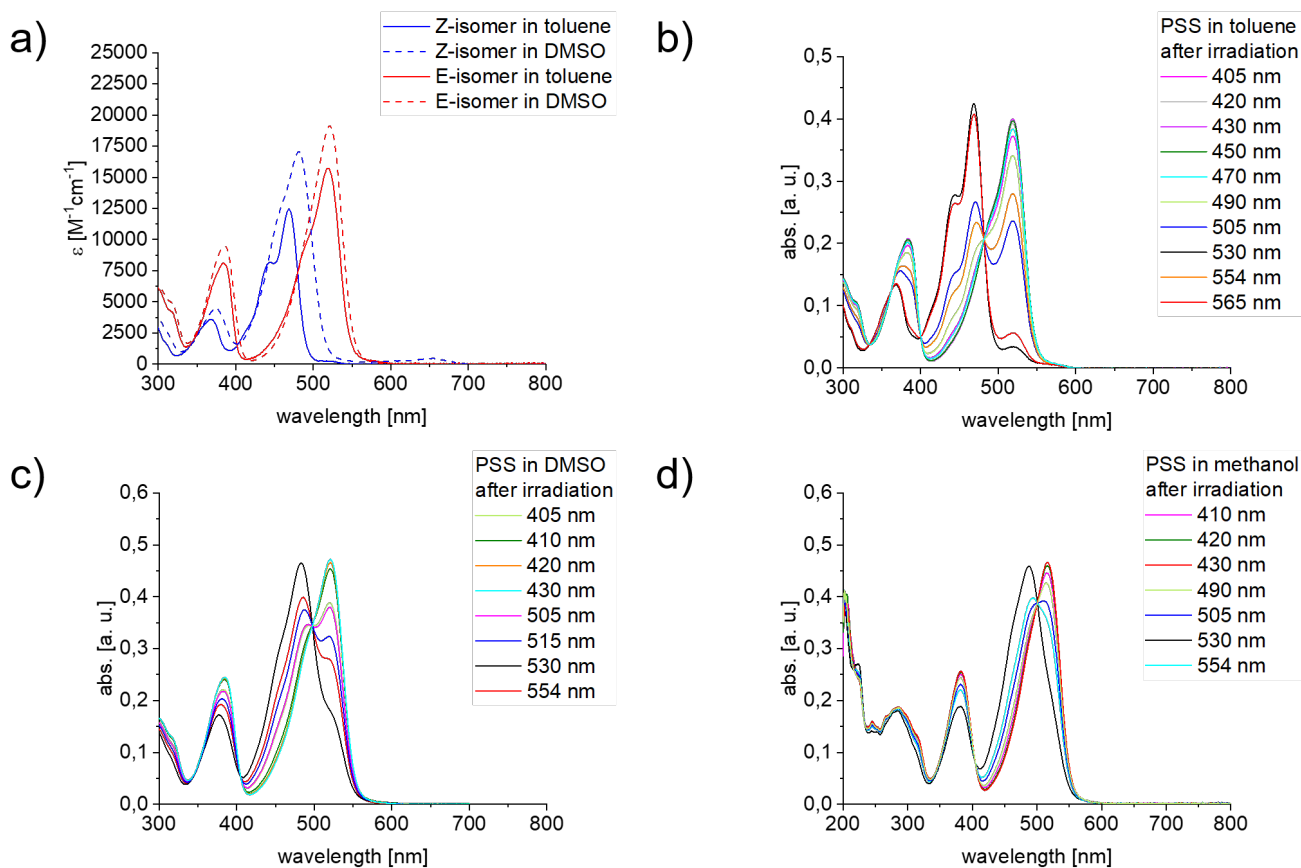
Figure S 8: a) Molar extinction coefficients of pure *Z* (blue) and *E* (red) isomer of compound **4** in toluene (solid line) and DMSO (dashed line); b) UV/Vis absorption spectra of *Z* and *E* isomer measured in toluene at 23 °C after irradiation with various wavelengths; c) UV/Vis absorption spectra of *Z* and *E* isomer measured in DMSO at 23 °C after irradiation with various wavelengths; d) UV/Vis absorption spectra of *Z* and *E* isomer measured in methanol at 23 °C after irradiation with various wavelengths.
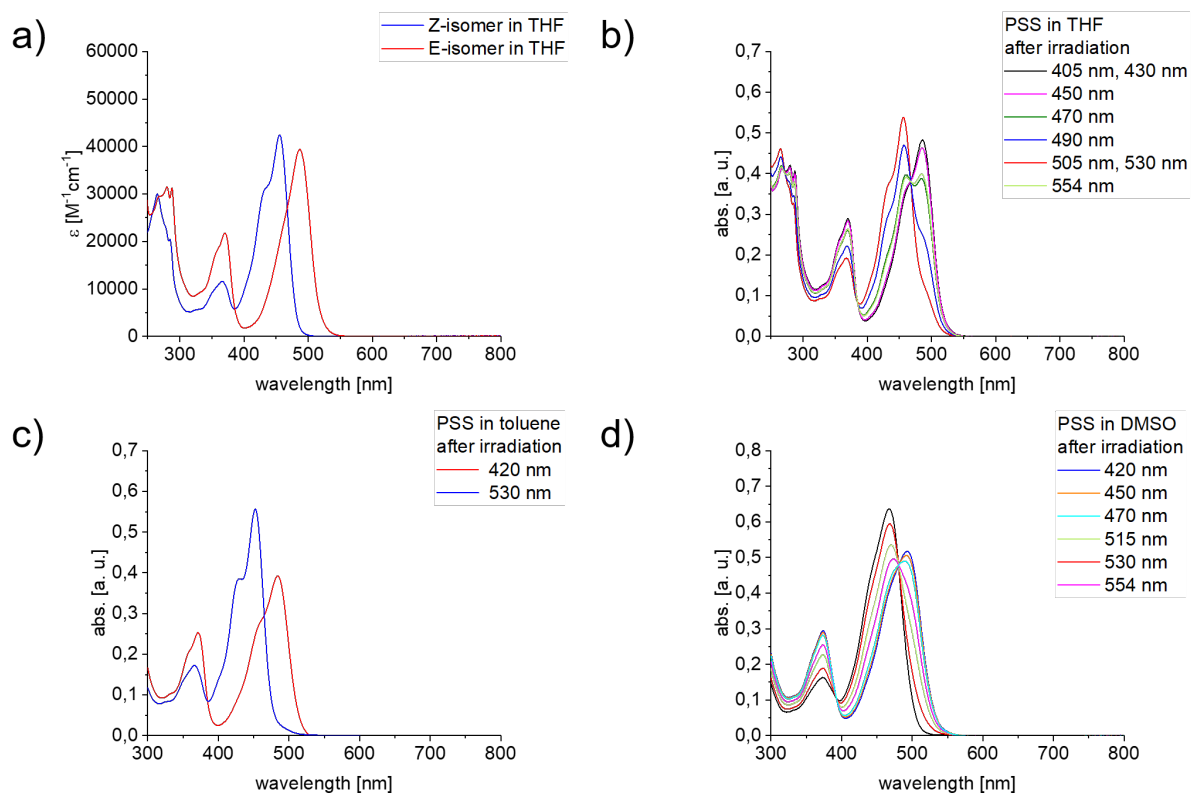
Figure S 9: a) Molar extinction coefficients of pure *Z* (blue) and *E* (red) isomer of compound **5** in THF; b) UV/Vis absorption spectra of *Z* and *E* isomer measured in THF at 23 °C after irradiation with various wavelengths; c) UV/Vis absorption spectra of *Z* and *E* isomer measured in toluene at 23 °C after irradiation with various wavelengths; d) UV/Vis absorption spectra of *Z* and *E* isomer measured in DMSO at 23 °C after irradiation with various wavelengths.
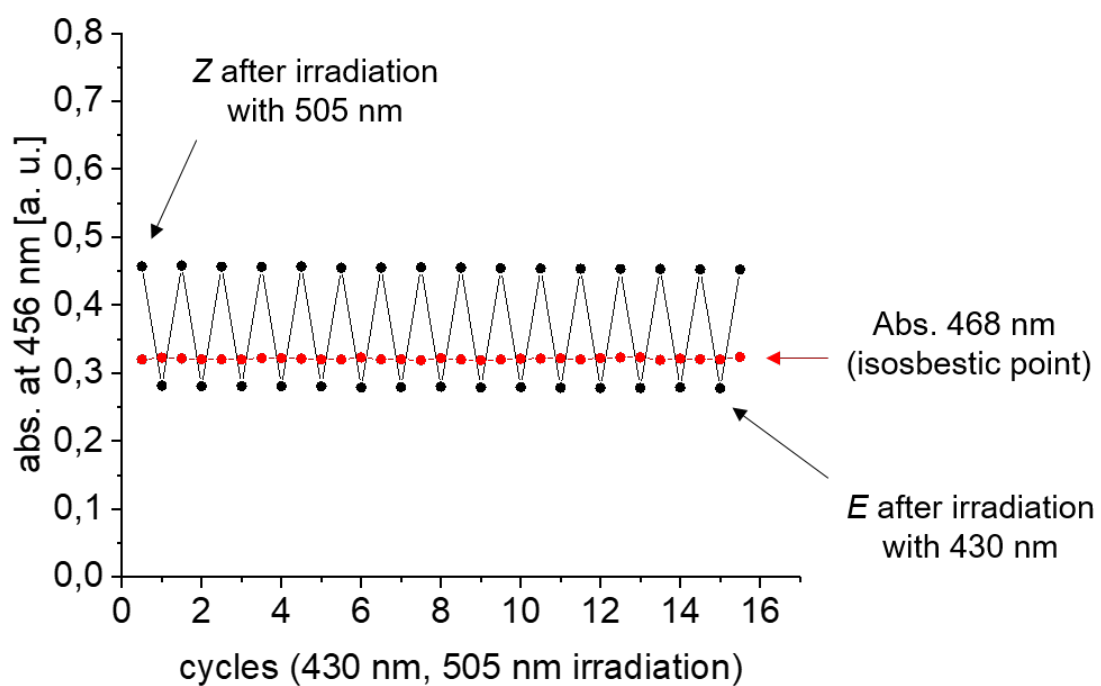
Figure S 10: The photochemical stability analysis of compound **5** in tetrahydrofuran. The *Z* isomer was enriched by irradiating at 505 nm and the *E* isomer by irradiating at 430 nm. The absorbance at 456 nm and 468 nm (isosbestic point) were compared for each cycle.
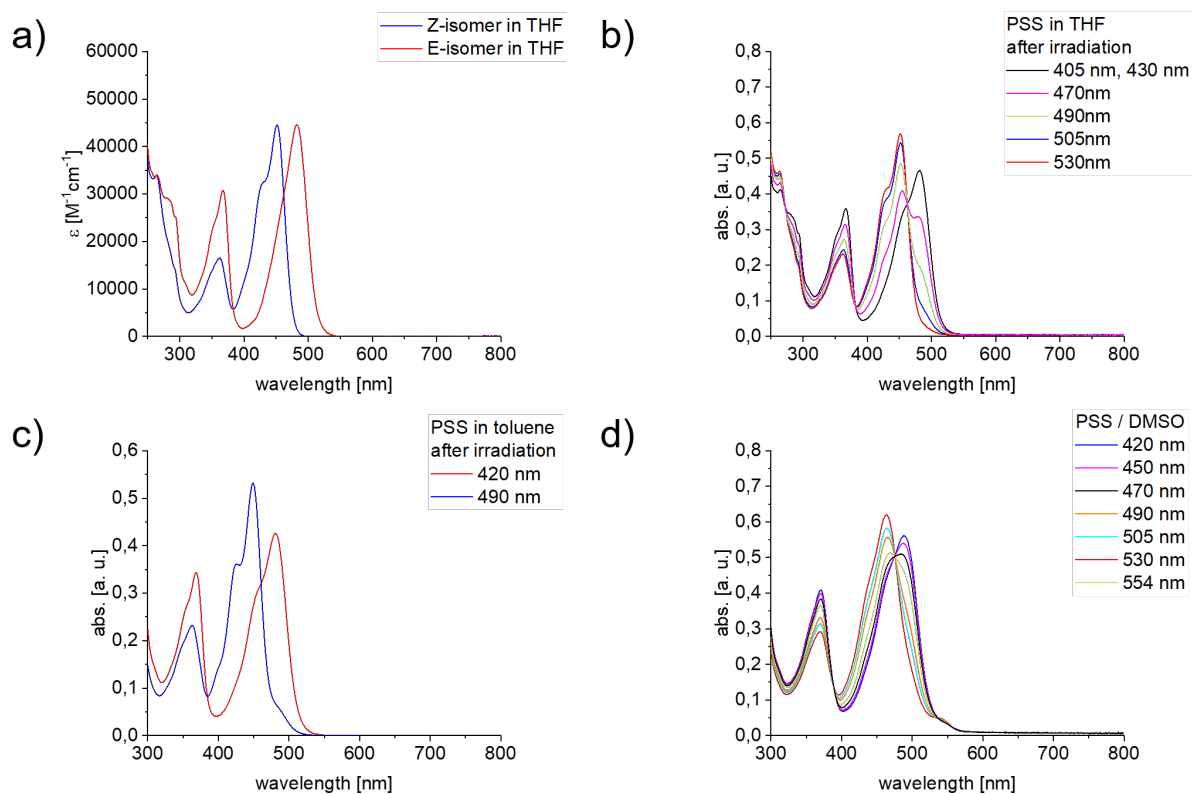
Figure S 11: a) Molar extinction coefficients of pure *Z* (blue) and *E* (red) isomer of compound **6** in THF; b) UV/Vis absorption spectra of *Z* and *E* isomer measured in THF at 23 °C after irradiation with various wavelengths; c) UV/Vis absorption spectra of *Z* and *E* isomer measured in toluene at 23 °C after irradiation with various wavelengths; d) UV/Vis absorption spectra of *Z* and *E* isomer measured in DMSO at 23 °C after irradiation with various wavelengths.
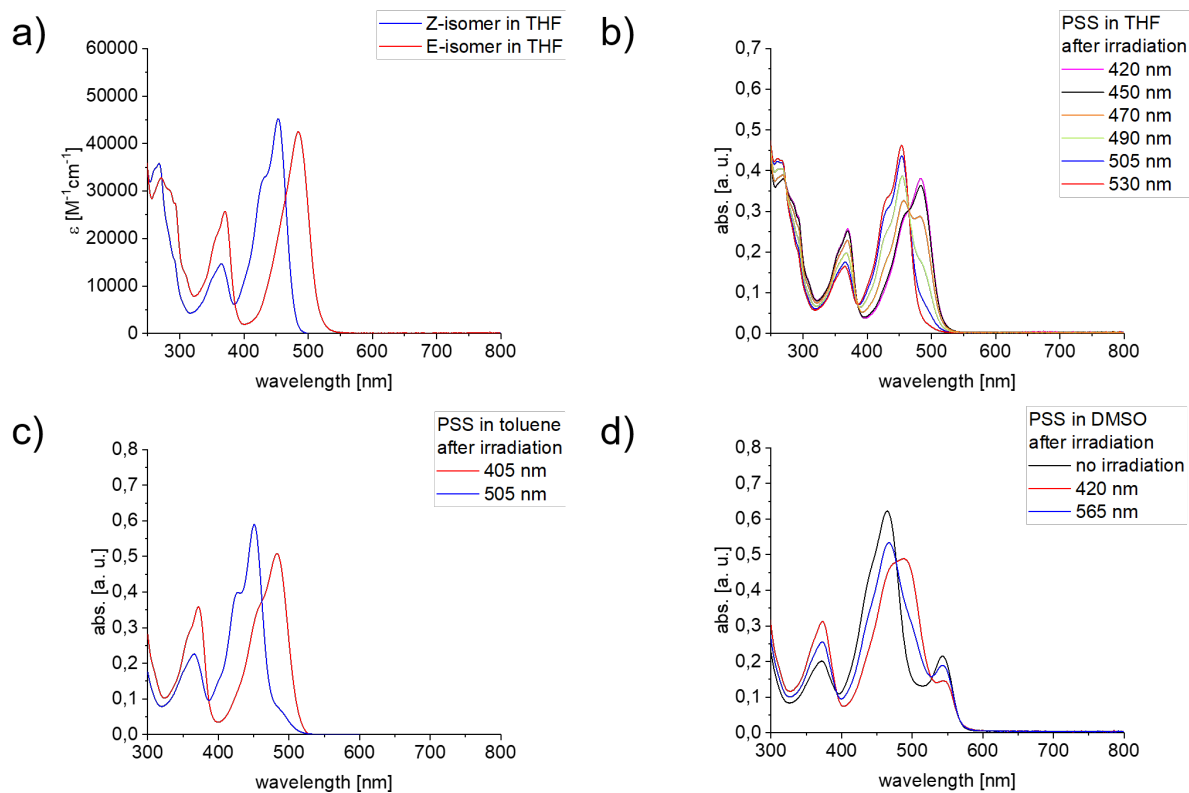
Figure S 12: a) Molar extinction coefficients of pure *Z* (blue) and *E* (red) isomer of compound **7** in THF; b) UV/Vis absorption spectra of *Z* and *E* isomer measured in THF at 23 °C after irradiation with various wavelengths; c) UV/Vis absorption spectra of *Z* and *E* isomer measured in toluene at 23 °C after irradiation with various wavelengths; d) UV/Vis absorption spectra of *Z* and *E* isomer measured in DMSO at 23 °C after irradiation with various wavelengths.
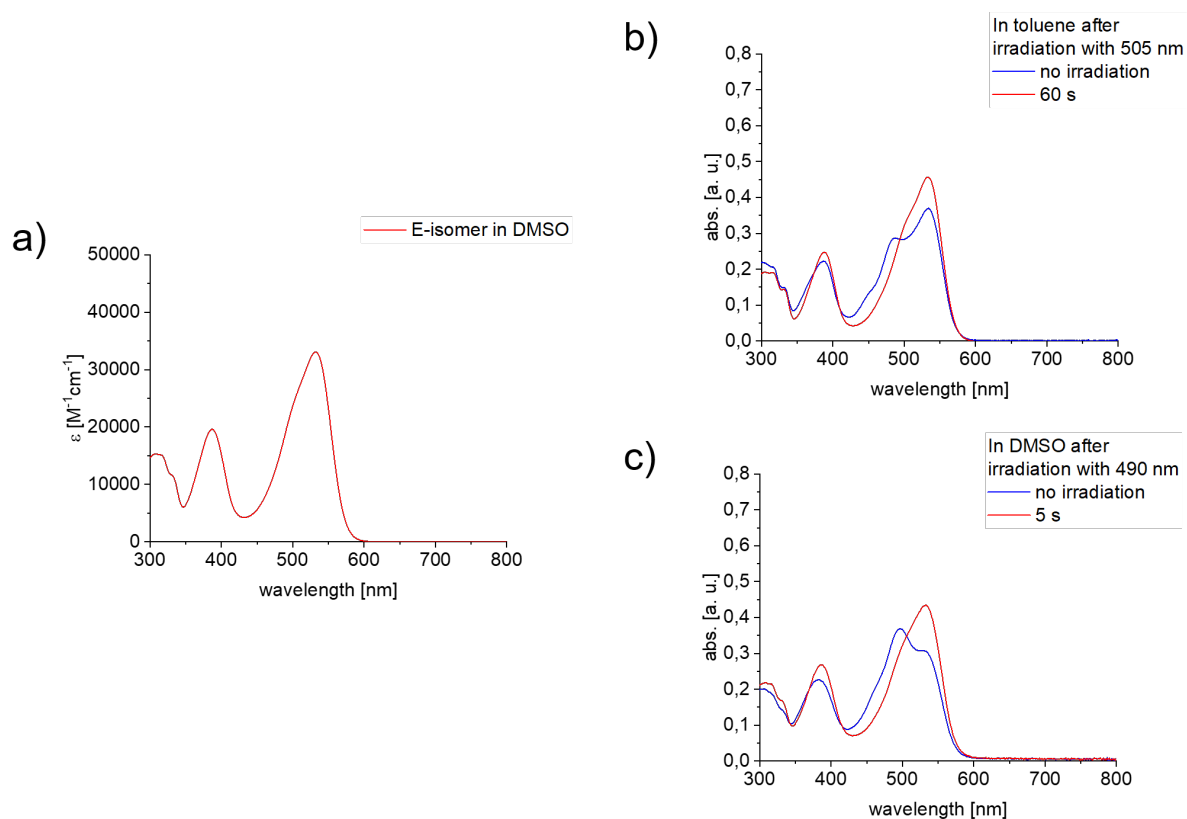
Figure S 13: a) a) Molar extinction coefficients of pure *E* isomer (red) isomer of compound **8** in DMSO; b), UV/Vis absorption spectra of compound **8** in toluene at 23 °C. After dissolving the solid material, a small amount of *Z* isomer is observed (blue spectra), which is converted fully to the E isomer after irradiation with 505 nm; c) UV/Vis absorption spectra of compound **8** in DMSO at 23 °C. After dissolving the solid material, a small amount of *Z* isomer is observed (blue spectra), which is converted fully to the *E* isomer after irradiation with 490 nm. Only one-way switching to the *E* isomer is possible but no *E* to *Z* photoisomerization can be observed.
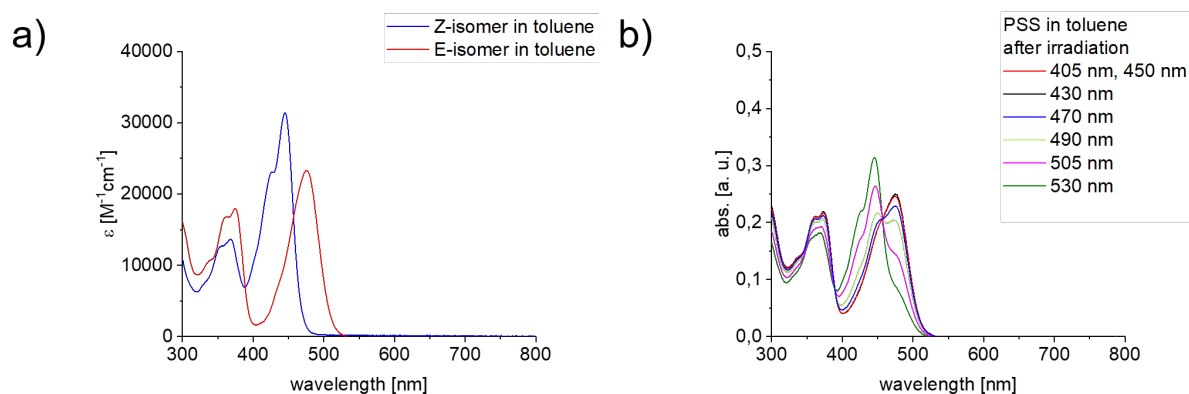
Figure S 14: a) Molar extinction coefficients of pure *Z* (blue) and *E* (red) isomer of compound **9** in toluene; b) UV/Vis absorption spectra of *Z* and *E* isomer measured in toluene at 23 °C after irradiation with various wavelengths.

Figure S 15: To investigate the photochemical stability of compound **9** in toluene, the *Z* isomer was enriched at 490 nm and the *E* isomer at 450 nm. The absorbance at 447 nm and 457 nm (isosbestic point) were compared for each cycle.

Figure S 16: a) Molar extinction coefficients of pure *Z* (blue) and *E* (red) isomer of compound **10** in toluene (solid line) and acetonitrile (dashed line); b) UV/Vis absorption spectra of *Z* and *E* isomer measured in toluene at 23 °C after irradiation with various wavelengths; c) UV/Vis absorption spectra of *Z* and *E* isomer measured acetonitrile in at 23 °C after irradiation with various wavelengths.

Figure S 17: a) Molar extinction coefficients of pure *Z* (blue) and *E* (red) isomer of compound **11** in toluene; b) UV/Vis absorption spectra of *Z* and *E* isomer measured in toluene at 23 °C after irradiation with various wavelengths.
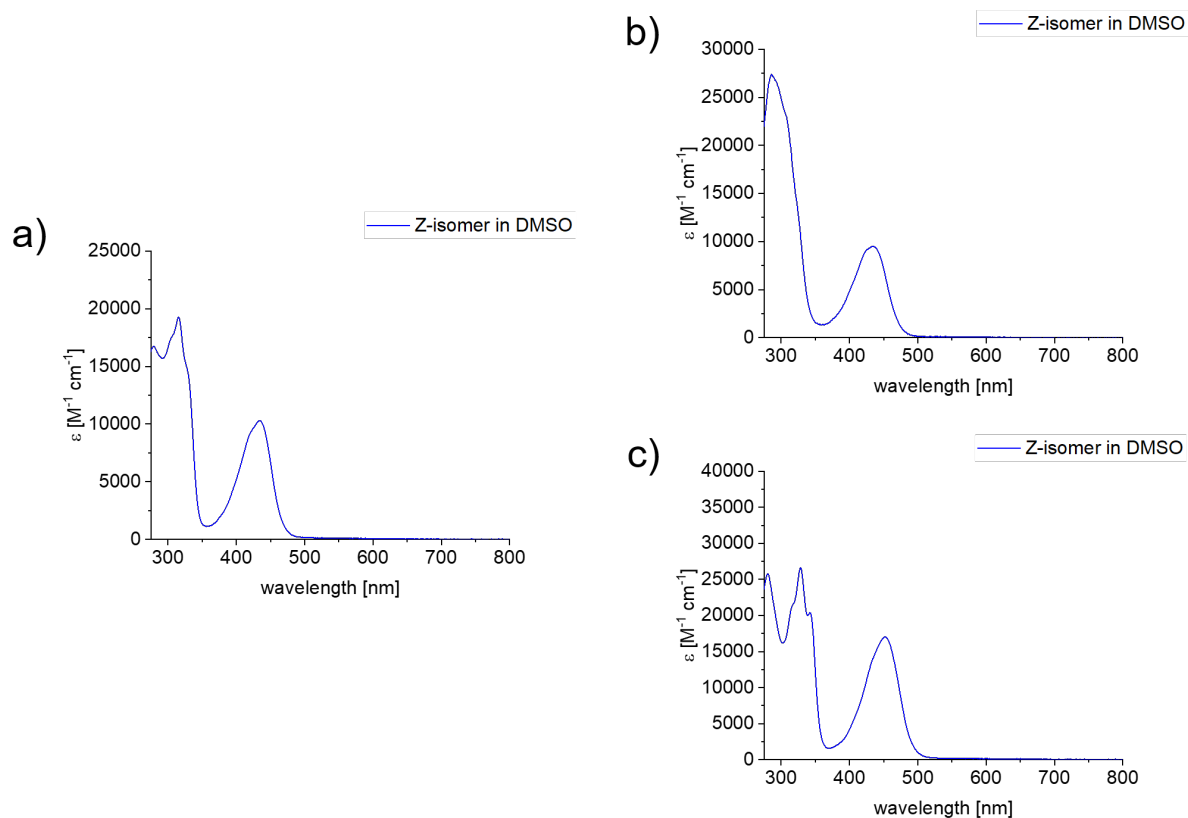
Figure S 18: a) Molar extinction coefficients of pure *Z* isomer of compound **12** in DMSO; b) Molar extinction coefficients of pure *Z* isomer of compound **13** in DMSO; c) Molar extinction coefficients of pure *Z* isomer of compound **14** in DMSO.
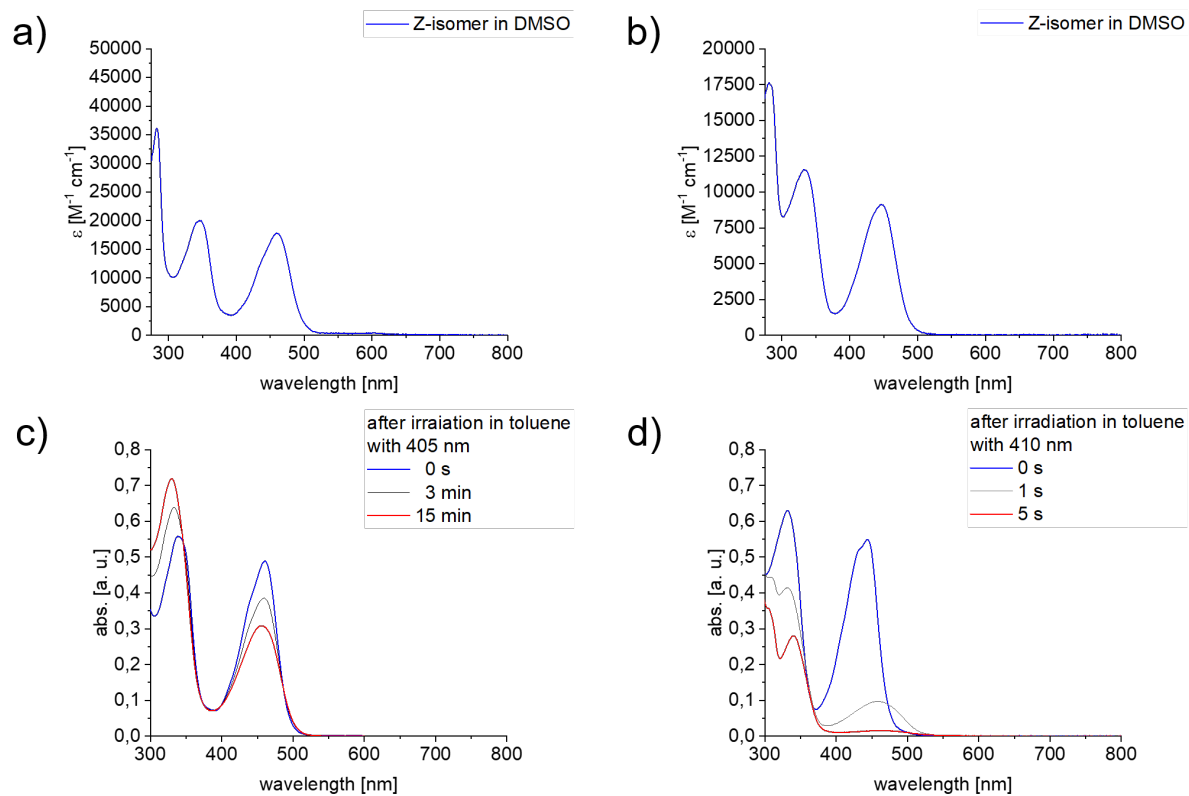
Figure S 19: a) Molar extinction coefficients of pure *Z* (blue) isomer of compound **15** in DMSO; b) Molar extinction coefficients of pure *Z* (blue) isomer of compound **16** in DMSO; c) UV/Vis absorption spectra of **15** in benzene at 23 °C. Irradiation with 405 nm results in the decomposition of the molecule; d) UV/Vis absorption spectra of 1**6** in benzene at 23 °C. Irradiation with 410 nm results in the decomposition of the molecule.

NMR Irradiation Experiments

The isomer ratio of the enriched *E/Z* isomers was ascertained by ^{1}H NMR experiments. Compounds **1**, **3-7** and **9-10**, **12-16** ($1.95 \odot 10^{-3} - 8.25 \odot 10^{-3}$ mol/L) were dissolved in deuterated solvents (toluene-d_8, DMSO-d_6, benzene-d_6, acetonitrile-d_3, methanol-d_4 or THF-d_8) and transferred to an NMR tube. The NMR sample was irradiated with different wavelengths for defined time intervals and ^{1}H NMR spectra were collected. The pss was accomplished if the isomer ratio remained unchanged. A suitable signal of each *E* and *Z* isomer was selected and integrated. One signal integral was set to 1 and the other signal can thus be described as integral *i*. The isomer ratio was then calculated as follows:

$$\frac{I_1}{I_2} = \frac{1}{1+i} \qquad\qquad\text{(eq.8)}$$

with I_1 and I_2 as isomer 1 and isomer 2.
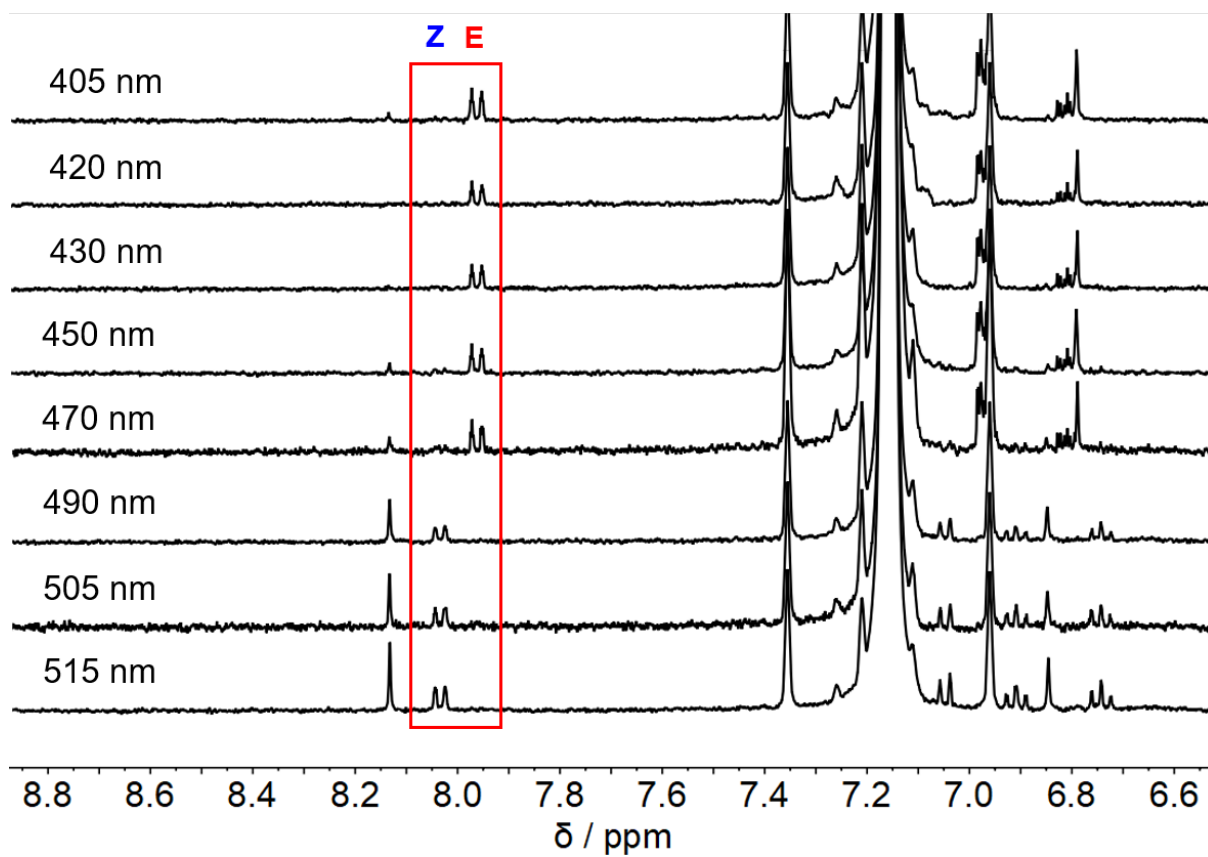
Figure S 20: Extracts from ^{1}H-NMR spectra of compound **1** (400 MHz, benzene-d_6, 26 °C) showing enriched *E* and *Z* isomer after irradiation with 405 nm, 420 nm, 430 nm, 450 nm, 470 nm, 490 nm, 505 nm, and 515 nm light. The signal of proton 1 was selected to determine the isomeric ratio.
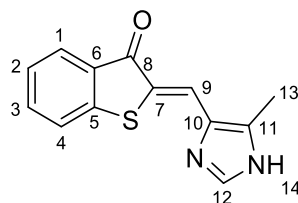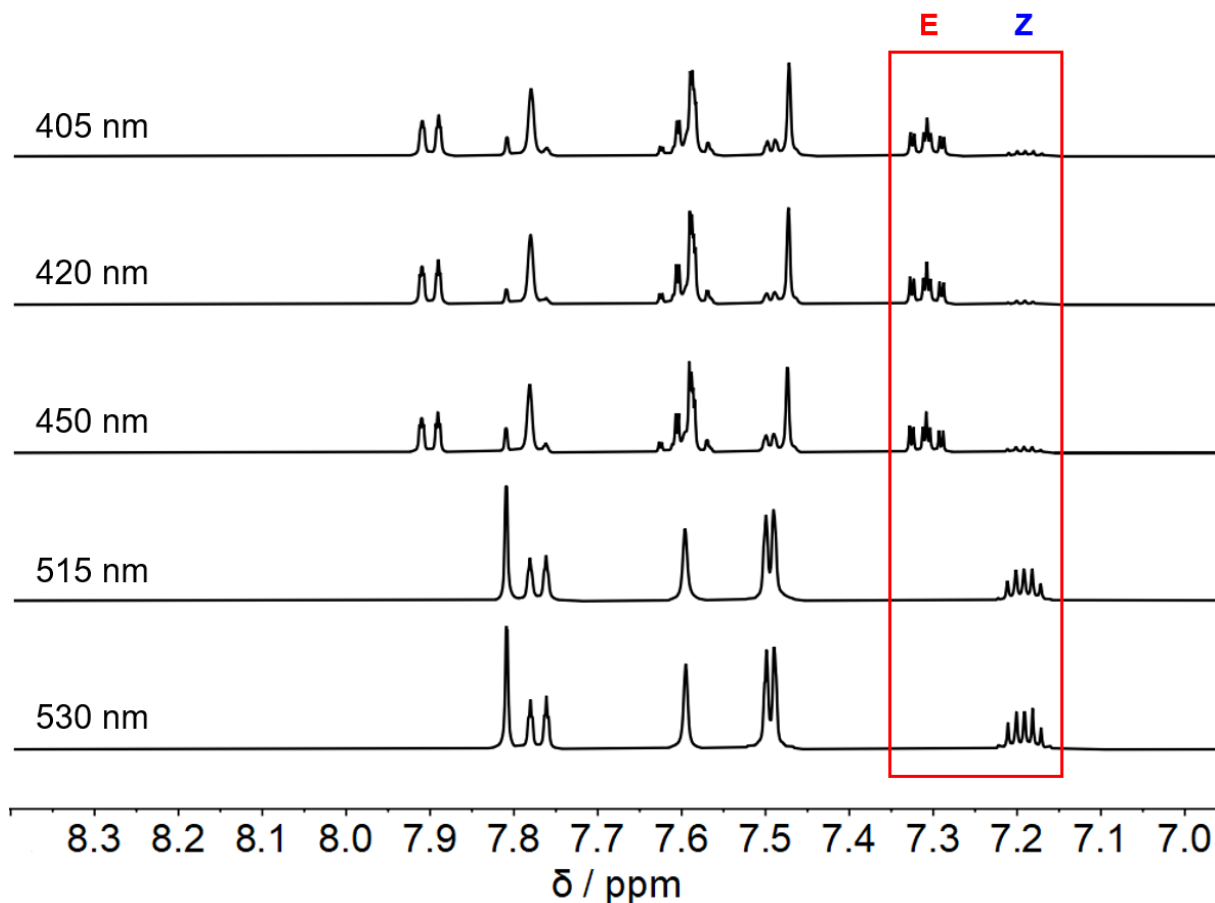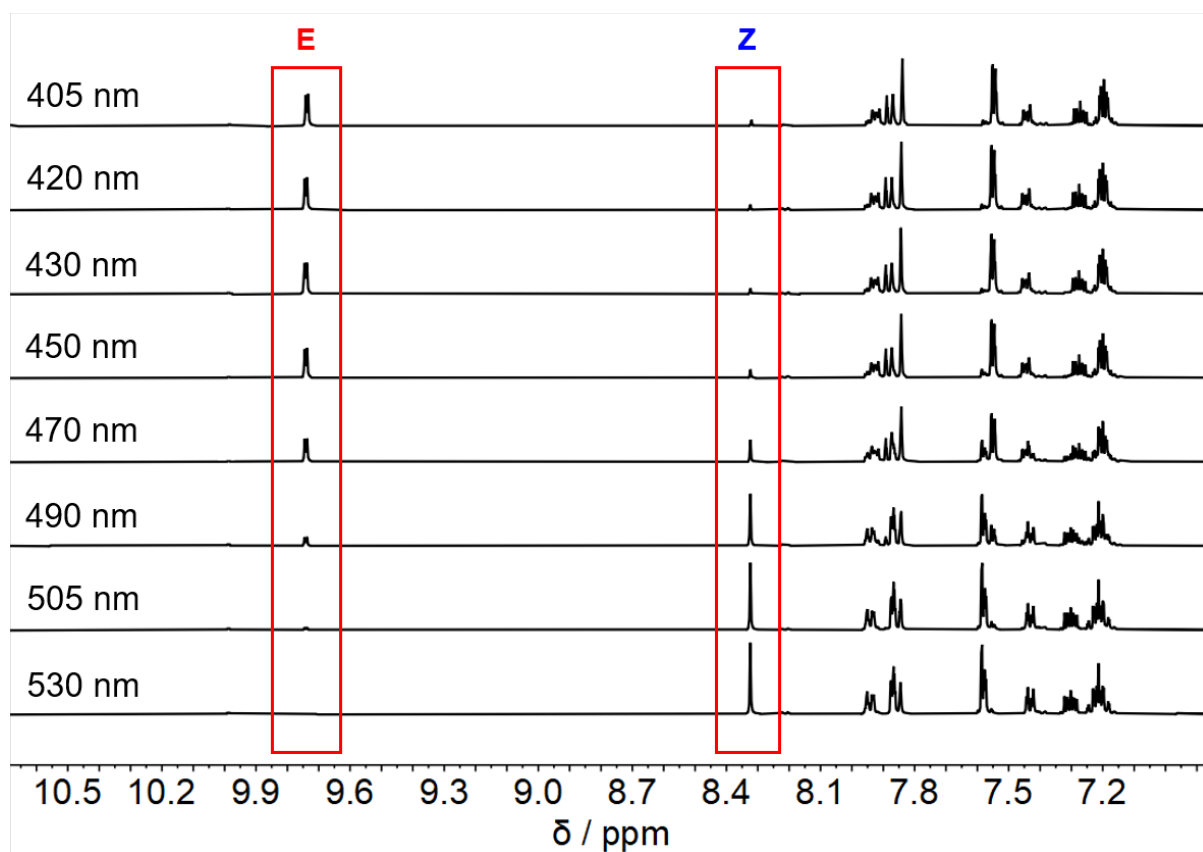
Figure S 21: Extracts from ^{1}H-NMR spectra of compound **1** (400 MHz, tetrahydrofuran-d_8, 26 °C) showing enriched *E* and *Z* isomer after irradiation with 405 nm, 430 nm, 450 nm, 515 nm, and 530 nm light. The signal of proton 2 was selected to determine the isomeric ratio.
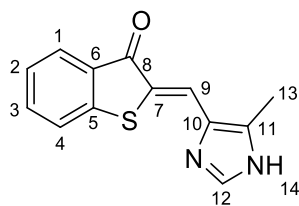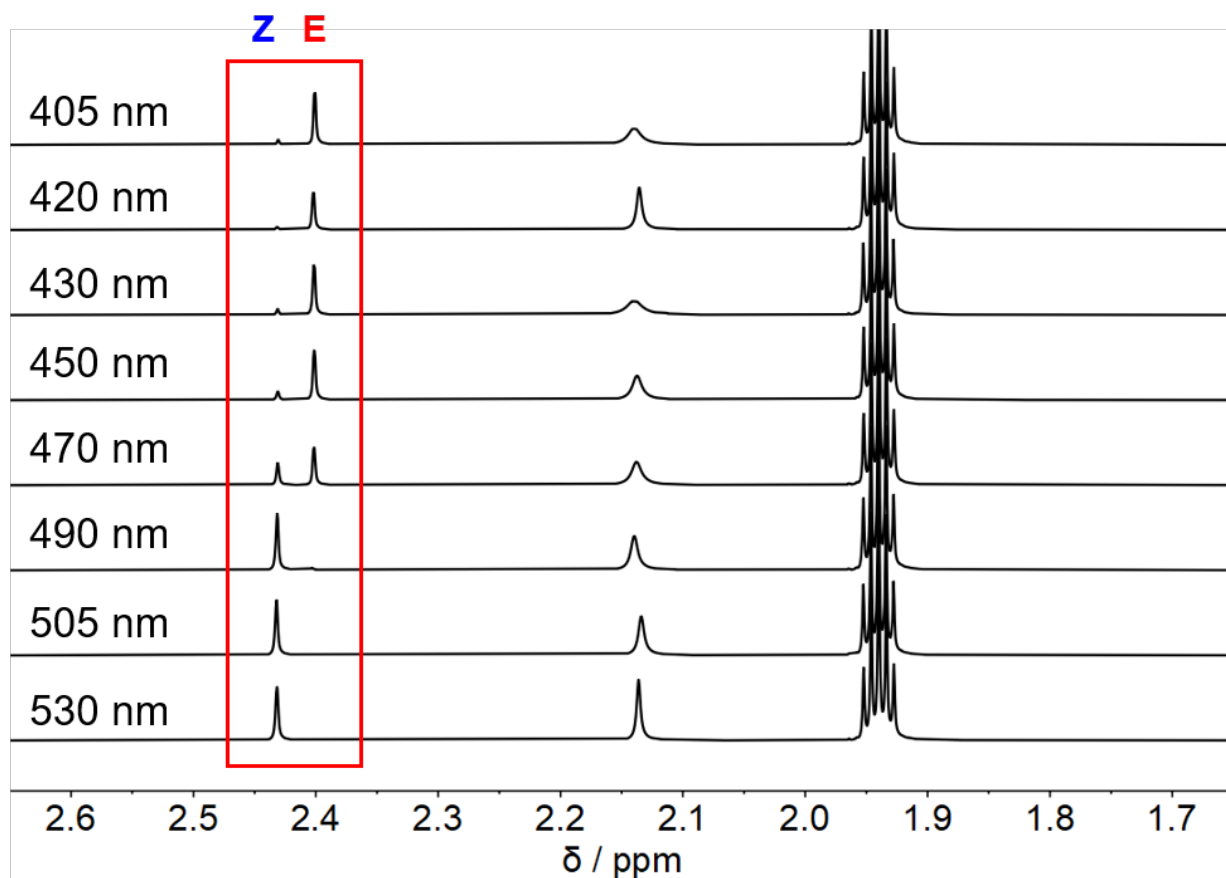
Figure S 22: Extracts from ^{1}H-NMR spectra of compound **1** (400 MHz, acetonitrile-d_3, 26 °C) showing enriched *E* and *Z* isomer after irradiation with 405 nm, 420 nm, 430 nm, 450 nm, 470 nm, 490 nm, 505 nm, and 530 nm light. The signal of proton 13 was selected to determine the isomeric ratio.
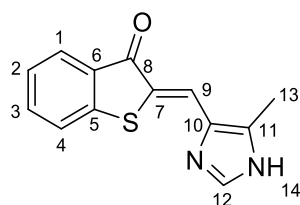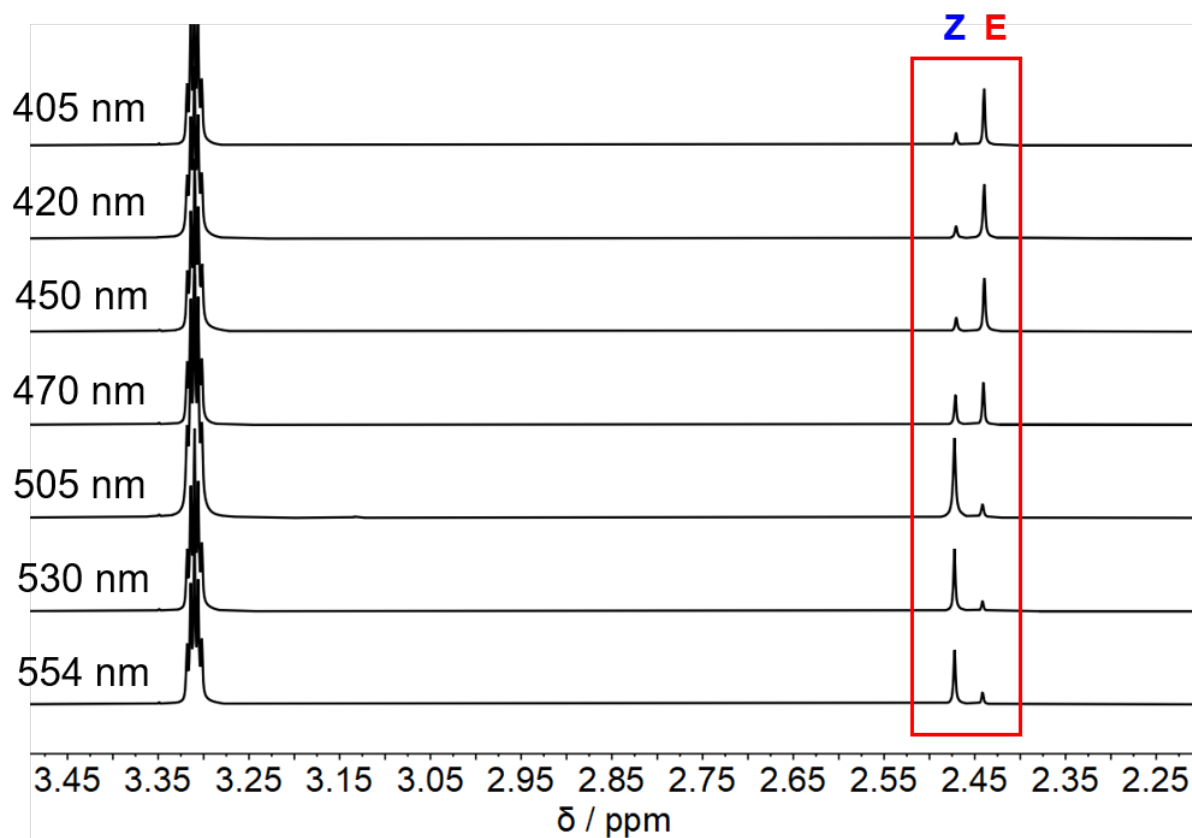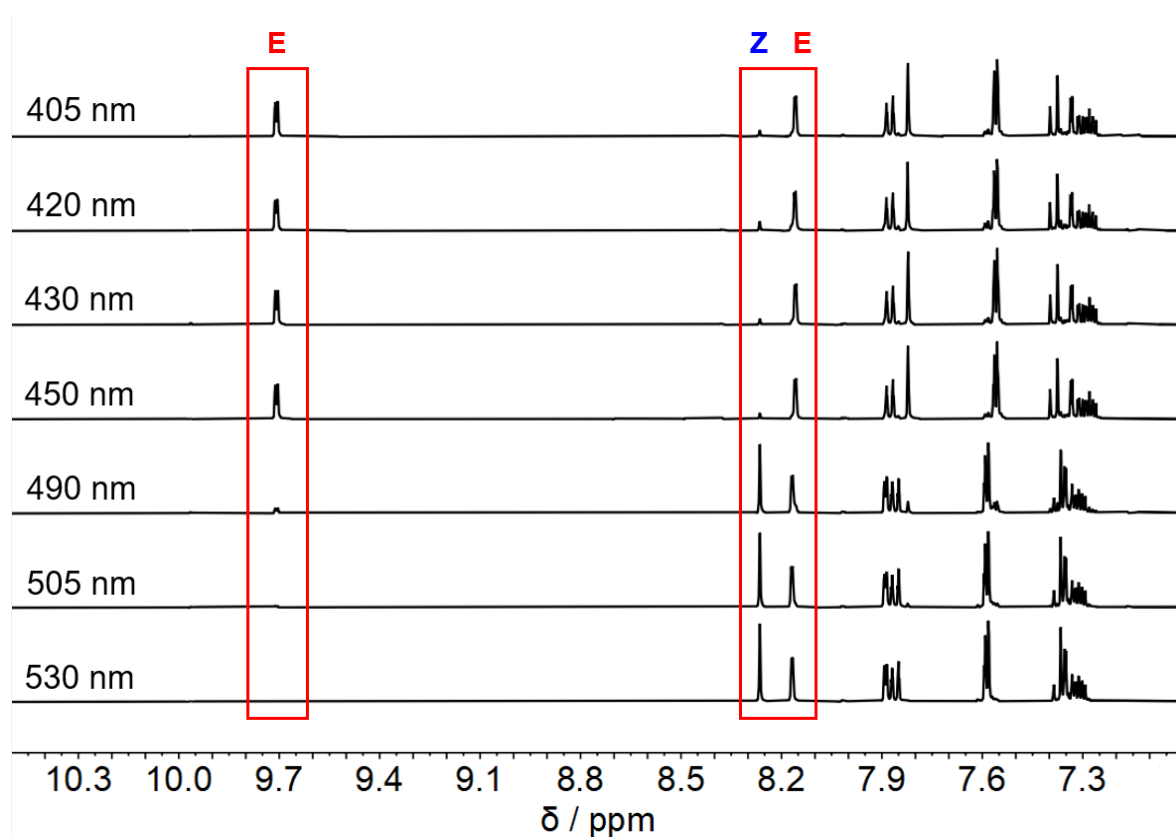
Figure S 23: Extracts from ¹H-NMR spectra of compound **1** (400 MHz, methanol-d_4, 26 °C) showing enriched *E* and *Z* isomer after irradiation with 405 nm, 420 nm, 450 nm, 470 nm, 490 nm, 505 nm, 530 nm, and 554 nm light. The signal of proton 13 was selected to determine the isomeric ratio.
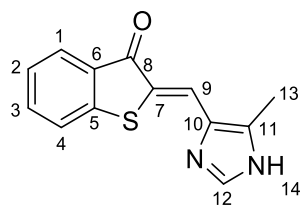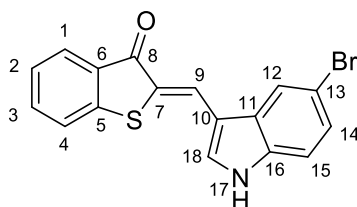
Table S 1: *E*/*Z* isomeric ratios of compound **1** obtained in the pss after irradiation with light of different wavelengths. All values given were determined using ^{1}H NMR spectroscopy at 26 °C.

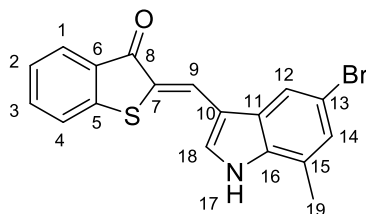| solvent	irr. wavelength [nm]	% Z isomer	% E isomer
benzene-*d$_6$*	405	21	79
	420	0	100
	430	0	100
	450	20	80
	470	31	69
	490	100	0
	505	100	0
	515	100	0
THF-*d$_8$*	405	14	86
	430	9	91
	450	17	83
	515	97	3
	530	100	0
acetonitrile-*d$_3$*	405	7	93
	420	10	90
	430	10	90
	450	14	86
	470	37	63
	490	95	5
	505	97	3
	530	100	0
methanol-*d$_4$*	405	20	80
	420	20	80
	450	19	81
	470	42	58
	505	85	15
	530	83	17
	554	80	20
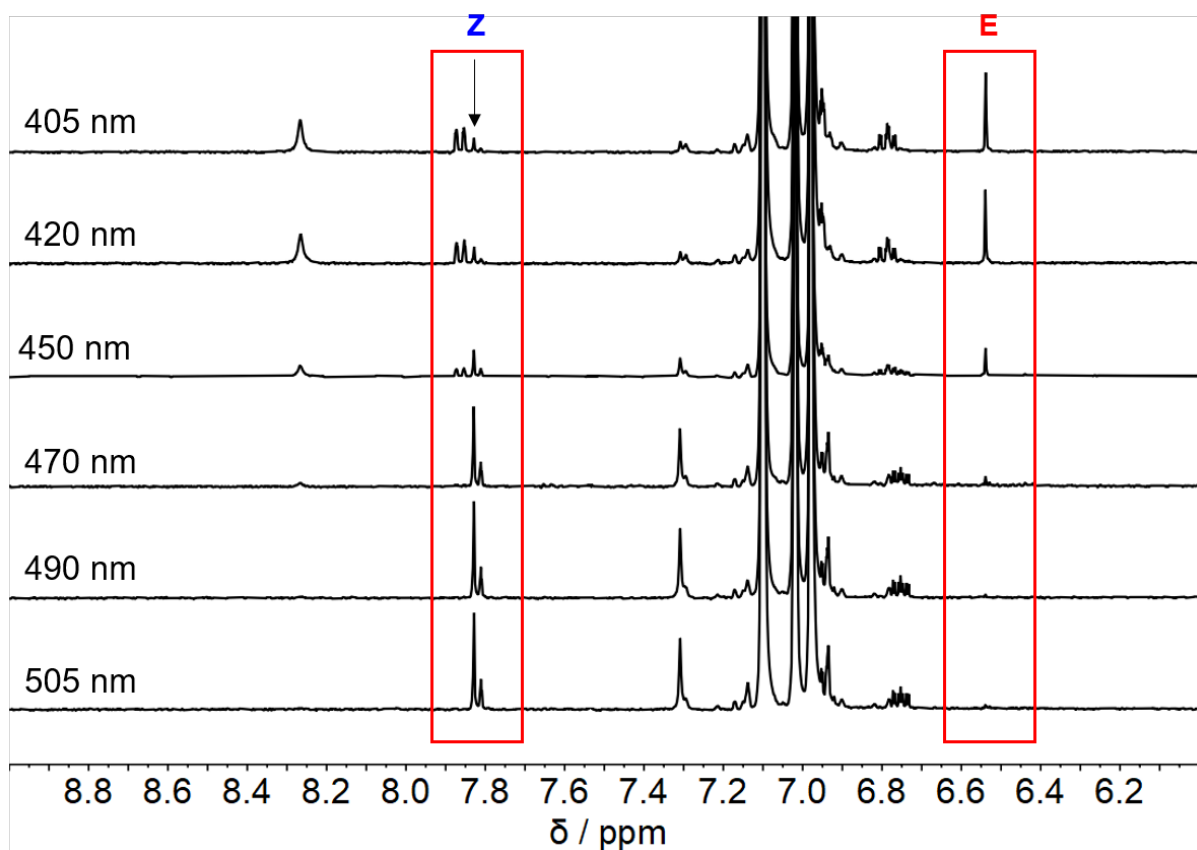
Figure S 24: Extracts from ^{1}H-NMR spectra of compound **3** (400 MHz, toluene-d_8, 26 °C) showing enriched *E* and *Z* isomer after irradiation with 405 nm, 420 nm, 450 nm, 470 nm, 490 nm, and 505 nm light. The signals of protons 1 and 9 were selected to determine the isomeric ratio.
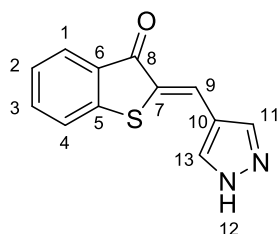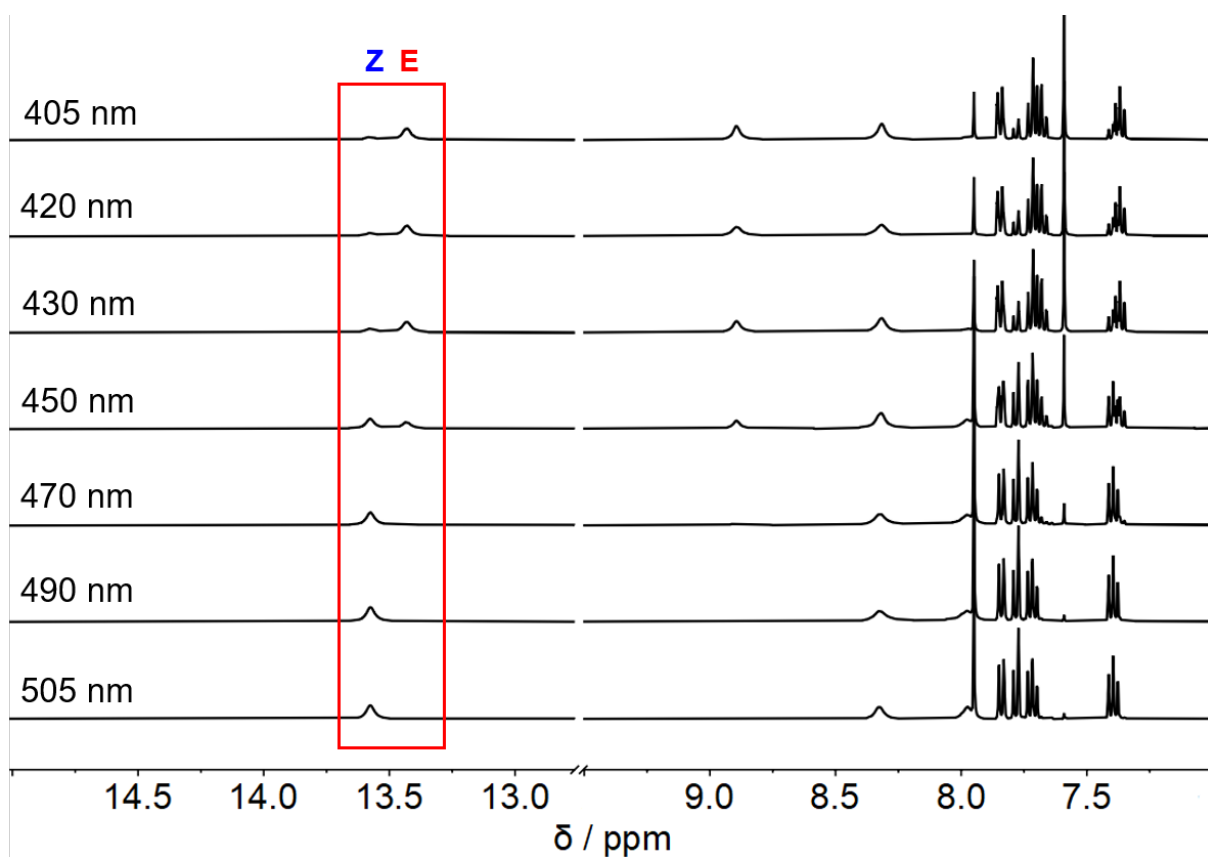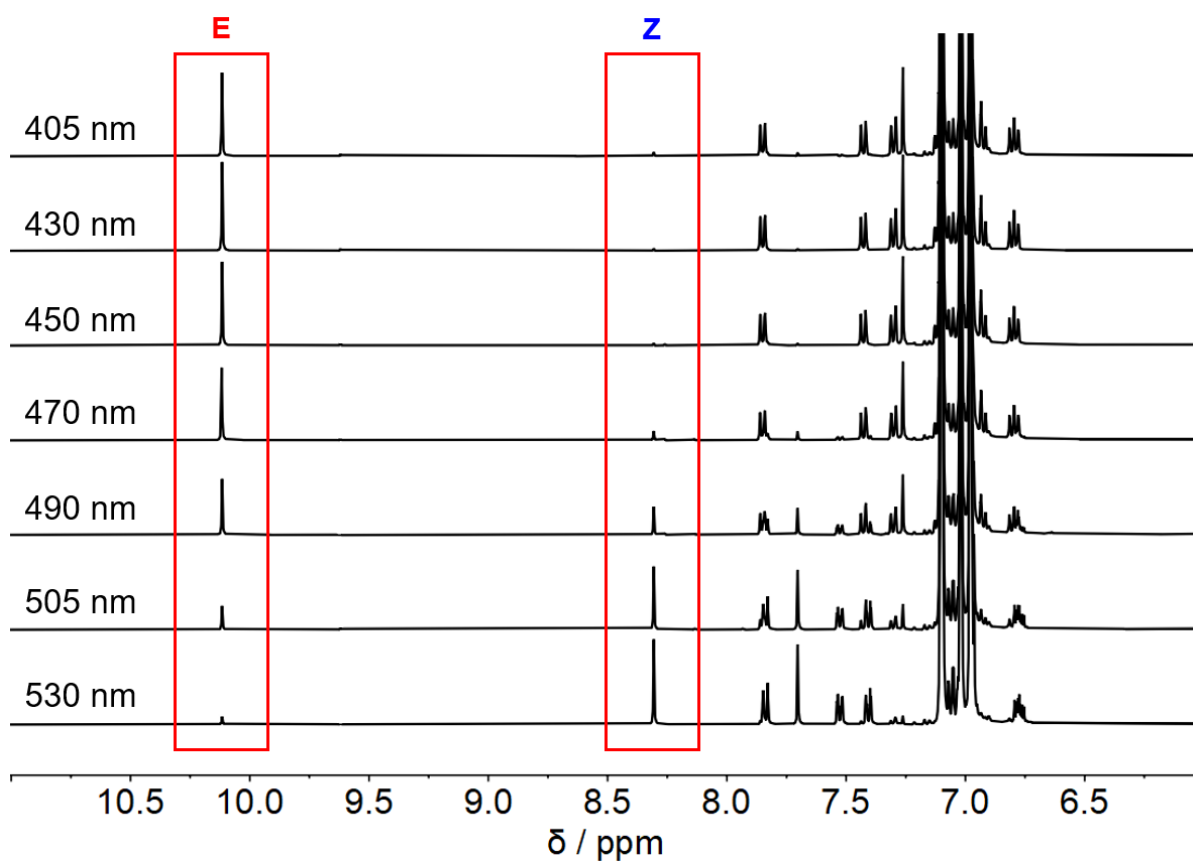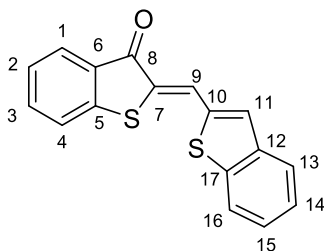
Figure S 25: Extracts from ^{1}H-NMR spectra of compound **3** (400 MHz, DMSO-d_6, 26 °C) showing enriched *E* and *Z* isomer after irradiation with 405 nm, 420 nm, 430 nm, 450 nm, 470 nm, 490 nm, and 505 nm light. The signal of proton 12 was selected to determine the isomeric ratio.
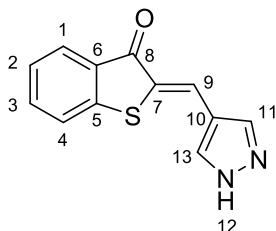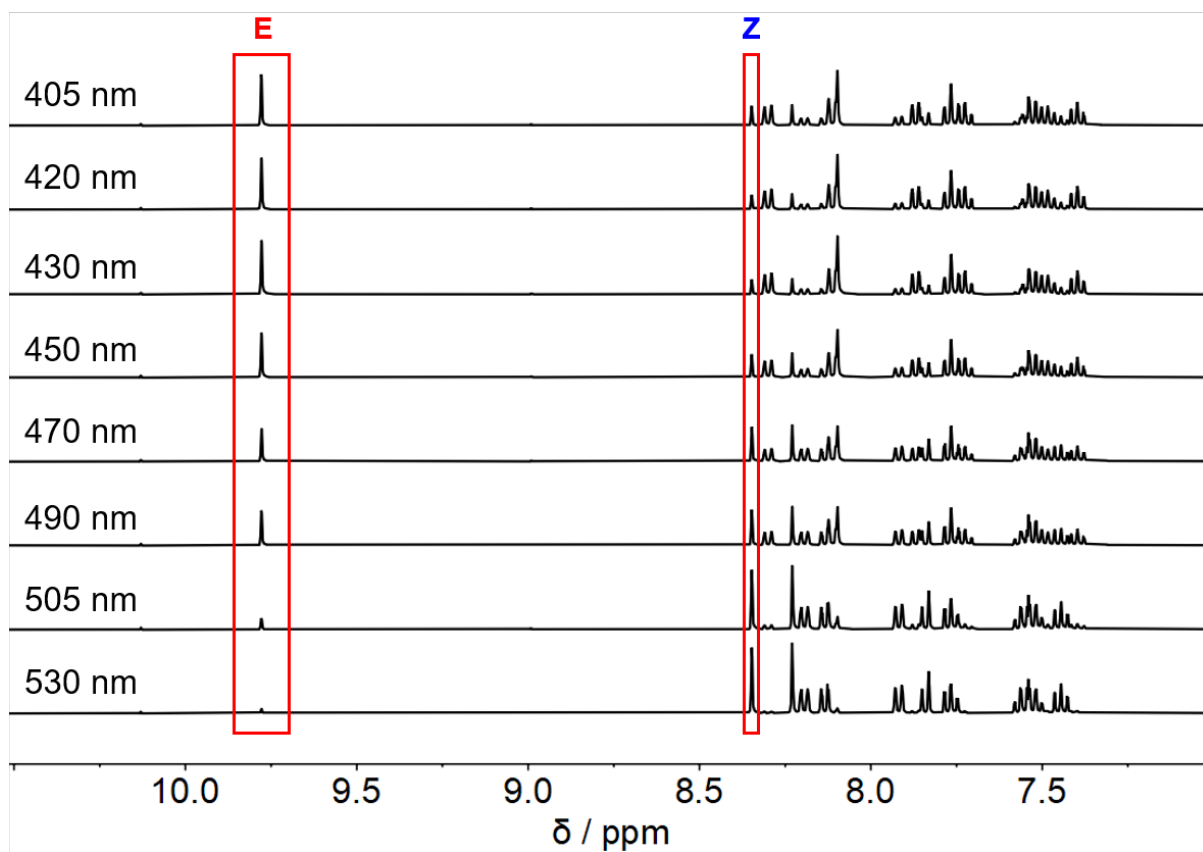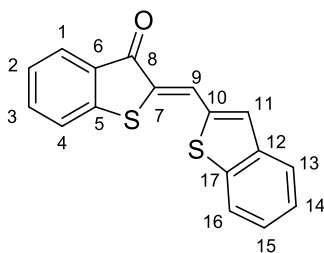
Table S2: *E*/*Z* isomeric ratios of compound **3** obtained in the pss after irradiation with light of different wavelengths. All values given were determined using ^{1}H NMR spectroscopy at 26 °C.

solvent	irr. wavelength [nm]	% Z isomer	% E isomer
toluene-*d$_8$*	405	16	84
	420	24	76
	450	41	59
	470	66	34
	490	82	18
	505	100	0
DMSO-*d$_6$*	405	24	76
	420	29	71
	430	30	70
	450	65	35
	470	89	11
	490	97	3
	505	97	3
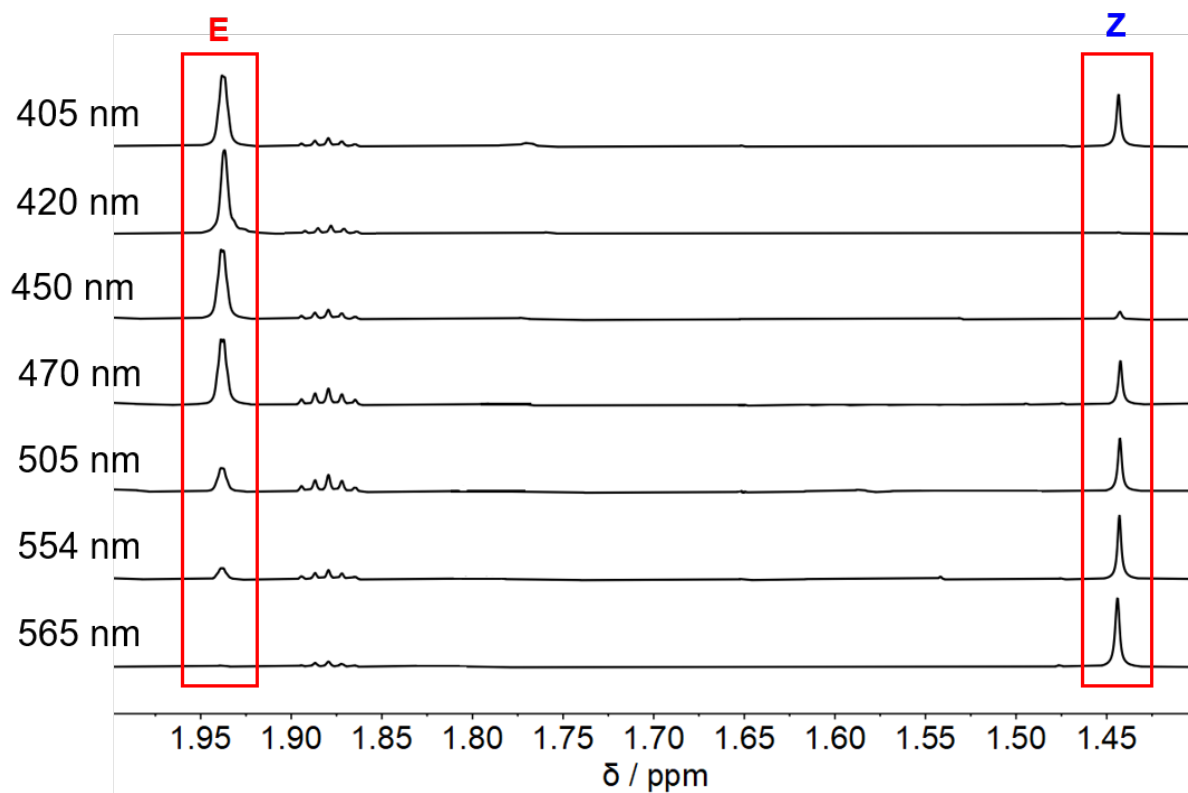
Figure S 26: Extracts from ^{1}H-NMR spectra of compound **4** (400 MHz, toluene-d_8, 26 °C) showing enriched *E* and *Z* isomer after irradiation with 405 nm, 420 nm, 450 nm, 470 nm, 505 nm, 530 nm, 554 nm, and 565 nm light. The signal of proton 14 was selected to determine the isomeric ratio.
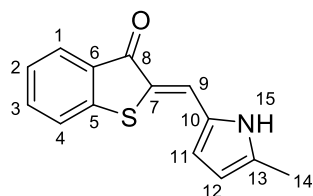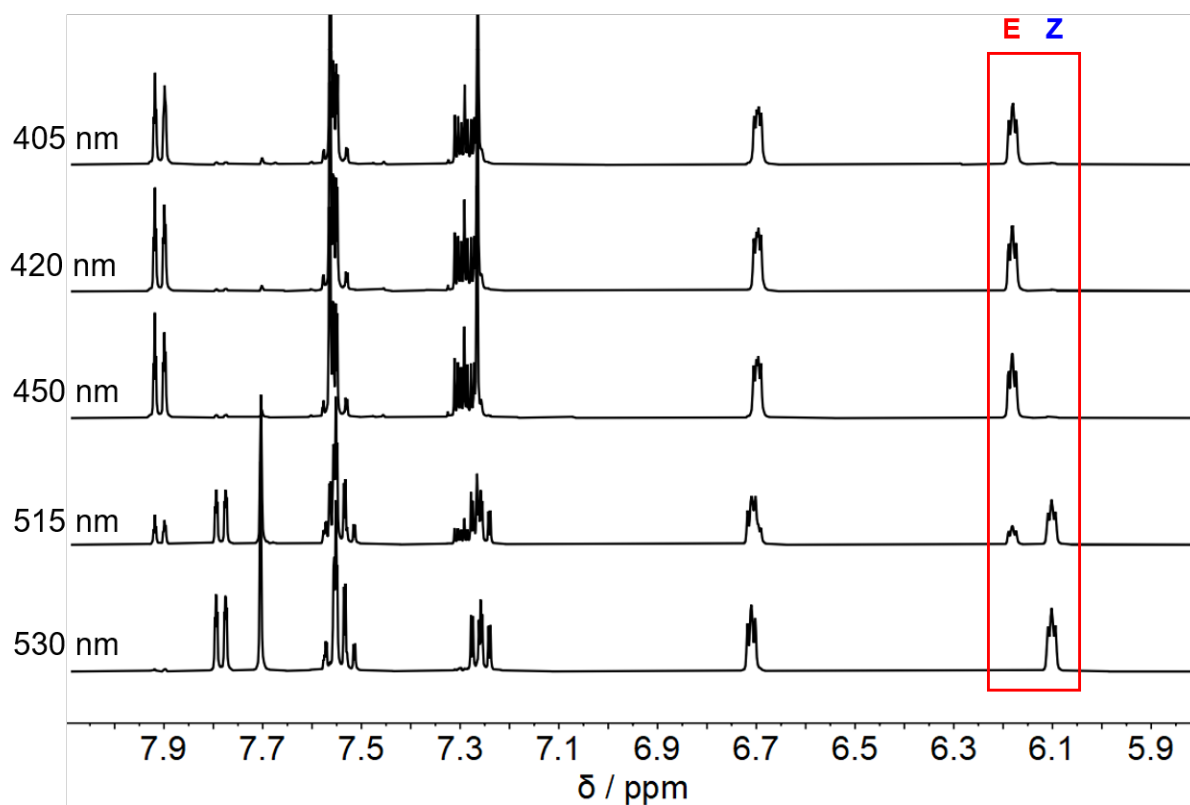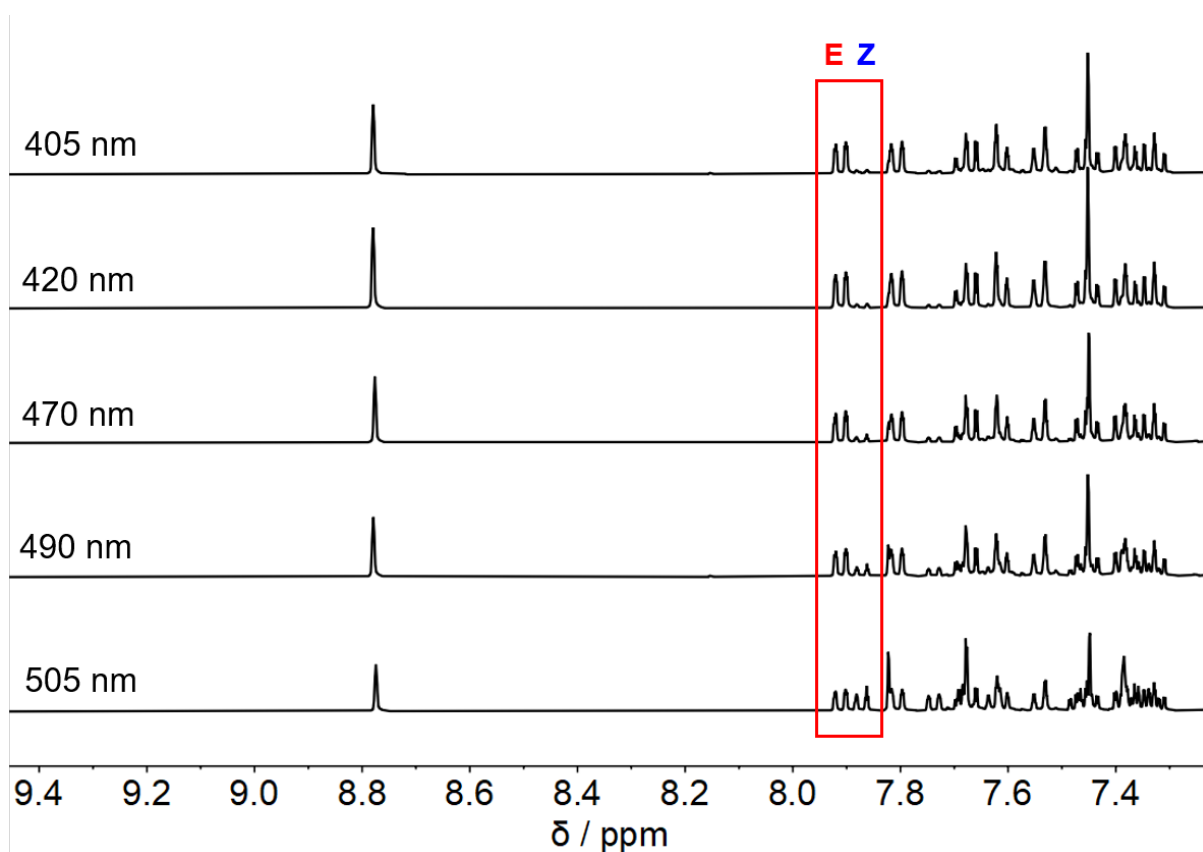
Figure S 27: Extracts from ¹H-NMR spectra of compound **4** (400 MHz, tetrahydrofuran-d_8, 26 °C) showing enriched *E* and *Z* isomer after irradiation with 405 nm, 430 nm, 450 nm, 515 nm, and 530 nm light. The signal of proton 12 was selected to determine the isomeric ratio.
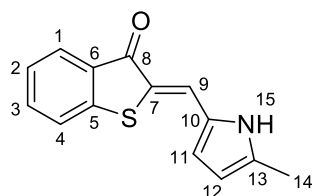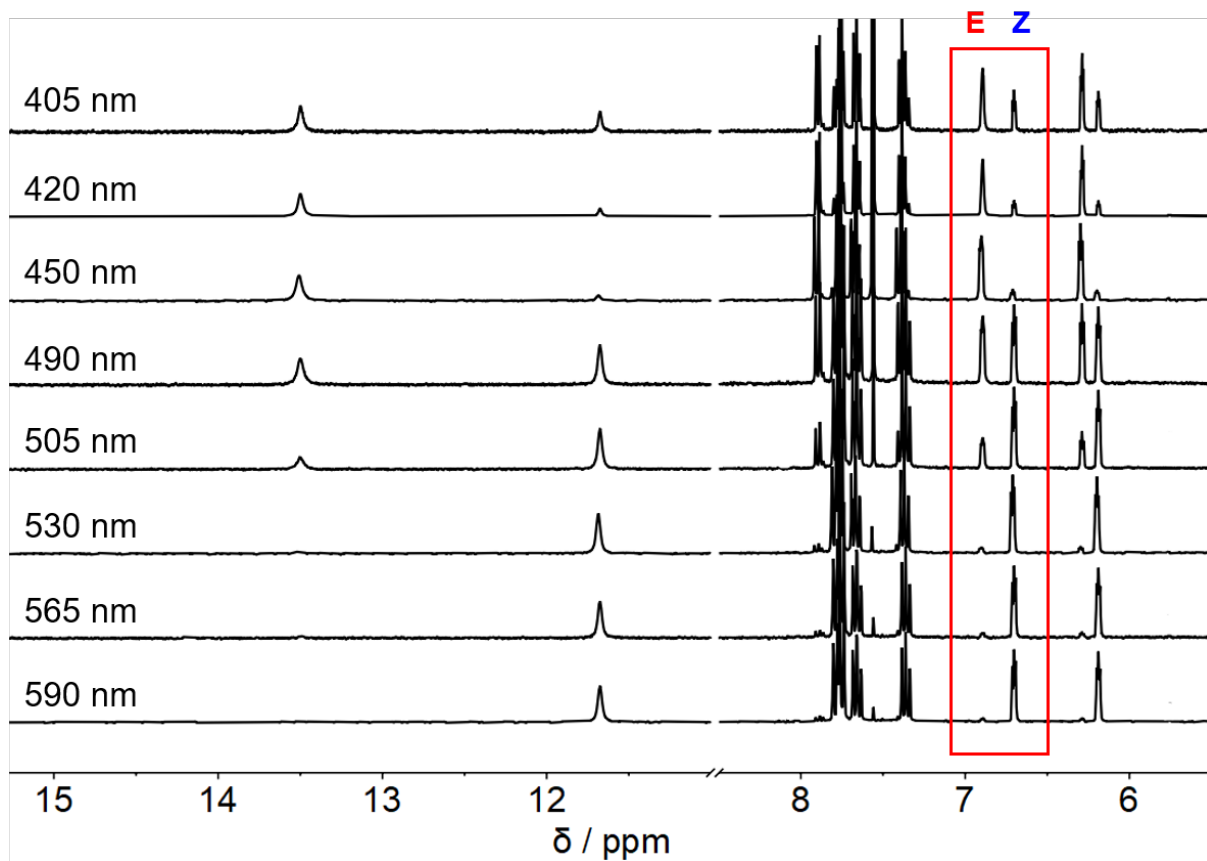
Figure S 28: Extracts from ^{1}H-NMR spectra of compound **4** (400 MHz, DMSO-d_6, 26 °C) showing enriched *E* and *Z* isomer after irradiation with 405 nm, 420 nm, 450 nm, 490 nm, 505 nm, 530 nm, 565 nm, and 590 nm light. The signal of proton 11 was selected to determine the isomeric ratio.
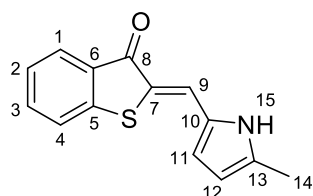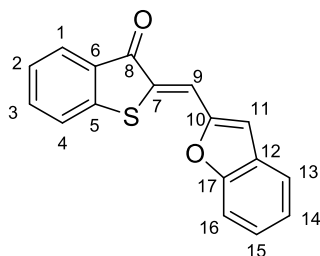
Table S 3: *E/Z* isomeric ratios of compound **4** obtained in the pss after irradiation with light of different wavelengths. All values given were determined using ^{1}H NMR spectroscopy at 26 °C.

solvent	irr. wavelength [nm]	% Z isomer	% E isomer
toluene-d_8	405	30	70
	420	0	100
	450	8	92
	470	29	71
	505	53	47
	554	75	25
	565	94	6
THF-d_8	405	6	94
	430	6	94
	450	5	95
	515	70	30
	530	95	5
DMSO-d_6	405	33	67
	420	13	87
	450	13	87
	490	50	50
	505	69	31
	530	93	7
	565	93	7
	590	95	5

Figure S 29: Extracts from ^{1}H-NMR spectra of compound **5** (400 MHz, THF-d_8, 26 °C) showing enriched *E* and *Z* isomer after irradiation with 405 nm, 420 nm, 430 nm, 450 nm, 470 nm, 490 nm, 505 nm, and 530 nm light. The signal of proton 9 was selected to determine the isomeric ratio.
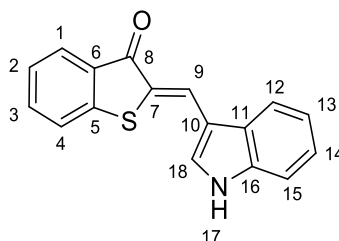
Table S 4: *E*/*Z* isomeric ratios of compound **5** obtained in the pss after irradiation with light of different wavelengths. All values given were determined using ^{1}H NMR spectroscopy at 26 °C.

solvent	irr. wavelength [nm]	% Z isomer	% E isomer
THF-*d₈*	405	11	89
	420	12	88
	430	15	85
	450	17	83
	470	65	35
	490	70	30
	505	82	18
	530	92	8

Figure S 30: Extracts from ^{1}H-NMR spectra of compound **6** (400 MHz, THF-d_8, 26 °C) showing enriched *E* and *Z* isomer after irradiation with 405 nm, 420 nm, 430 nm, 450 nm, 490 nm, 505 nm, and 530 nm light. The signal of proton 9 was selected to determine the isomeric ratio.

Table S 5: *E/Z* isomeric ratios of compound **6** obtained in the pss after irradiation with light of different wavelengths. All values given were determined using ^{1}H NMR spectroscopy at 26 °C.

solvent	irr. wavelength [nm]	% Z isomer	% E isomer
THF-d_8	405	13	87
	420	16	84
	430	13	87
	450	15	85
	490	81	19
	505	89	11
	530	100	0
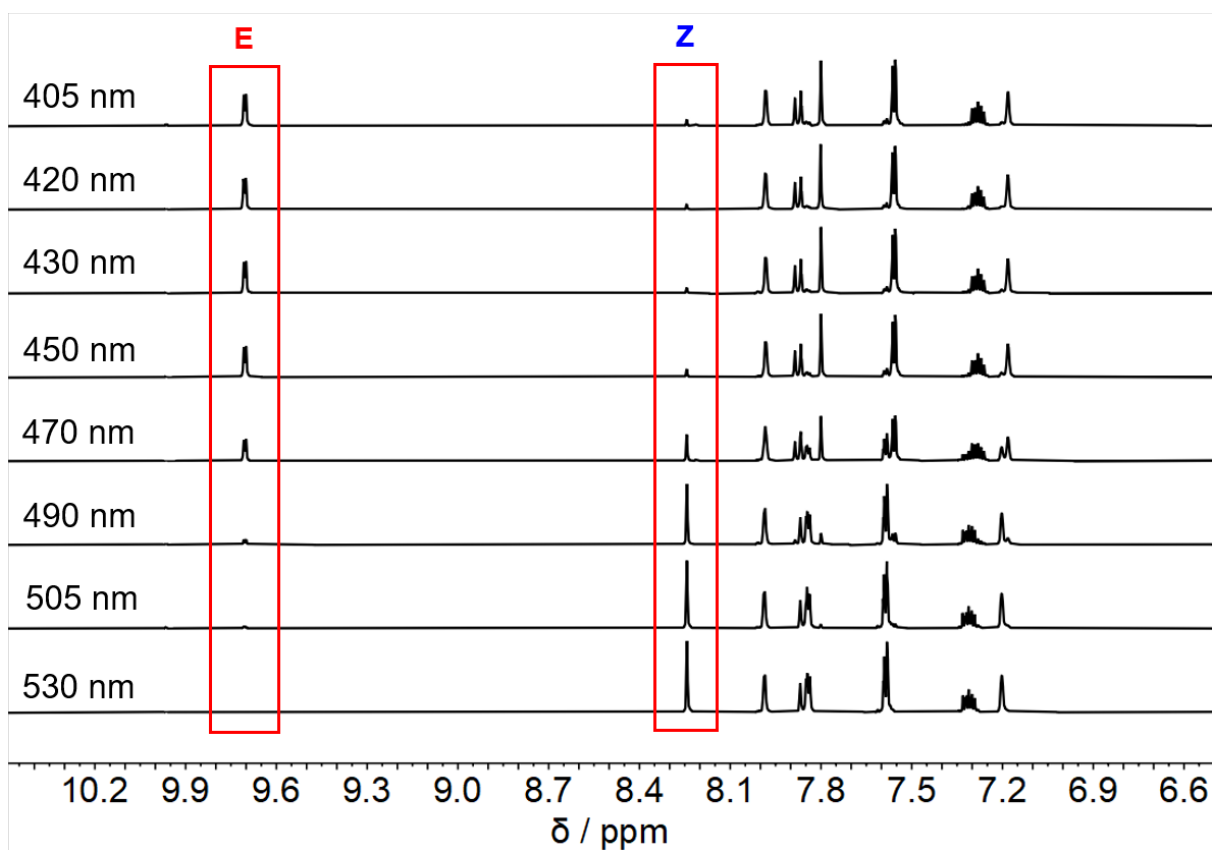
Figure S 31: Extracts from ^{1}H-NMR spectra of compound **7** (400 MHz, THF-d_8, 26 °C) showing enriched *E* and *Z* isomer after irradiation with 405 nm, 420 nm, 430 nm, 450 nm, 470 nm, 490 nm, 505 nm, and 530 nm light. The signal of proton 9 was selected to determine the isomeric ratio.

Table S 6: *E*/*Z* isomeric ratios of compound **7** obtained in the pss after irradiation with light of different wavelengths. All values given were determined using ^{1}H NMR spectroscopy at 26 °C.

solvent	irr. wavelength [nm]	% Z isomer	% E isomer
THF-d_8	405	15	85
	420	16	84
	430	16	84
	450	16	84
	470	75	25
	490	80	20
	505	87	13
	530	100	0

Figure S 32: Extracts from ^{1}H-NMR spectra of compound **9** (400 MHz, toluene-d_8, 26 °C) showing enriched *E* and *Z* isomer after irradiation with 405 nm, 430 nm, 450 nm, 470 nm, 490 nm, 505 nm, and 530 nm light. The signal of proton 9 was selected to determine the isomeric ratio.

Figure S 33: Extracts from ^{1}H-NMR spectra of compound **9** (400 MHz, DMSO-d_6, 26 °C) showing enriched *E* and *Z* isomer after irradiation with 405 nm, 420 nm, 430 nm, 450 nm, 470 nm, 490 nm, 505 nm, and 530 nm light. The signal of proton 12 was selected to determine the isomeric ratio.

Table S 7: *E/Z* isomeric ratios of compound **9** obtained in the pss after irradiation with light of different wavelengths. All values given were determined using ^{1}H NMR spectroscopy at 26 °C.

solvent	irr. wavelength [nm]	% Z isomer	% E isomer
toluene-*d$_8$*	405	9	91
	430	6	94
	450	5	95
	470	13	87
	490	69	31
	505	69	31
	530	88	12
DMSO-*d$_6$*	405	25	75
	420	22	78
	430	19	81
	450	32	68
	470	46	54
	490	48	52
	505	79	21
	530	81	19

Figure S 34: Extracts from ^{1}H-NMR spectra of compound **10** (400 MHz, acetonitrile-d_3, 26 °C) showing enriched *E* and *Z* isomer after irradiation with 405 nm, 420 nm, 470 nm, 490 nm and 505 nm light. The signal of proton 1 was selected to determine the isomeric ratio.

Table S 8: *E*/*Z* isomeric ratios of compound **10** obtained in the pss after irradiation with light of different wavelengths. All values given were determined using ^{1}H NMR spectroscopy at 26 °C.

solvent	irr. wavelength [nm]	% Z isomer	% E isomer
acetonitrile-d_3	405	20	80
	420	17	83
	470	23	77
	490	31	69
	505	46	54
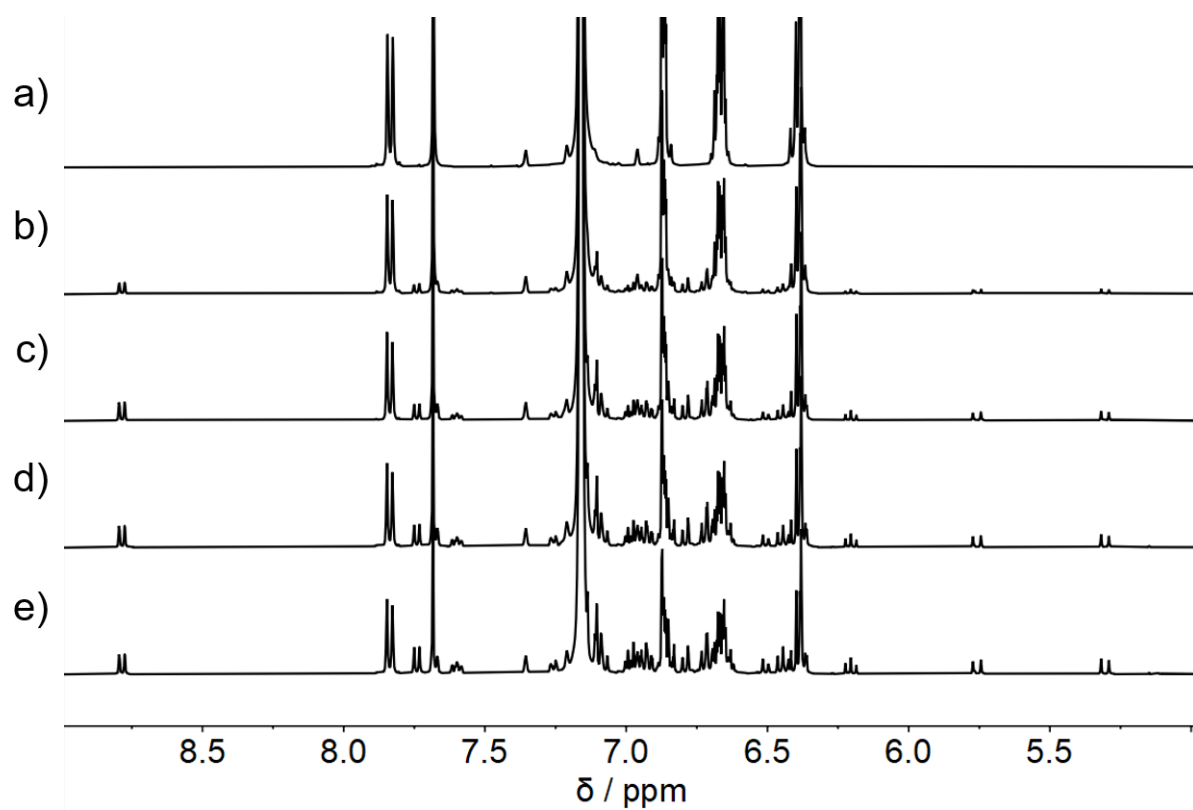
Figure S 35: Extracts from ^{1}H-NMR spectra of compound *Z*-**12** (400 MHz, benzene-*d₆*, 26 °C) after irradiation with 450 nm light. Photodegradation occurs; a) no irradiation; b) 1 min; c) 5 min; d) 10 min; e) 15 min.
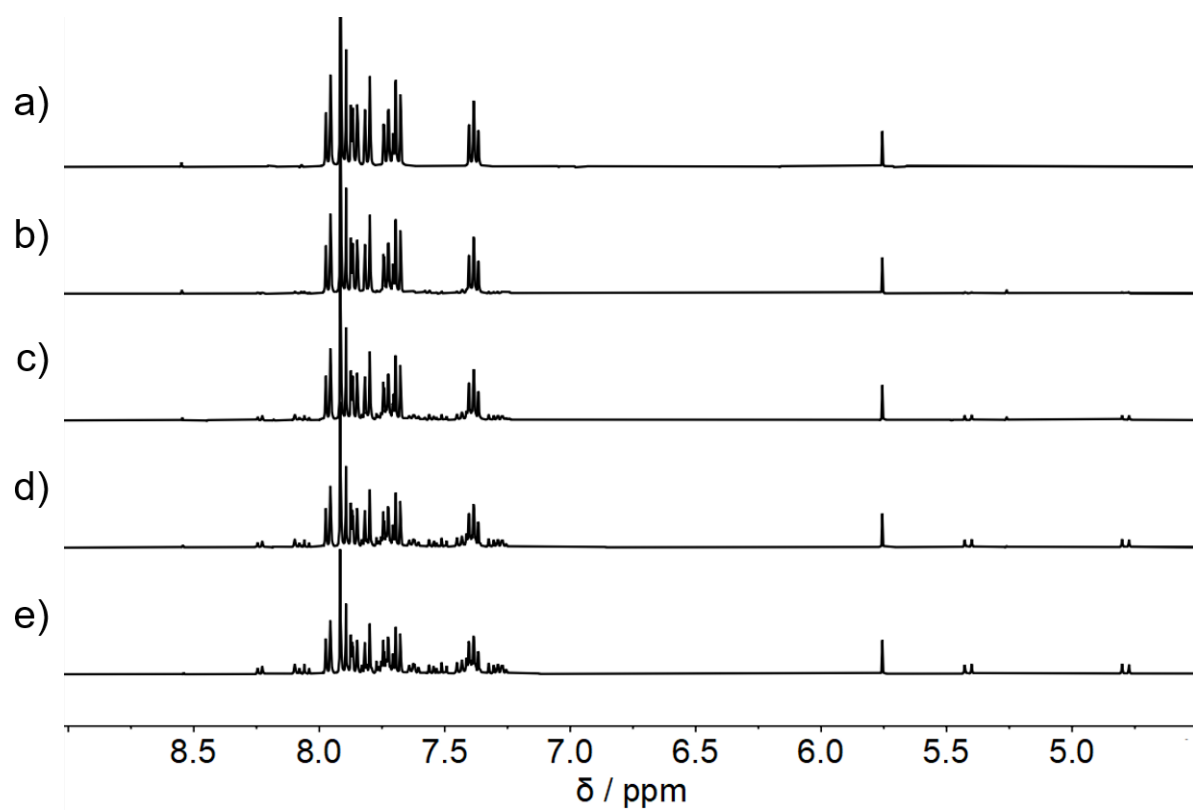
Figure S 36: Extracts from ^{1}H-NMR spectra of compound *Z*-**12** (400 MHz, DMSO-*d$_6$*, 26 °C) after irradiation with 450 nm light. Photodegradation occurs; a) no irradiation; b) 1 min; c) 5 min; d) 10 min; e) 15 min.
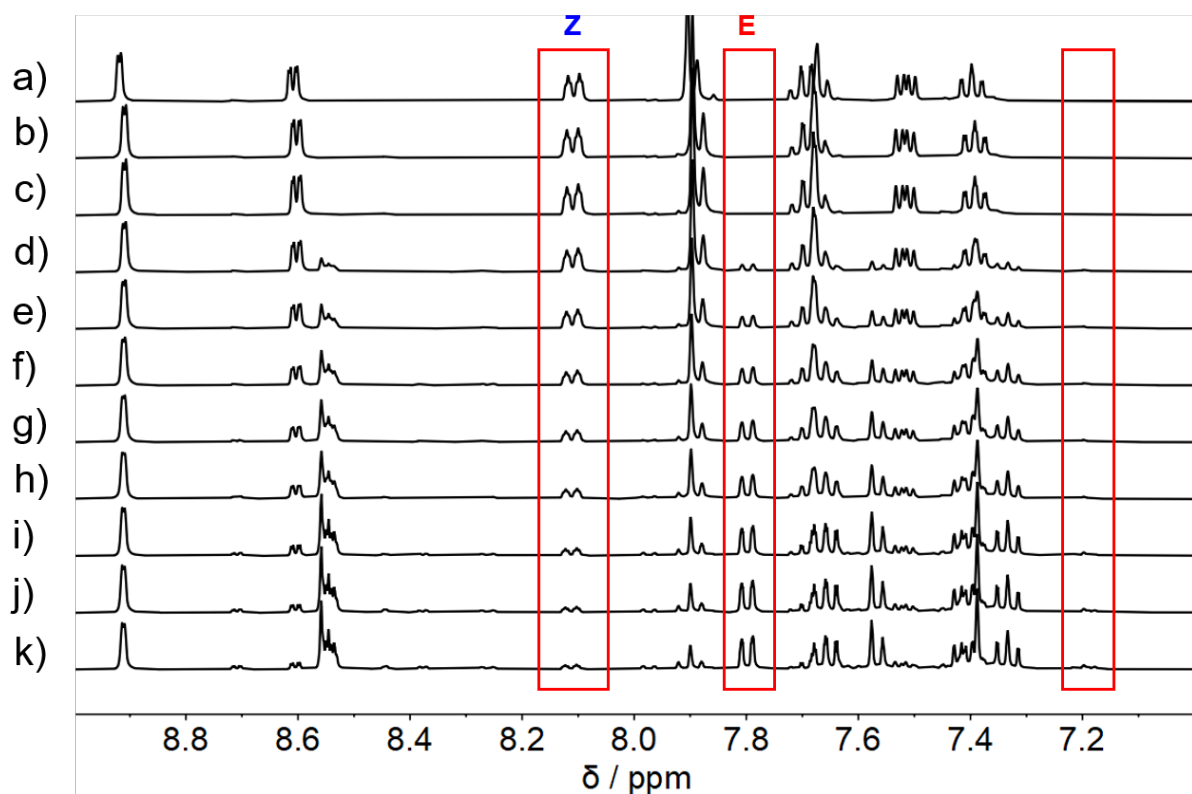
Figure S 37: Extracts from ^{1}H-NMR spectra of compound **13** (400 MHz, acetonitrile-d_3, 26 °C, 0 °C) showing enriched *E* and *Z* isomer after irradiation with 420 nm light; a) no irradiation 26 °C; b) no irradiation 0 °C; c) 1 min; d) 5 min; e) 10 min; f) 15 min; g) 20 min; h) 25 min; i) 35 min; j) 45 min; k) 55 min. Signals signifying decomposition can be seen i.a. at 7.2 ppm. The signal of proton 4 was selected to determine the isomeric ratio.
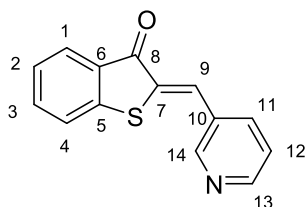
Table S 9: *E/Z* isomeric ratios of compound **13** obtained in the pss after irradiation with 420 nm light as determined by ^{1}H NMR spectroscopy at 0 °C.

solvent	irr. wavelength [nm]	% Z isomer	% E isomer	% decomposition product
acetonitrile-d_3	420	14	70	16
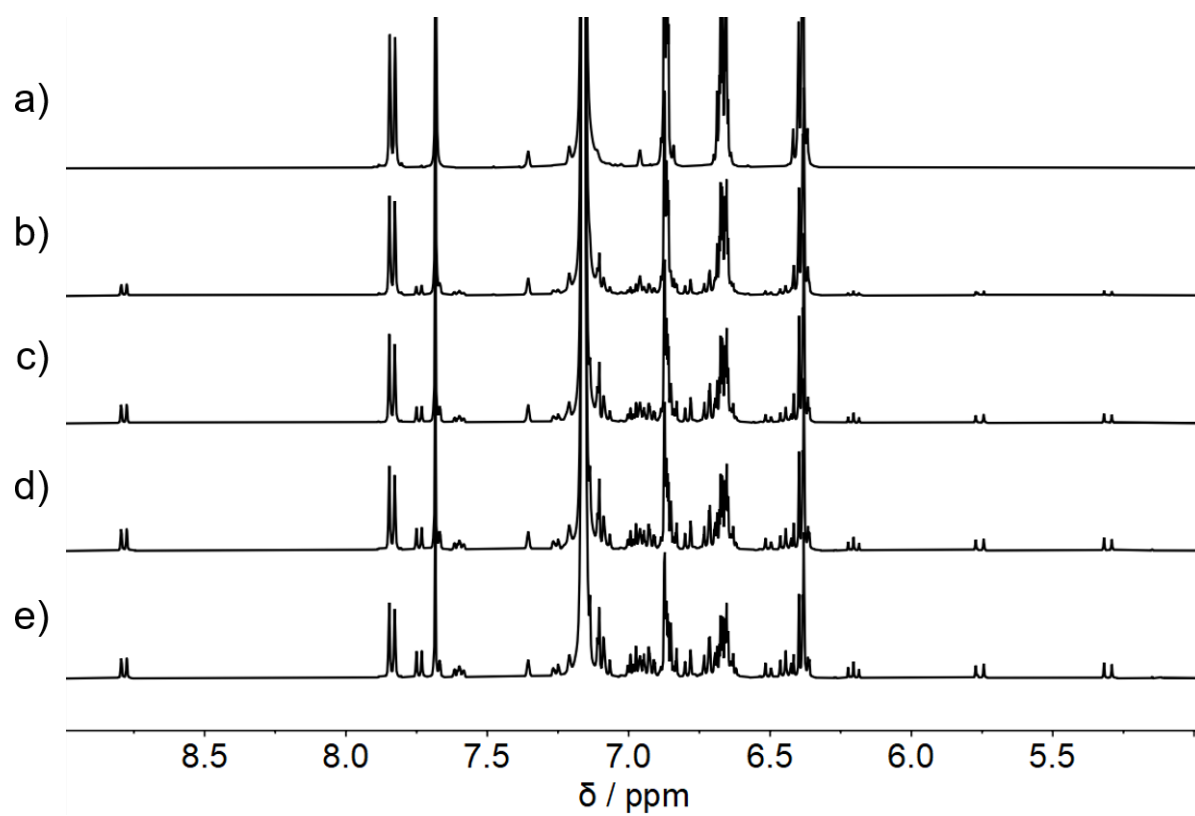
Figure S 38: Extracts from ^{1}H-NMR spectra of compound *Z*-**14** (400 MHz, benzene-*d₆*, 26 °C) after irradiation with 420 nm light. Photodegradation occurs; a) no irradiation; b) 1 min; c) 3 min; d) 5 min; e) 7 min.
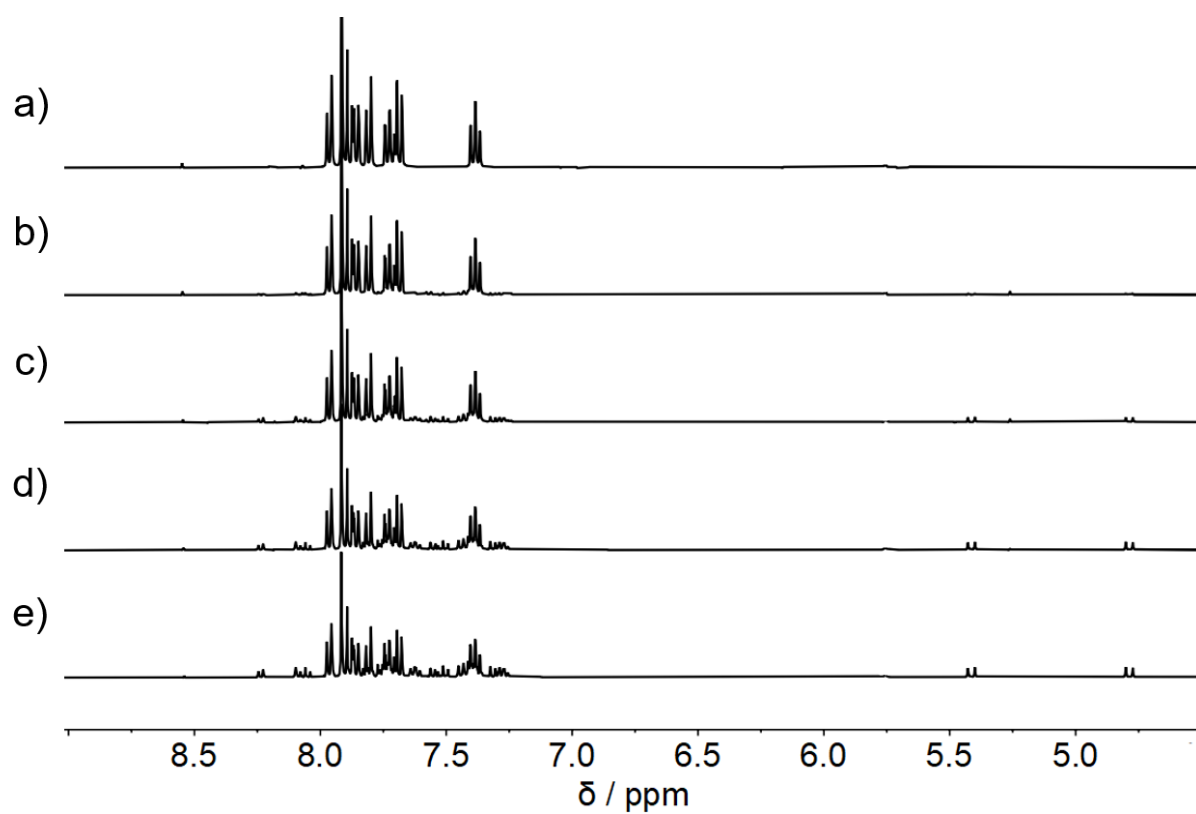
Figure S 39: Extracts from ^{1}H-NMR spectra of compound *Z*-**14** (400 MHz, DMSO-d_6, 26 °C) after irradiation with 420 nm light. Photodegradation occurs; a) no irradiation; b) 10 min; c) 30 min; d) 1 h; e) 1,5 h.
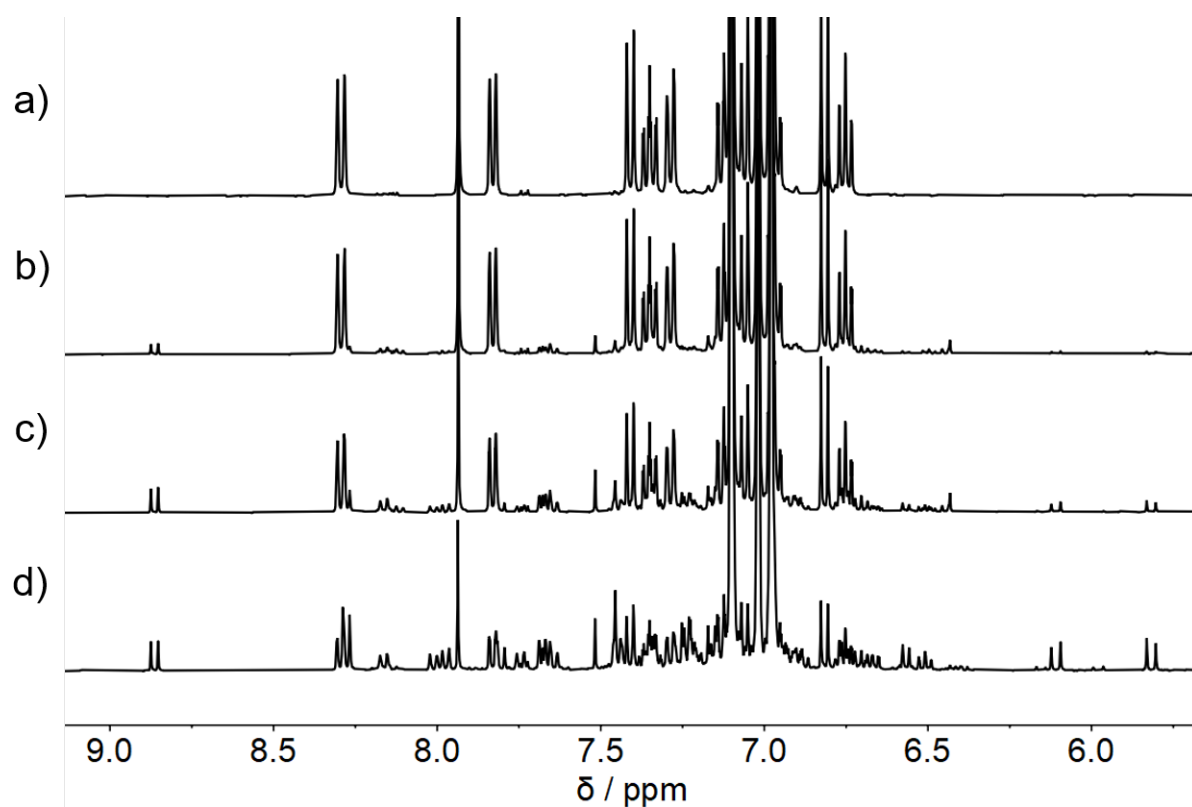
Figure S 40: Extracts from ^{1}H-NMR spectra of compound *Z*-**15** (400 MHz, toluene-*d₈*, 26 °C) after irradiation with 450 nm light. Photodegradation occurs; a) no irradiation; b) 1 min; c) 5 min; d) 10 min.
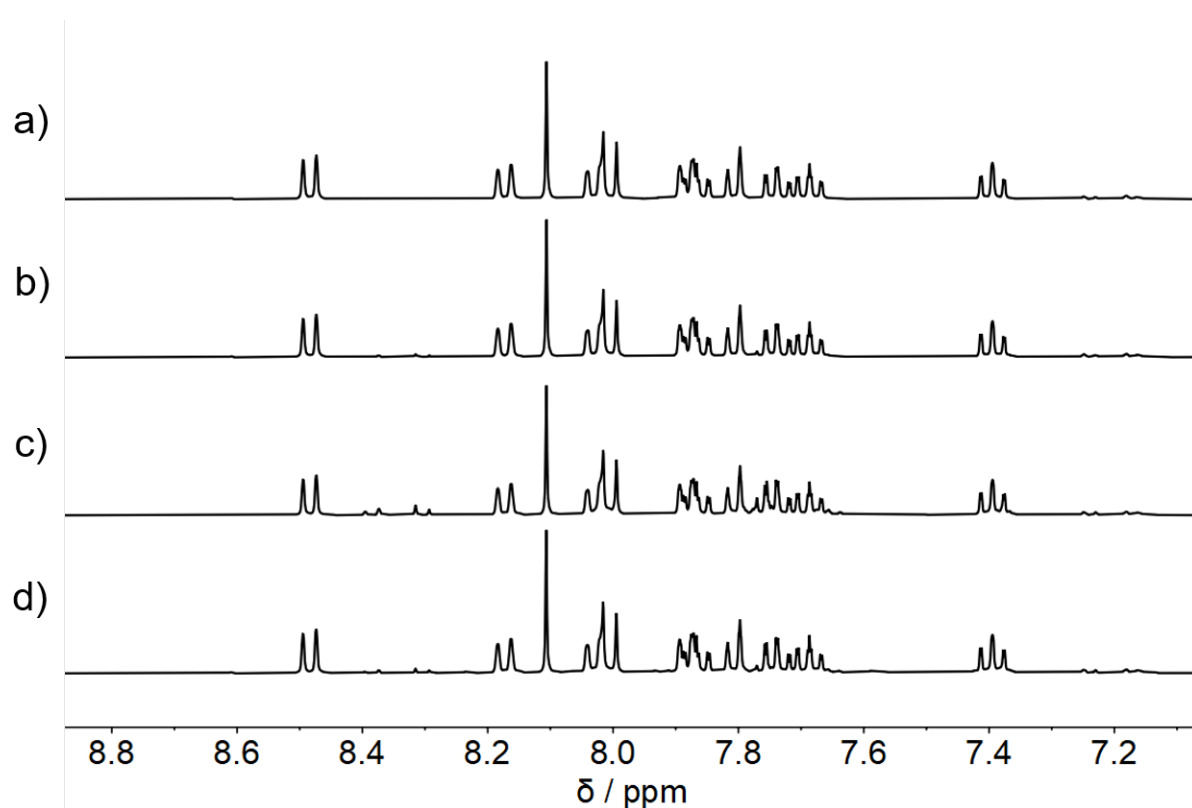
Figure S 41: Extracts from ^{1}H-NMR spectra of compound *Z*-**15** (400 MHz, DMSO-*d₆*, 26 °C) after irradiation with 450 nm light. Photodegradation occurs; a) no irradiation; b) 1 min; c) 5 min; d) 10 min.
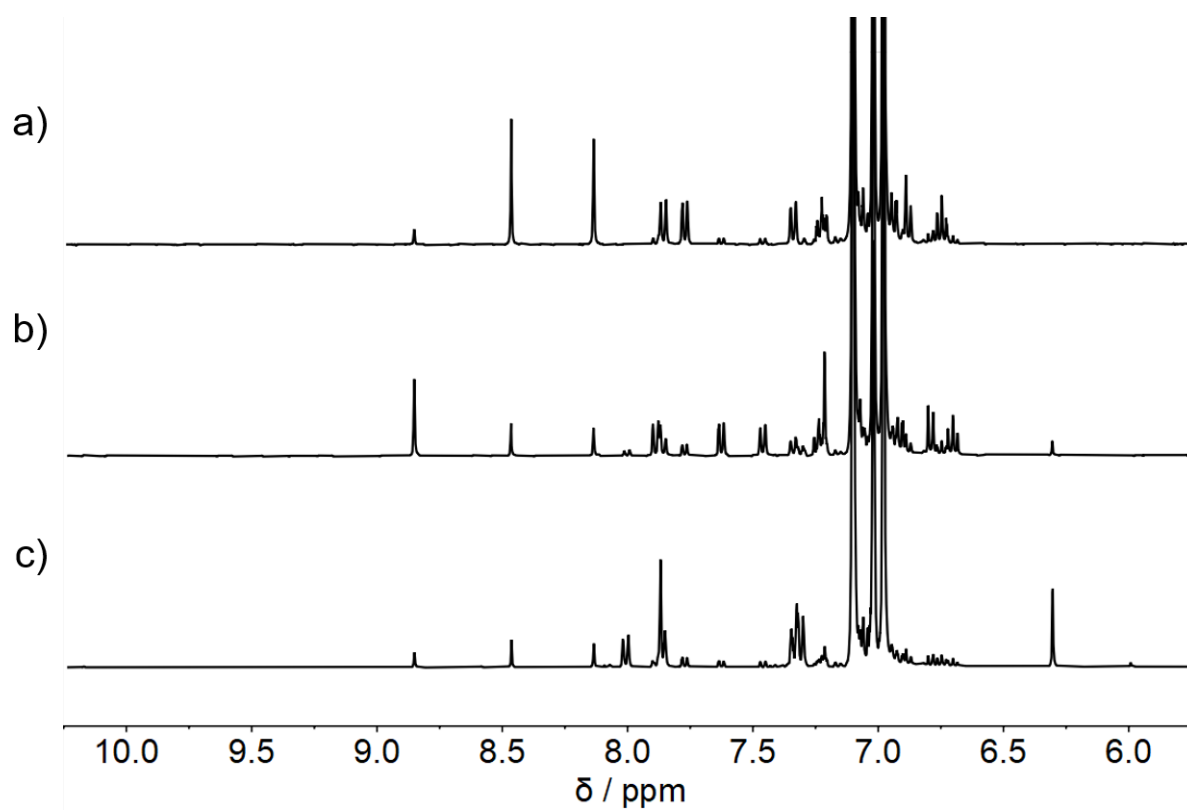
Figure S 42: Extracts from ^{1}H-NMR spectra of compound *Z*-**16** (400 MHz, toluene-*d₈*, 26 °C) after irradiation with 450 nm. Photodegradation occurs; a) no irradiation; b) 1 min; c) 5 min.
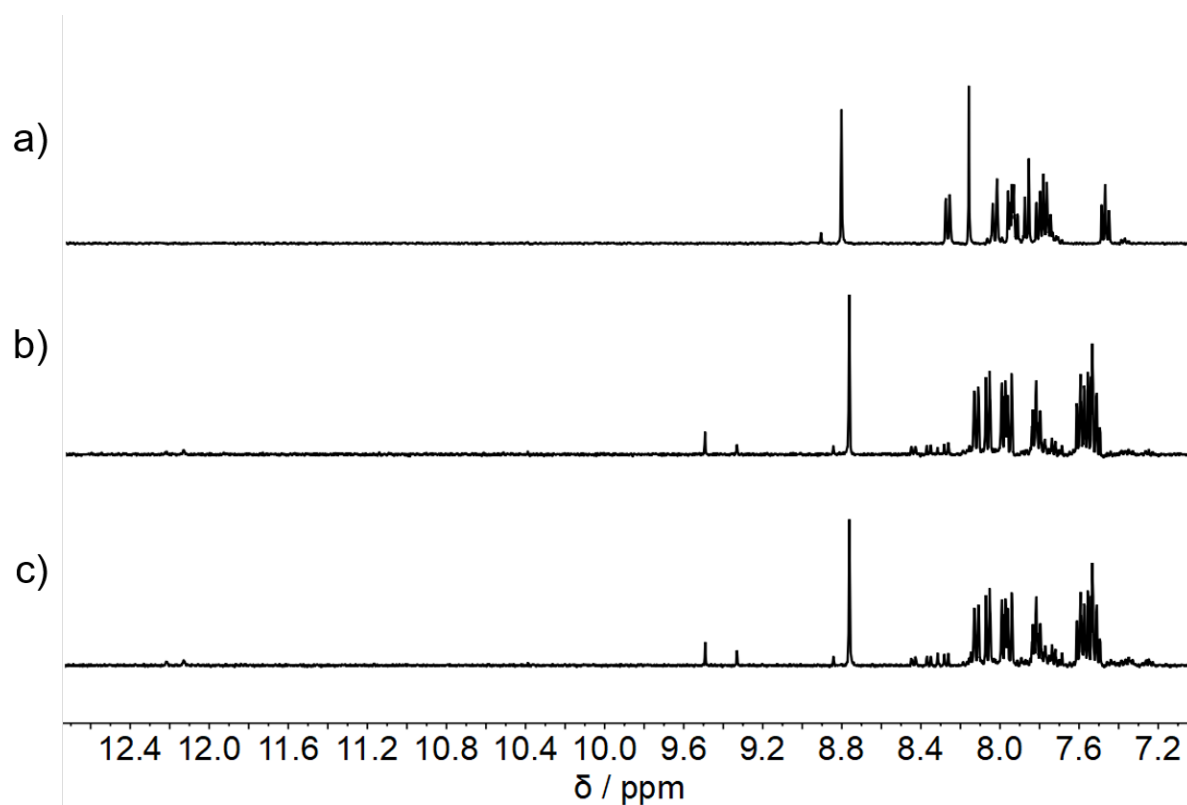
Figure S 43: Extracts from ^{1}H-NMR spectra of compound *Z*-**16** (400 MHz, DMSO-*d₆*, 26 °C) after irradiation with 450 nm light. Photodegradation occurs; a) no irradiation; b) 1 min; c) 5 min.

Thermal Double Bond Isomerization Experiments

To investigate the thermal double bond isomerization of compound **1**-**7** and **9**-**11**, an NMR tube was filled with 1.26 mg to 2.13 mg of compound dissolved in 0.7 mL of deuterated solvent (toluene-d_8, DMSO-d_6, benzene-d_6, acetonitrile-d_3 or THF-d_8). For enrichment of the metastable isomer, the NMR sample was irradiated with 405 nm – 450 nm. An initial spectrum was recorded and subsequently the NMR tube was left in darkness at a suitable temperature (20 °C – 100 °C) and the isomerization was observed at specific time periods by ^{1}H NMR spectroscopy. The experiment was finished once thermal equilibrium between *E* and *Z* isomer was reached or the metastable isomer completely re-isomerized into the most stable isomer.

The thermal double bond isomerization is an unimolecular first order reaction towards an equilibrium between two isomers (isomer I_1 and isomer I_2):

$$\ln\left(\frac{[I_1]_{t0}-[I_1]_{eq}}{[I_1]_t-[I_1]_{eq}}\right) = \left(k_{I_1/I_2} + k_{I_2/I_1}\right)t \tag{eq.9}$$

with $[I_1]_{t0}$ as the initial concentration of isomer 1 at time t = 0, $[I_1]_{eq}$ as the concentration of isomer 1 in the equilibrium, $[I_1]_t$ as the concentration of isomer 1 at a defined time t, k_{I_1/I_2} as the rate constant for the isomerization of isomer 1 to isomer 2, k_{I_2/I_1} as the rate constant for the isomerization of isomer 2 to isomer 1 and t as the elapsed time. The slope *m* obtained from the plot of the logarithmic part in eq.9 includes the rate constants for both isomerization processes in the presence of equilibrium. As a result, the rate constant can be determined by:

$$k_{I_1/I_2} = \frac{m}{1+\frac{[I_1]_{eq}}{[I_2]_{eq}}} \tag{eq.10}$$

A special case, where the chemical equilibrium of the reaction is 100% on the side of an isomer corresponds to the following relationship between the rate constants:

$$k_{I_1 \rightarrow I_2} \gg k_{I_2 \rightarrow I_1} \tag{eq.11}$$

Therefore, equation 22 can be simplified:

$$\ln\left(\frac{[I_1]_{t0}}{[I_1]_t}\right) = k_{I_1 \rightarrow I_2} \cdot t = m \cdot t \tag{eq. 12}$$

and the slope m of the straight line corresponds directly to the rate constant *k* for one isomerization direction.

The *Law of Mass Action* must be taken into account:

$$\frac{[I_1]_{eq}}{[I_2]_{eq}} = \frac{k_{I_2/I_1}}{k_{I_1/I_2}} \tag{eq.13}$$

The *Gibbs energy of activation $\Delta G^{\ddagger}$* can be calculated by using the *Eyring* equation:

$$k = \frac{k_B T}{h} e^{\frac{-\Delta G^{\ddagger}}{RT}}$$
(eq.14)

with the *Boltzmann* constant k_B (1.381·10⁻²³ JK⁻¹), temperature T, *Planck* constant h (6.62610⁻³⁴ Js), gas constant R (8.314 J·K⁻¹·mol⁻¹) and the rate constant k. After rearrangement of eq.12 the *Gibbs energy of activation $\Delta G^{\ddagger}$* is received:

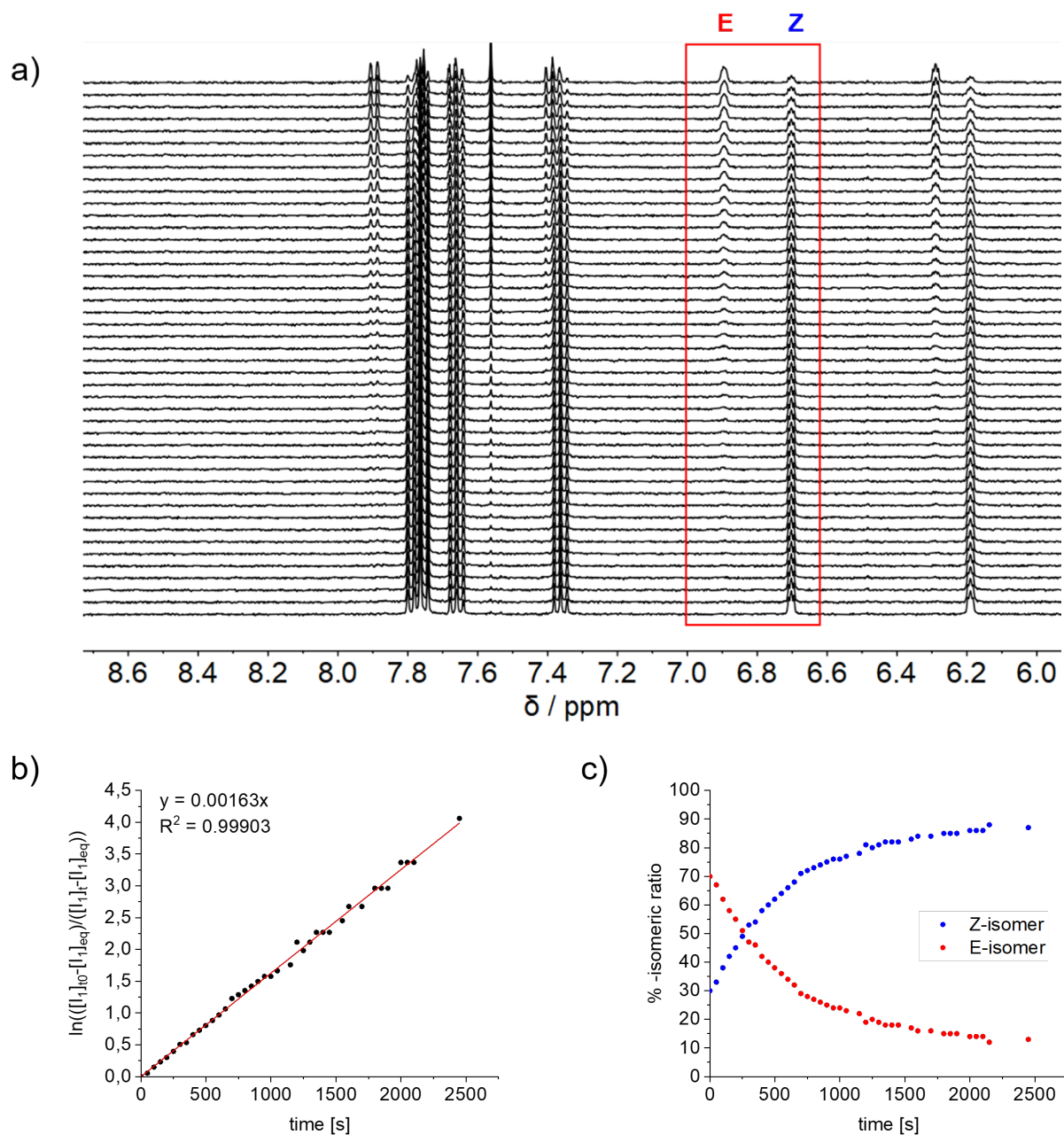$$\Delta G^* = -RTln\left(\frac{kh}{k_B T}\right)$$
(eq.15)
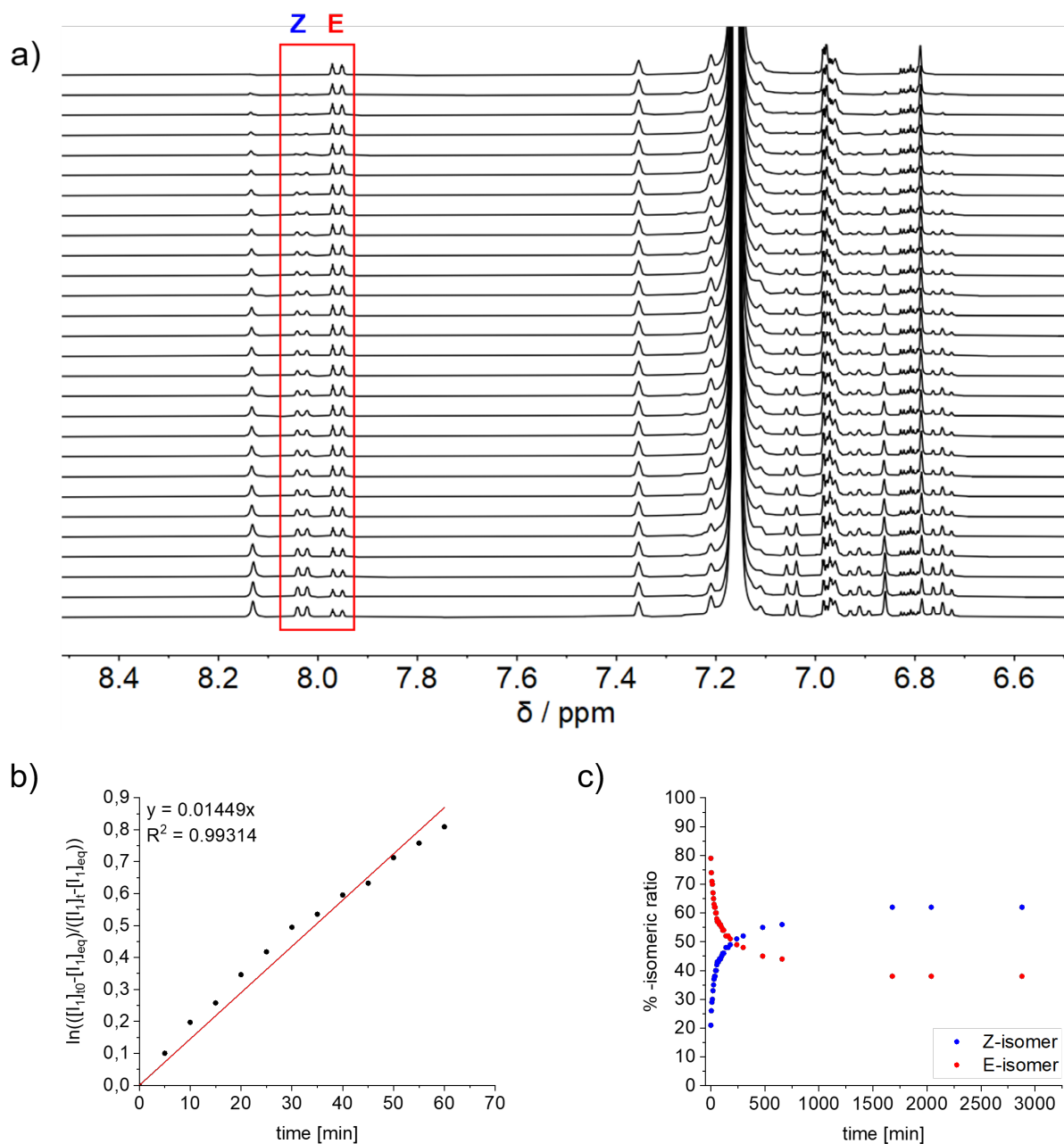
Figure S 44: Kinetic analysis of thermal E to Z isomerization of compound **1** at 60 °C in C_6D_6 in the dark. a) Indicative ^{1}H NMR (400 MHz, C_6D_6, 26 °C) signals that were used for determination of isomeric ratio; b) First order kinetic analysis of the thermal isomerization of E isomer. The first order rate constant for the thermal isomerization is obtained from the slope of the linear plot and is $k_{Z/E} = 8.98 \cdot 10^{-2}$ s^{-1}, which corresponds to a *Gibbs energy of activation* $\Delta G^* = 27.7$ kcal mol^{-1}; c) Changing isomeric ratio over time determined by integration of ^{1}H NMR signals.
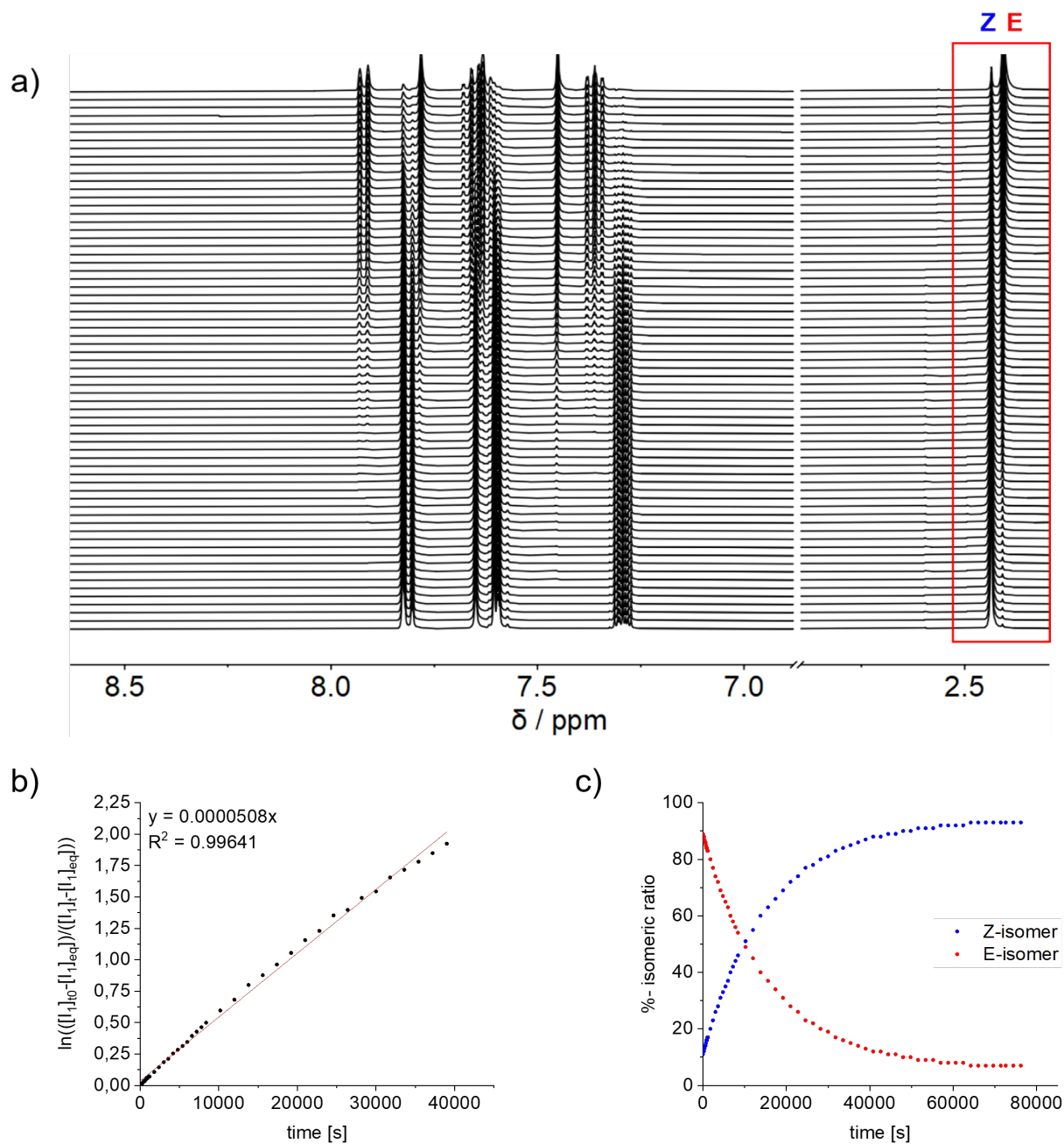
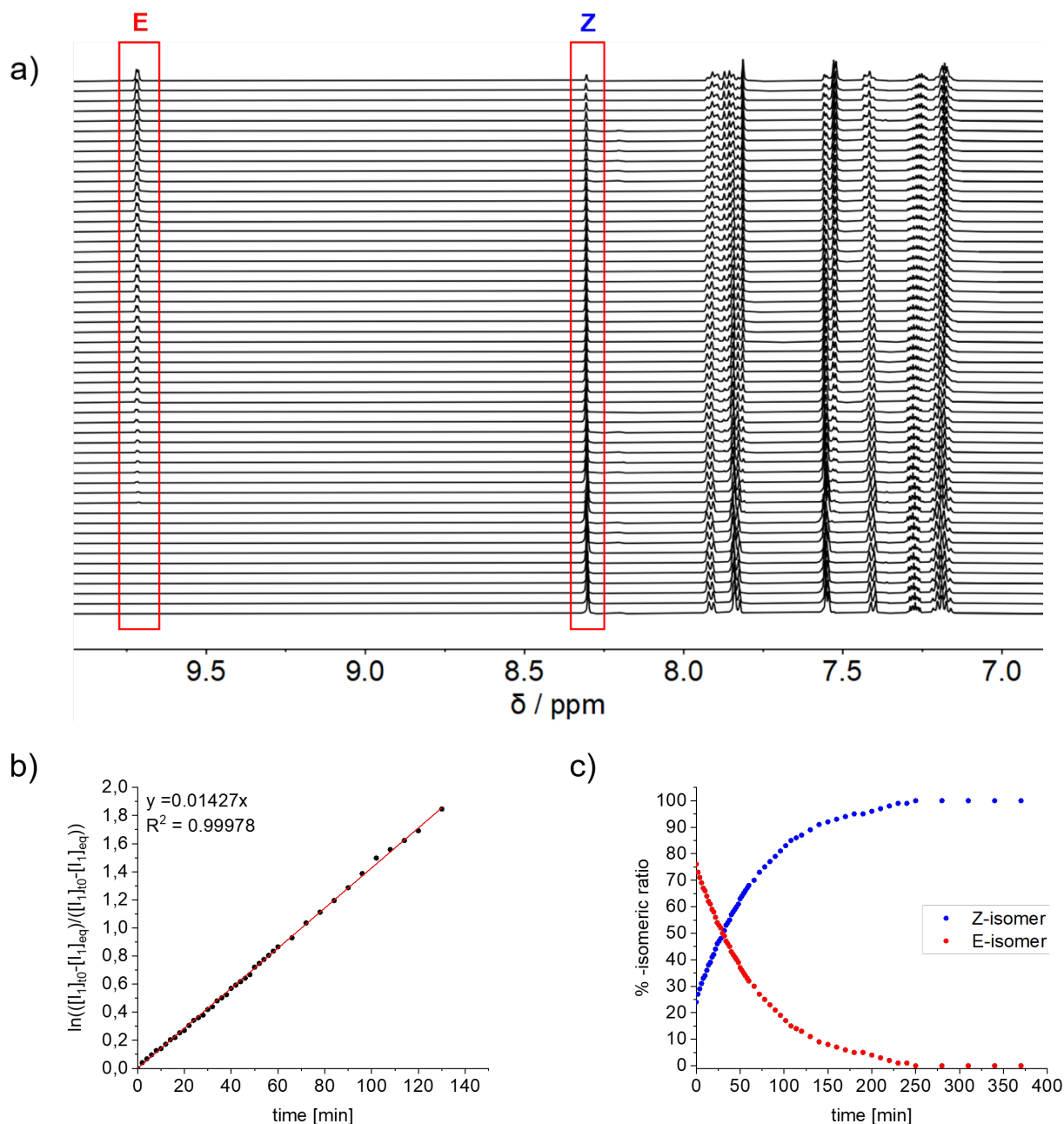**Figure S 45:** Kinetic analysis of the thermal isomerization of E to Z of compound **1** at 35 °C in acetonitrile-d_3 in the dark. a) Indicative ^{1}H NMR (400 MHz, acetonitrile-d_3, 35 °C) signals used to determine the isomer ratio; b) Kinetic analysis of the first-order thermal isomerization of the E isomer. The first-order rate constant for thermal isomerization is inferred from the slope of the linear plot and is $k_{Z/E} = 4.73 \cdot 10^{-5}$ s^{-1}, corresponding to a *Gibbs energy of activation* $\Delta G^* = 24.2$ kcal mol^{-1}; c) Change in isomer ratio over time determined by integration of the ^{1}H NMR signals.
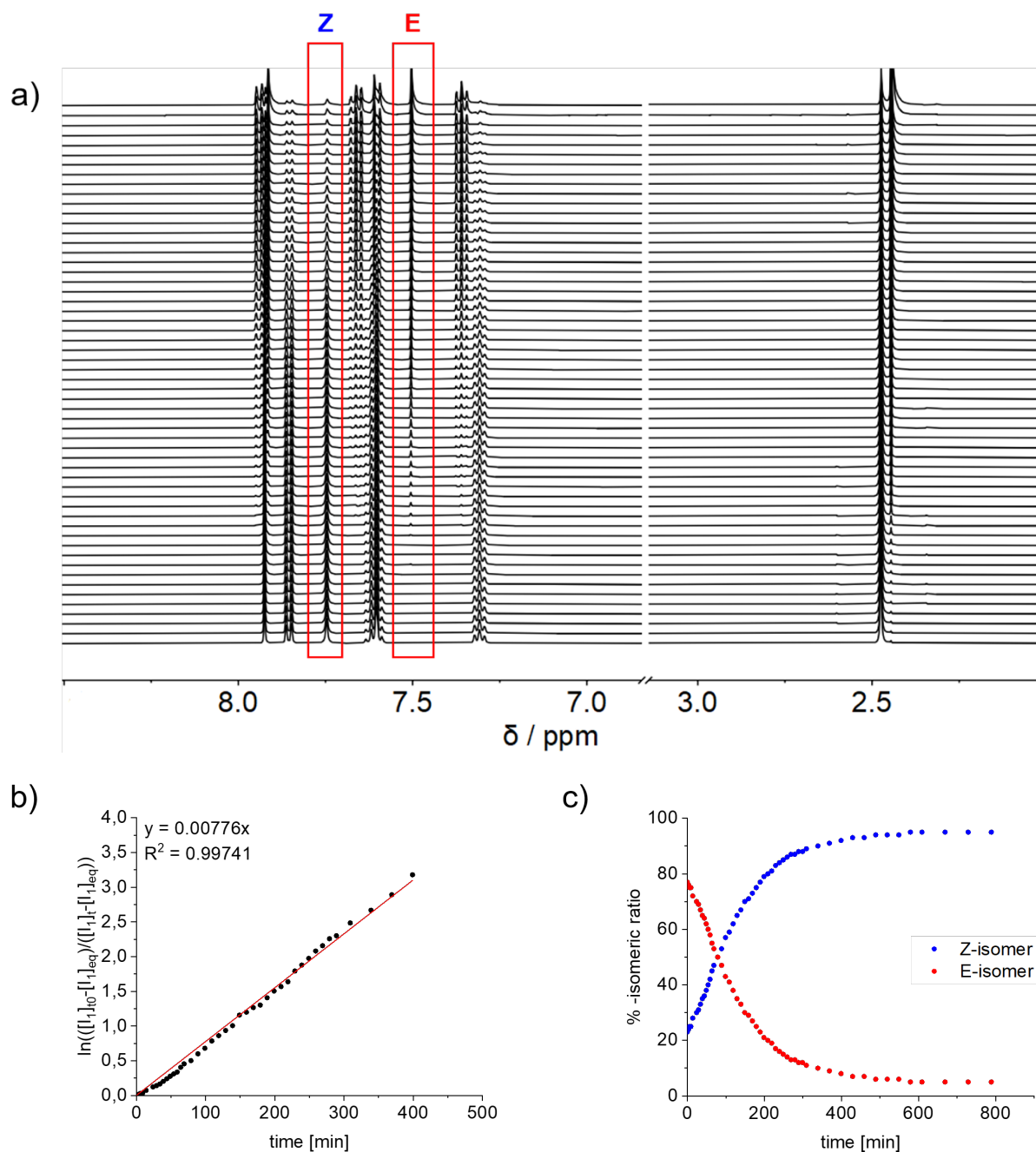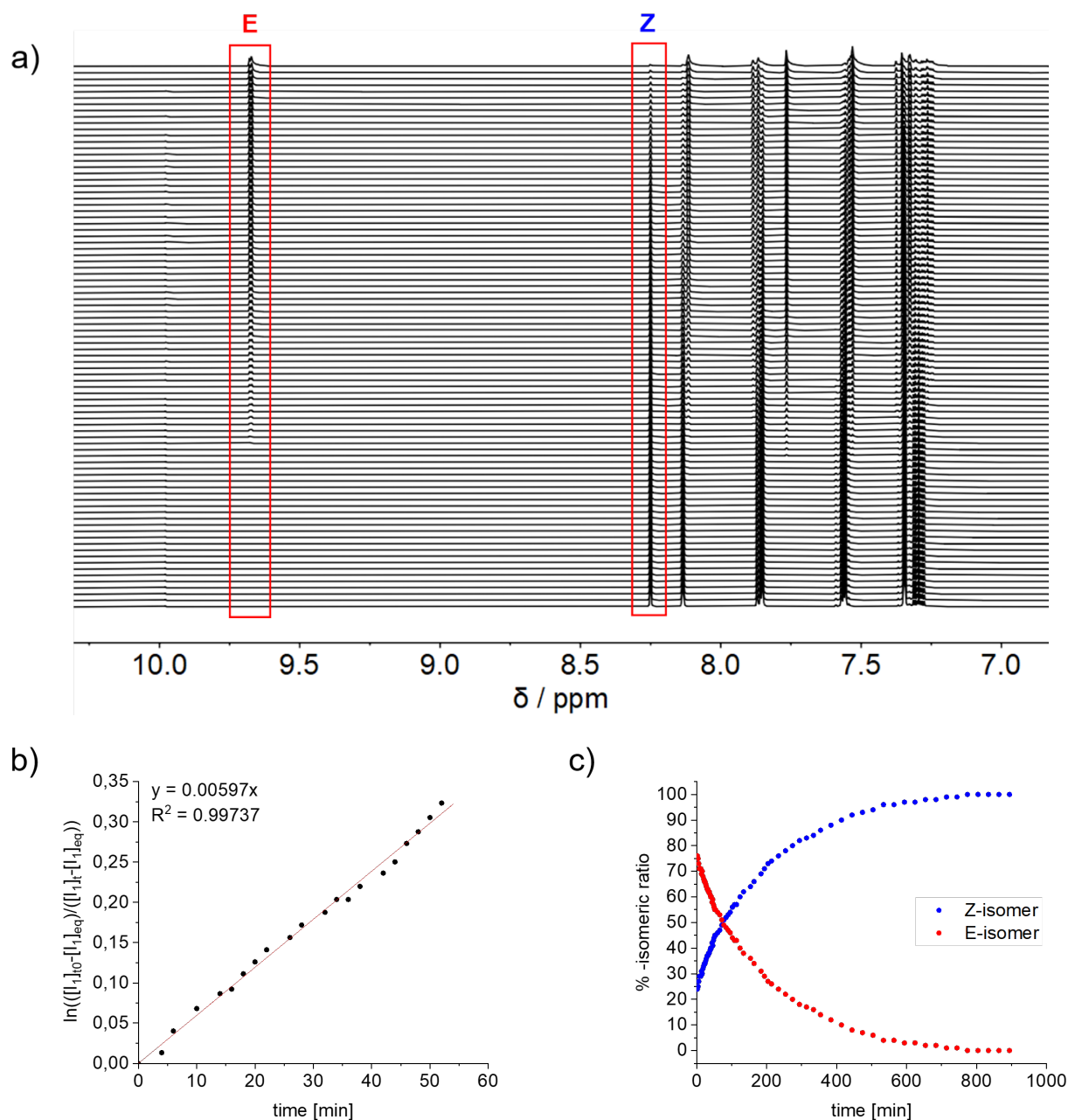
Figure S 46: Kinetic analysis of thermal *E* to *Z* isomerization of compound **1** at 20 °C in methanol-d_4 in the dark. a) Indicative ^{1}H NMR (500 MHz, methanol-d_4, 20 °C) signals that were used for determination of isomeric ratio; b) First order kinetic analysis of the thermal isomerization of *E* isomer. The first order rate constant for the thermal isomerization is obtained from the slope of the linear plot and is $k_{Z/E}$ = 7.37 · 10^{-3} s^{-1}, which corresponds to a *Gibbs energy of activation* ΔG^* = 20.0 kcal mol^{-1}; c) Changing isomeric ratio over time determined by integration of ^{1}H NMR signals.
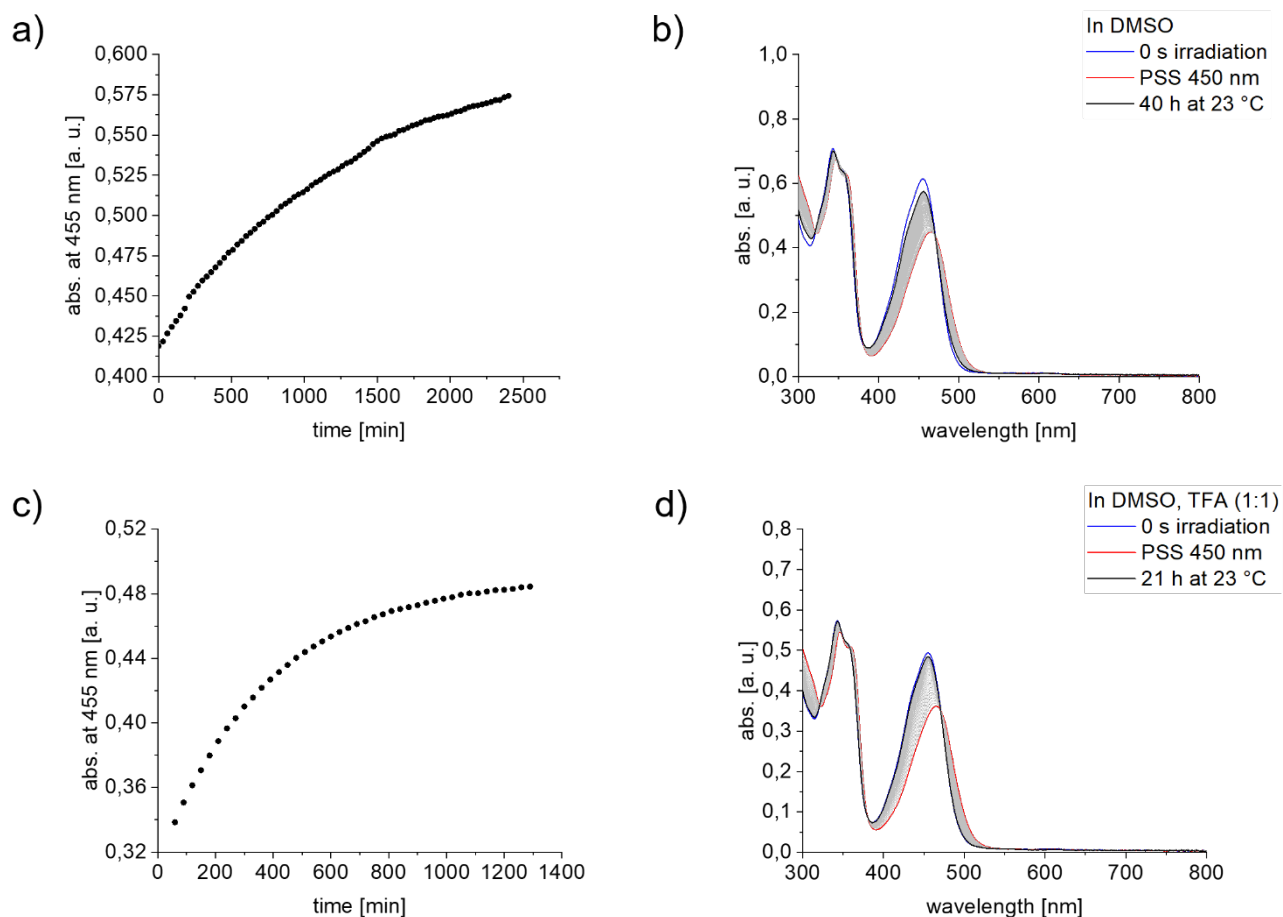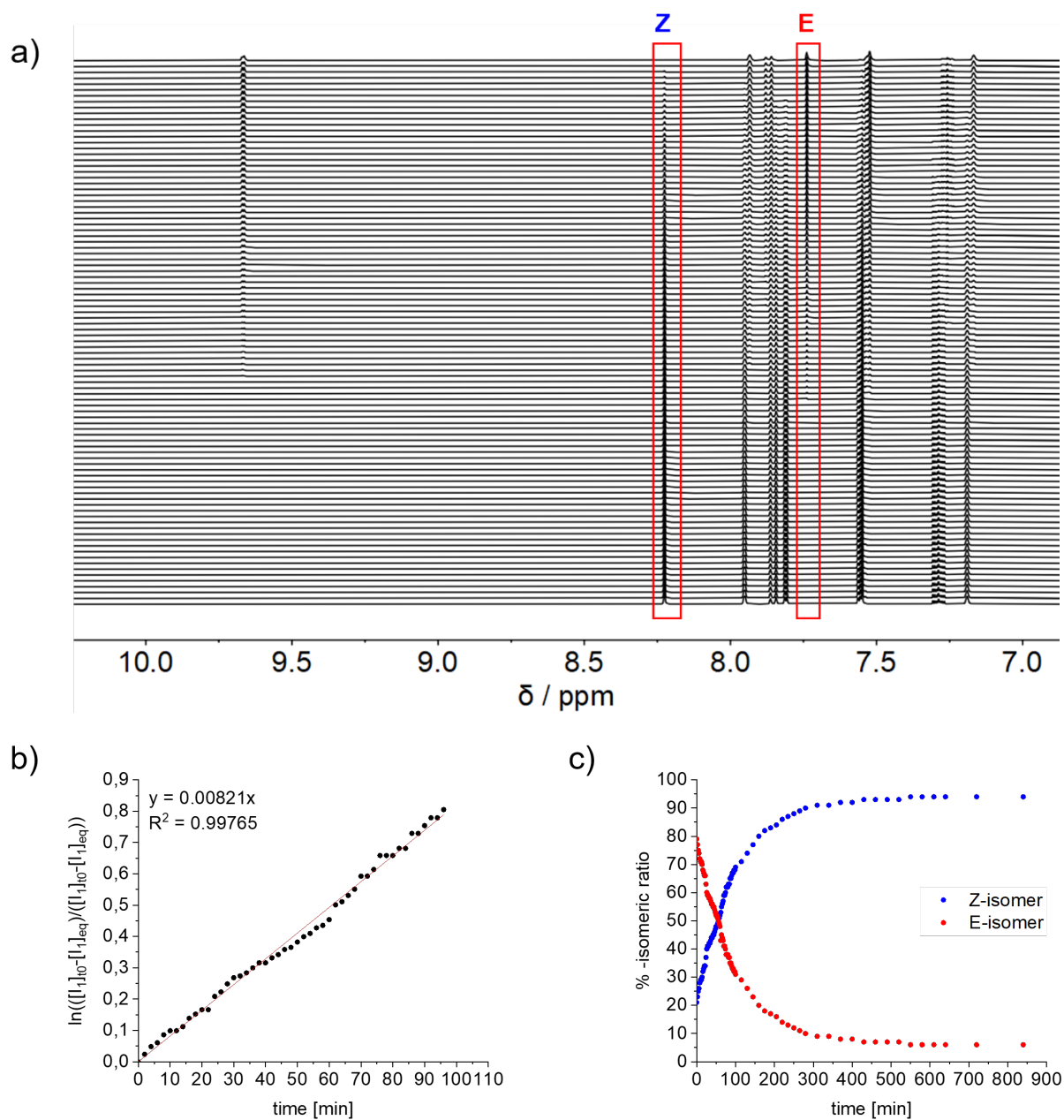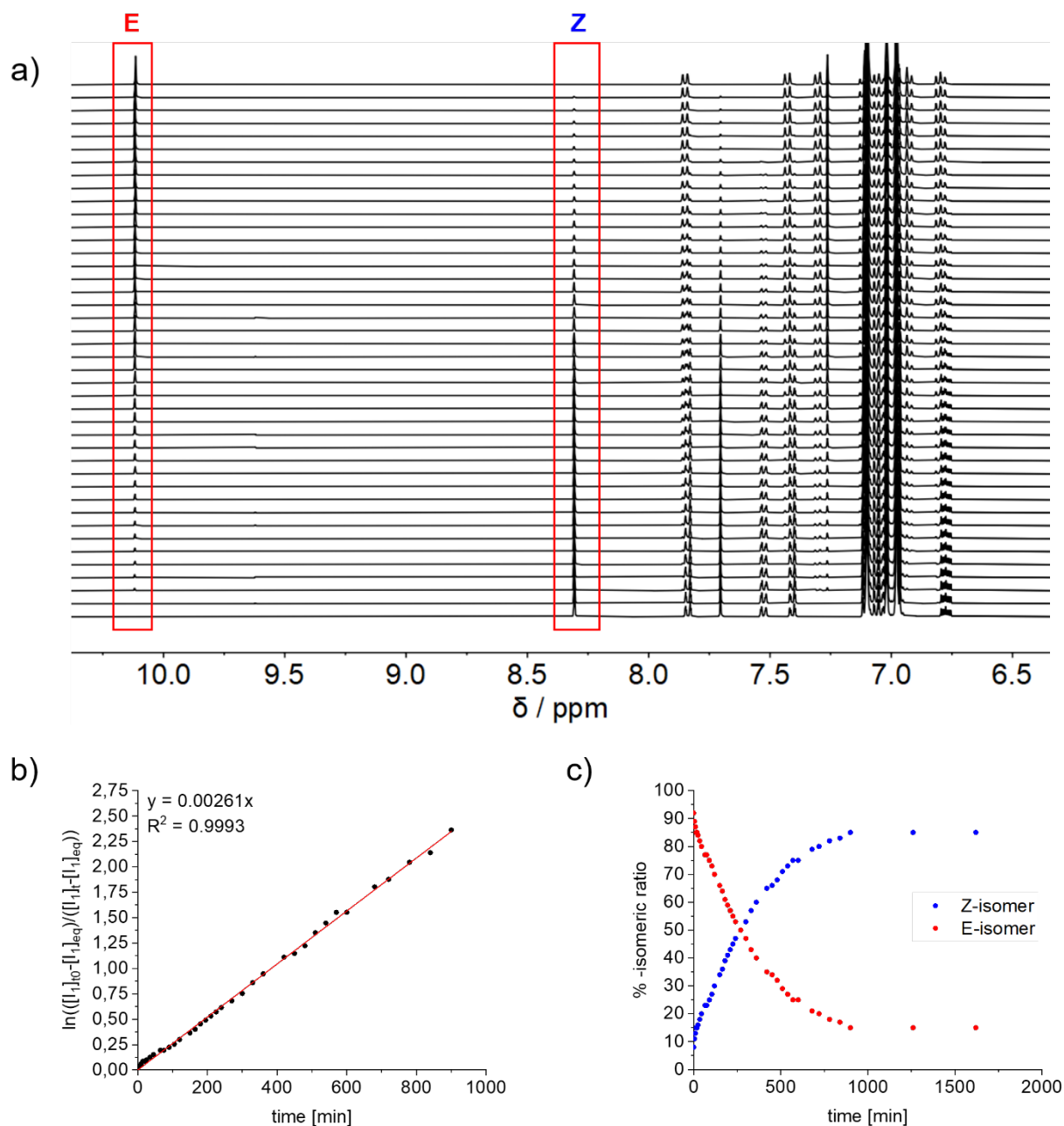
Figure S 47: Kinetic analysis of the thermal *E* to *Z* isomerization of compound **2** at 23 °C in DMSO-*d₆* in the dark. a) Change in absorbance of compound **2** in DMSO-*d₆* monitored at 455 nm over time. b) UV/Vis spectra of compound **2** in DMSO-*d₆* before irradiation (blue line), after irradiation with 450 nm light (red line) and after 40 h in darkness at 23 °C (black line). c) Increase in absorbance of compound **2** in DMSO-*d₆* with TFA (1:1) monitored at 455 nm over time. d) UV/Vis spectra of compound **2** in DMSO-*d₆* taken before irradiation (blue line), after irradiation with 450 nm light (red line) and after 21 h in darkness at 23 °C (black line). Thermal double bond isomerization is slower without TFA compared to with TFA (1:1) addition.
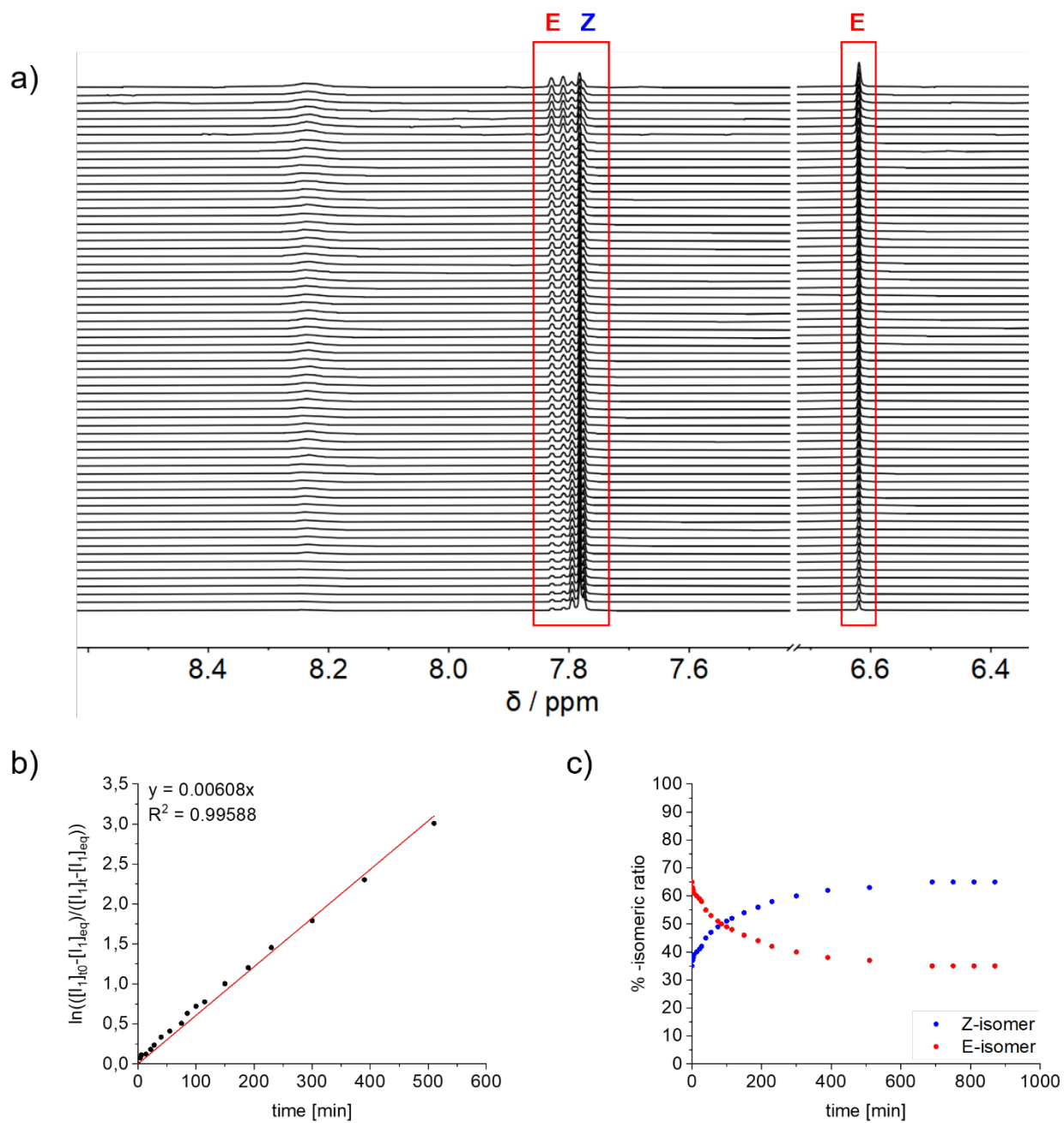
Figure S 48: Kinetic analysis of thermal *E* to *Z* isomerization of compound **3** at 70 °C in toluene-d_8 in the dark. a) Indicative ^{1}H NMR (500 MHz, toluene-d_8, 70 °C) signals that were used for determination of isomeric ratio; b) First order kinetic analysis of the thermal isomerization of *E* isomer. The first order rate constant for the thermal isomerization is obtained from the slope of the linear plot and is $k_{Z/E} = 3.95 \cdot 10^{-3}$ s^{-1}, which corresponds to a *Gibbs energy of activation* $\Delta G^* = 24.0$ kcal mol^{-1}; c) Changing isomeric ratio over time determined by integration of ^{1}H NMR signals.
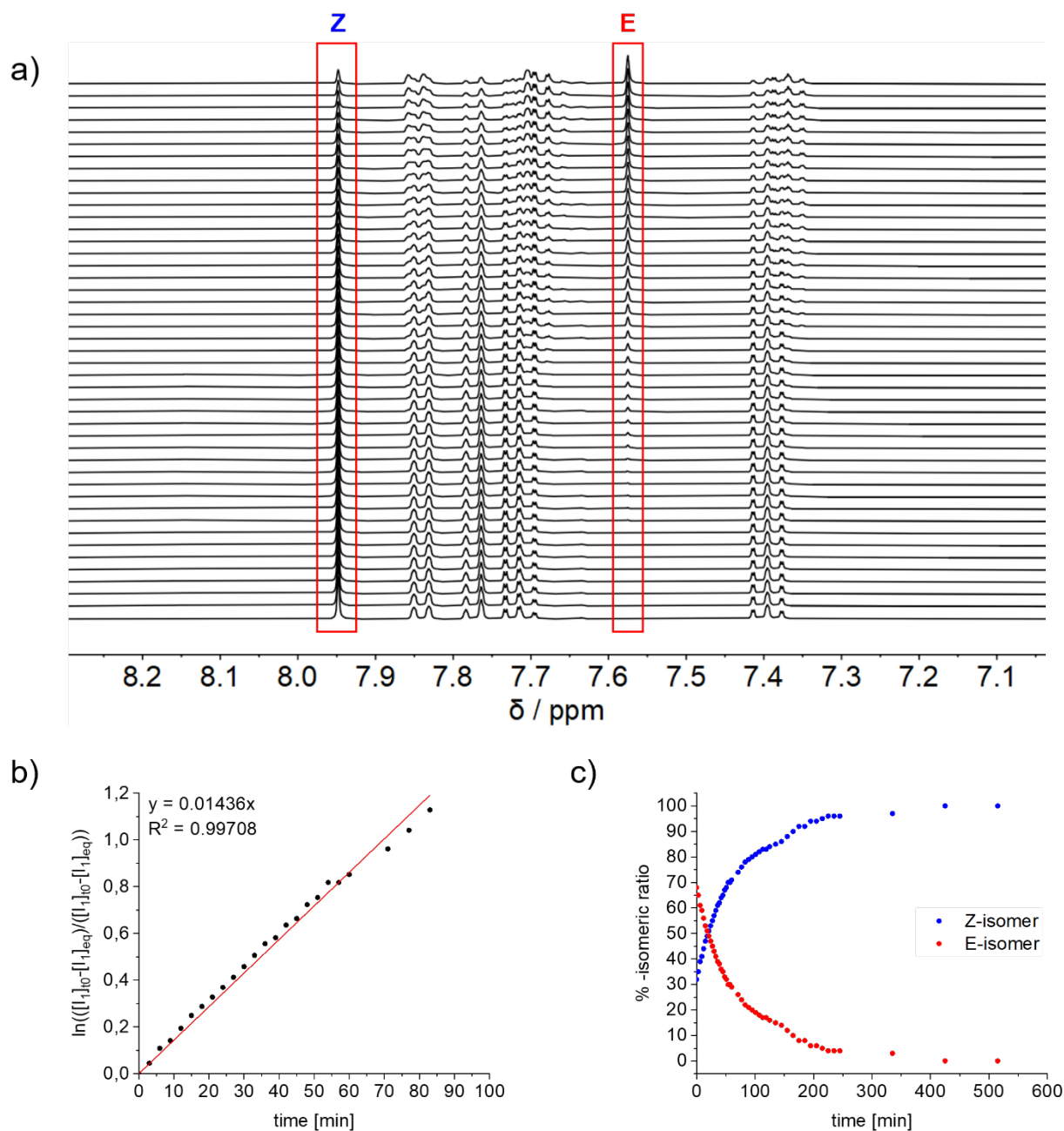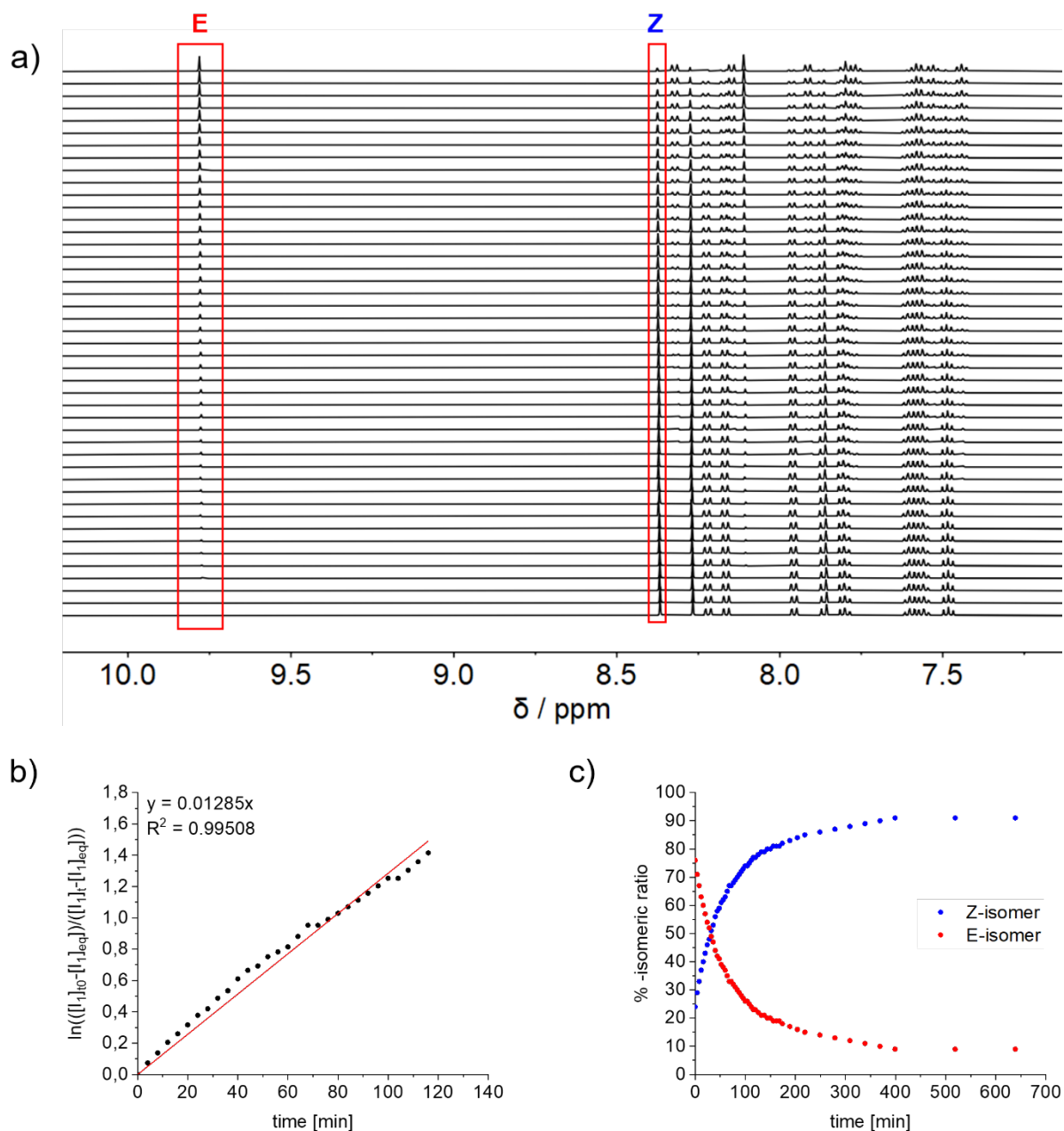
Figure S 49: Kinetic analysis of thermal *E* to *Z* isomerization of compound **3** at 40 °C in DMSO-*d₆* in the dark. a) Indicative ¹H NMR (400 MHz, DMSO-*d₆*, 40 °C) signals that were used for determination of isomeric ratio; b) First order kinetic analysis of the thermal isomerization of *E* isomer. The first order rate constant for the thermal isomerization is obtained from the slope of the linear plot and is $k_{E \to Z}$ = 1.34 · 10^{-2} s^{-1}, which corresponds to a *Gibbs energy of activation* ΔG^* = 21.0 kcal mol^{-1}; c) Changing isomeric ratio over time determined by integration of ¹H NMR signals.
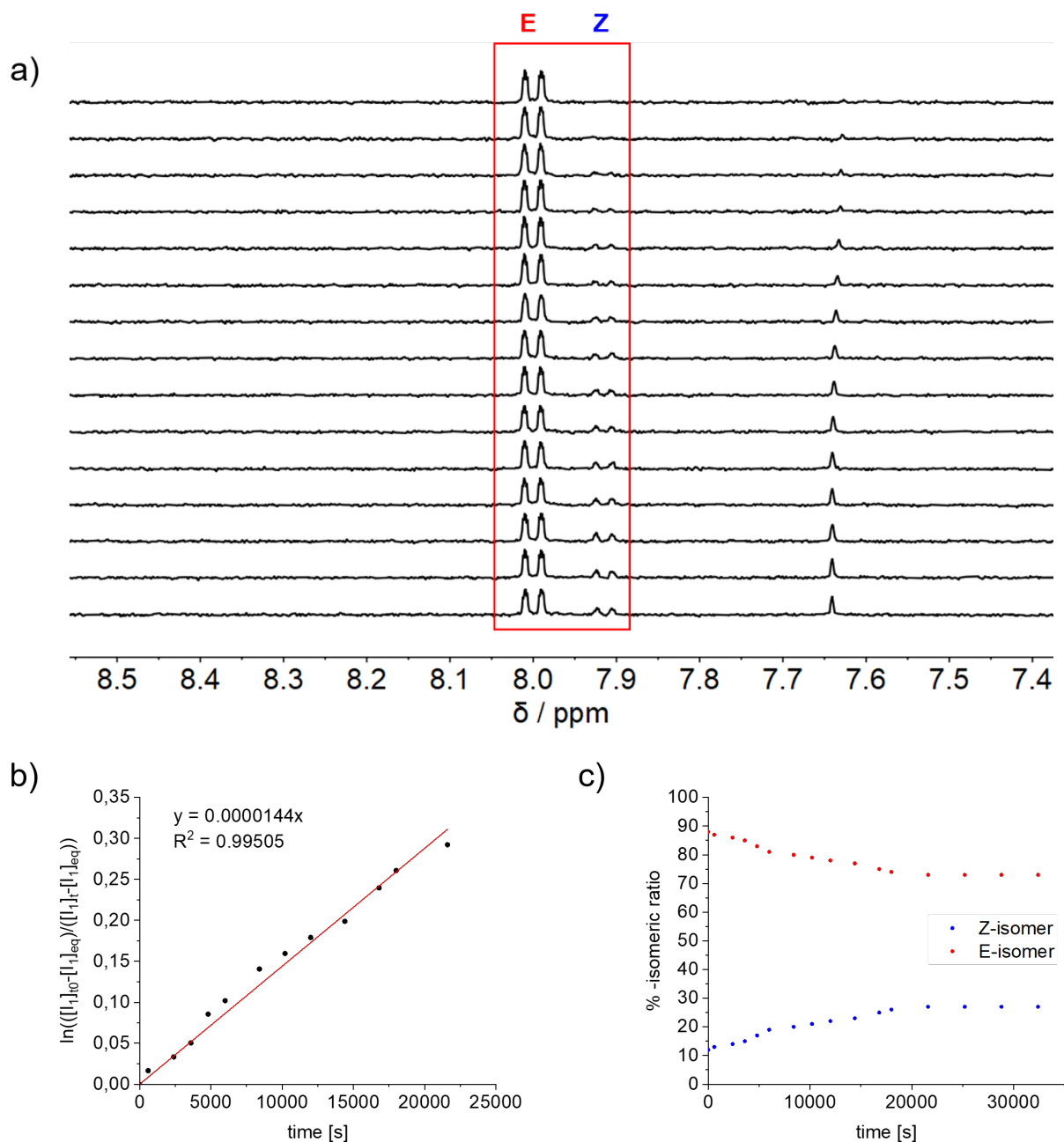
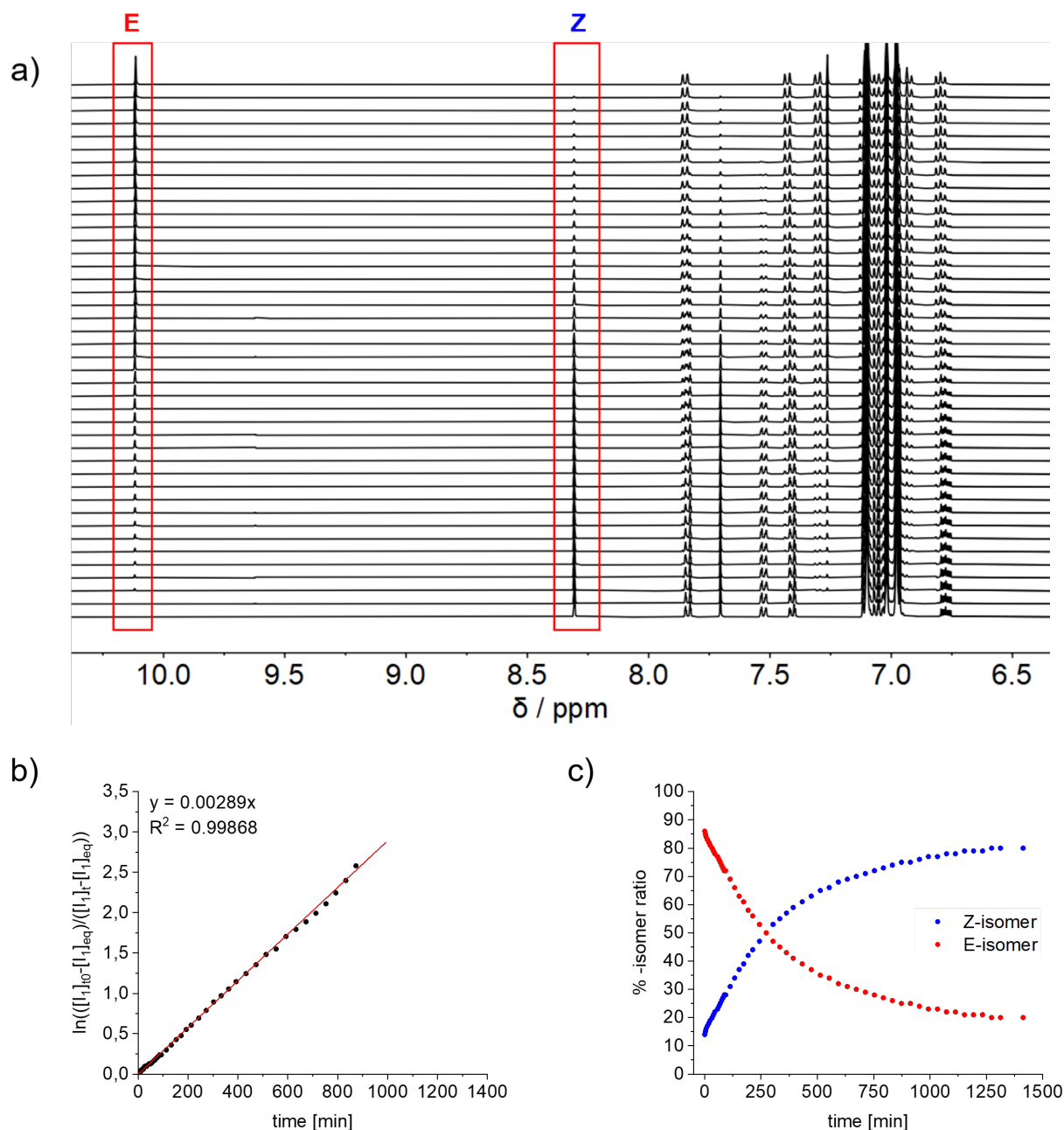**Figure S 50:** Kinetic study of the thermal isomerization of *E* to *Z* of compound **4** at 100 °C in toluene-d_8 in the dark. a) Indicative ^{1}H NMR (400 MHz, toluene-d_8, 26 °C) signals to determine the isomer ratio; b) Kinetic analysis of the first-order thermal isomerization of the *E* isomer. The first-order rate constant for thermal isomerization is derived from the slope of the linear plot and is $k_{Z/E}$ = 1.05 · 10^{-5} s^{-1}, representing a *Gibbs energy of activation* Δ*G** = 30.5 kcal mol^{-1}; c) Change in isomer ratio over time measured by integration of the ^{1}H NMR signals.

Figure S 51: Kinetic analysis of thermal E to Z isomerization of compound **4** at 22 °C in DMSO-d_6 in the dark. a) Indicative ^{1}H NMR (400 MHz, DMSO-d_6, 22 °C) signals that were used for determination of isomeric ratio; b) First order kinetic analysis of the thermal isomerization of E isomer. The first order rate constant for the thermal isomerization is obtained from the slope of the linear plot and is $k_{Z/E} = 1.43 \cdot 10^{-3}$ s^{-1}, which corresponds to a *Gibbs energy of activation* $\Delta G^* = 21.1$ kcal mol^{-1}; c) Changing isomeric ratio over time determined by integration of ^{1}H NMR signals.

Figure S 52: Kinetic analysis of thermal *E* to *Z* isomerization of compound **5** at 30 °C in THF-*d₈* in the dark. a) Indicative ¹H NMR (400 MHz, THF-*d₈*, 30 °C) signals that were used for determination of isomeric ratio; b) First order kinetic analysis of the thermal isomerization of *E* isomer. The first order rate constant for the thermal isomerization is obtained from the slope of the linear plot and is $k_{E \rightarrow Z}$ = 1.33 · 10^{-2} s⁻¹, which corresponds to a *Gibbs energy of activation* ΔG^{*} = 20.4 kcal mol⁻¹; c) Changing isomeric ratio over time determined by integration of ¹H NMR signals.

Figure S 53: Kinetic analysis of the thermal isomerization of *E* to *Z* of compound **6** at 55 °C in THF-*d₈* in the dark. a) Indicative ¹H NMR (400 MHz, THF-*d₈*, 55 °C) signals used to determine the isomer ratio; b) Kinetic analysis of the first-order thermal isomerization of the *E* isomer. The first-order rate constant for thermal isomerization is inferred from the slope of the linear plot and is $k_{E \to Z}$ = 5.97 · 10^{-3} s⁻¹, corresponding to a *Gibbs energy of activation* ΔG^* = 22.6 kcal mol⁻¹; c) Change in isomer ratio over time determined by integration of the ¹H NMR signals.

Figure S 54: Kinetic analysis of thermal *E* to *Z* isomerization of compound **7** at 55 °C in THF-*d₈* in the dark. a) Indicative ¹H NMR (400 MHz, THF-*d₈*, 55 °C) signals that were used for determination of isomeric ratio; b) First order kinetic analysis of the thermal isomerization of *E* isomer. The first order rate constant for the thermal isomerization is obtained from the slope of the linear plot and is $k_{Z/E}$ = 8.21 · 10⁻³ s⁻¹, which corresponds to a *Gibbs energy of activation* Δ*G** = 22.4 kcal mol⁻¹; c) Changing isomeric ratio over time determined by integration of ¹H NMR signals.

Figure S 55: Kinetic analysis of the thermal isomerization of *E* to *Z* of compound **9** at 100 °C in toluene-d_8 in the dark. a) Indicative ^{1}H NMR (400 MHz, toluene-d_8, 26 °C) signals used to determine the isomer ratio; b) Kinetic analysis of the first-order thermal isomerization of the *E* isomer. The first-order rate constant for thermal isomerization is inferred from the slope of the linear plot and is $k_{Z/E}$ = 2.61 · 10^{-3} s^{-1}, corresponding to a *Gibbs energy of activation* ΔG^* = 26.5 kcal mol^{-1}; c) Change in isomer ratio over time determined by integration of the ^{1}H NMR signals.

Figure S 56: Kinetic analysis of thermal *E* to *Z* isomerization of compound **9** at 40 °C in DMSO-d_6 in the dark. a) Indicative ^{1}H NMR (500 MHz, DMSO-d_6, 40 °C) signals that were used for determination of isomeric ratio; b) First order kinetic anaylsis of the thermal isomerization of *E* isomer. The first order rate constant for the thermal isomerization is obtained from the slope of the linear plot and is $k_{Z/E}$ = 1.17 · 10^{-2} s^{-1}, which corresponds to a *Gibbs energy of activation* ΔG^* = 21.1 kcal mol^{-1}; c) Changing isomeric ratio over time determined by integration of ^{1}H NMR signals.
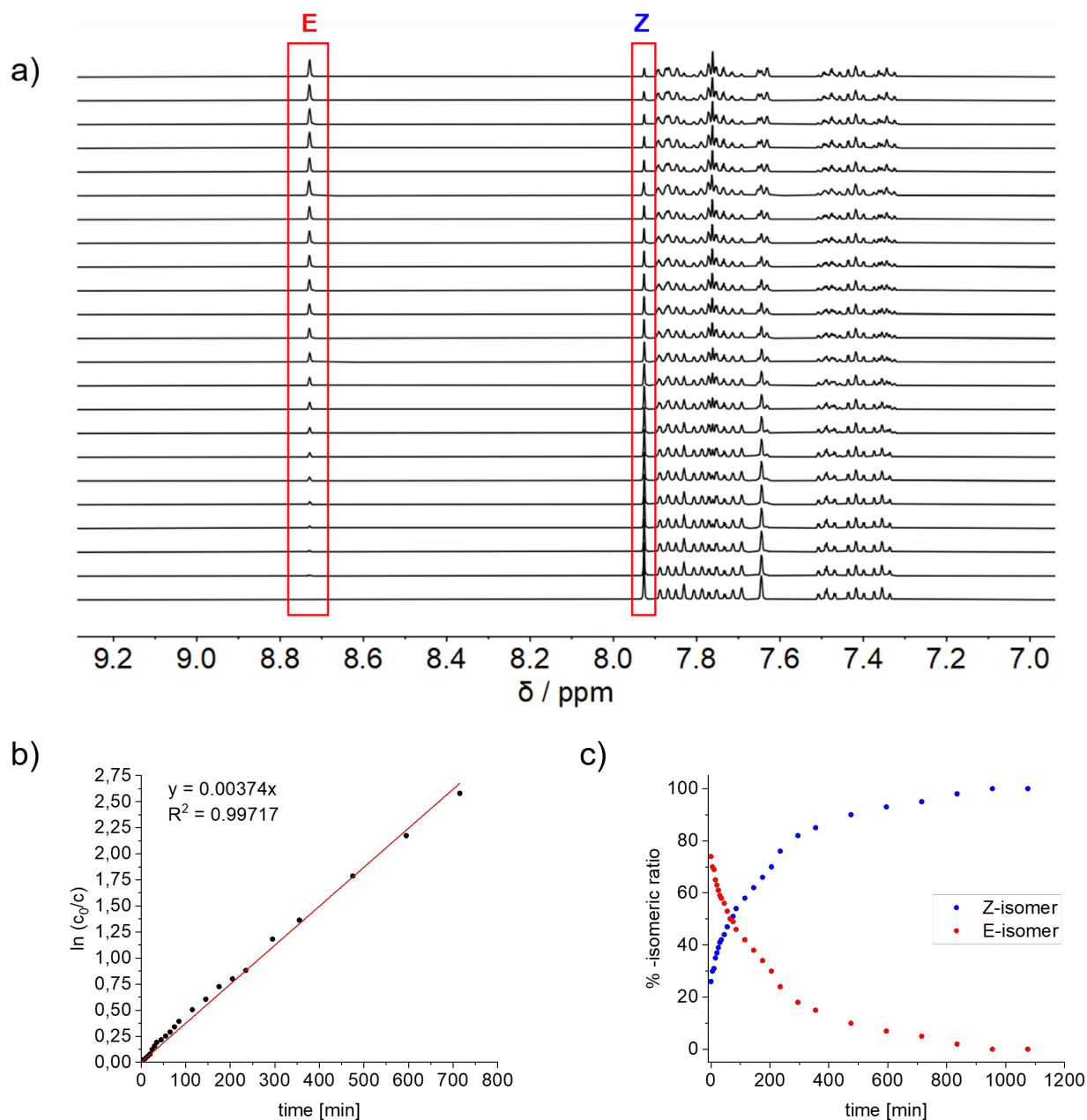
Figure S 57: Kinetic analysis of thermal *E* to *Z* isomerization of compound **10** at 90 °C in DMSO-d_6 in the dark. a) Indicative ^{1}H NMR (400 MHz, DMSO-d_6, 26 °C) signals that were used for determination of isomeric ratio; b) First order kinetic analysis of the thermal isomerization of *E* isomer. The first order rate constant for the thermal isomerization is obtained from the slope of the linear plot and is $k_{E \to Z}$ = 3.40 · 10^{-3} s^{-1}, which corresponds to a *Gibbs energy of activation* ΔG^* = 25.5 kcal mol^{-1}; c) Changing isomeric ratio over time determined by integration of ^{1}H NMR signals.

Figure S 58: Kinetic analysis of the thermal isomerization of *E* to *Z* of compound **11** at 70 °C in DMSO-d_6 in the dark. a) Indicative ^{1}H NMR (500 MHz, DMSO-d_6, 70 °C) signals used to determine the isomer ratio; b) Kinetic analysis of the first-order thermal isomerization of the *E* isomer. The first-order rate constant for thermal isomerization is inferred from the slope of the linear plot and is $k_{Z/E}$ = 2.31 ·10^{-3} s^{-1}, corresponding to a *Gibbs energy of activation* ΔG^* = 24.3 kcal mol^{-1}; c) Change in isomer ratio over time determined by integration of the ^{1}H NMR signals.

Measurement of the Quantum Yield

For determination of photoisomerization quantum yields a published procedure was used.[5,6]

Photoisomerization quantum yield Φ is defined as the ratio of the number of isomerized molecules *n(isomerized molecules)* and the number of absorbed photons *n(absorbed photons)*:

$$\Phi = \frac{n(isomerized\ molecules)}{n(absorbed\ photons)} \qquad \text{(eq.15)}$$

To obtain the photoisomerization quantum yield Φ, a sample with known concentration was prepared in tetrahydrofuran, acetonitrile, or DMSO and was irradiated with a focused LED beam of 415 nm, 450 nm and 505 nm. The number of absorbed photons *n(absorbed photons)* were received directly from the measured change of power ΔP at the thermal photometer:

$$n(h\nu) = \frac{\Delta P \cdot \lambda_{exc} \cdot t}{c \cdot h} \qquad \text{(eq.16)}$$

with speed of light c ($2.99792 \cdot 10^8\ \text{m·s}^{-1}$) and the Planck constant h ($6.62607 \cdot 10^{-34}$ Js). The excitation wavelength is given as λ_{exc} in meter and t is the irradiation period. The change of power ΔP is obtained by the difference of the power of the blank sample (P_0) and the power of the sample (P_t) in the indicated irradiation time intervals.

The rate of the photoisomerization from E to E depends on the concentration of E isomer present during irradiation and can be described by the following equitation:

$$r_{Z \to E} = \Phi_{Z \to E} \cdot I_0 \cdot \varepsilon_Z \cdot d \cdot [Z] \cdot \left(\frac{1 - e^{-d\varepsilon_E[E]}}{d \cdot \varepsilon_E \cdot [E]}\right) \qquad \text{(eq.17)}$$

with the photoisomerization quantum yield for the phototransition from Z to E isomer $\Phi_{Z \to E}$, the photon flux I_0 ($\text{L}^{-1}\text{s}^{-1}$), the molar extinction coefficient of Z and E isomer at the wavelength of irradiation ε_Z, ε_E and the pathway of the cuvette d.

Table S 10: Comparison of the quantum yields for the compounds **1**, **3** – **7**, **9** – **10** and **18** (for comparison with the independently measured, literature reported value of 23%).

compound	solvent	irr. wavelength [nm]	Φ (Z to E) in %	Φ (E to Z) in %
1	acetonitrile	415	43	
		505		17
	tetrahydrofuran	415	69	
		515		43
3	toluene	405	34	
		490		17
4	THF	405	65	
		565		41
	DMSO	430	36	
		530		43
5	tetrahydrofuran	450	35	
		505		26
6	tetrahydrofuran	405	42	
		530		54
7	tetrahydrofuran	405	39	
		530		48
9	toluene	450	53	
10	acetonitrile	415	19	
		505		8
18[7]	CH$_2$Cl$_2$	415	25 (23)[7]	
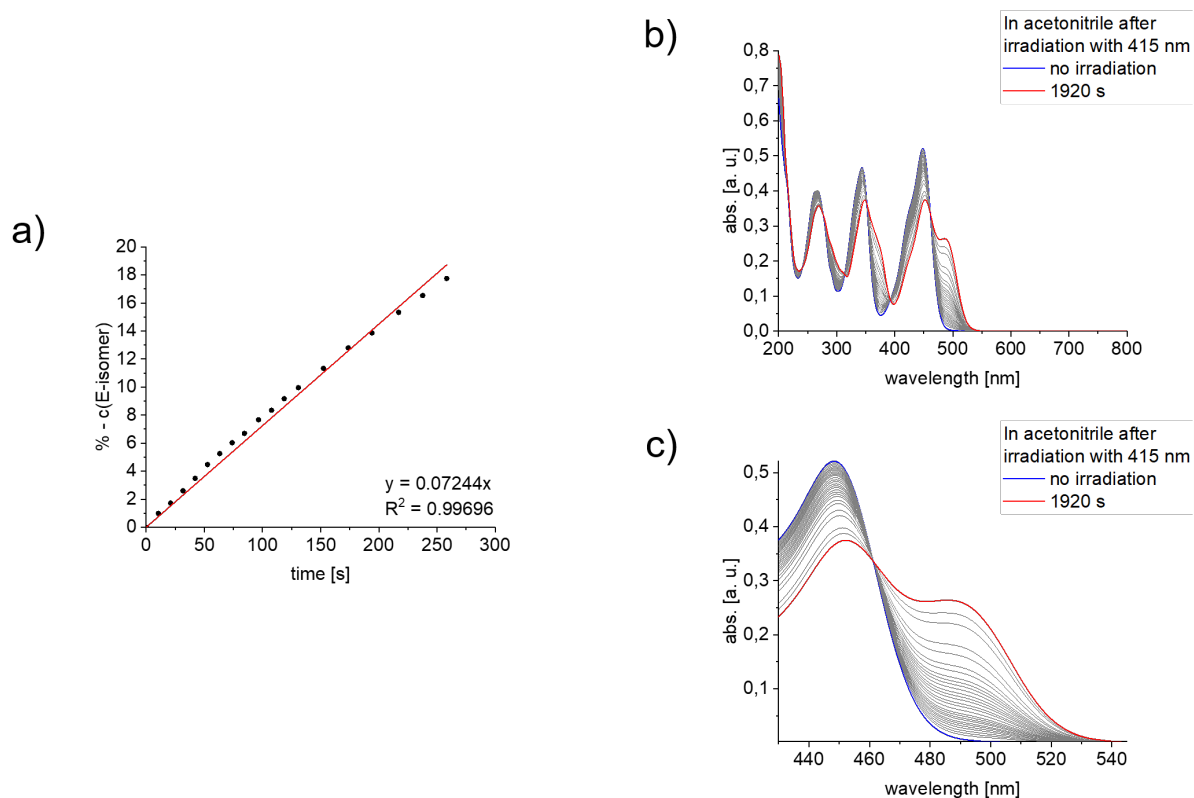
Figure S 59: Quantum yield determination of photoisomerization from *Z*-isomer to *E*-isomer of compound **1** in acetonitrile during irradiation with 415 nm; a) Plot of the change of concentration of *E*-isomer during phototransition by irradiation with 415 nm; b) UV/Vis absorption spectra received during irradiation of Het-HTI **1** with 415 nm in acetonitrile; c) UV/Vis spectrum excerpt: isosbestic point at 461 nm and the quantum yield was determined at 487 nm.
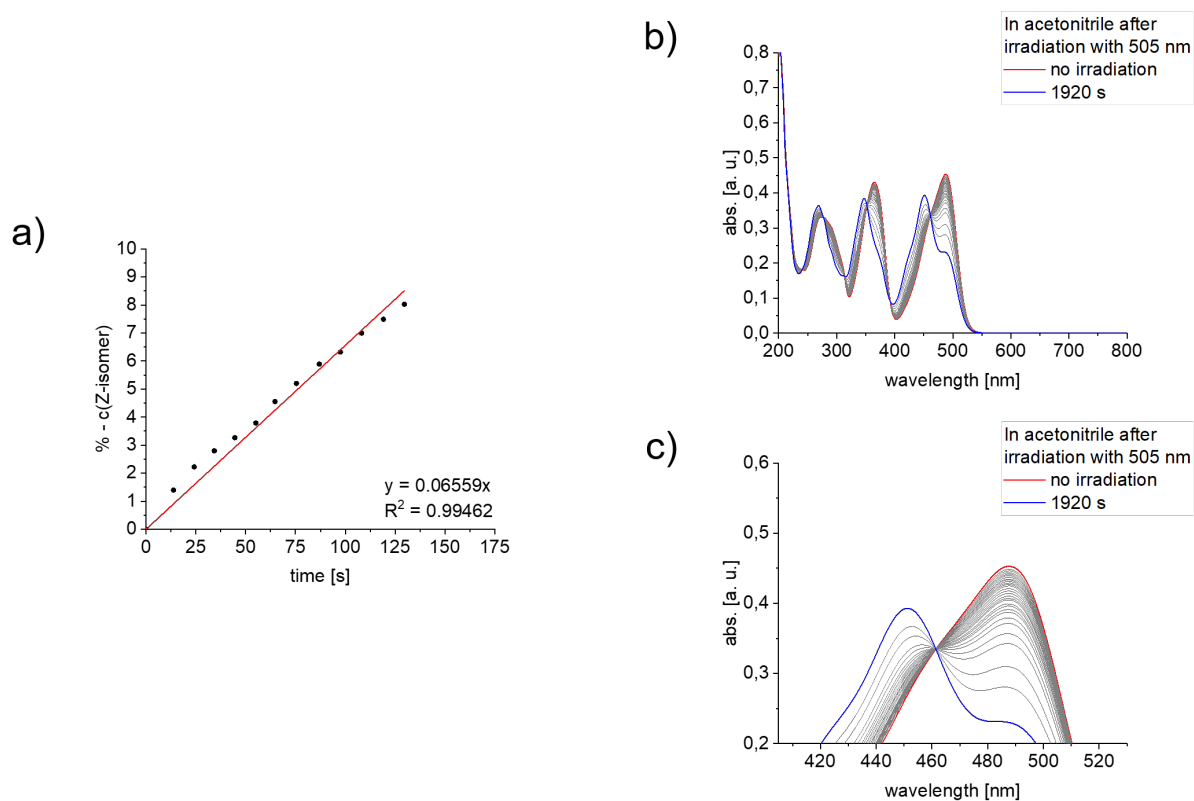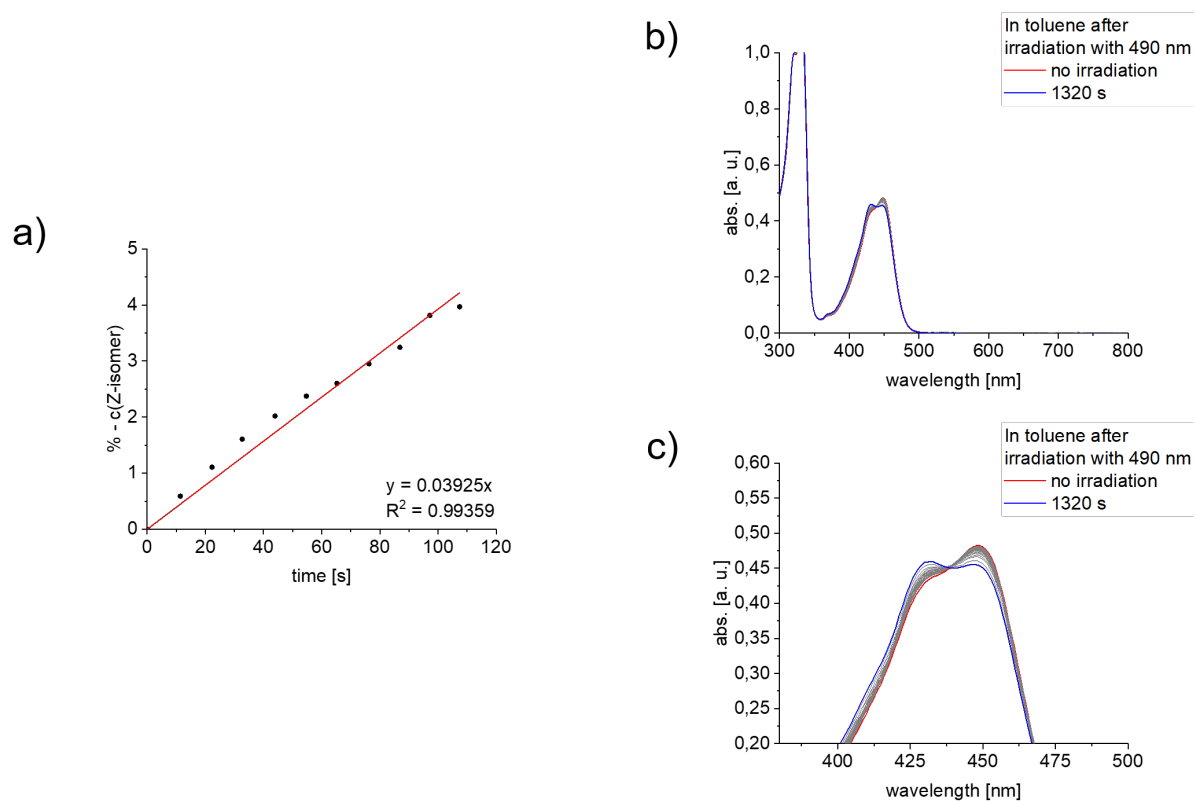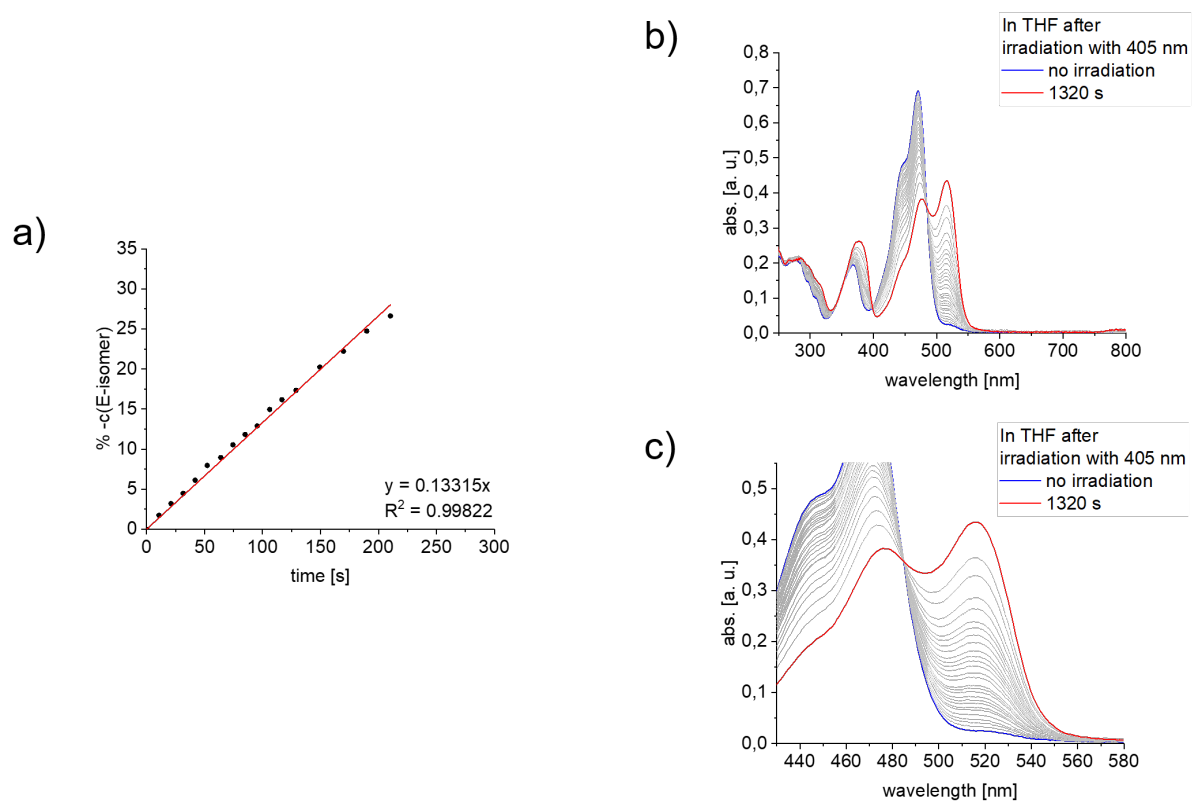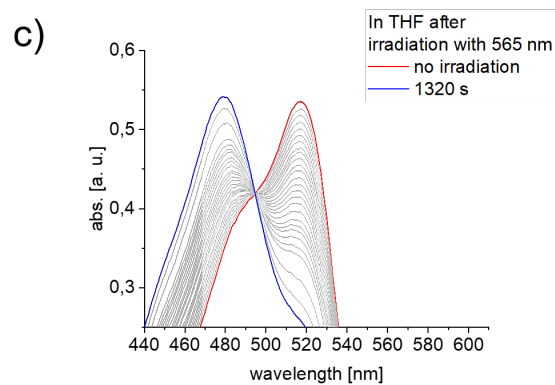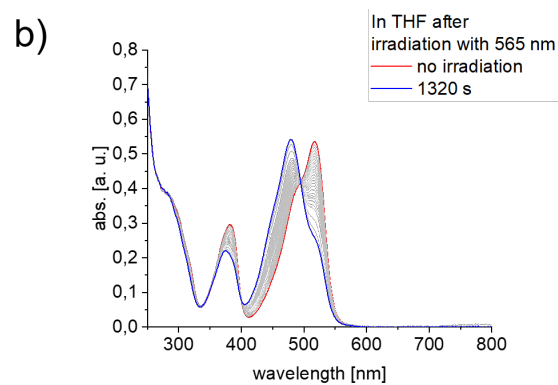
Figure S 60: Quantum yield determination of photoisomerization from *E*-isomer to *Z*-isomer of compound **1** in acetonitrile during irradiation with 505 nm; a) Plot of the concentration of *Z*-isomer during photoconversion by irradiation with 505 nm; b) UV/Vis absorption spectra received during irradiation of Het-HTI **1** with 505 nm in acetonitrile; c) UV/Vis spectrum excerpt: isosbestic point at 461 nm and the quantum yield was obtained at 450 nm.
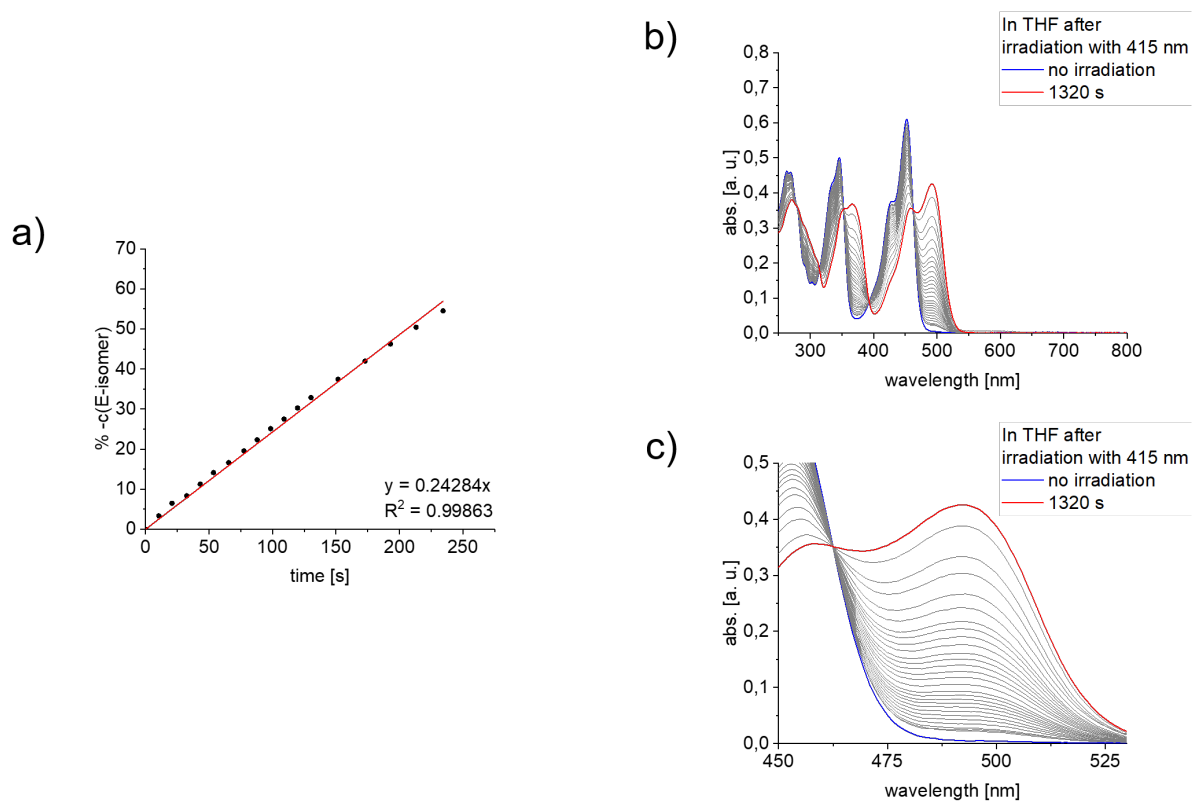
Figure S 61: Quantum yield determination of photoisomerization from *Z*-isomer to *E*-isomer of compound **1** in THF during irradiation with 415 nm; a) Plot of the concentration of *E*-isomer during photoconversion by irradiation with 415 nm; b) UV/Vis absorption spectra received during irradiation of Het-HTI **1** with 415 nm in tetrahydrofuran; c) UV/Vis spectrum excerpt: isosbestic point at 463 nm and the quantum yield was determined at 492 nm.
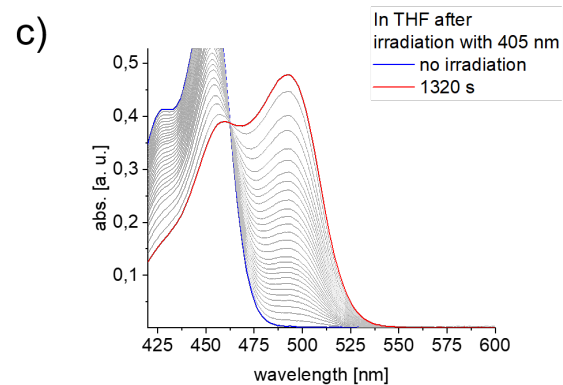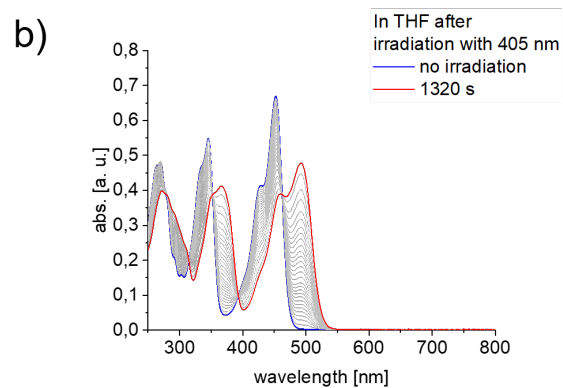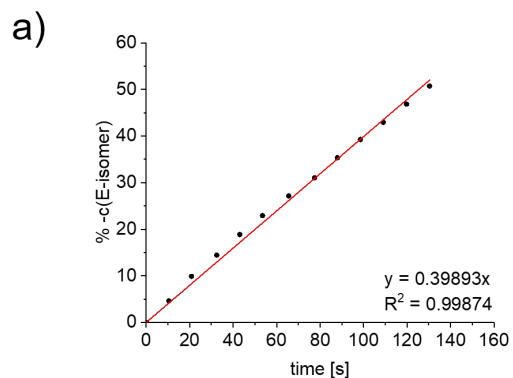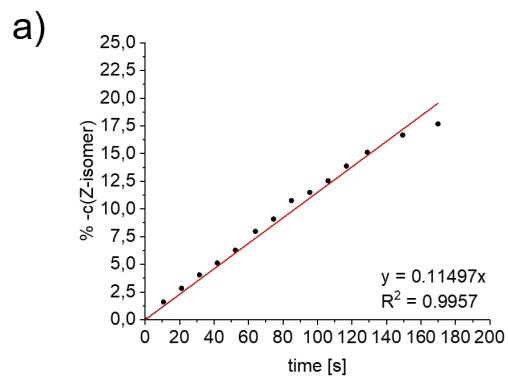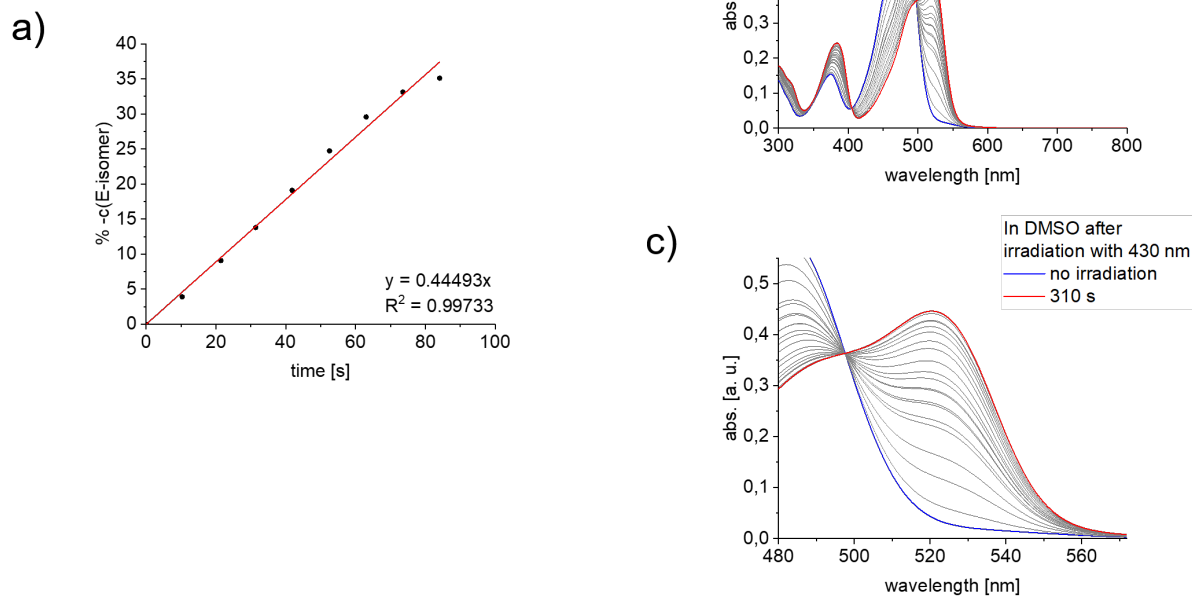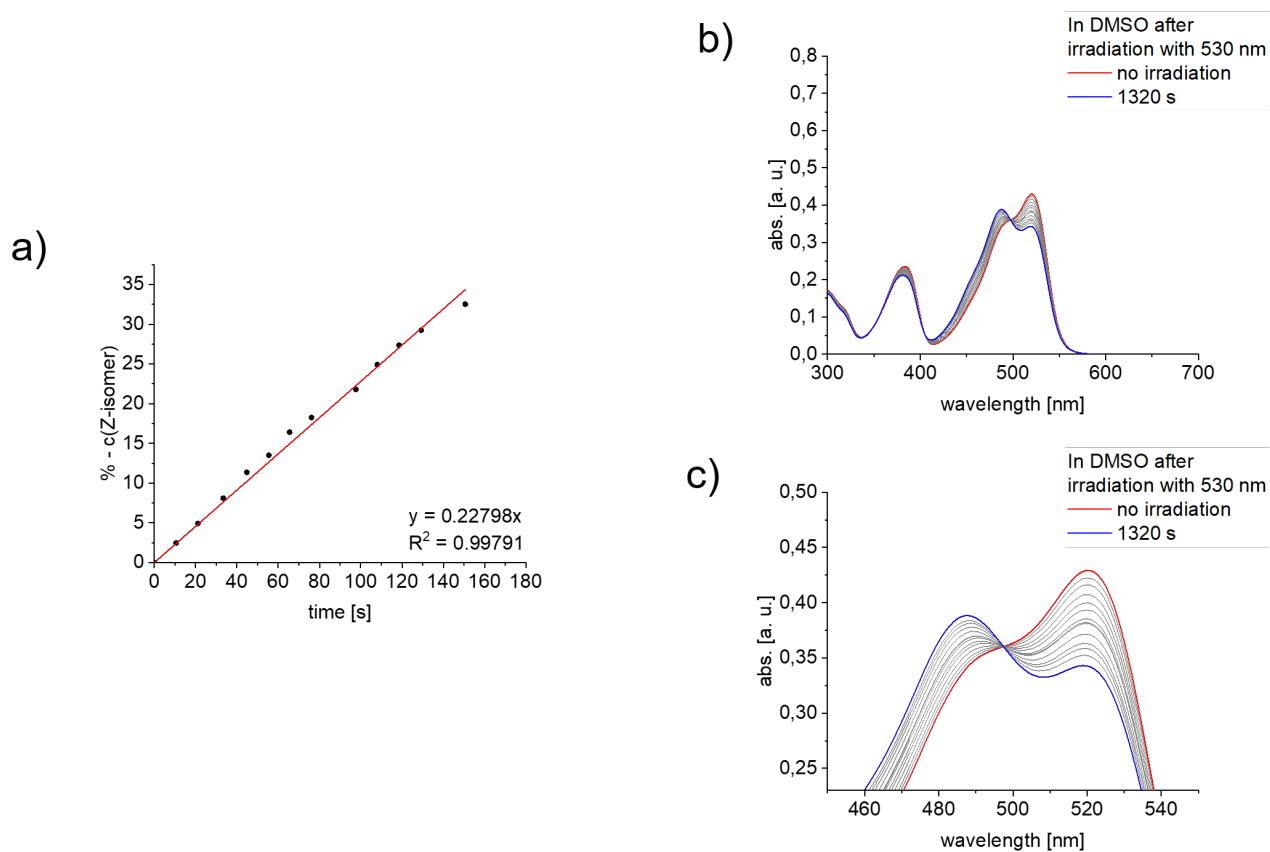
Figure S 62: Quantum yield determination of photoisomerization from *Z*-isomer to *E*-isomer of compound **1** in THF during irradiation with 405 nm; a) Plot of the concentration of *E*-isomer during photoconversion by irradiation with 405 nm; b) UV/Vis absorption spectra received during irradiation of Het-HTI **1** with 405 nm in tetrahydrofuran; c) UV/Vis spectrum excerpt: isosbestic point at 463 nm and the quantum yield was determined at 492 nm.
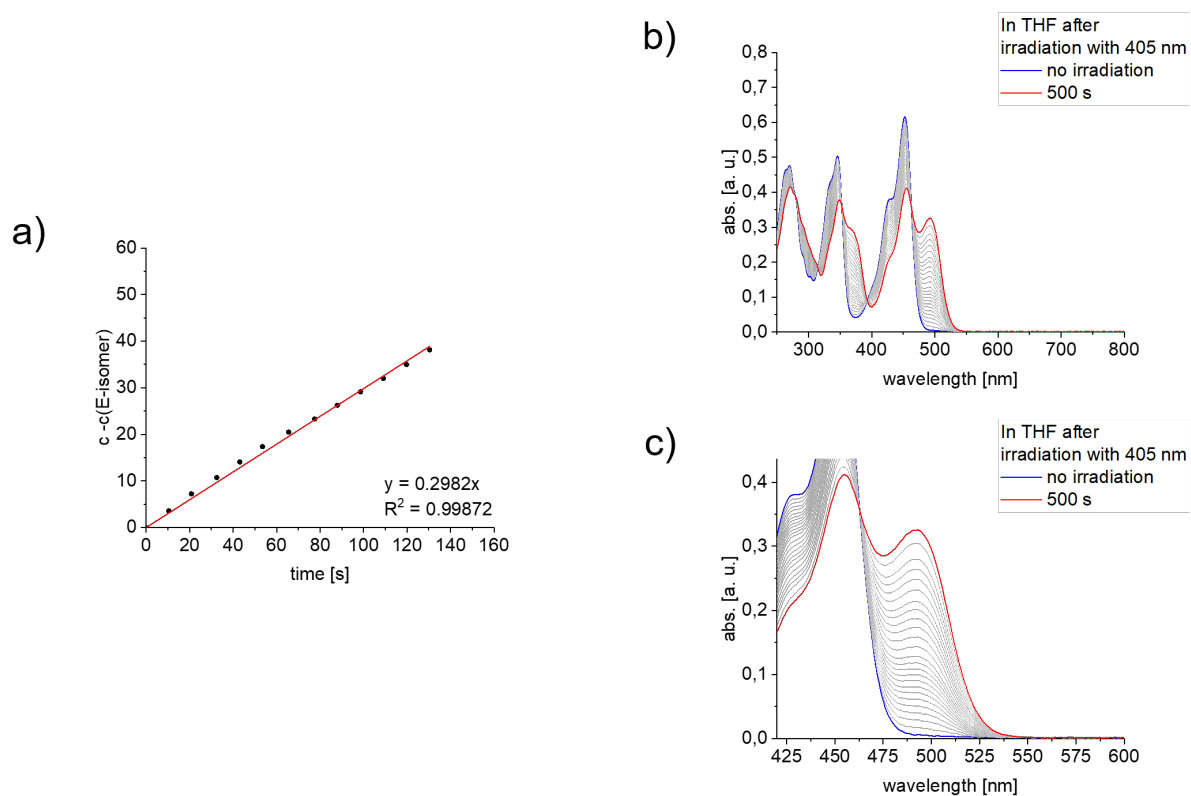
Figure S 63: Quantum yield determination of photoisomerization from *Z*-isomer to *E*-isomer of compound **1** in tetrahydrofuran during irradiation with 405 nm; a) Plot of the concentration of *E*-isomer during photoconversion by irradiation with 405 nm; b) UV/Vis absorption spectra received during irradiation of Het-HTI **1** with 405 nm in tetrahydrofuran; c) UV/Vis spectrum excerpt: isosbestic point at 463 nm and the quantum yield was determined at 492 nm.
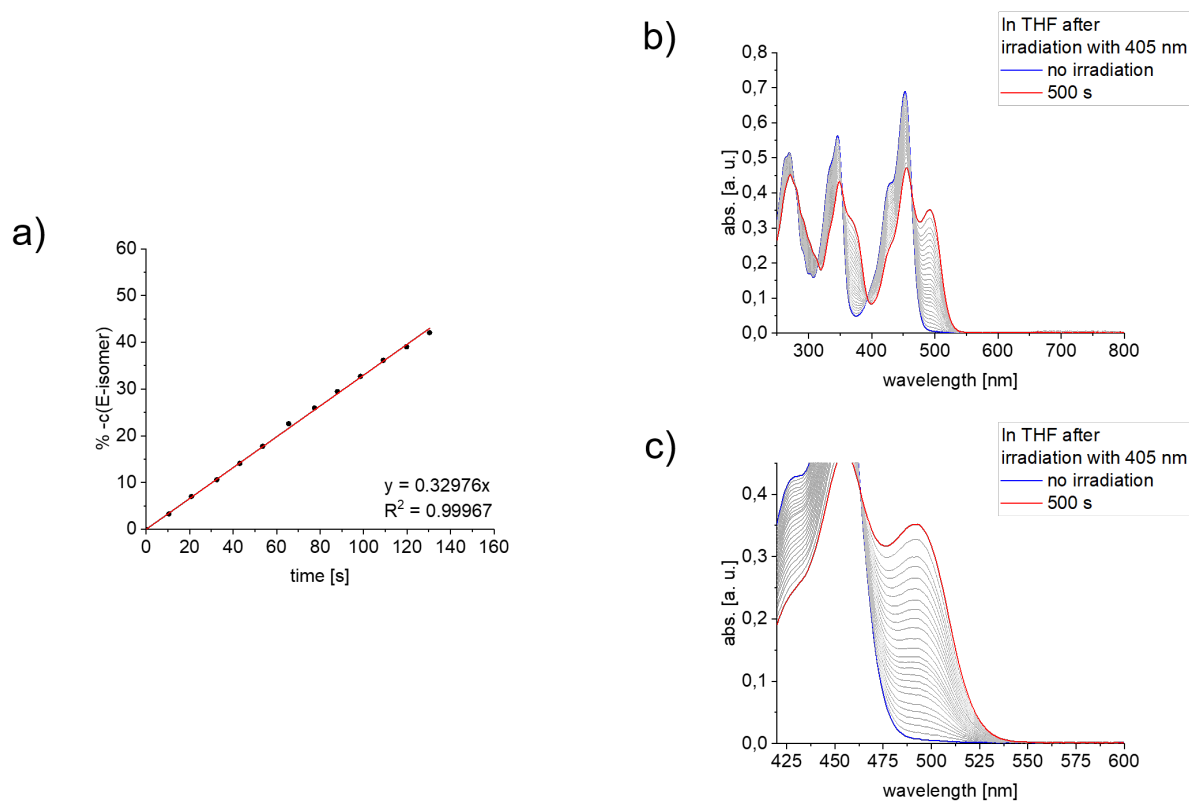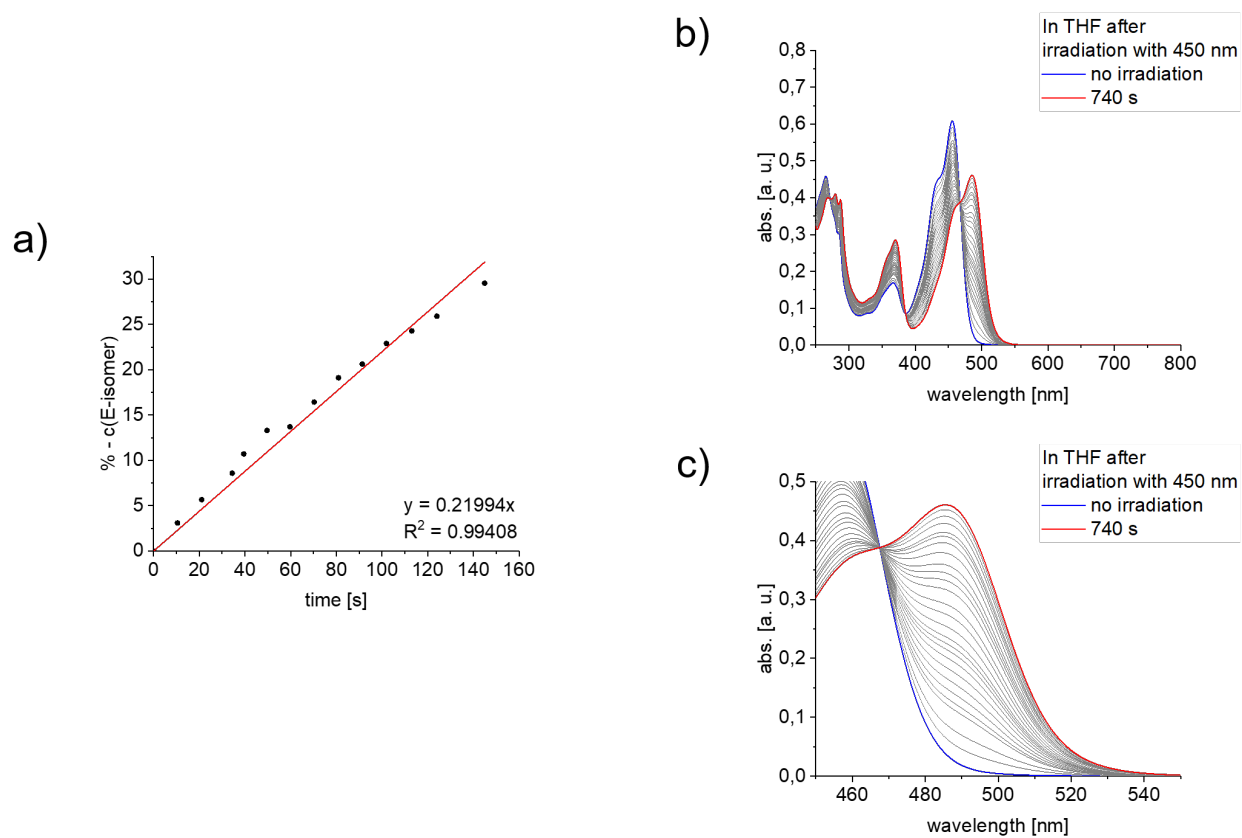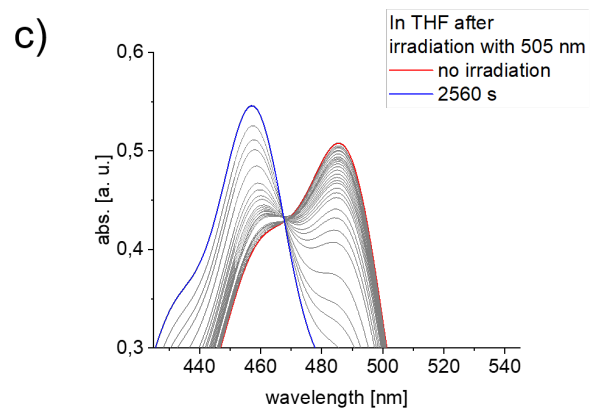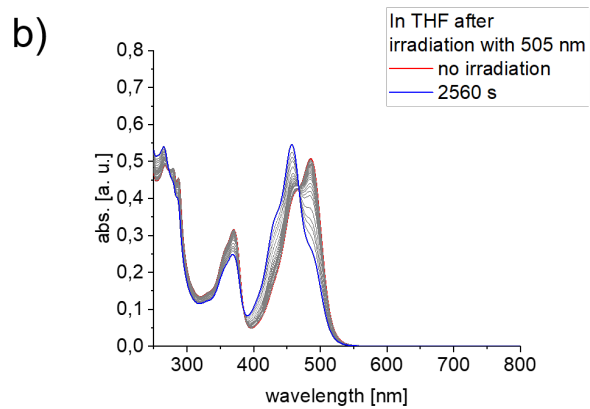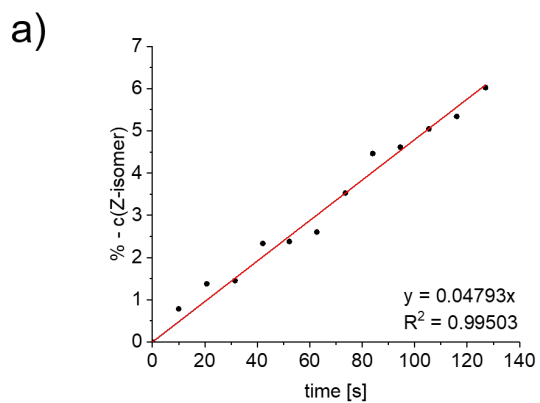
Figure S 64: Quantum yield determination of photoisomerization from *Z*-isomer to *E*-isomer of compound **1** in tetrahydrofuran during irradiation with 405 nm; a) Plot of the concentration of *E*-isomer during photoconversion by irradiation with 405 nm; b) UV/Vis absorption spectra received during irradiation of Het-HTI **1** with 405 nm in tetrahydrofuran; c) UV/Vis spectrum excerpt: isosbestic point at 463 nm and the quantum yield was determined at 492 nm.

Table S 11: Comparison of the quantum yields for compound **1** in THF. The average value of the measurement results is 69% and the standard deviation is 4%.

compound	solvent	irr. wavelength [nm]	Φ *(Z to E)* in %
1	THF	415	74
	THF	405	70
	THF	405	66
	THF	405	67
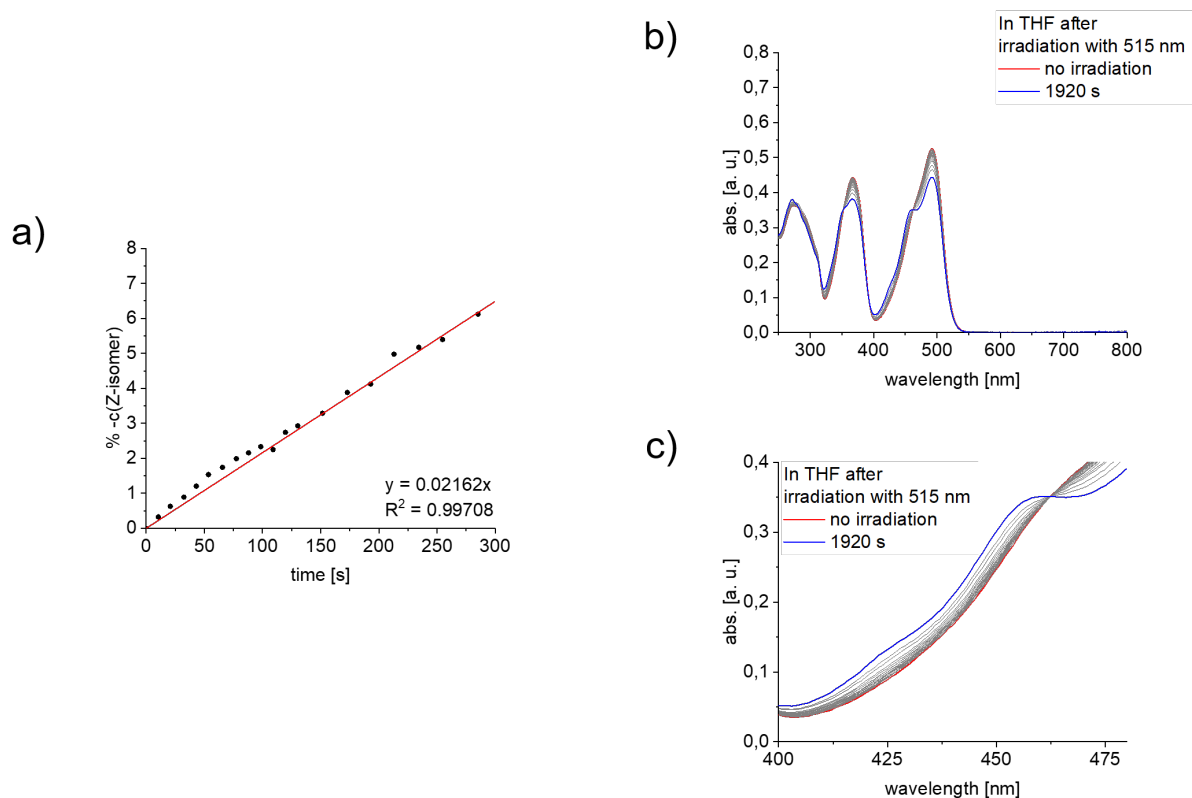
Figure S 65: Quantum yield determination of photoisomerization from *E*-isomer to *Z*-isomer of compound **1** in THF during irradiation with 515 nm light; a) Plot of the concentration of *Z*-isomer during photoconversion by irradiation with 515 nm; b) UV/Vis absorption spectra received during irradiation of Het-HTI **1** with 515 nm in tetrahydrofuran; c) UV/Vis spectrum excerpt: isosbestic point at 463 nm and the quantum yield was determined at 452 nm.
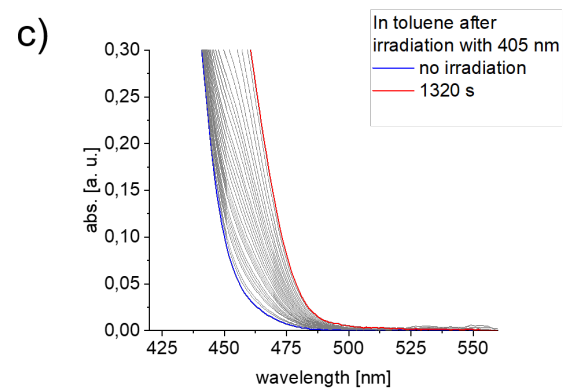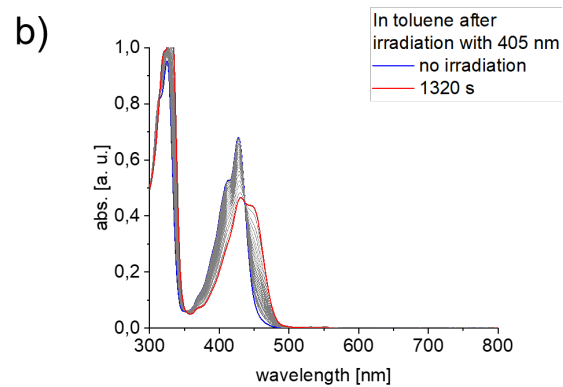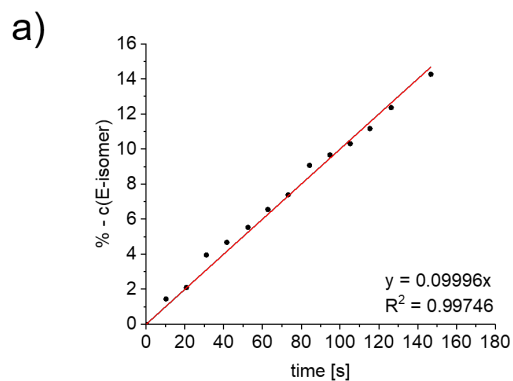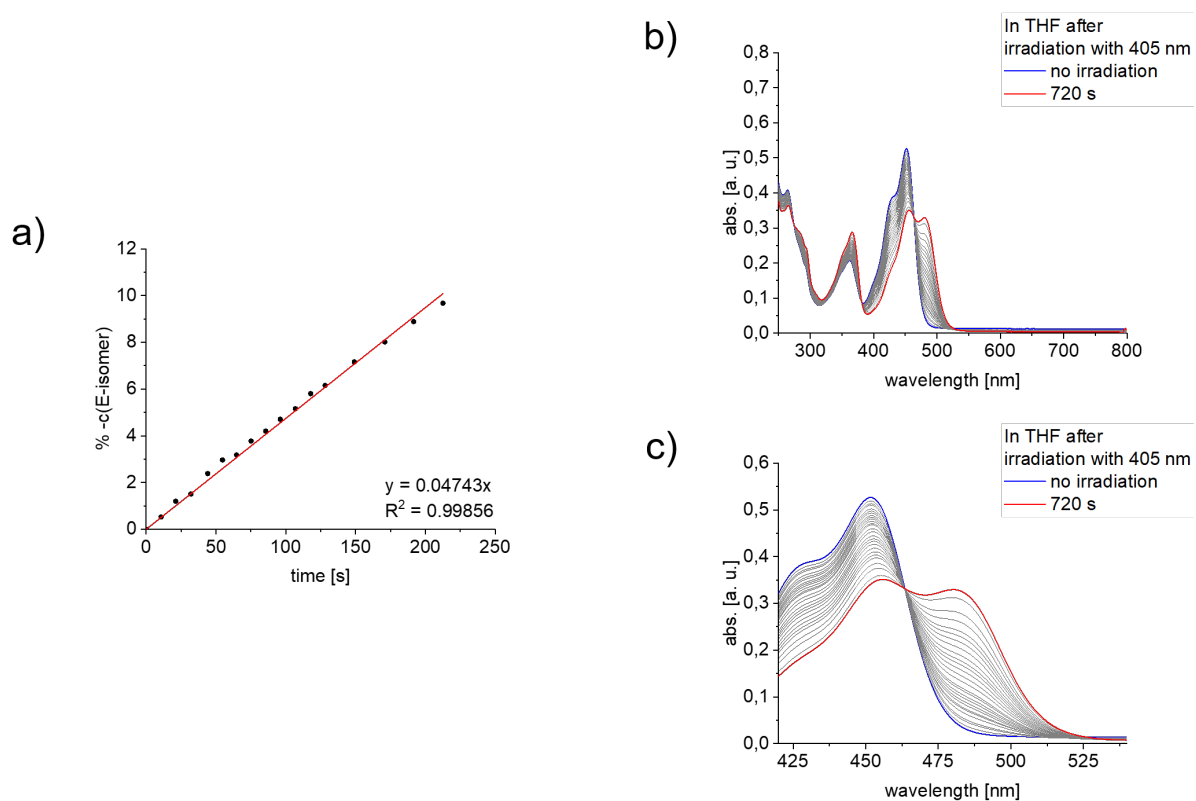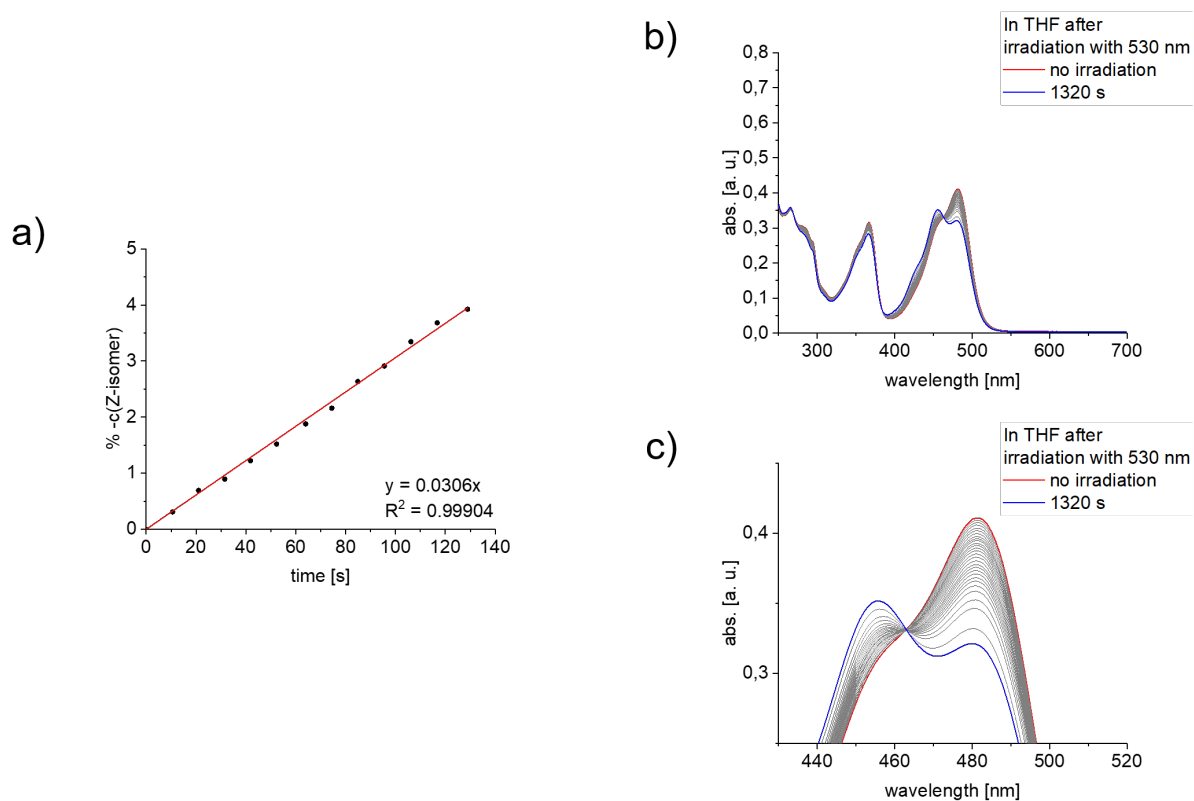
Figure S 66: Quantum yield determination of photoisomerization from *Z*-isomer to *E*-isomer of compound **3** in toluene during irradiation with 405 nm; a) Plot of the concentration of *E*-isomer during photoconversion by irradiation with 405 nm; b) UV/Vis absorption spectra received during irradiation of Het-HTI **3** with 405 nm in toluene; c) UV/Vis spectrum excerpt: isosbestic point at 437 nm and the quantum yield was determined at 451 nm.

a)

y = 0.03925x
R² = 0.99359

b) In toluene after irradiation with 490 nm
— no irradiation
— 1320 s

c) In toluene after irradiation with 490 nm
— no irradiation
— 1320 s

Figure S 67: Quantum yield determination of photoisomerization from *E*-isomer to *Z*-isomer of compound **3** in toluene during irradiation with 490 nm; a) Plot of the concentration of *Z*-isomer during photoconversion by irradiation with 490 nm; b) UV/Vis absorption spectra received during irradiation of Het-HTI **3** with 490 nm in toluene; c) UV/Vis spectrum excerpt: isosbestic point at 437 nm and the quantum yield was determined at 427 nm.
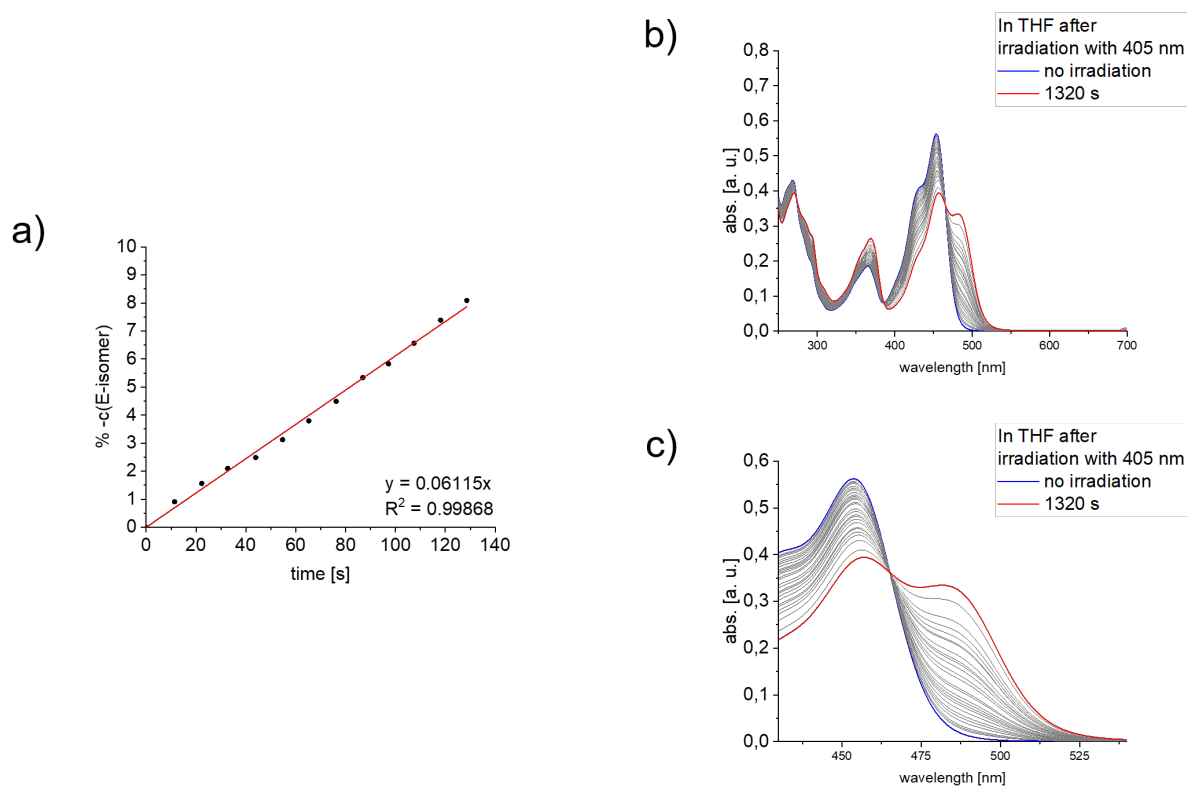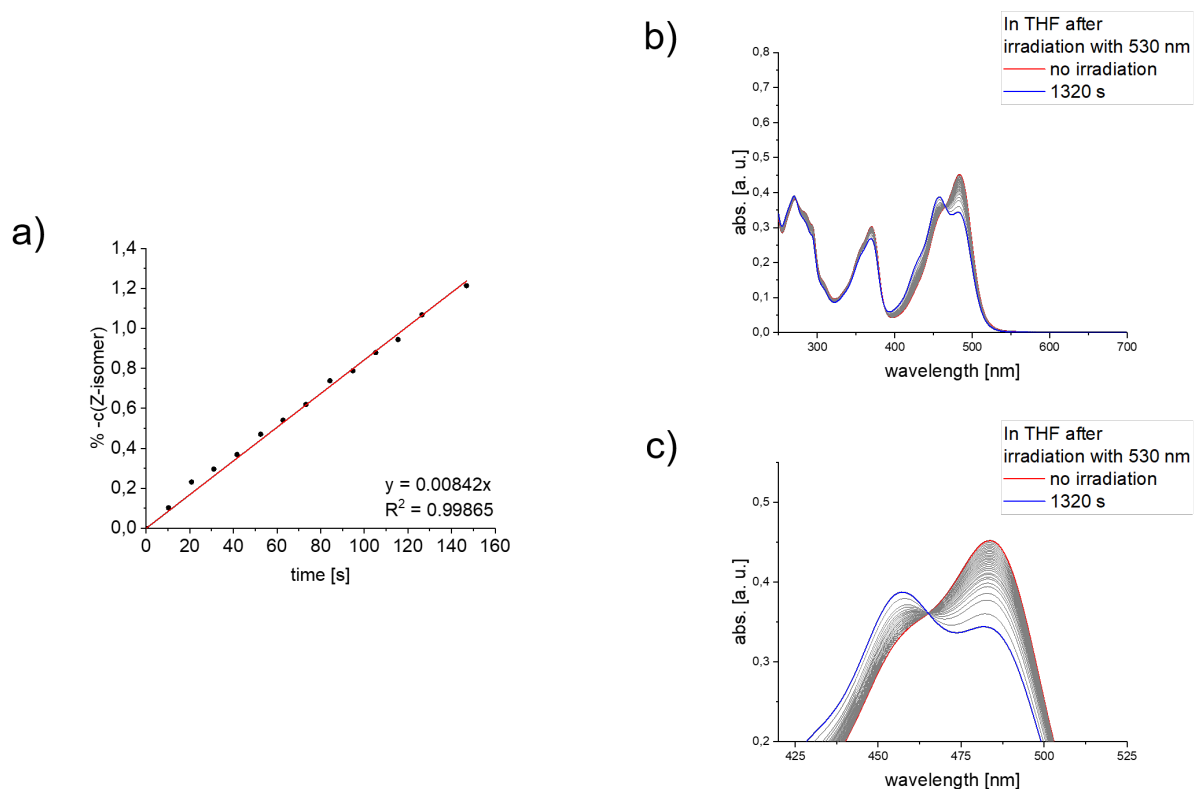
Figure S 68: Quantum yield determination of photoisomerization from *Z*-isomer to *E*-isomer of compound **4** in tetrahydrofuran during irradiation with 405 nm; a) Plot of the concentration of *E*-isomer during photoconversion by irradiation with 405 nm; b) UV/Vis absorption spectra received during irradiation of Het-HTI **4** with 405 nm in tetrahydrofuran; c) UV/Vis spectrum excerpt: isosbestic point at 495 nm and the quantum yield was determined at 516 nm.

Figure S 69: Quantum yield determination of photoisomerization from *E*-isomer to *Z*-isomer of compound **4** in tetrahydrofuran during irradiation with 565 nm; a) Plot of the concentration of *Z*-isomer during photoconversion by irradiation with 565 nm; b) UV/Vis absorption spectra received during irradiation of Het-HTI **4** with 565 nm in tetrahydrofuran; c) UV/Vis spectrum excerpt: isosbestic point at 495 nm and the quantum yield was determined at 471 nm.
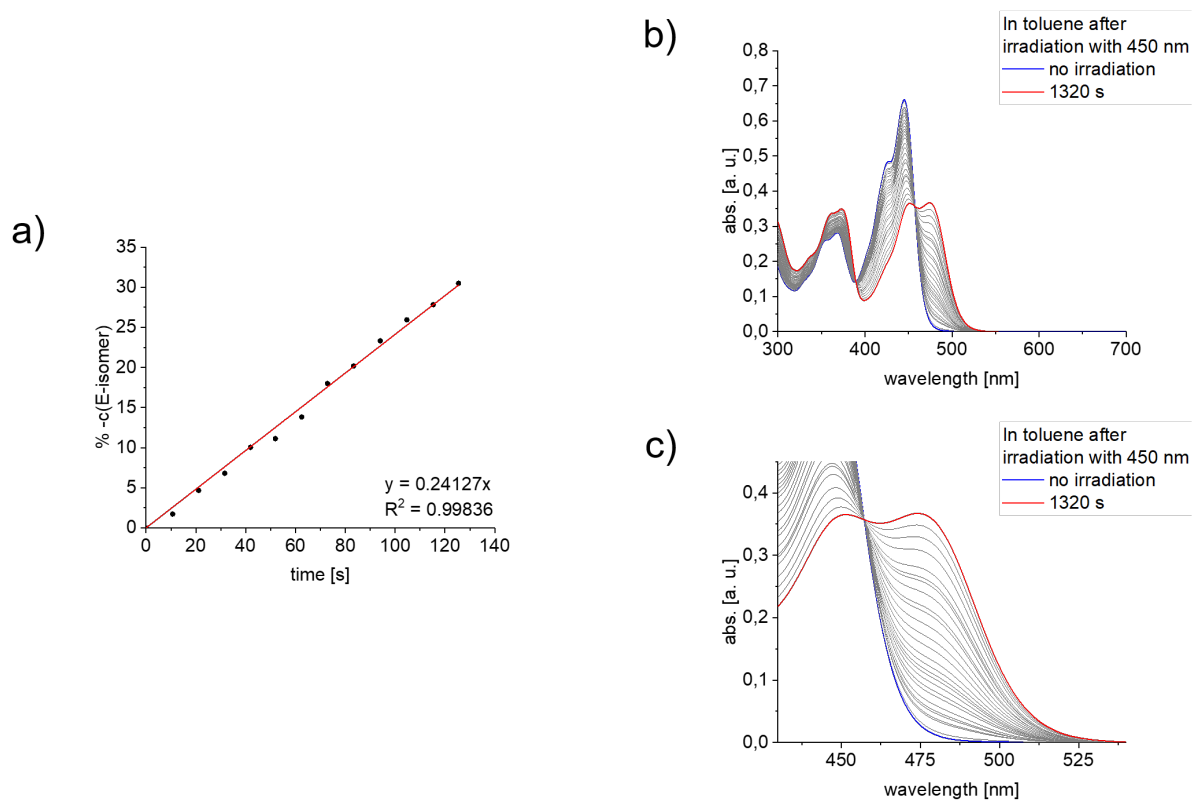
Figure S 70: Quantum yield determination of photoisomerization from *Z*-isomer to *E*-isomer of compound **4** in DMSO during irradiation with 430 nm; a) Plot of the concentration of *E*-isomer during phototransition by irradiation with 430 nm; b) UV/Vis absorption spectra received during irradiation of Het-HTI **4** with 430 nm in DMSO; c) UV/Vis spectrum excerpt: isosbestic point at 497 nm and the quantum yield was measured at 520 nm.
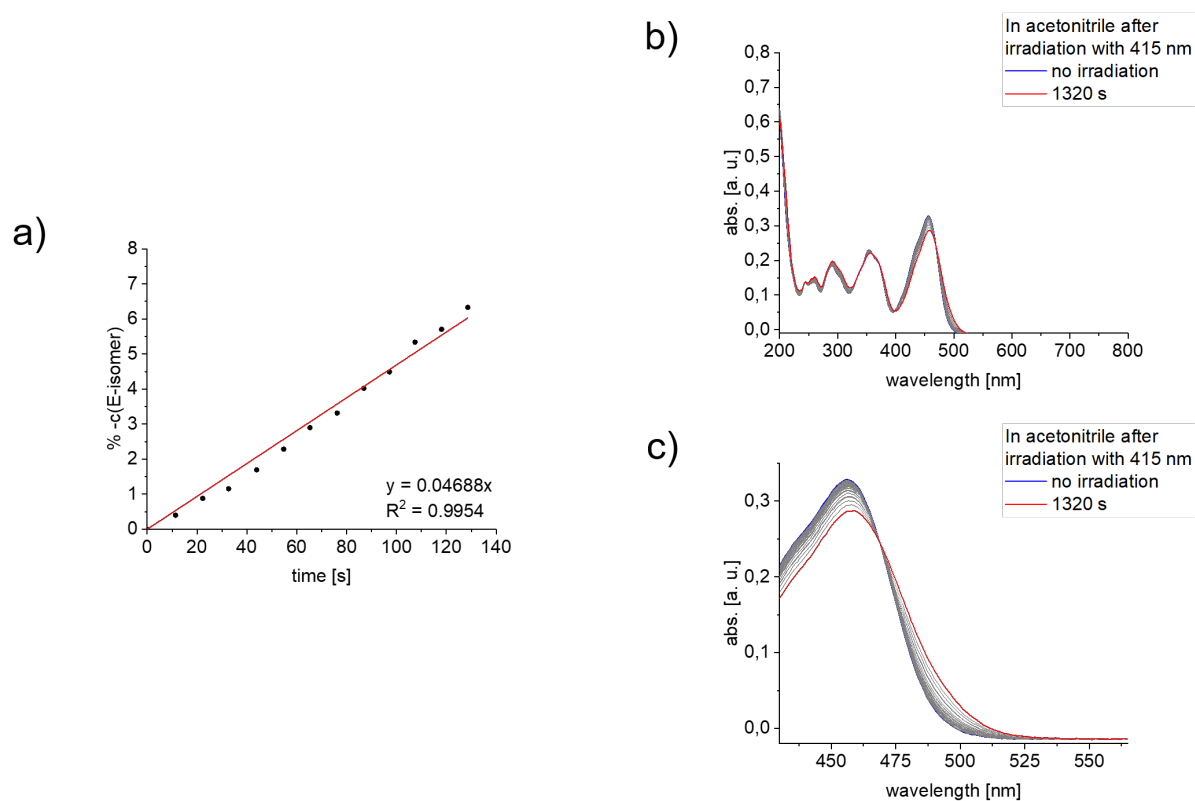
Figure S 71: Quantum yield determination of photoisomerization from *E*-isomer to *Z*-isomer of compound **4** in DMSO during irradiation with 530 nm; a) Plot of the concentration of *Z*-isomer during photoconversion by irradiation with 530 nm; b) UV/Vis absorption spectra received during irradiation of Het-HTI **4** with 530 nm in DMSO; c) UV/Vis spectrum excerpt: isosbestic point at 497 nm and the quantum yield was determined at 487 nm.
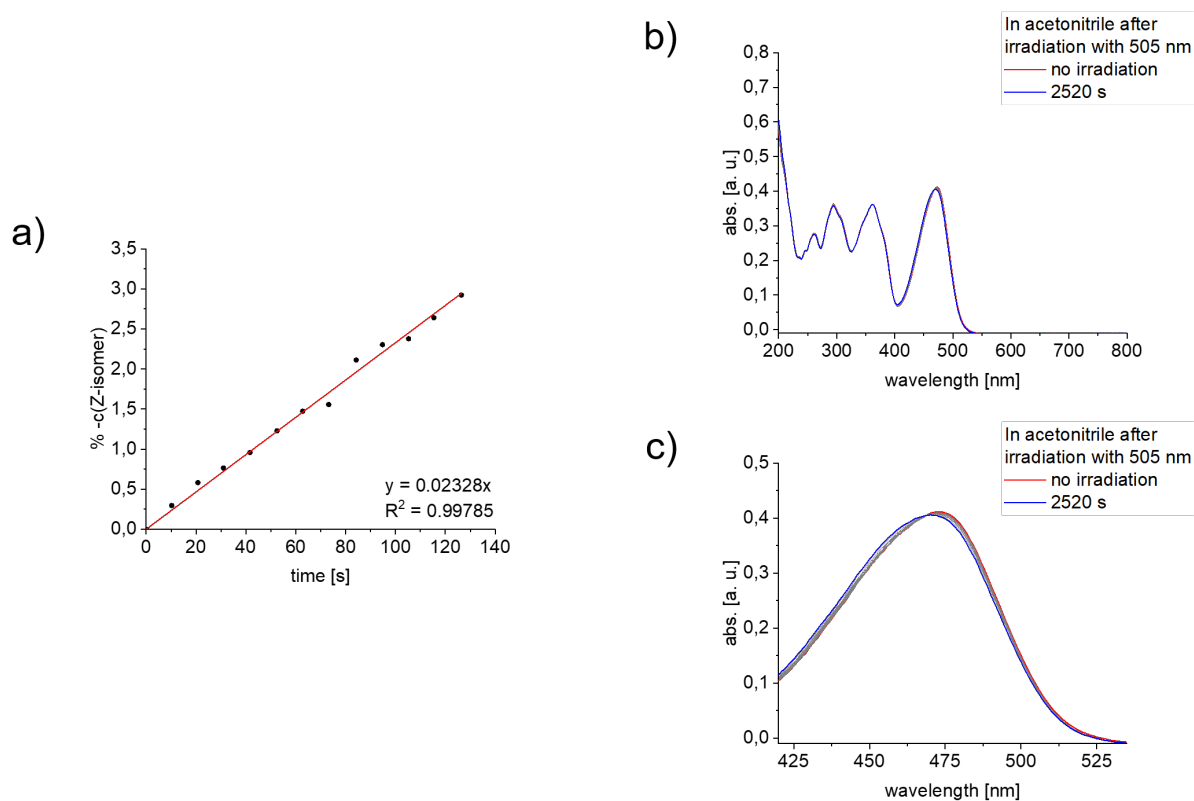
Figure S 72: Quantum yield determination of photoisomerization from *Z*-isomer to *E*-isomer of compound **5** in tetrahydrofuran during irradiation with 450 nm; a) Plot of the concentration of *E*-isomer during phototransition by irradiation with 450 nm; b) UV/Vis absorption spectra received during irradiation of Het-HTI **5** with 450 nm in tetrahydrofuran; c) UV/Vis spectrum excerpt: isosbestic point at 467 nm and the quantum yield was obtained at 486 nm.
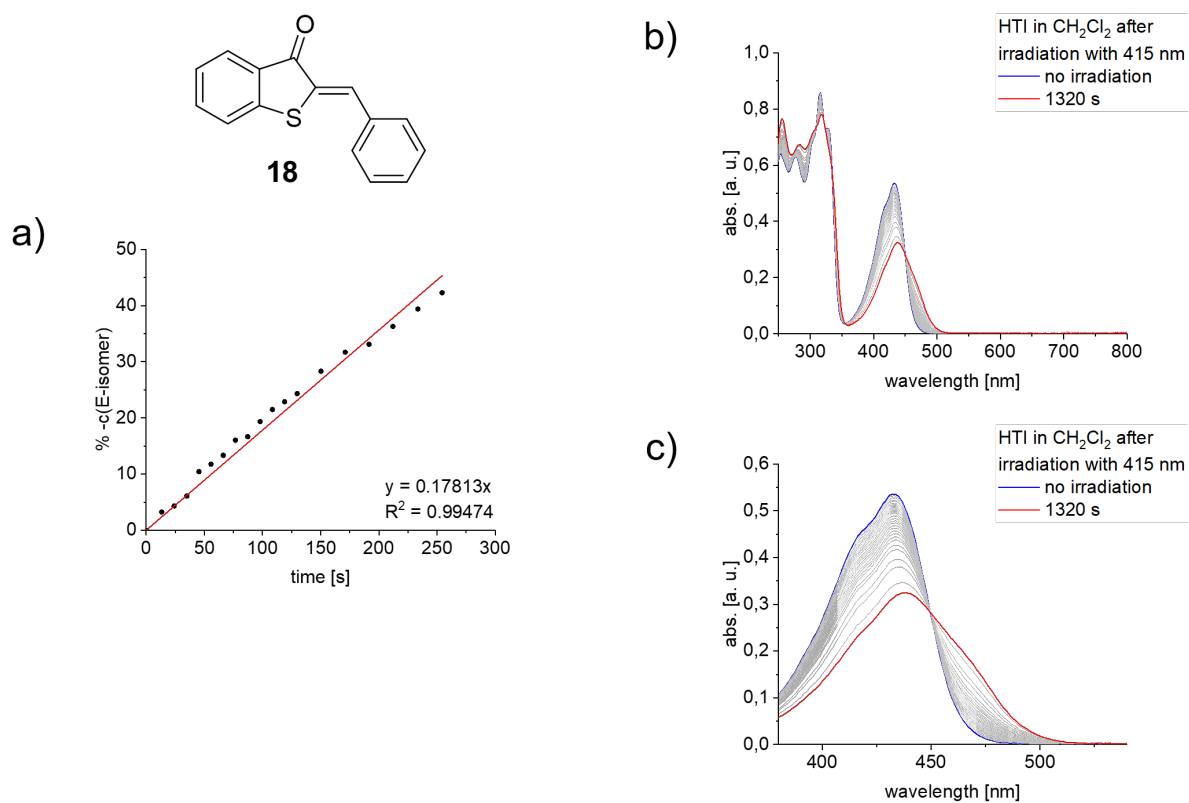
Figure S 73: Quantum yield determination of photoisomerization from *E*-isomer to *Z*-isomer of compound **5** in tetrahydrofuran during irradiation with 530 nm; a) Plot of the concentration of *E*-isomer during photoconversion by irradiation with 530 nm; b) UV/Vis absorption spectra received during irradiation of Het-HTI **5** with 530 nm in tetrahydrofuran; c) UV/Vis spectrum excerpt: isosbestic point at 467 nm and the quantum yield was measured at 457 nm.
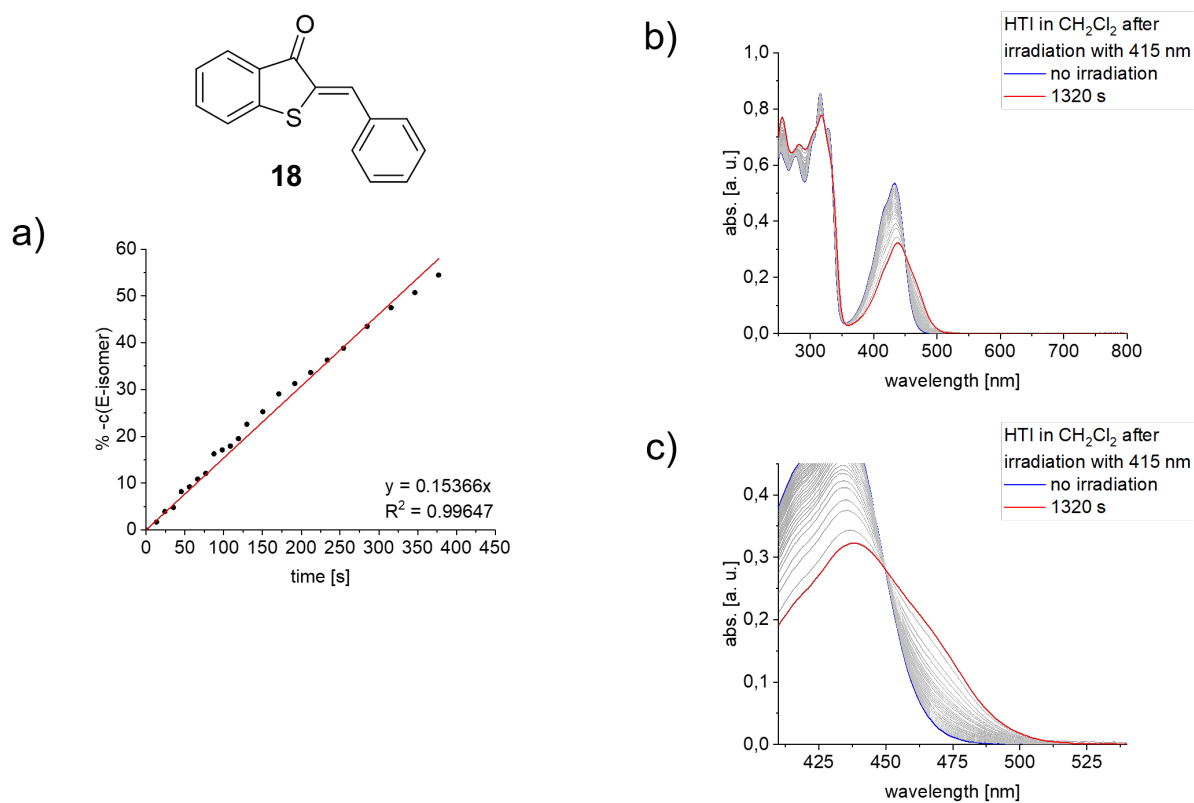
Figure S 74: Quantum yield determination of photoisomerization from *Z*-isomer to *E*-isomer of compound **6** in tetrahydrofuran during irradiation with 405 nm; a) Plot of the concentration of *E*-isomer during phototransition by irradiation with 405 nm; b) UV/Vis absorption spectra received during irradiation of Het-HTI **6** with 405 nm in tetrahydrofuran; c) UV/Vis spectrum excerpt: isosbestic point at 463 nm and the quantum yield was obtained at 482 nm.
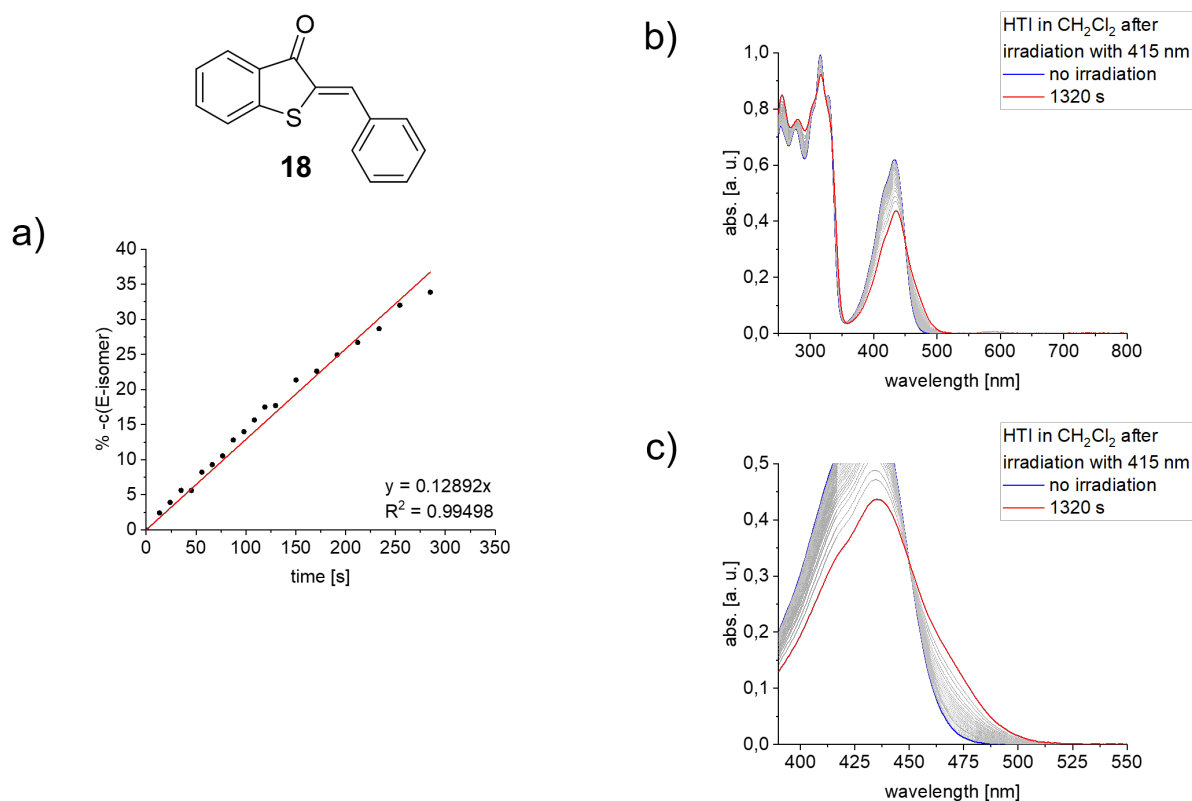
Figure S 75: Quantum yield determination of photoisomerization from *E*-isomer to *Z*-isomer of compound **6** in tetrahydrofuran during irradiation with 530 nm; a) Plot of the concentration of *Z*-isomer during photoconversion by irradiation with 530 nm; b) UV/Vis absorption spectra received during irradiation of Het-HTI **6** with 530 nm in tetrahydrofuran; c) UV/Vis spectrum excerpt: isosbestic point at 463 nm and the quantum yield was determined at 452 nm.

Figure S 76: Quantum yield determination of photoisomerization from *Z*-isomer to *E*-isomer of compound **7** in tetrahydrofuran during irradiation with 405 nm; a) Plot of the concentration of *E*-isomer during phototransition by irradiation with 405 nm; b) UV/Vis absorption spectra received during irradiation of Het-HTI **7** with 405 nm in tetrahydrofuran; c) UV/Vis spectrum excerpt: isosbestic point at 465 nm and the quantum yield was obtained at 483 nm.

Figure S 77: Quantum yield determination of photoisomerization from *E*-isomer to *Z*-isomer of compound **7** in tetrahydrofuran during irradiation with 530 nm; a) Plot of the concentration of *Z*-isomer during photoconversion by irradiation with 530 nm; b) UV/Vis absorption spectra received during irradiation of Het-HTI **7** with 530 nm in tetrahydrofuran; c) UV/Vis spectrum excerpt: isosbestic point at 465 nm and the quantum yield was determined at 457 nm.

Figure S 78: Quantum yield determination of photoisomerization from *Z*-isomer to *E*-isomer of compound **9** in acetonitrile during irradiation with 450 nm; a) Plot of the change of concentration of *E*-isomer during phototransition by irradiation with 450 nm; b) UV/Vis absorption spectra received during irradiation of Het-HTI **9** with 450 nm in acetonitrile; c) UV/Vis spectrum excerpt: isosbestic point at 457 nm and the quantum yield was determined at 475 nm.

Figure S 79: Quantum yield determination of photoisomerization from *Z*-isomer to *E*-isomer of compound **10** in acetonitrile during irradiation with 415 nm; a) Plot of the concentration of *E*-isomer during photoconversion by irradiation with 415 nm; b) UV/Vis absorption spectra received during irradiation of Het-HTI **10** with 415 nm in acetonitrile; c) UV/Vis spectrum excerpt: isosbestic point at 469 nm and the quantum yield was obtained at 477 nm.

Figure S 80: Quantum yield determination of photoisomerization from *E*-isomer to *Z*-isomer of compound **10** in acetonitrile during irradiation with 505 nm; a) Plot of the concentration of *Z*-isomer during photoconversion by irradiation with 505 nm; b) UV/Vis absorption spectra received during irradiation of Het-HTI **10** with 505 nm in acetonitrile; c) UV/Vis spectrum excerpt: isosbestic point at 469 nm and the quantum yield was determined at 462 nm.

Figure S 81: Quantum yield determination of photoisomerization from *Z*-isomer to *E*-isomer of compound **18** in CH₂Cl₂ during irradiation with 415 nm; a) Plot of the change of concentration of *E*-isomer during phototransition by irradiation with 415 nm; b) UV/Vis absorption spectra received during irradiation of HTI **18** with 450 nm in acetonitrile; c) UV/Vis spectrum excerpt: isosbestic point at 450 nm and the quantum yield was determined at 457 nm.

Figure S 82: Quantum yield determination of photoisomerization from *Z*-isomer to *E*-isomer of compound **18** in CH_2Cl_2 during irradiation with 415 nm; a) Plot of the change of concentration of *E*-isomer during phototransition by irradiation with 415 nm; b) UV/Vis absorption spectra received during irradiation of HTI **18** with 450 nm in acetonitrile; c) UV/Vis spectrum excerpt: isosbestic point at 450 nm and the quantum yield was determined at 457 nm.

Figure S 83: Quantum yield determination of photoisomerization from *Z*-isomer to *E*-isomer of compound **18** in CH_2Cl_2 during irradiation with 415 nm; a) Plot of the change of concentration of *E*-isomer during phototransition by irradiation with 415 nm; b) UV/Vis absorption spectra received during irradiation of HTI **18** with 450 nm in acetonitrile; c) UV/Vis spectrum excerpt: isosbestic point at 450 nm and the quantum yield was determined at 457 nm.

Table S 12: Comparison of the quantum yields for compound **18** in THF. The average value of the measurement results is 25% and the standard deviation is 3%.

compound	solvent	irr. wavelength [nm]	$\varPhi$ *(Z* to *E)* in %
18[7]	CH_2Cl_2	415	22
	CH_2Cl_2	415	28
	CH_2Cl_2	415	26

Structure Analysis

2-((4-methyl-1*H*-imidazol-5-yl)methylene)benzo[*b*]thiophen-3(2*H*)-one (1)
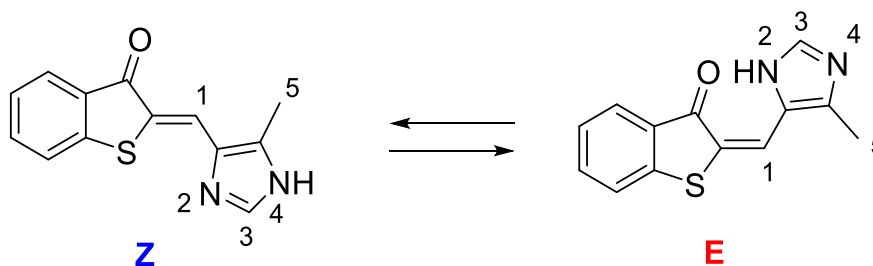
Figure S 84: Structure and conformation of compound **1** as *Z* and *E* isomer. The acidic hydrogen atom is at N(4) in the *Z* isomer because the chalcogen bonding with the sulfur is predominant and at N(2) in the *E* isomer where a hydrogen bond is developed with the carbonyl.
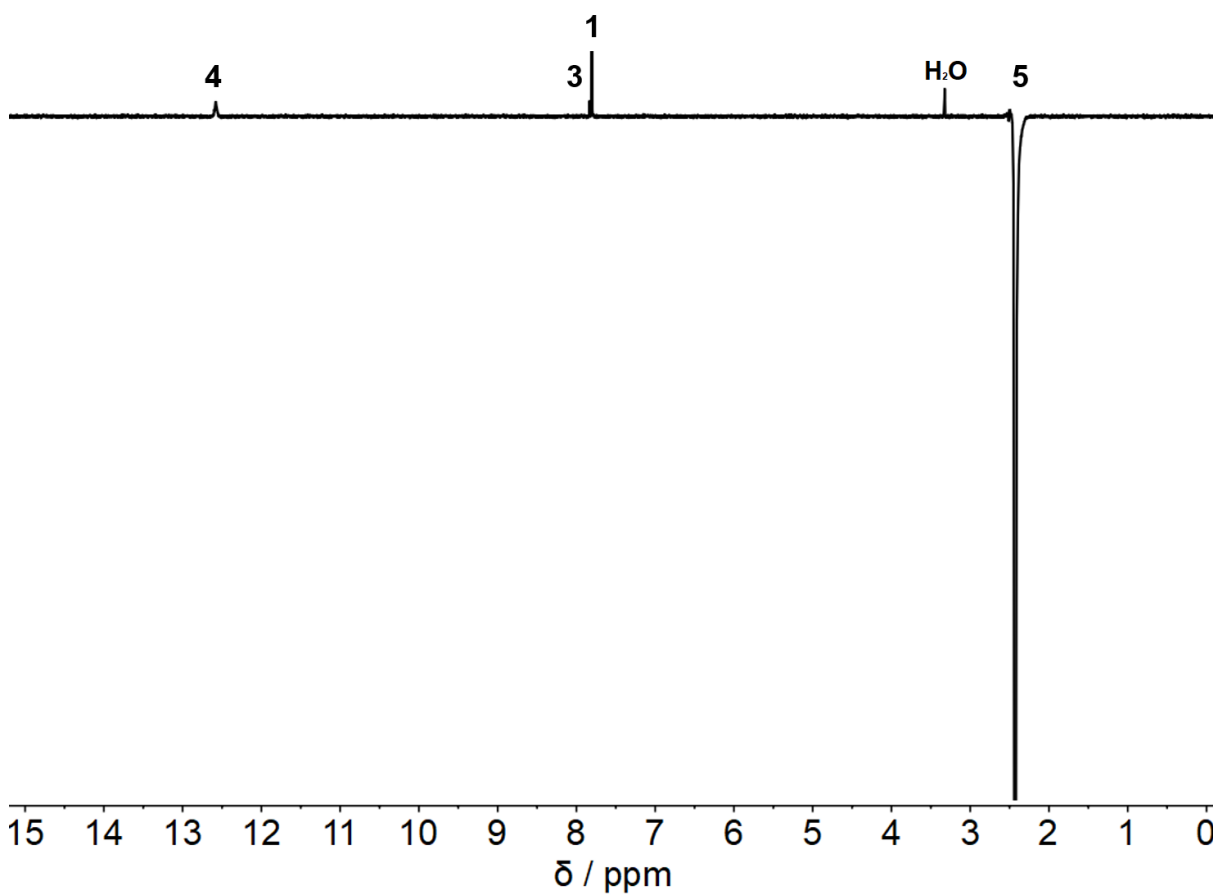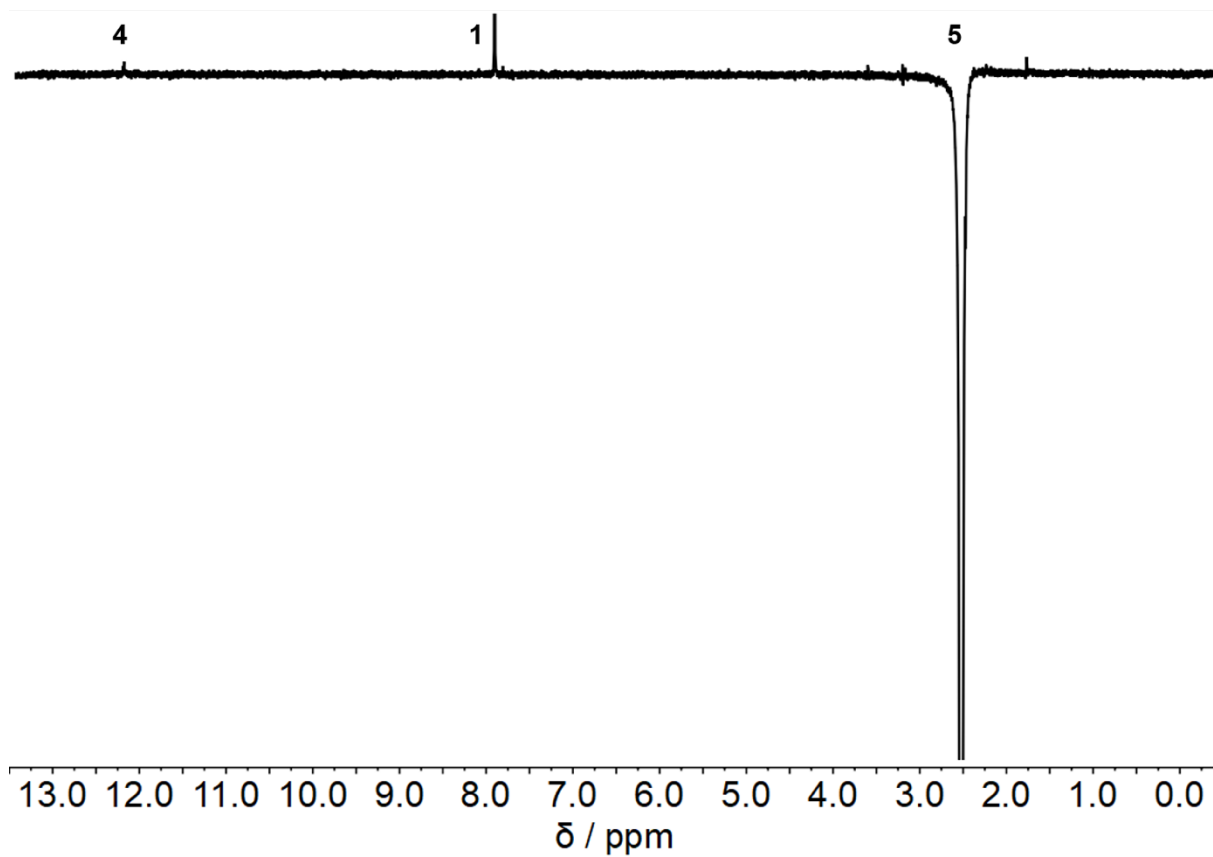

Figure S 85: 1D NOE (600 MHz, DMSO-d_6, 25 °C) spectrum of the *Z* isomer of compound **1**. Selective irradiation of the protons of the methyl group (5) reveals a through-space coupling to H(1) and H(4). The position of the acidic hydrogen at the N(4) is thus evidenced.
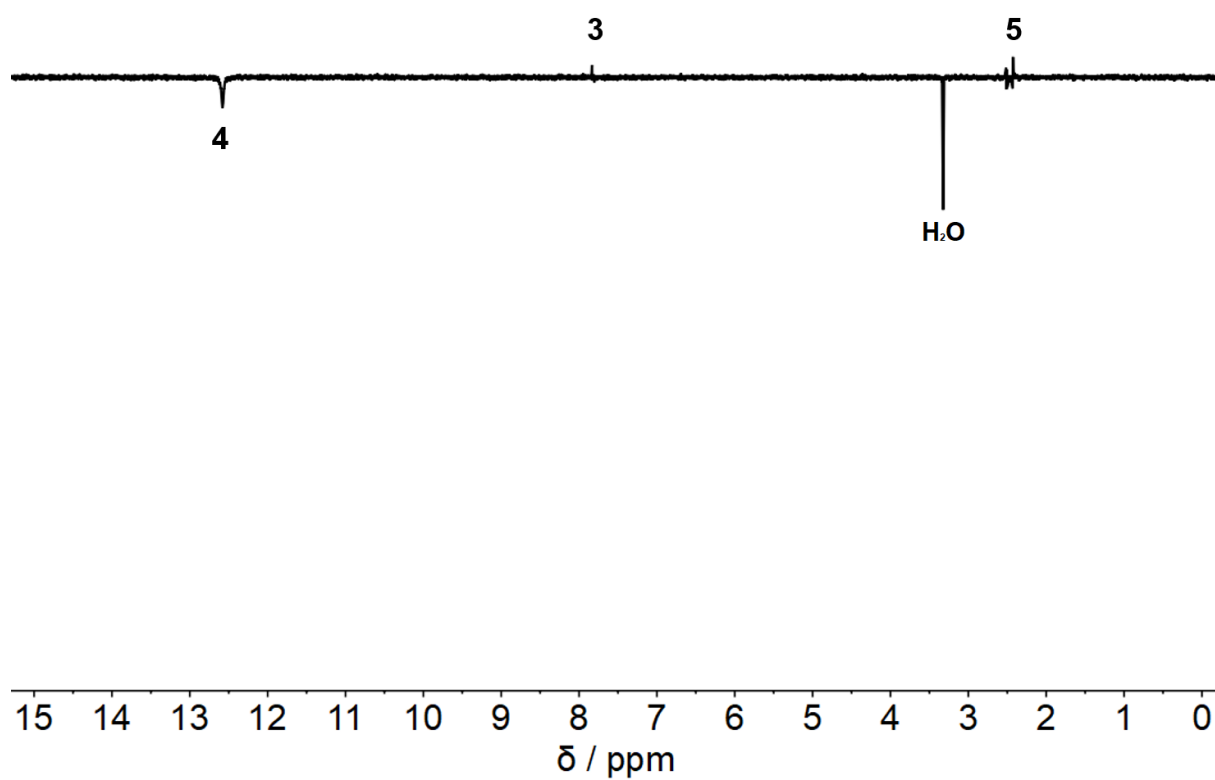
Figure S 86: 1D NOE (600 MHz, DMSO-d_6, 25 °C) spectrum of the *Z* isomer of compound **1**. Selective irradiation of the proton of the NH-group (4) reveals a through-space coupling to the aromatic proton of the imidazole H (3) and protons of the methyl group H (5). The position of the hydrogen at the N (4) is thus evidenced.
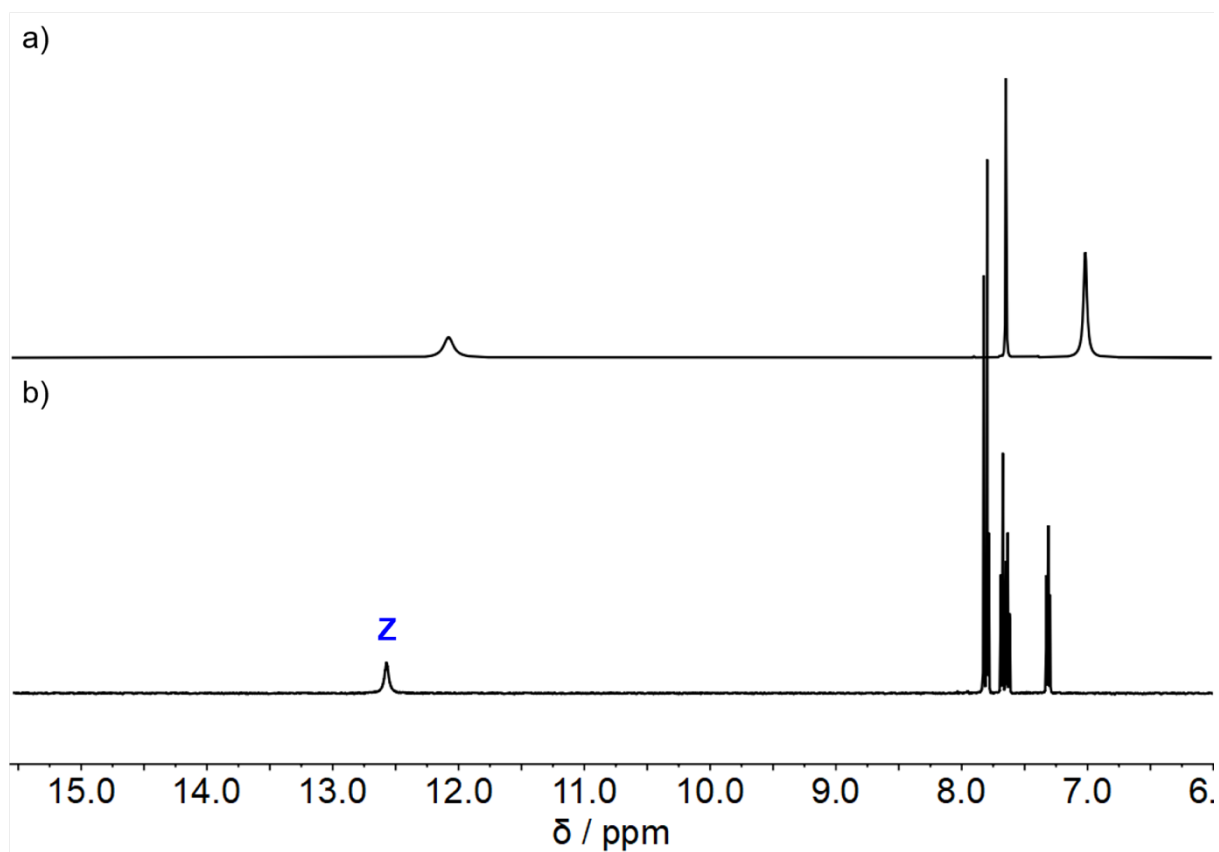
Figure S 87: ^{1}H NMR (400 MHz, DMSO-d_6, 25 °C); a) ^{1}H NMR spectrum of 1H-imidazole in DMSO-d_6; b) ^{1}H NMR spectrum of the Z isomer of compound **1**. The NH in the 1H-imidazole and in the Z-**1** have a comparable chemical shift. This supports the interpretation that intermolecular hydrogen bonding is preferred in the Z isomer and intramolecular hydrogen bonding is prominent in the E isomer.
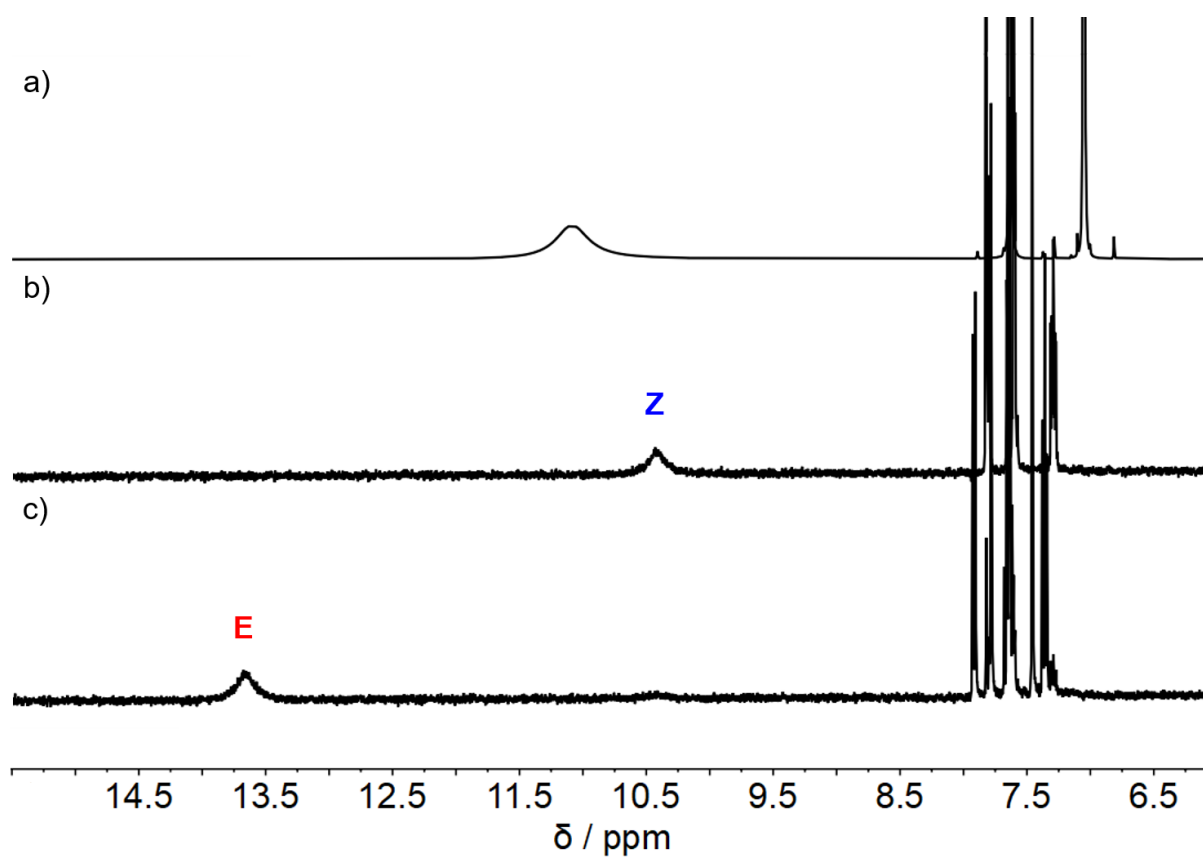
Figure S 88: ^{1}H NMR (400 MHz, acetonitrile-d_3, 25 °C); a) ^{1}H NMR spectrum of 1H-imidazole in acetonitrile-d_3; b) ^{1}H NMR spectrum of the Z isomer of compound **1**; c) ^{1}H NMR spectrum of the E isomer of compound **1**. In the E isomer, the NH hydrogen is significantly shifted downfield compared to the NH hydrogen in the Z isomer. The NH in the 1H-imidazole and in the Z-**1** have a comparable chemical shift. This supports the interpretation that intermolecular hydrogen bonding is preferred in the Z isomer and intramolecular hydrogen bonding is prominent in the E isomer.
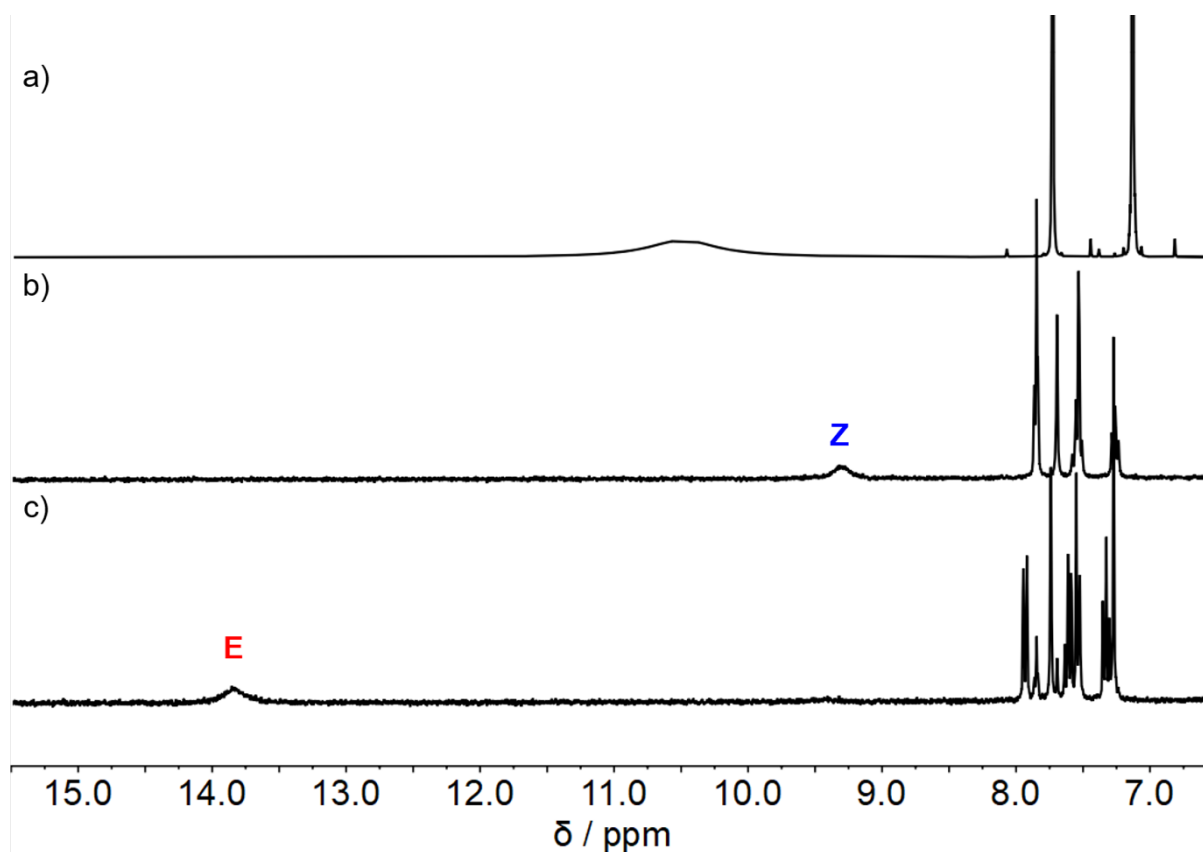
Figure S 89: ^1H NMR (400 MHz, CD$_2$Cl$_2$, 25 °C); a) ^1H NMR spectrum of 1H-imidazole in CD$_2$Cl$_2$; b) ^1H NMR spectrum of the Z isomer of compound **1**; c) ^1H NMR spectrum of the E isomer of compound **1**. In the E isomer, the NH hydrogen is significantly shifted downfield compared to the NH hydrogen in the Z isomer. The NH in the 1H-imidazole and in the Z-**1** have a comparable chemical shift. This supports the interpretation that intermolecular hydrogen bonding is preferred in the Z isomer and intramolecular hydrogen bonding is prominent in the E isomer.
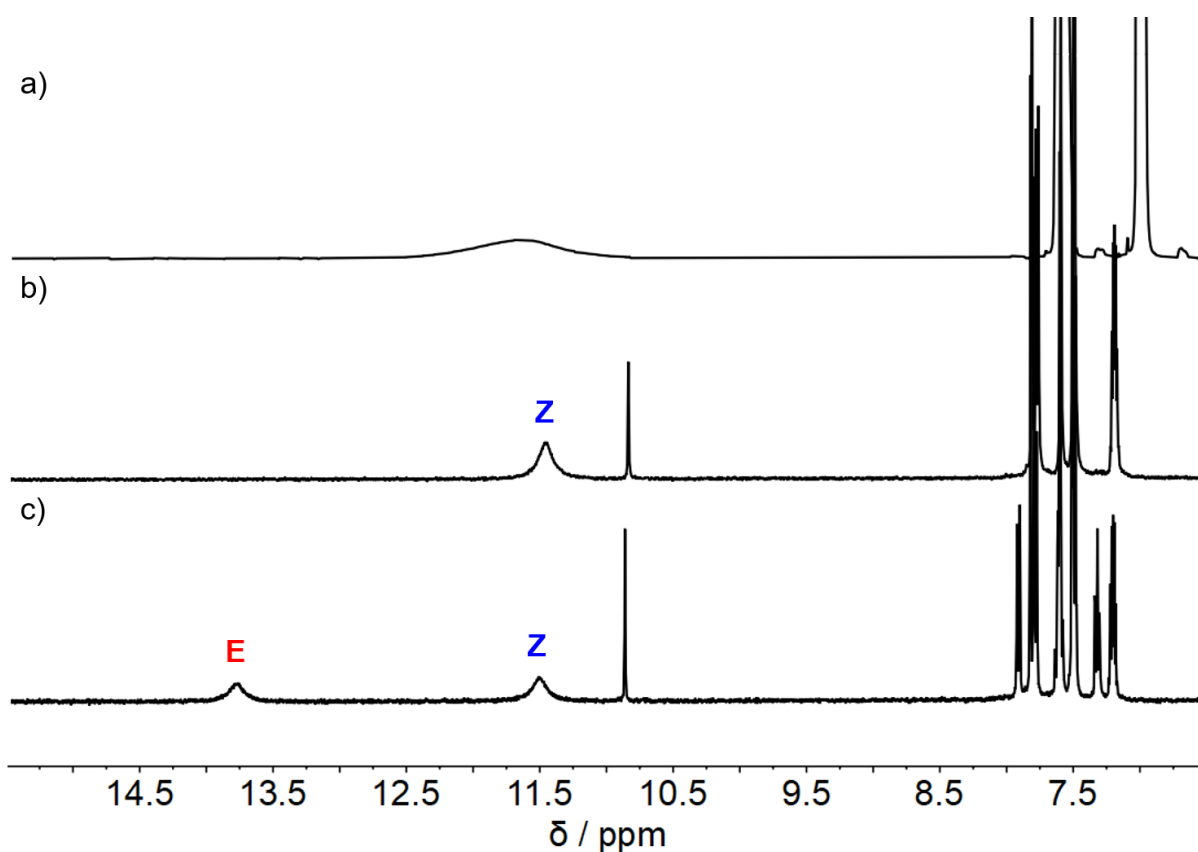
Figure S 90: ^{1}H NMR (400 MHz, THF-d_8, 25 °C); a) ^{1}H NMR spectrum of 1*H*-imidazole in THF-d_8; b) ^{1}H NMR spectrum of the *Z* isomer of compound **1**; c) ^{1}H NMR spectrum of the enriched *E* isomer of compound **1**. In the *E* isomer, the NH hydrogen is significantly shifted downfield compared to the NH hydrogen in the *Z* isomer. The NH in the 1*H*-imidazole and in the *Z*-**1** have a comparable chemical shift. This supports the interpretation that intermolecular hydrogen bonding is preferred in the *Z* isomer and intramolecular hydrogen bonding is prominent in the *E* isomer. The signal at 10.86 ppm belongs to the 2-hydroperoxytetrahydrofuran solvent impurity.
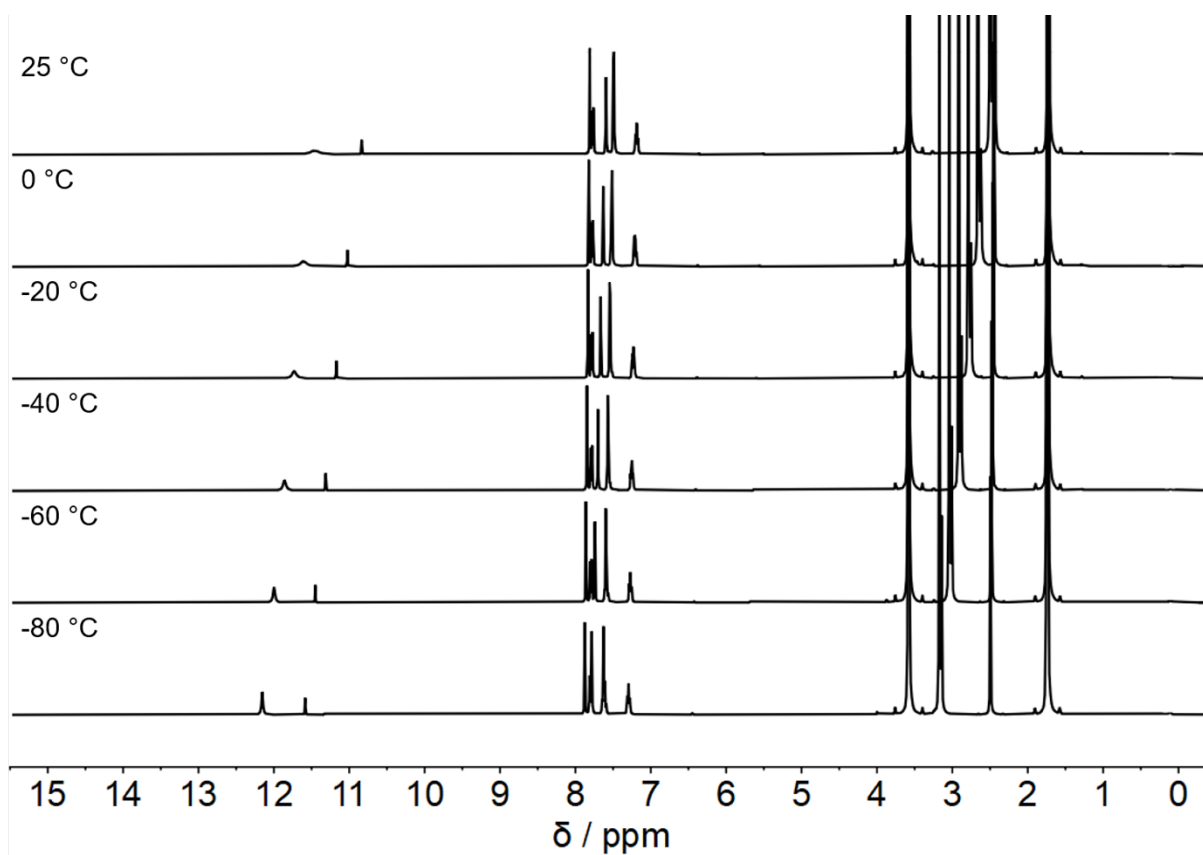
Figure S 91: Variable temperature ¹H NMR (400 MHz, THF-d_8) spectra of the *Z* isomer of compound **1** at 25 °C, 0 °C, -20 °C, -40 °C, -60 °C and -80 °C. The signal at 10.86 ppm corresponds to the 2-hydroperoxytetrahydrofuran solvent impurity.
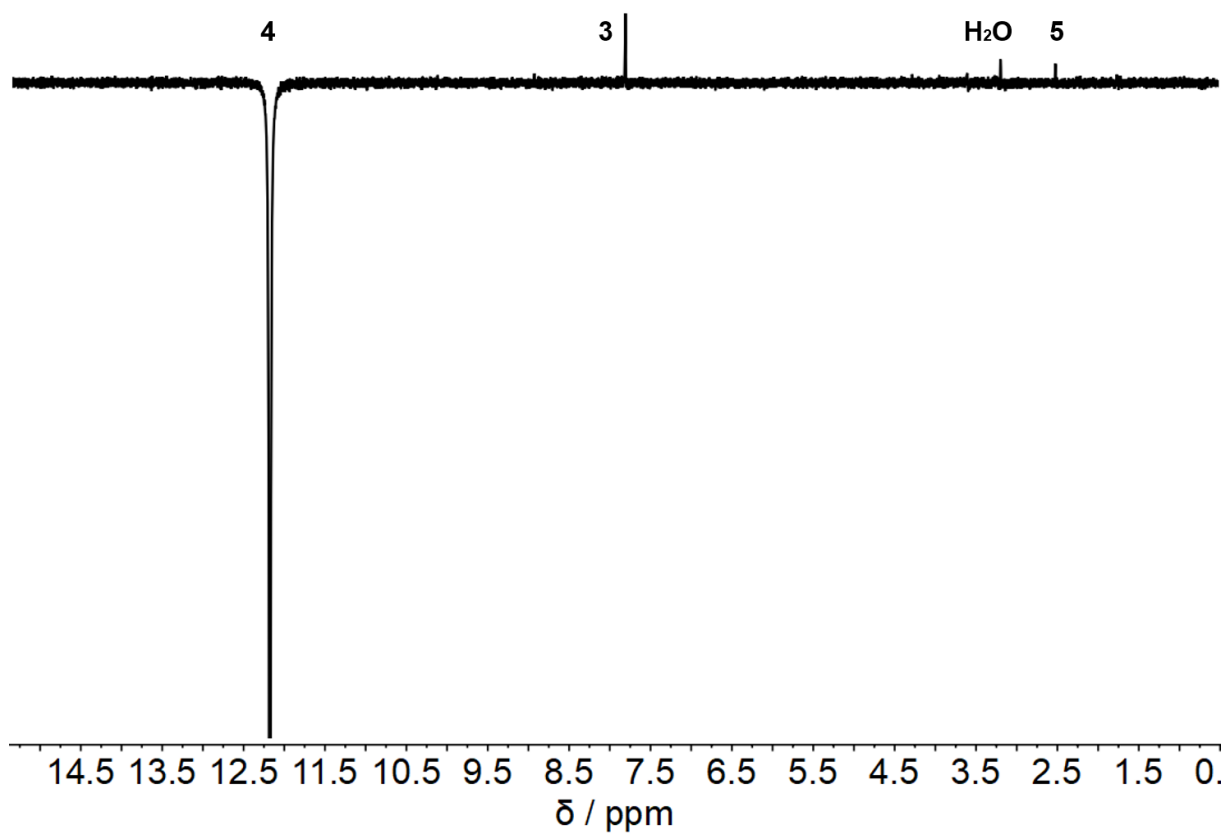
Figure S 92: 1D ROE (400 MHz, THF-d_8, -80 °C, 336 scans) spectrum of the *Z* isomer of compound **1**. Selective irradiation of the proton of NH(4) reveals a through-space coupling to H(3) and the methyl group (5). Furthermore, there is a cross signal to the water. This indicates a water exchange. The position of the hydrogen at the N(4) is thus evidenced.

Figure S 93: 1D ROE (400 MHz, THF-d_8, -80 °C, 512 scans) spectrum of the *Z* isomer of compound **1**. Selective irradiation of the protons of the methyl group (5) reveals a through-space coupling to H(1) and NH(4). The position of the hydrogen at the N(4) is thus evidenced and the methyl group points in the direction of H(1).
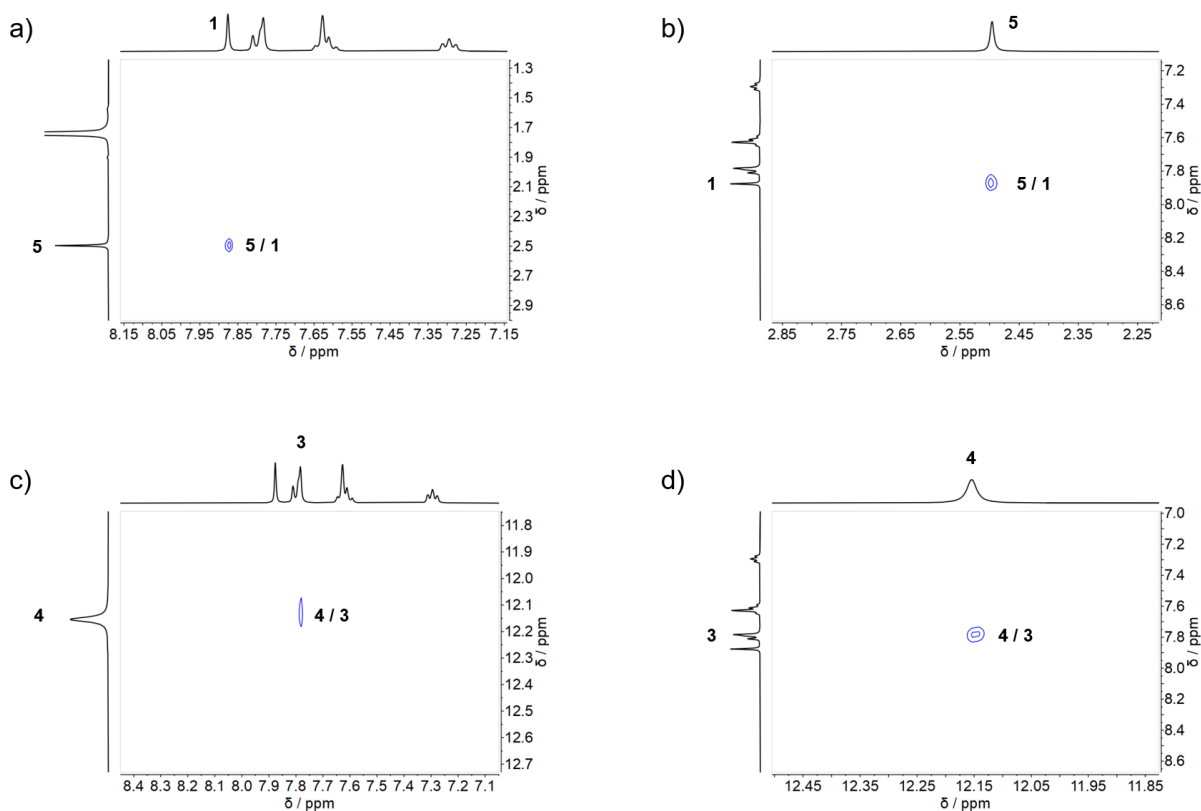
Figure S 94: ROSEY (400 MHz, THF-d_8, -80 °C, 88 scans) spectra of the *Z* isomer of compound **1**; showing: a) cross signal between olefinic H(1) and methyl group CH$_3$(5); b) cross signal between olefinic H(1) and methyl group CH$_3$(5); c) cross signal between NH(4) and H(3); d) cross signal between NH(4) and H(3). The cross signal from NH(4) to the methyl group (5) could not be detected in these experiments. To measure this cross signal, more scans would be needed. However, this was not possible due to the limited measurement time at -80 °C.
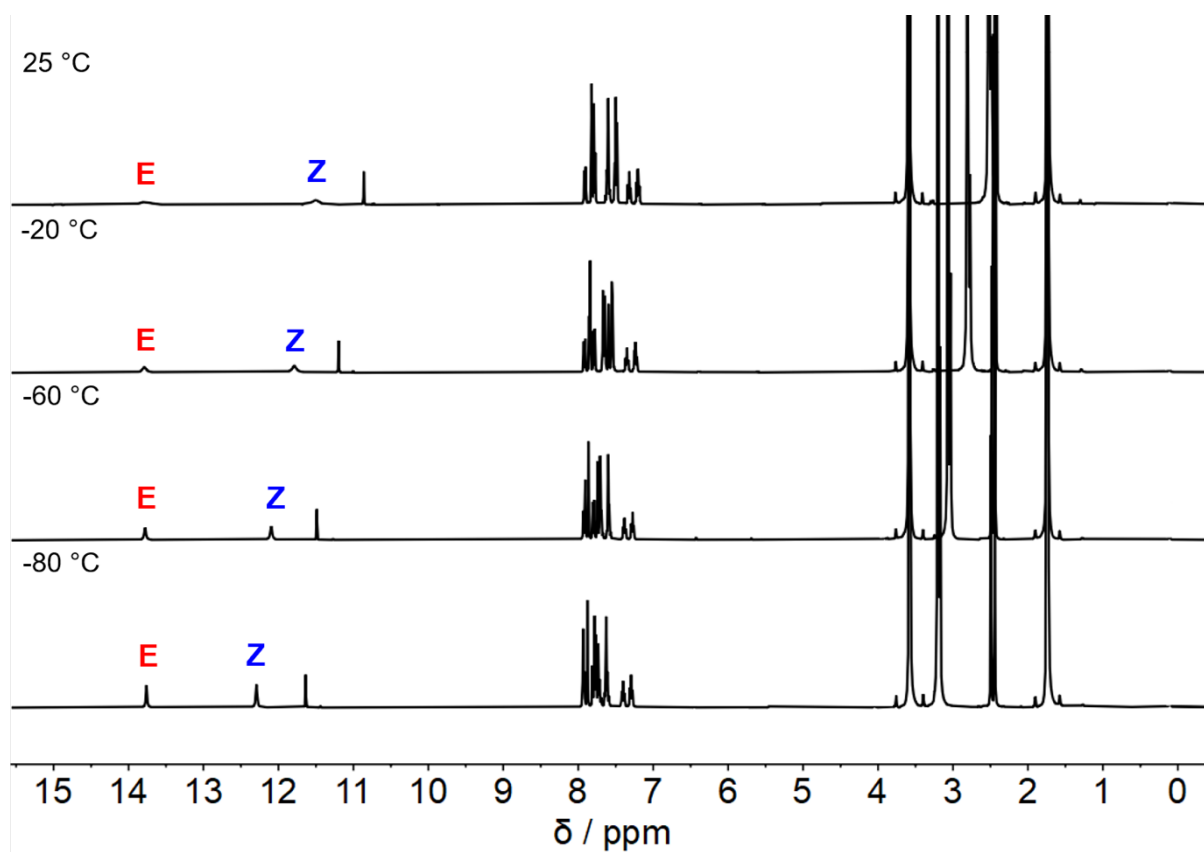
Figure S 95: Variable temperature ^{1}H NMR (400 MHz, THF-d_8) spectra of the enriched *E* isomer of compound **1** at 25 °C, -20 °C, -60 °C and -80 °C. The signal at 10.86 ppm corresponds to the 2-hydroperoxytetrahydrofuran solvent impurity.
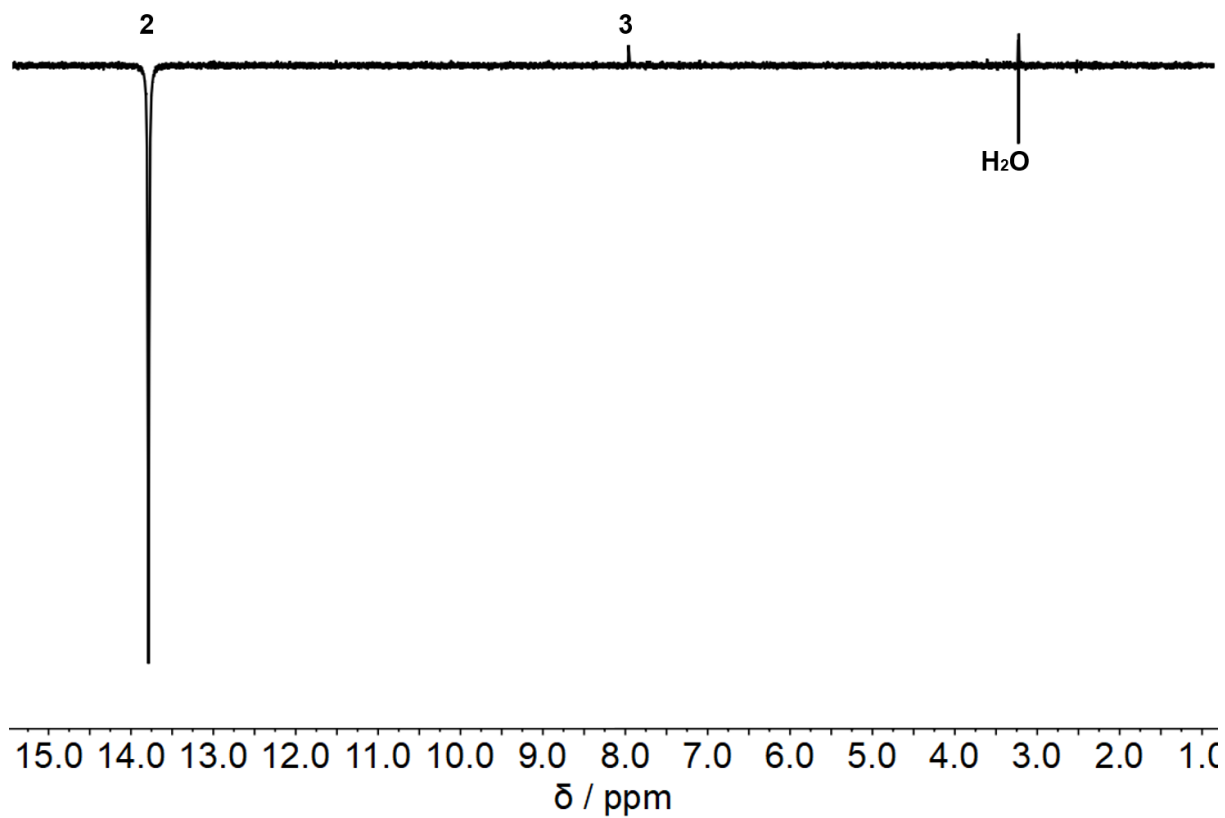
Figure S 96: 1D ROE (400 MHz, THF-d_8, -80 °C, 336 scans) spectrum of the enriched *E* isomer of compound **1**. Selective irradiation of the proton of NH(2) reveals a through-space coupling to H(3). Note that there is no cross signal to water. The water peak has not the same phase. The position of the hydrogen at N(2) is thus evidenced.
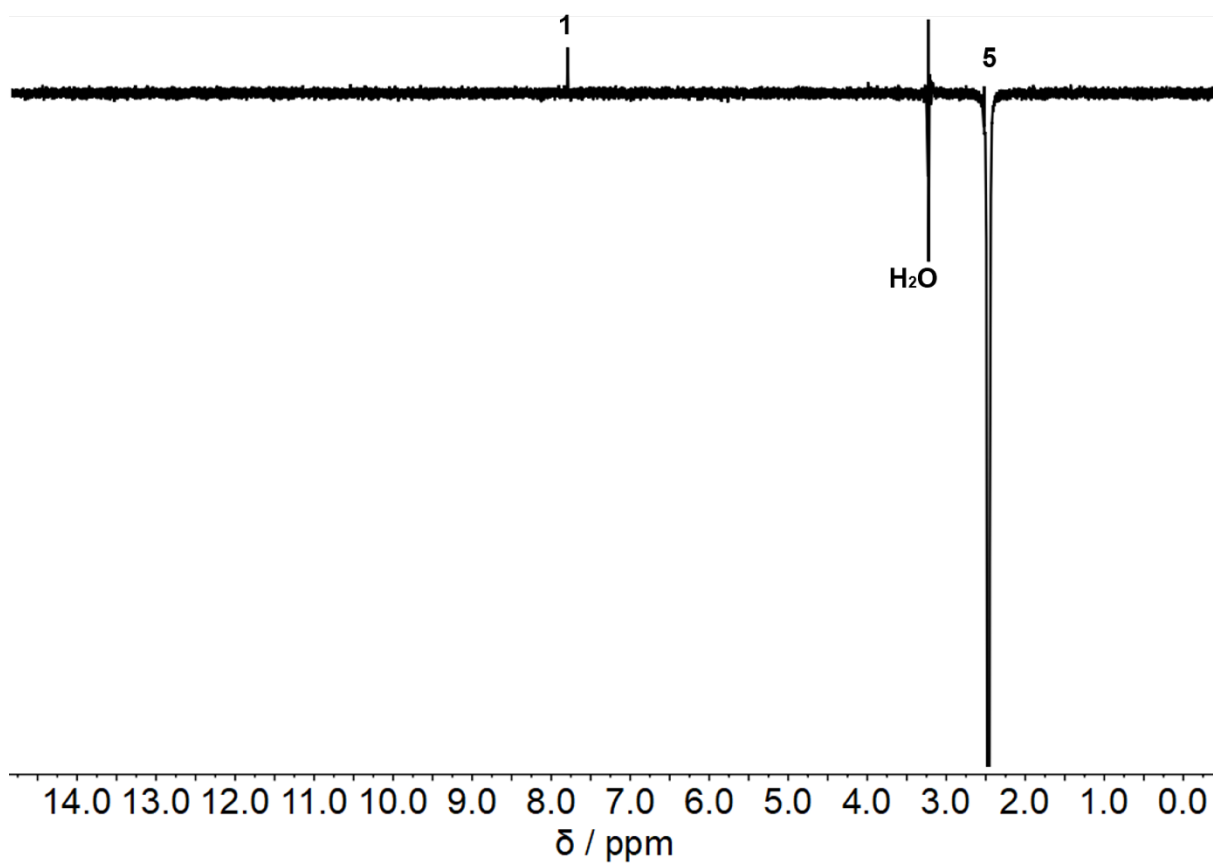
Figure S 97: 1D ROE (400 MHz, THF-d_8, -80 °C, 512 scans) spectrum of the enriched E isomer of compound **1**. Selective irradiation of the protons of the methyl group (5) reveals a through-space coupling to H(1). Note that there is no cross signal to water. The water peak has not the same phase. The position of the hydrogen at the N(2) is thus evidenced and the methyl group points in the direction of H(1).
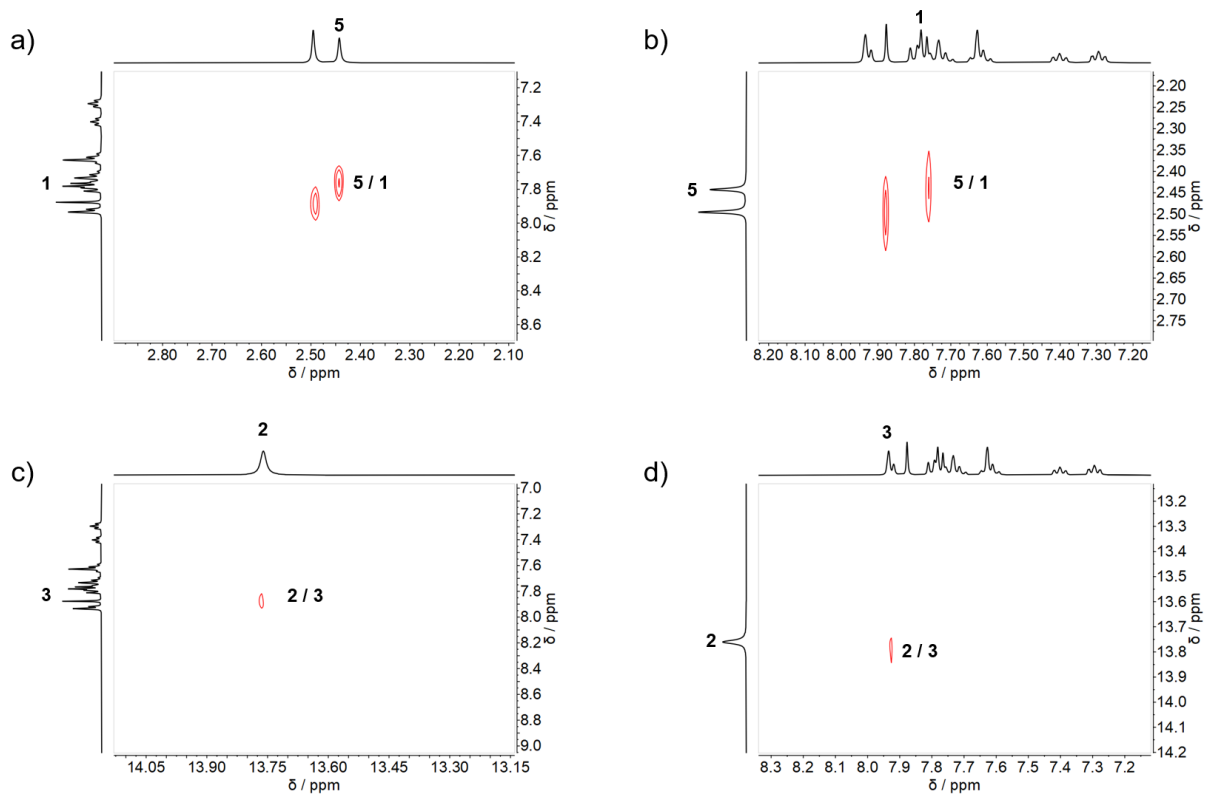
Figure S 98: ROSEY (400 MHz, THF-d_8, -80 °C, 88 scans) spectra of the enriched *E* isomer of compound **1**; showing: a) cross signal between olefinic H(1) and methyl group CH$_3$(5); b) cross signal between olefinic H(1) and methyl group CH$_3$(5); c) cross signal between NH(2) and H(3); d) cross signal between NH(2) and H(3).

2-((methyl-1*H*-pyrrol-2-yl)methylene)benzo[*b*]thiophen-3(2*H*)-one (4)
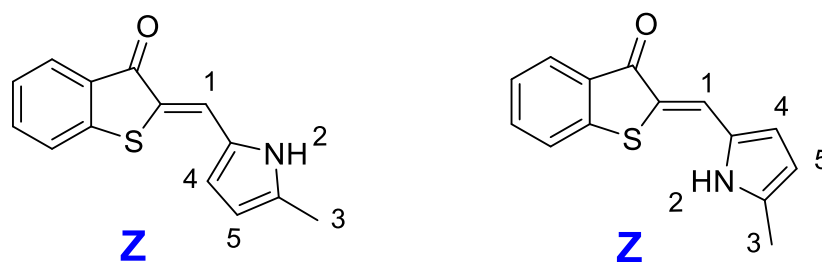
Figure S 99: Structure of the *Z* isomer of compound **4**.
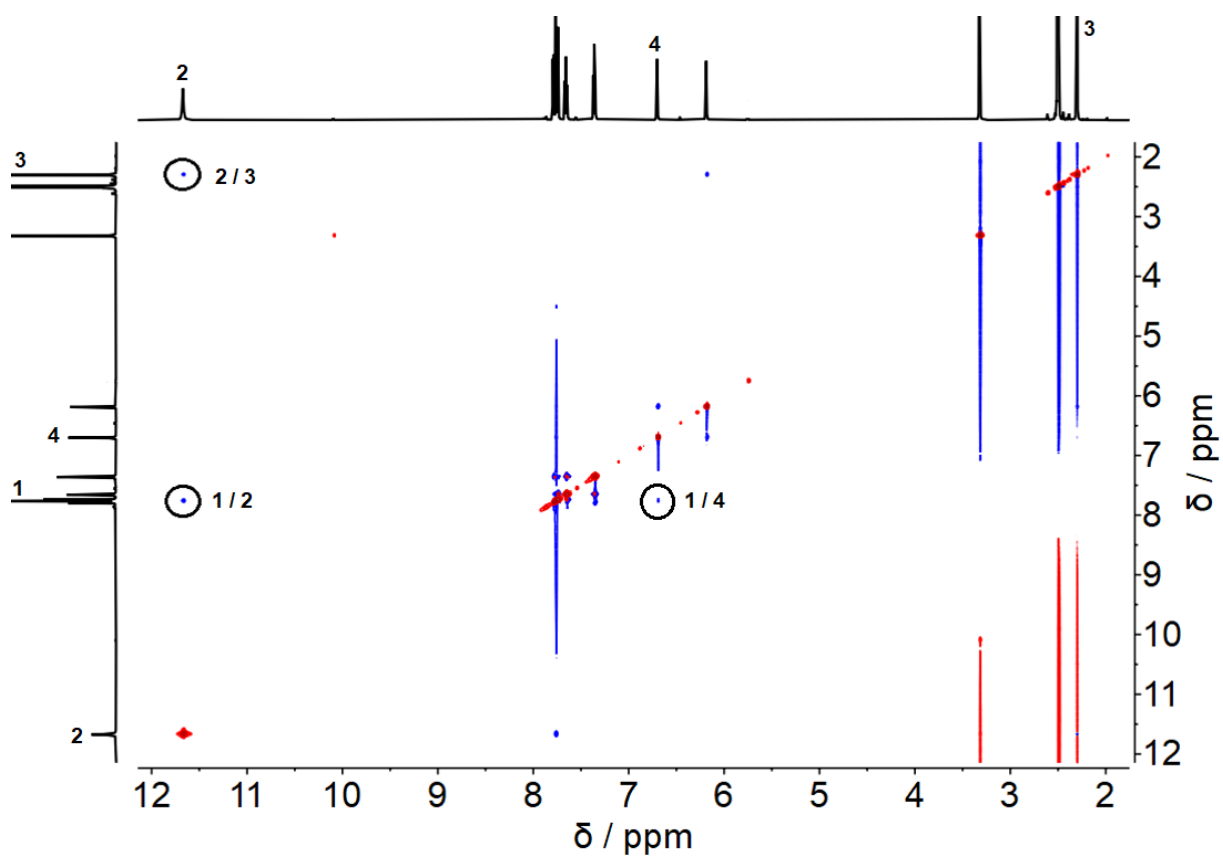
Figure S 100: NOESY (600 MHz, DMSO-*d₆*, 25 °C) spectrum of the *Z* isomer of compound **4**. Cross signals between protons H(2) and H(3) as well as between H(1) and H(2) and H(1) and H(4) are observed.

2-((1*H*-indol-3-yl)methylene)benzo[*b*]thiophen-3(2*H*)-one (5)
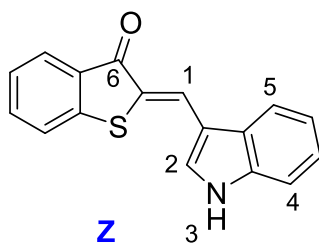
Figure S 101: Structure of the *Z* isomer of compound **5**.
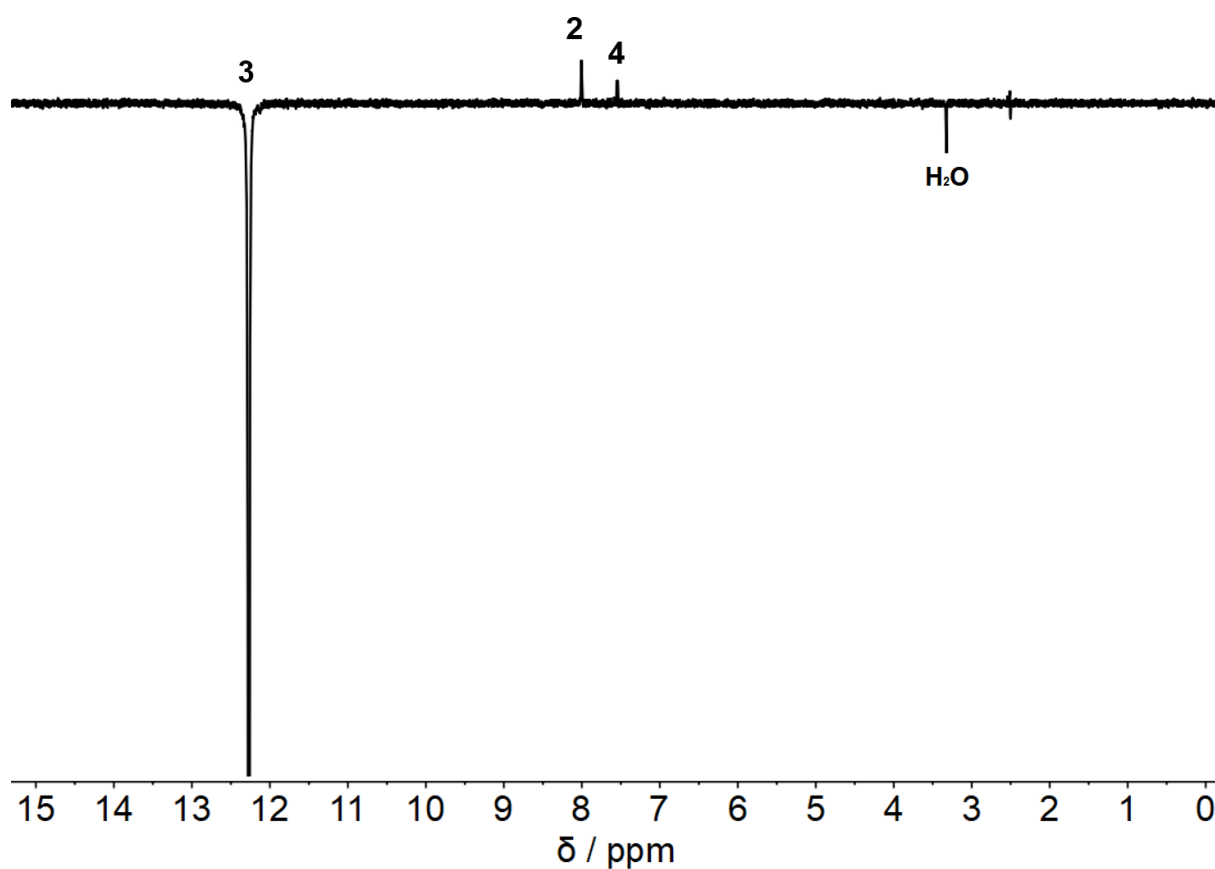
**Figure S 102:** 1D NOE (600 MHz, DMSO-d_6, 25 °C) spectrum of the *Z* isomer of compound **5**. Selective irradiation of the proton of NH-group (3) reveals a through-space coupling to the aromatic protons of the indole H(2) and H(4). No through-space coupling to the olefinic H(1) is observed.
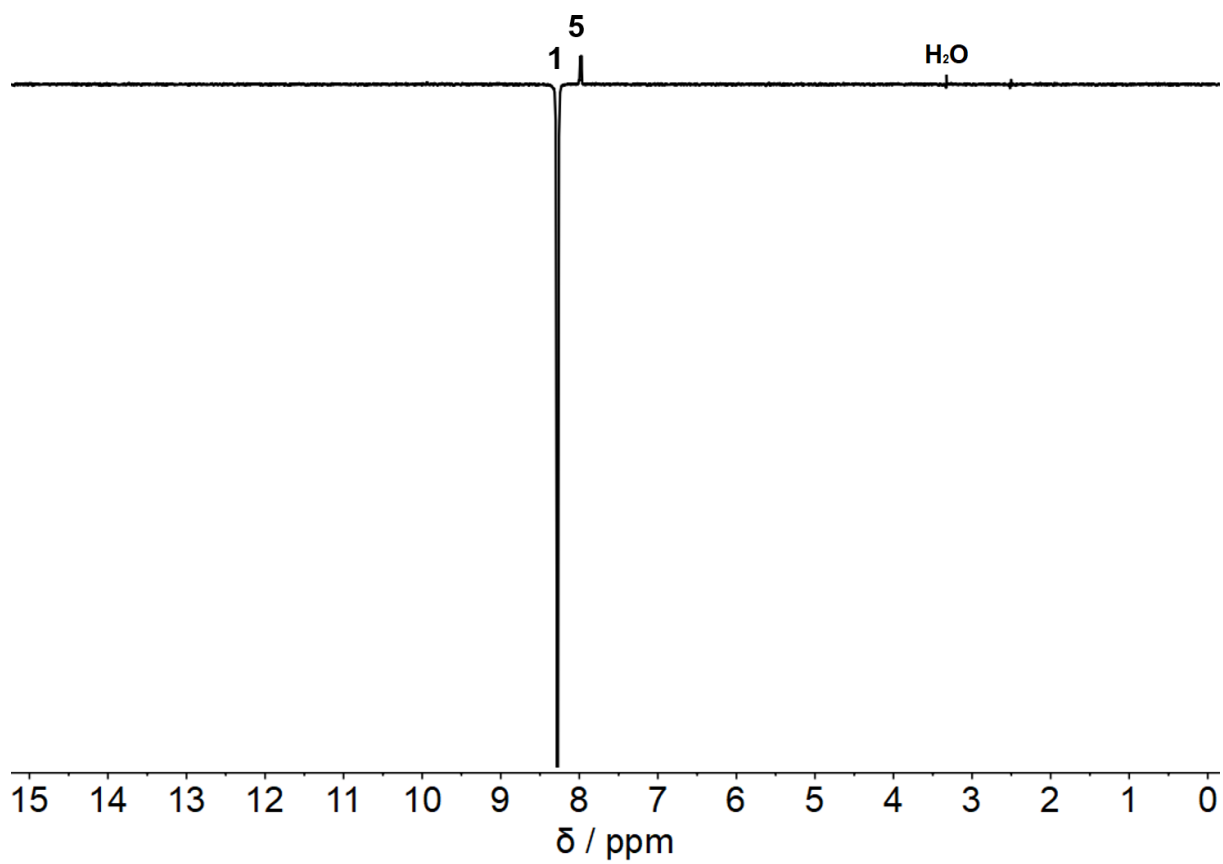
Figure S 103: 1D NOE (600 MHz, DMSO-d_6, 25 °C) spectrum of the *Z* isomer of compound **5**. Selective irradiation of the olefinic H(1) reveals a through-space coupling to the aromatic proton of the indole H(5).
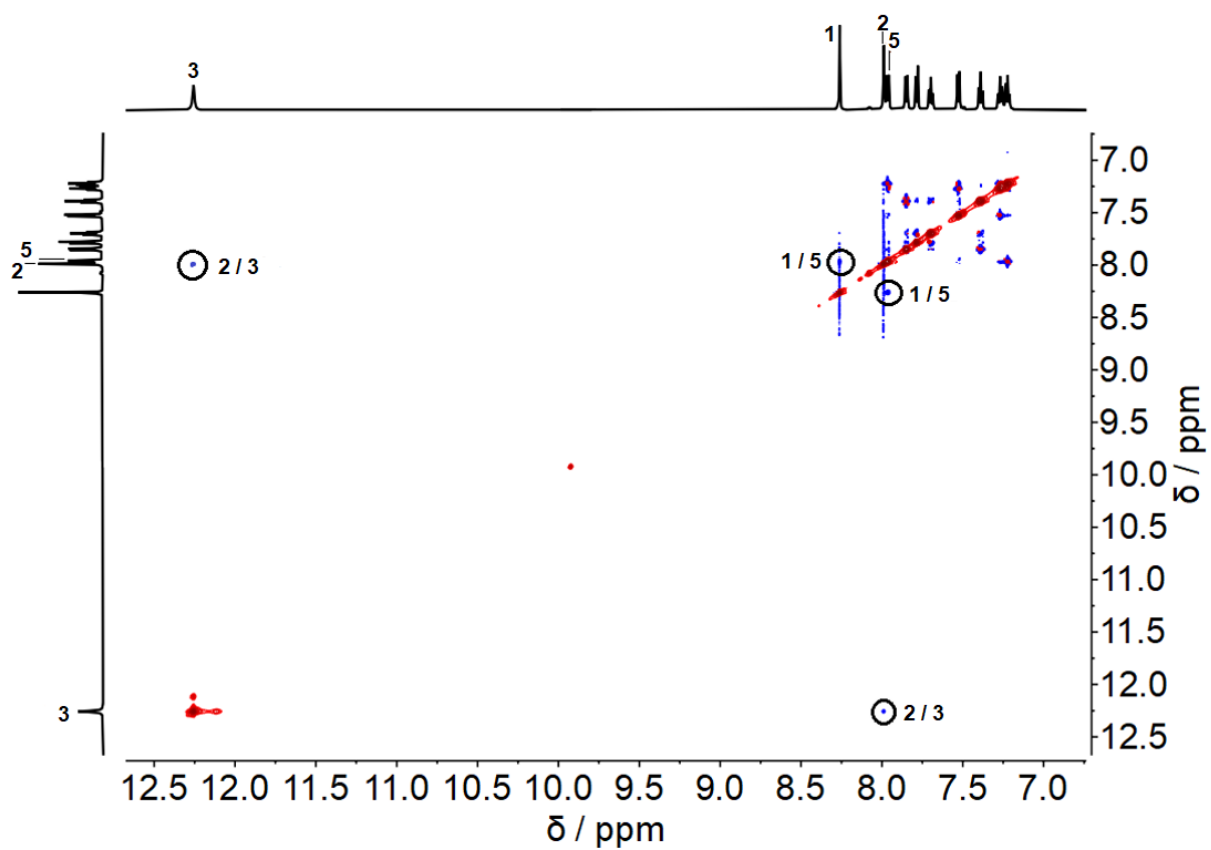
Figure S 104: NOESY (600 MHz, DMSO-d_6, 25 °C) spectrum of the *Z* isomer of compound **5**. Cross signals between protons H(2) and H(3) as well as between H(1) and H(5) are observed.
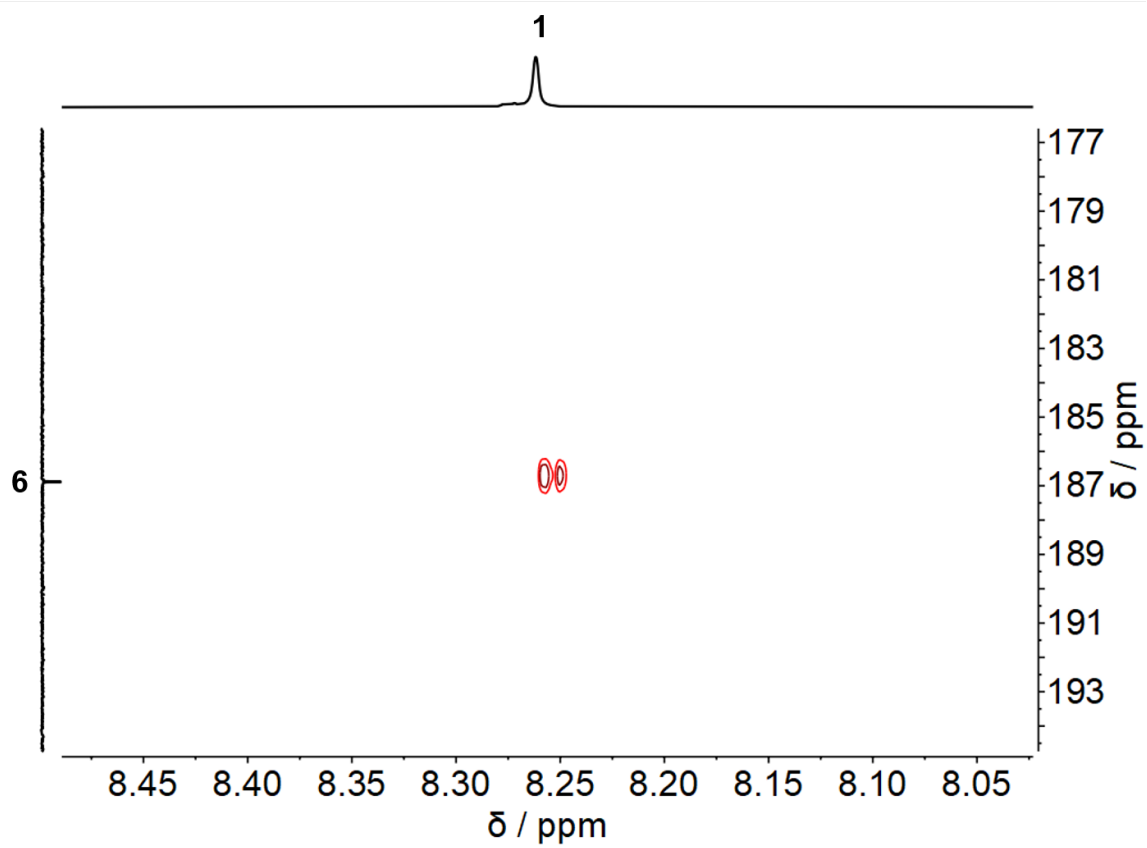
Figure S 105: selHSQMBC (600 MHz, DMSO-d_6, 25 °C) spectrum of the *Z* isomer of compound **5**. The coupling constant between C(6) and H(1) is 4.55 Hz and evidences the *Z* isomer.

2-((3-metyl-1*H*-indol-2-yl)methylene)benzo[*b*]thiophen-3(2*H*)-one (8)
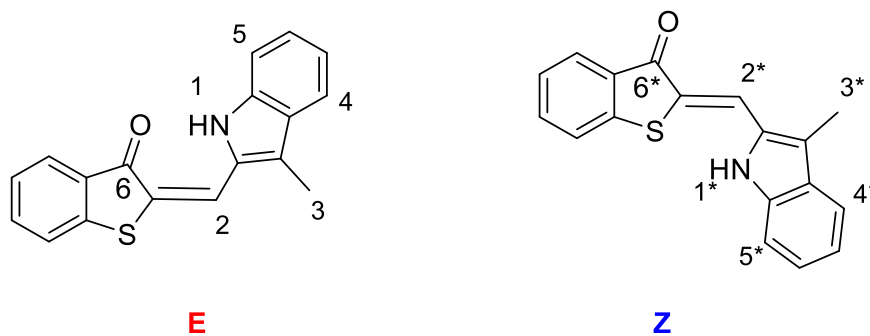
Figure S 106: Structure and conformation of the *Z* (assigned with *) and *E* isomer of compound **8**.
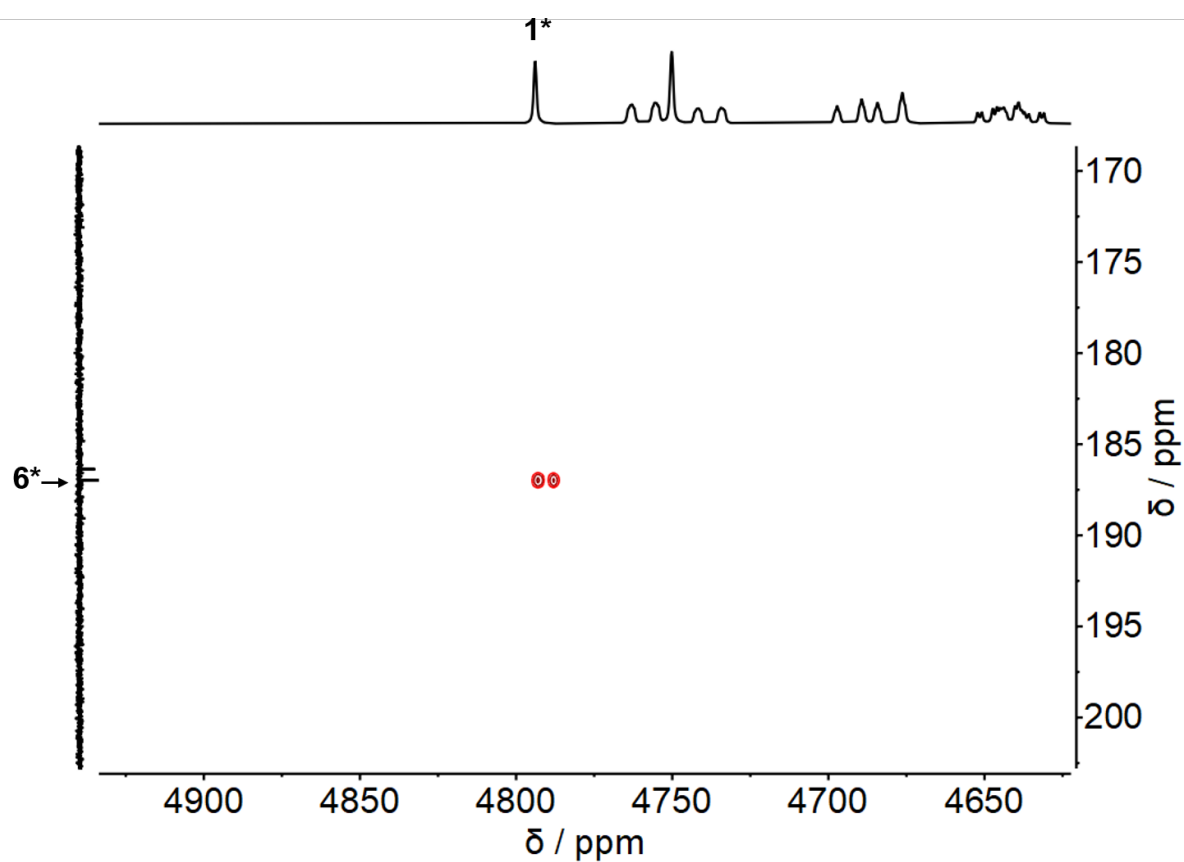
Figure S 107: selHSQMBC (600 MHz, DMSO-*d*₆, 25 °C) spectrum of a mixture of *Z* and *E* isomer of compound **8**. The coupling constant between C(6)* and H(2)* is 4.95 Hz and evidences the *Z* isomer.
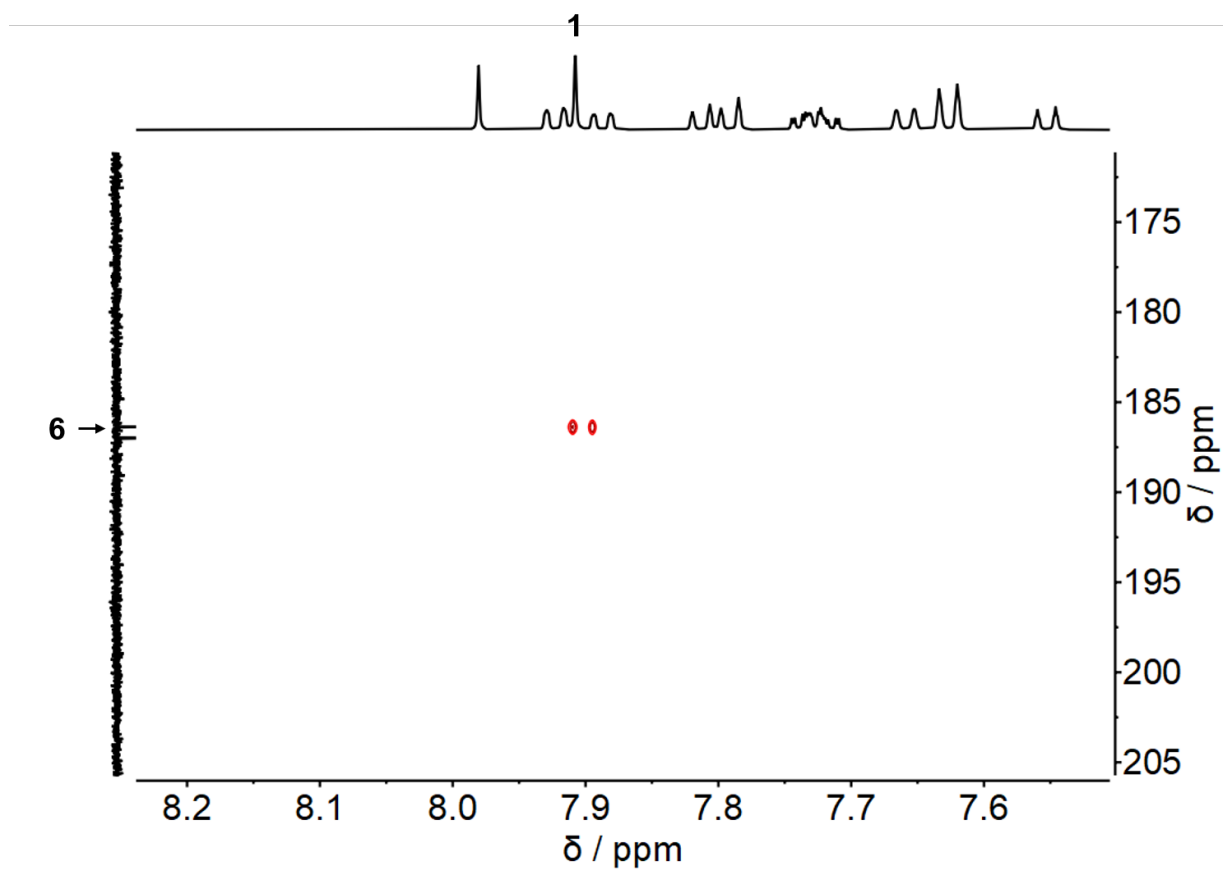
Figure S 108: selHSQMBC (600 MHz, DMSO-d_6, 25 °C) spectrum of a mixture of *Z* and *E* isomer of compound **8**. The coupling constant between C(6) and H(2) is 8.84 Hz and evidences the *E* isomer.
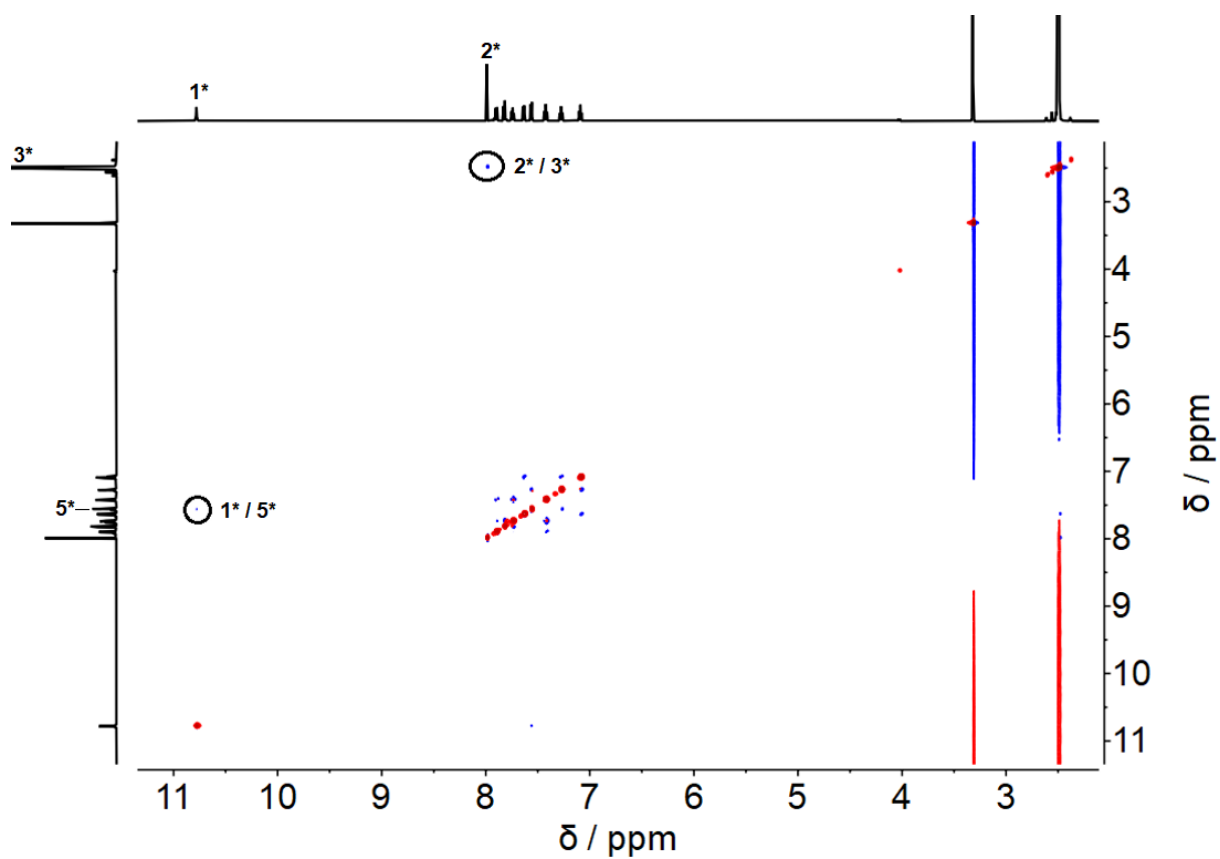
Figure S 109: NOESY (600 MHz, DMSO-d_6, 25 °C) spectrum of a mixture of *Z* and *E* isomer of compound **8**. Cross signals for the *Z* isomer between protons 2* and 3* as well as between 1* and 5* can be observed
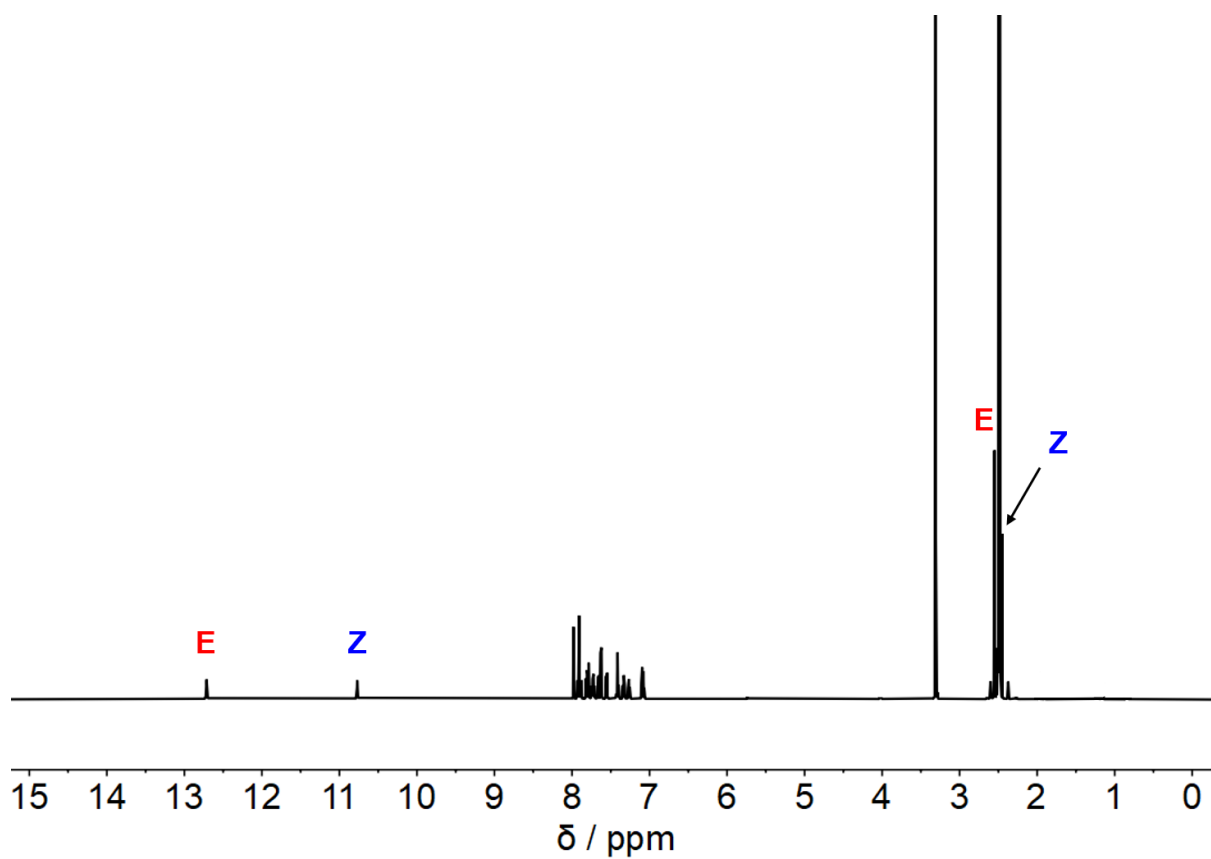
Figure S 110: ^{1}H NMR (600 MHz, DMSO-d_6, 25 °C) spectrum of a mixture of the *Z* isomer and *E* isomer of compound **8**. In the *E* isomer, the NH hydrogen is significantly downfield shifted compared to the NH hydrogen in the *Z* isomer.

2-(benzofuran-2-ylmethylene)benzo[*b*]thiophen-3(2*H*)-one (10)
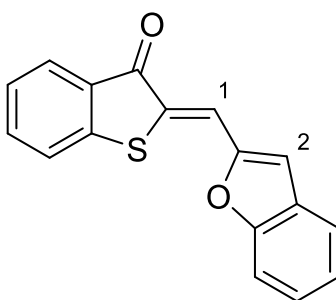
Figure S 111: Structure of the *Z* isomer of compound **10**.
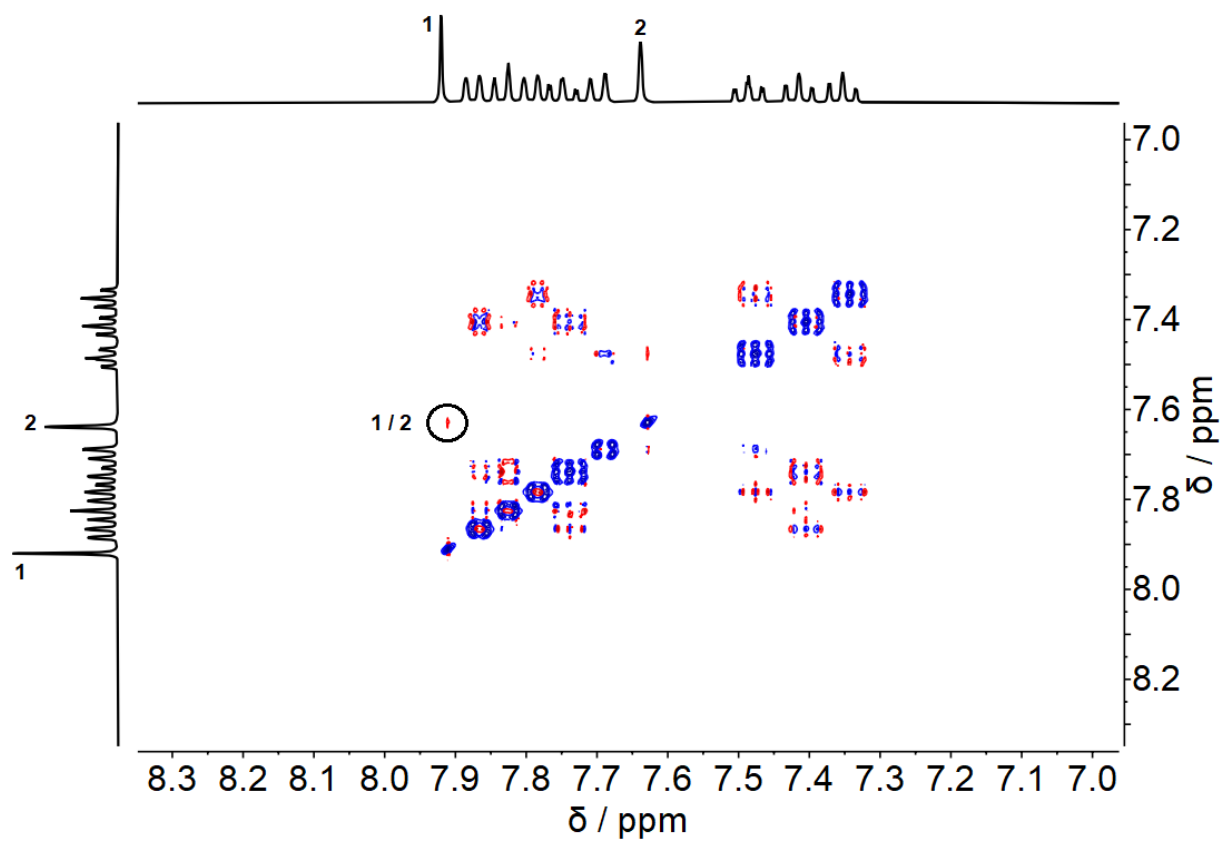
Figure S 112: NOESY (600 MHz, DMSO-*d₆*, 25 °C) spectrum of the *Z* isomer of compound **10**. Cross signal between protons 1 and 2 evidences the conformation shown in Figure S111.

Crystal Structural Data
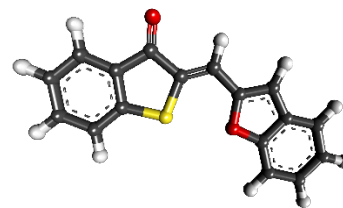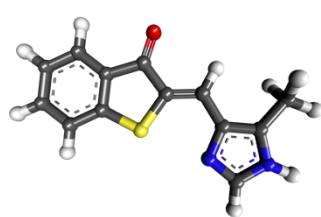
	Het-HTI 1 (VJ02_2) CCDC 2177529	Het-HTI 10 (VJ01_2) CCDC 2177531
Net formula	$C_{13}H_{10}N_2OS$	$C_{17}H_{10}O_2S$
$D_{calc.}$/ g cm^{-1}	1.433	1.504
μ/mm^{-1}	2.420	2.314
Formular weight	242.29	278.31
Colour	Clear orangish red	Clear orangish red
Shape	Block-shaped	Plate-shaped
Size/mm^3	0.33×0.26×0.09	0.21×0.07×0.05
T/K	153.00(10)	153.00(10)
Crystal System	orthorohmbic	orthorhombic
Flack Parameter		-0.03(3)
Hooft Parameter		-0.024(18)
Space Group	$Pnma$	$Pca2_1$
a/Å	14.7305(10)	28.1928(11)
b/Å	6.4680(7)	3.8475(2)
c/Å	11.7910(7)	11.3330(5)
α/$^\circ$	90	90
β/$^\circ$	90	90
γ/$^\circ$	90	90
V/ Å^3	1123.41(16)	1229.31(10)
Z	4	4
Z'	0,5	1
Wavelength/ Å	1.54184	1.54184
Radiation type	Cu K$_\alpha$	Cu K$_\alpha$
Q_{min}/$^\circ$	4.804	3.135
Q_{max}/$^\circ$	71.320	72.121
Measured Refl's	2355	3355
Indep't Refl's	1148	1794
Refl's I≥2 σ(I)	1027	1703
R_{int}	0.0376	0.0231
Parameters	107	181
Restraints	0	1
Largest Peak	0.240	0.260
Deepest Hole	-0.358	-0.219
GooF	1.095	1.068
wR_2 (all data)	0.1248	0.0856
wR_2	0.1202	0.0825
R_1 (all data)	0.0552	0.0346
R_1	0.0502	0.0322
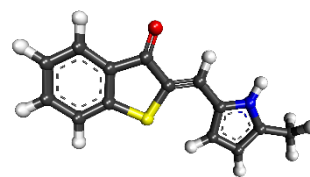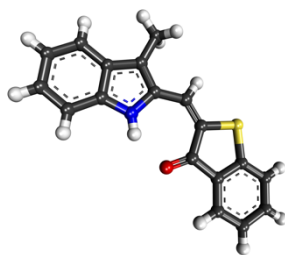
	Het-HTI 8 (VJ04) CCDC 2177530	Het-HTI 4 (VJ05) CCDC 2192395
Net formula	$C_{18}H_{13}NOS$	$C_{14}H_{11}NOS$
$D_{calc.}$/ g cm^{-1}	1.416	1.429
μ/mm^{-1}	2.070	2.394
Formular weight	291.35	241.30
Colour	Clear dark red	Clear dark red
Shape	Needle-shaped	Blocked-shaped
Size/mm^3	0.21×0.18×0.14	0.36×0.12×0.06
T/K	152.9(8)	153.0(3)
Crystal System	monoclinic	monoclinic
Flack Parameter		
Hooft Parameter		
Space Group	$P2_1/n$	$P2_1/n$
a/Å	6.7326(2)	12.5881(5)
b/Å	8.0758(2)	3.94440(10)
c/Å	25.2164(6)	23.2090(9)
α/°	90	90
β/°	94.539(2)	103.301(4)
γ/°	90	90
V/ Å^3	1366.74(6)	1121.47(7)
Z	4	4
Z'	1	1
Wavelength/ Å	1.54184	1.54184
Radiation type	Cu K$_\alpha$	Cu K$_\alpha$
Q_{min}/°	3.517	3.688
Q_{max}/°	71.544	71.477
Measured Refl's	4106	3174
Indep't Refl's	2494	2095
Refl's I≥2 σ(I)	2342	1771
R_{int}	0.0148	0.0258
Parameters	191	155
Restraints	0	0
Largest Peak	0.316	0.266
Deepest Hole	-0.238	-0.440
GooF	1.062	1.033
wR_2 (all data)	0.0970	0.1072
wR_2	0.0954	0.0994
R_1 (all data)	0.0371	0.0466
R_1	0.0355	0.0385

NMR Spectra of Compounds 1-16
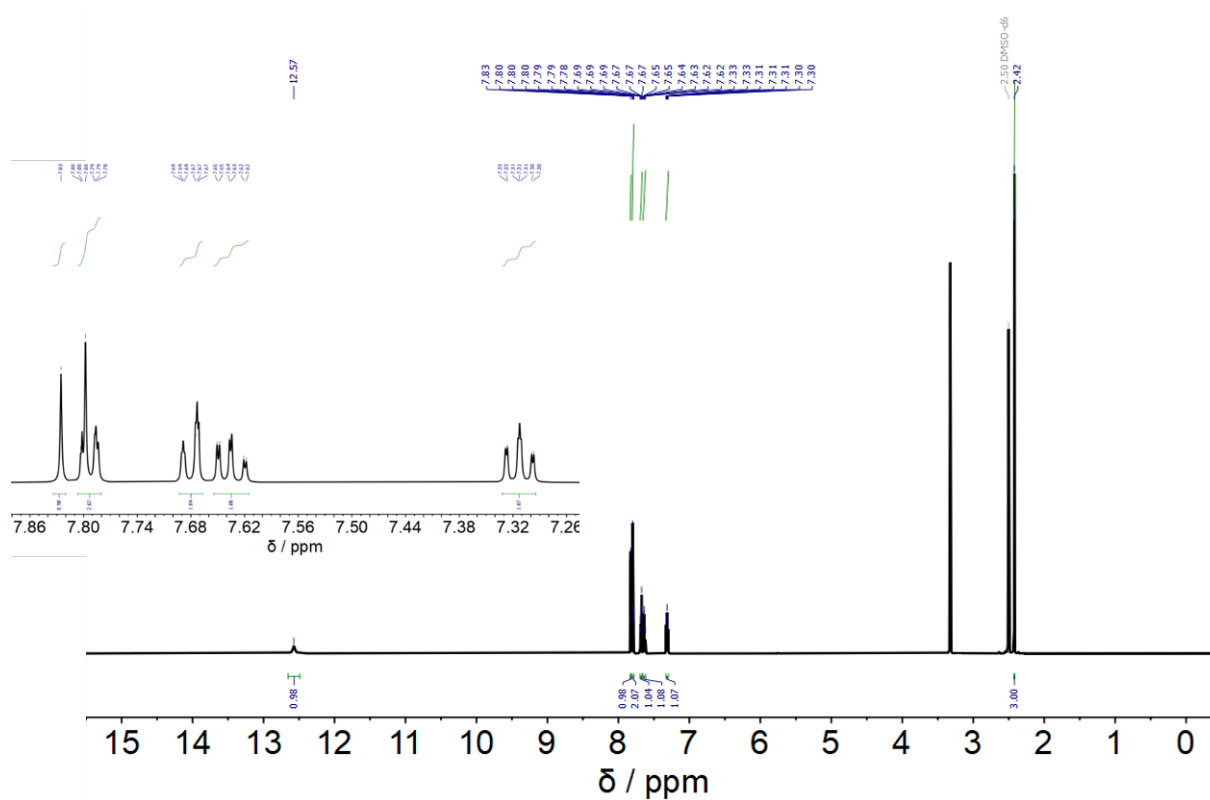
Figure S 113: ^{1}H NMR spectrum (500 MHz, DMSO-d_6, 26 °C) of **1**.
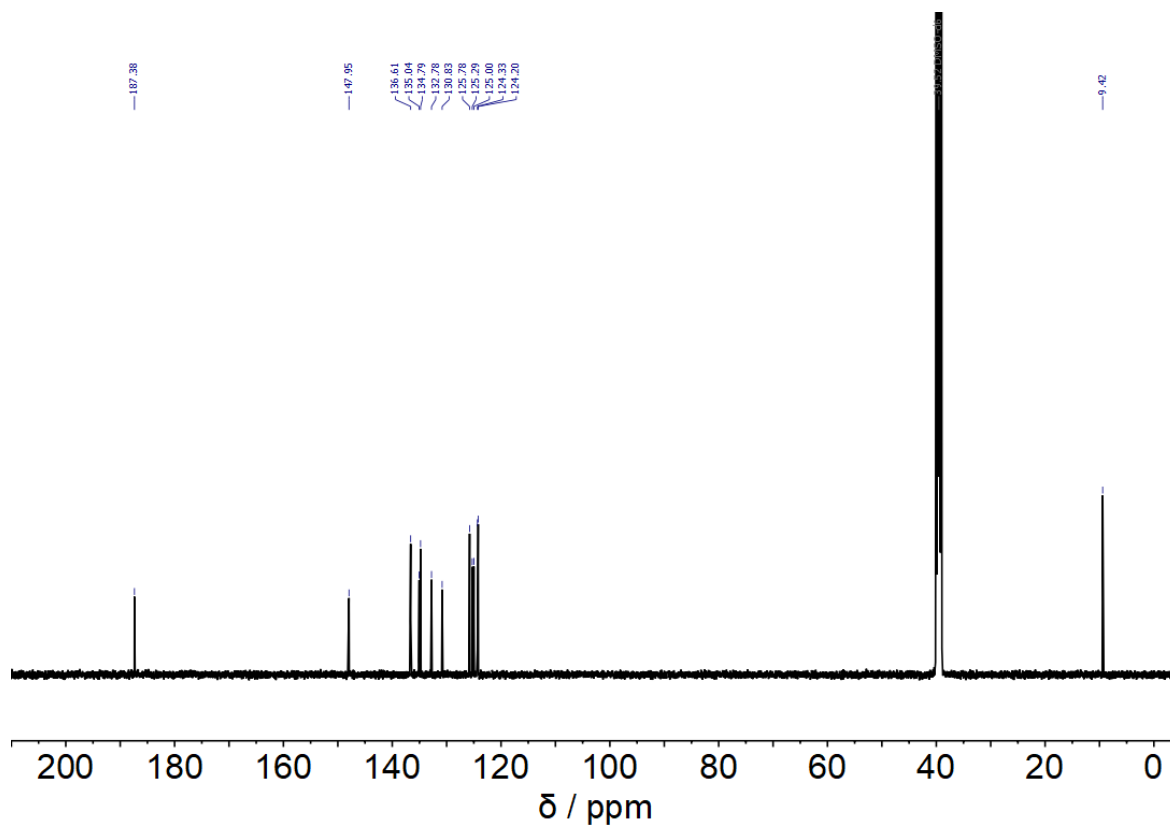
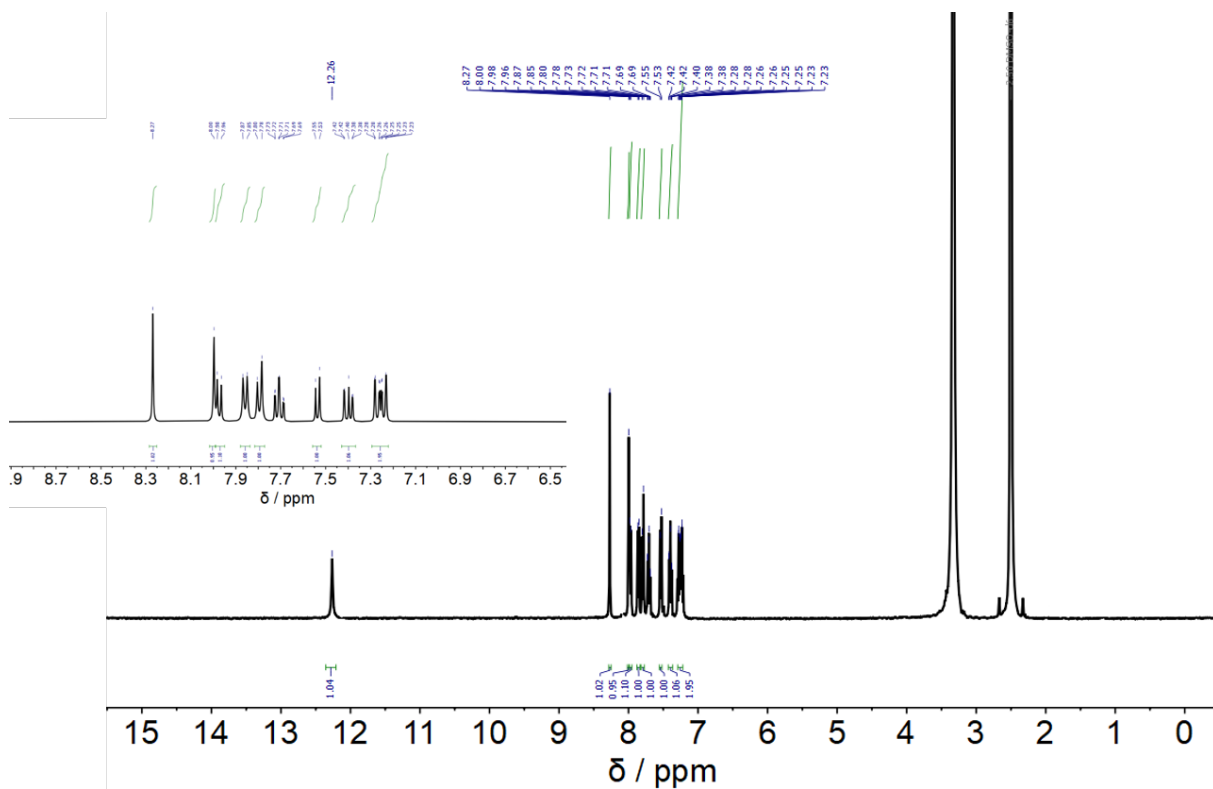**Figure S 114:** ^{13}C NMR spectrum (126 MHz, DMSO-d_6, 26 °C) of **1**.
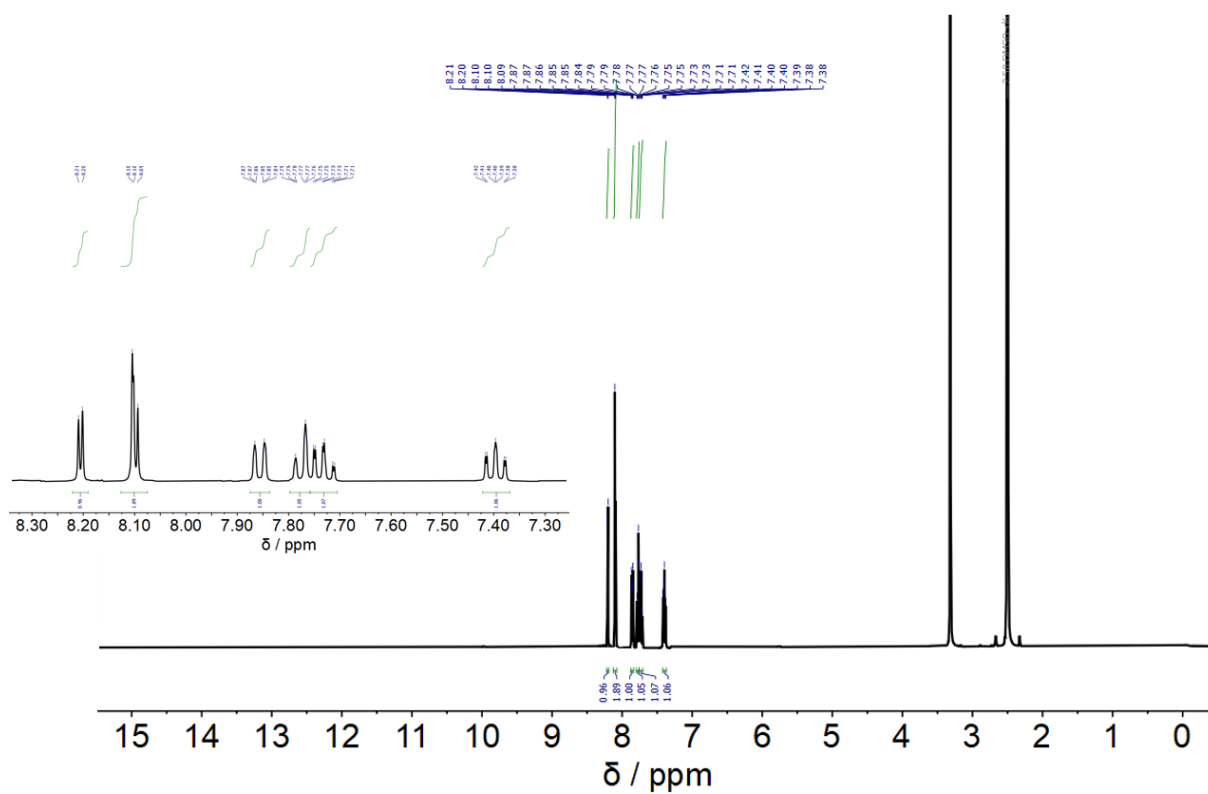
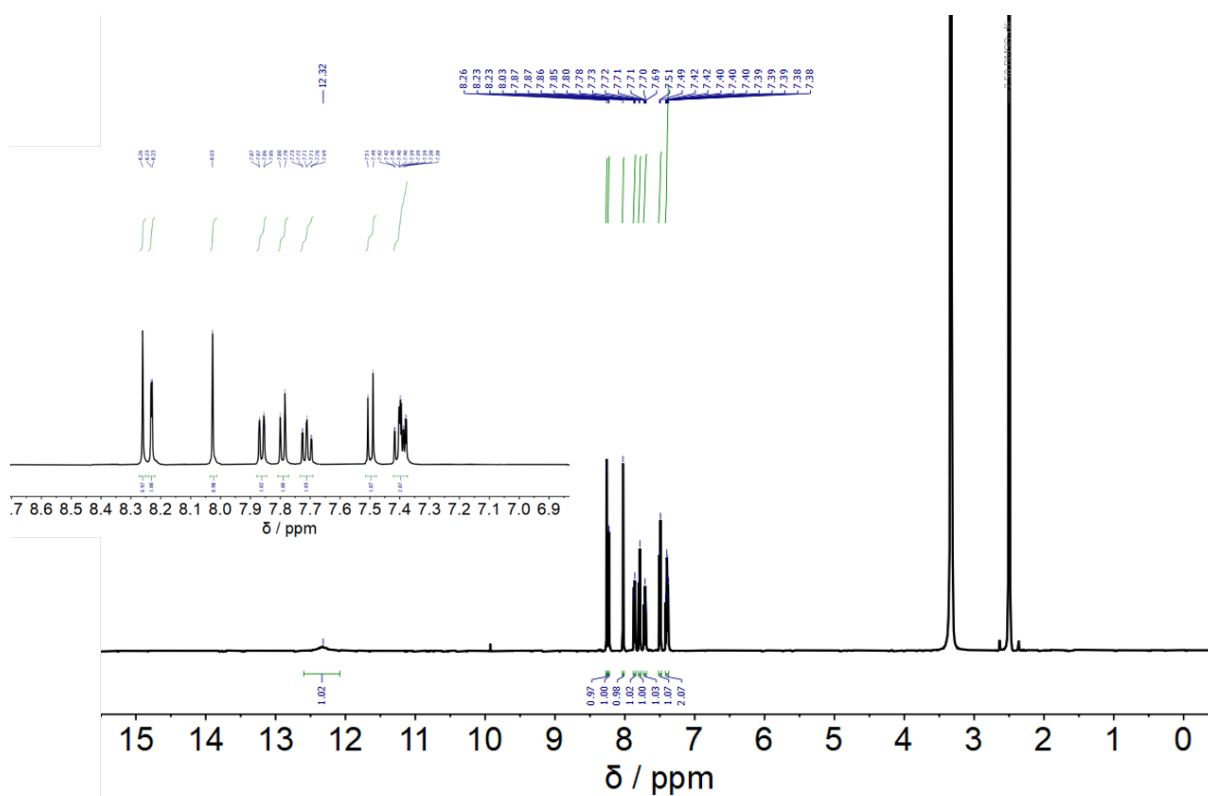**Figure S 115:** ^{1}H NMR spectrum (500 MHz, DMSO-d_6, 26 °C) of **2**.
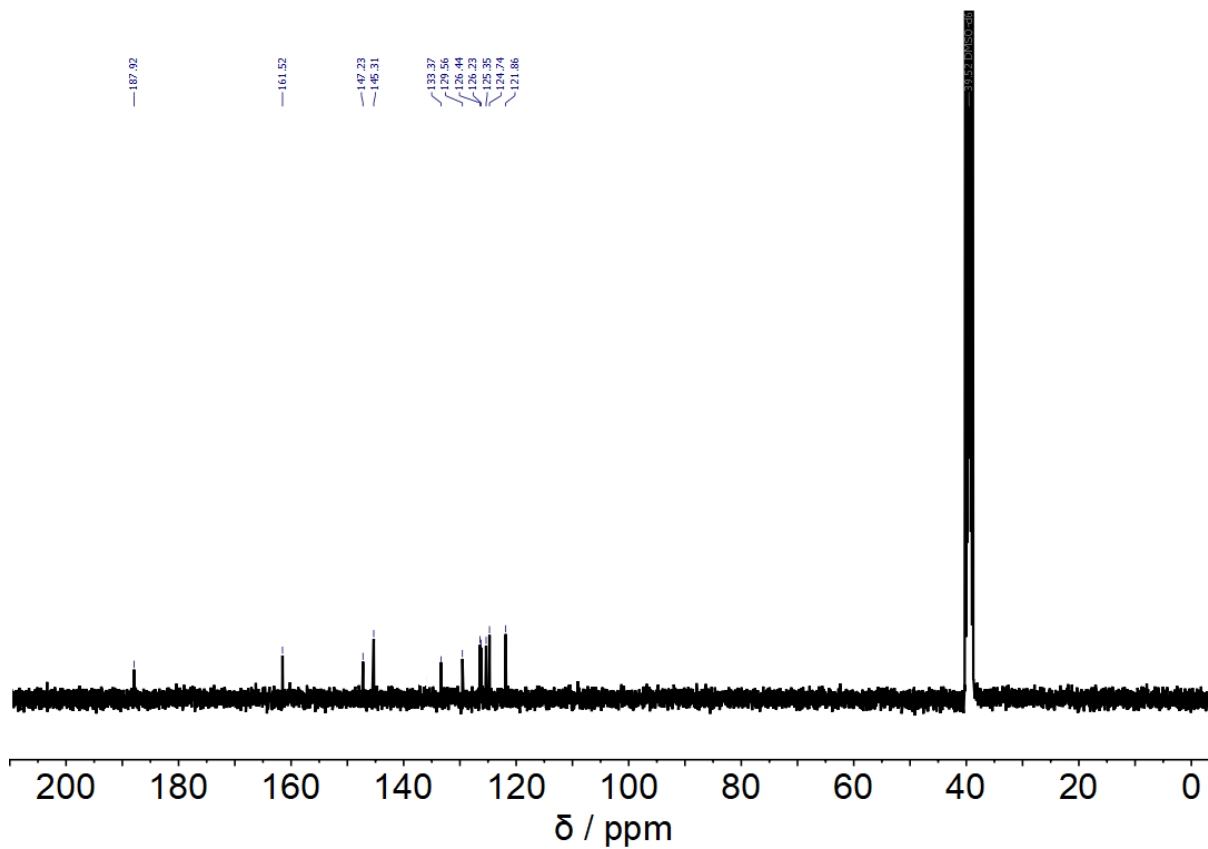
Figure S 116: ^{13}C NMR spectrum (126 MHz, DMSO-d_6, 26 °C) of **2**.
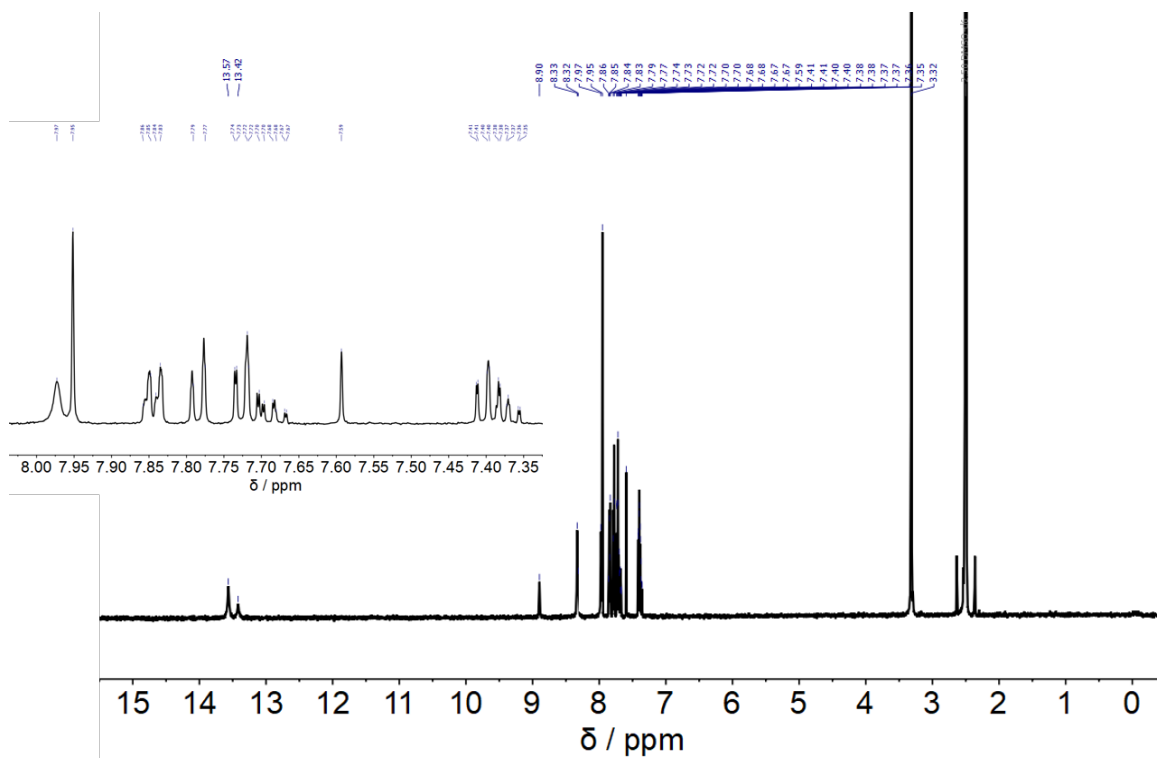
Figure S 117: ^{1}H NMR spectrum (500 MHz, DMSO-d_6, 26 °C)of *E*/*Z* isomer mixture of **3**. Due to the tautomerism on the pyrazole, the signal sets are doubled.
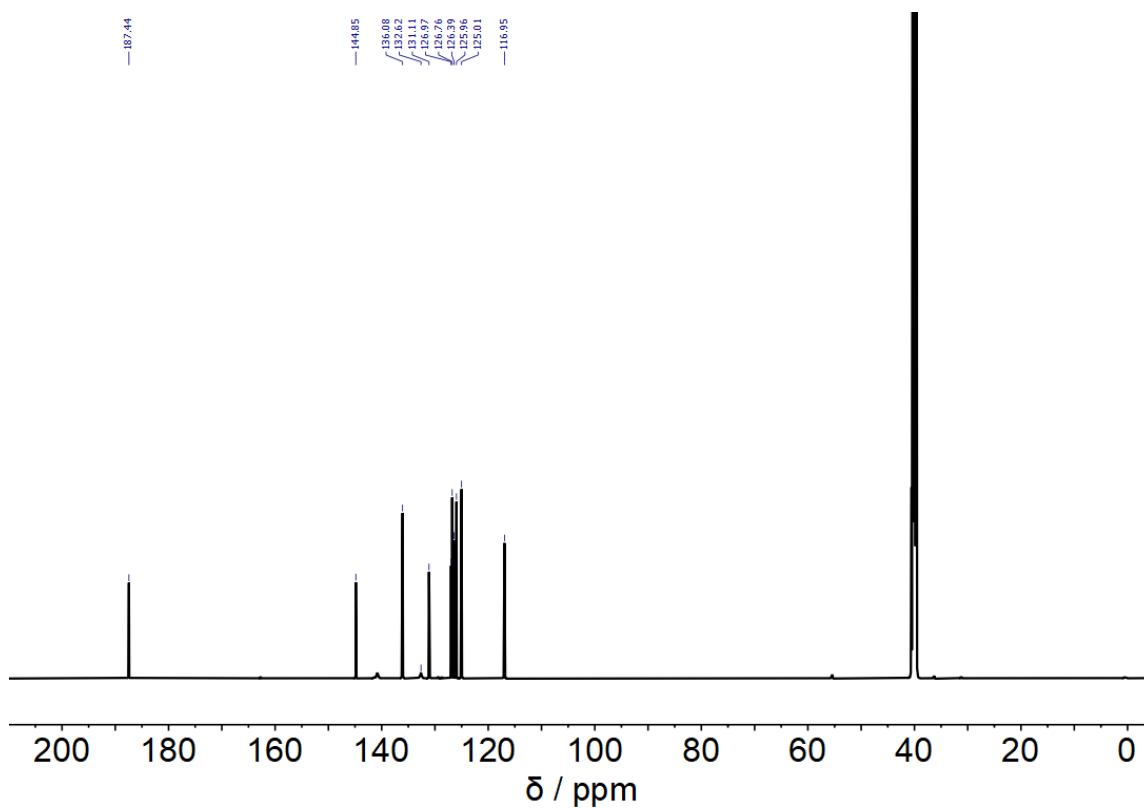
Figure S 118: ^{13}C NMR spectrum (126 MHz, DMSO-d_6, 26 °C) of *E*/*Z* isomer mixture of **3**. Due to the tautomerism on the pyrazole, the signal sets are doubled.
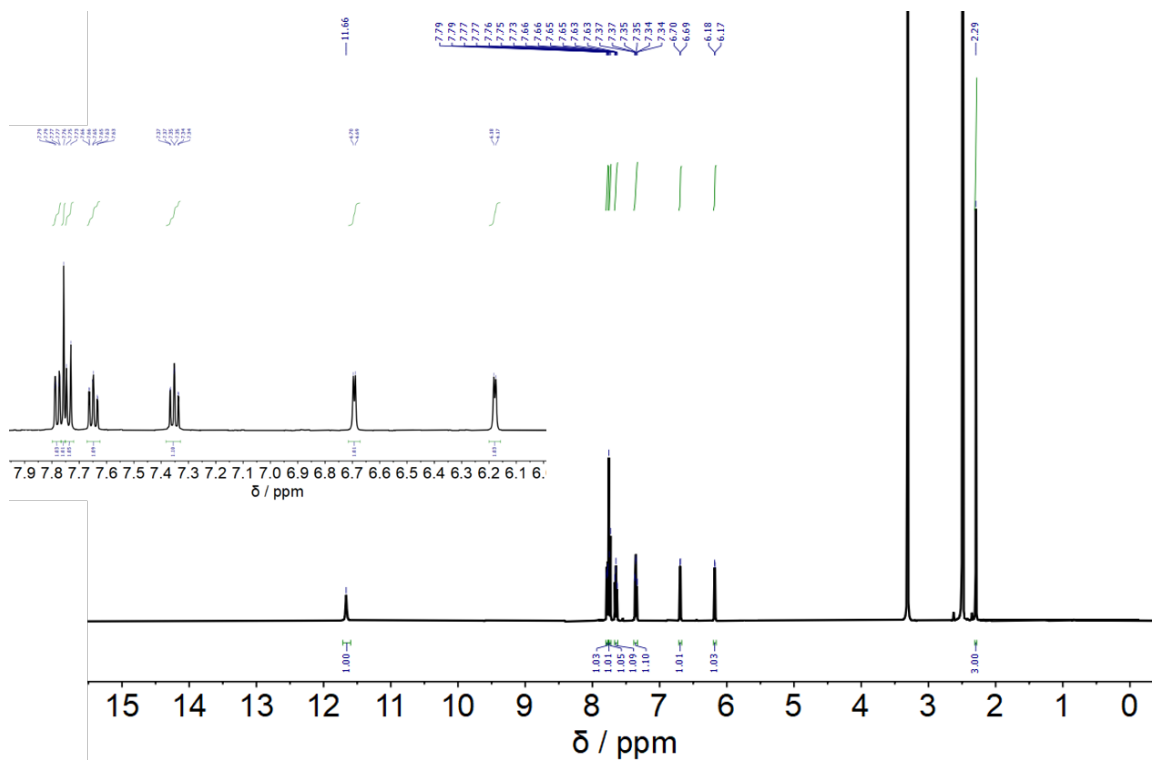
Figure S 119: ^{1}H NMR spectrum (500 MHz, DMSO-d_6, 26 °C) of **4**.
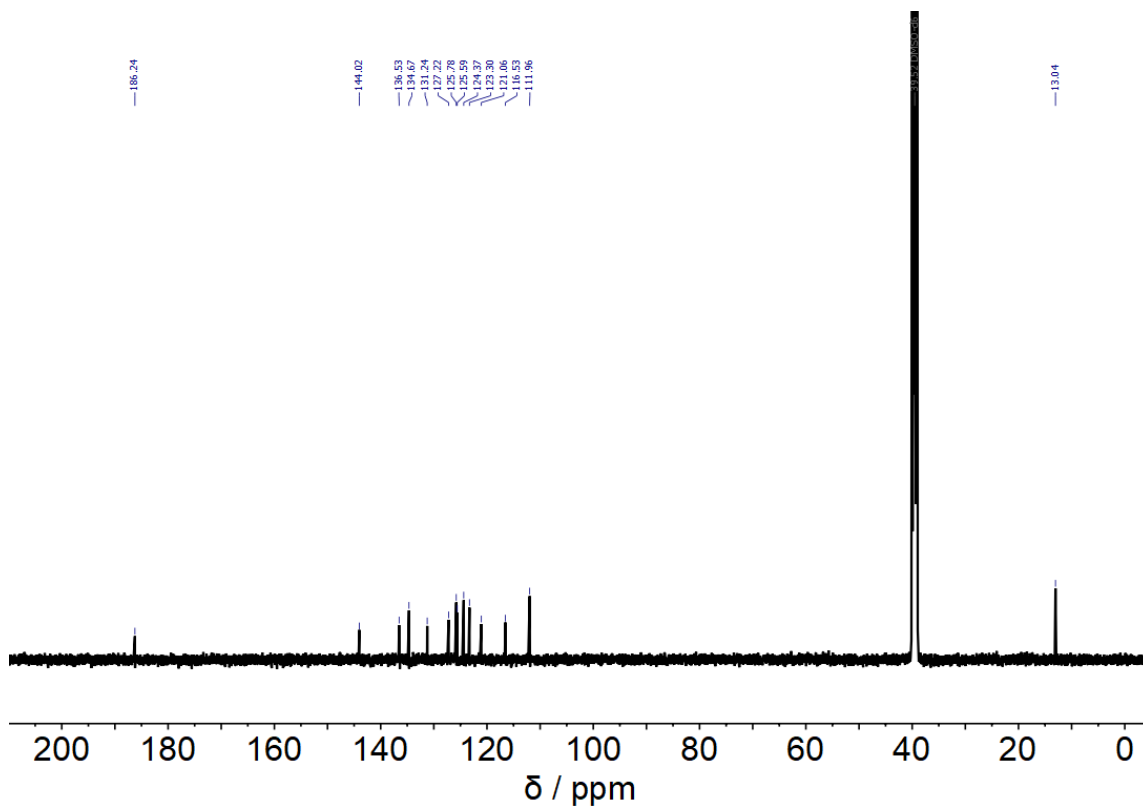
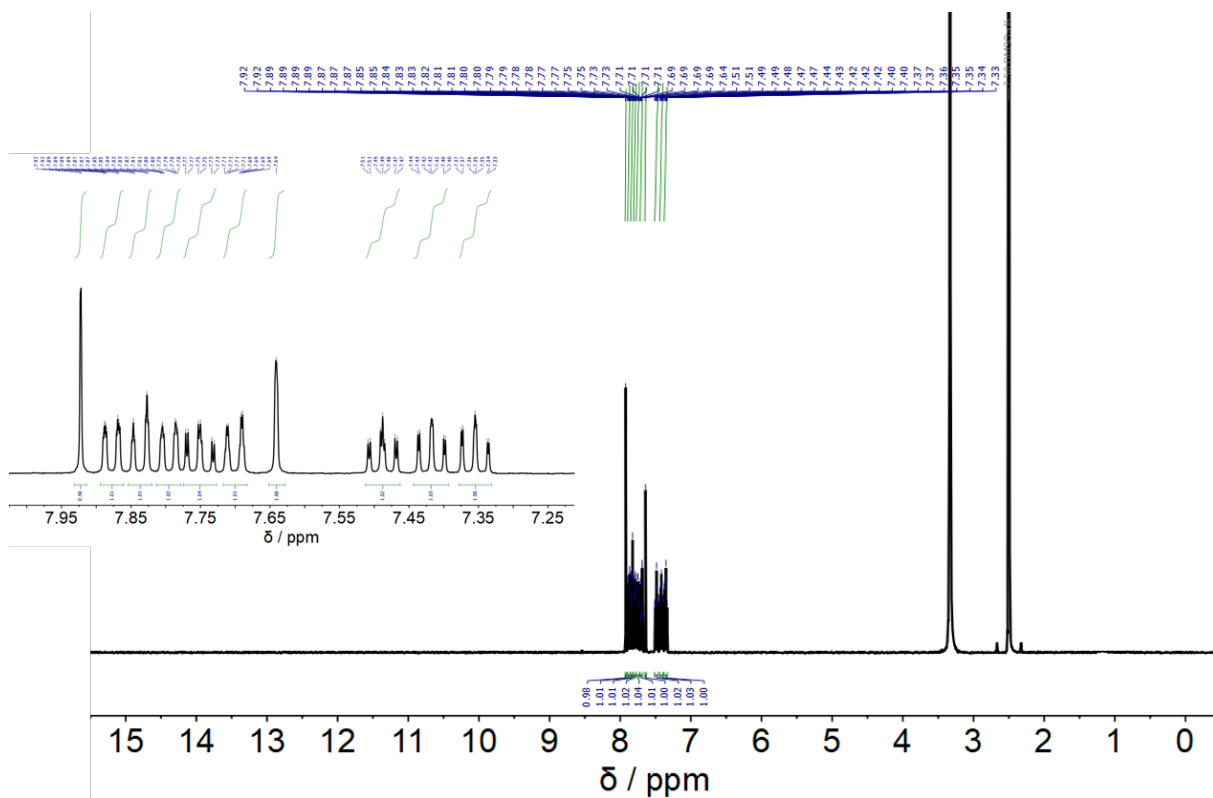**Figure S 120:** ^{13}C NMR spectrum (126 MHz, DMSO-d_6, 26 °C) of **4**.

Figure S 121: ^{1}H NMR spectrum (400 MHz, DMSO-d_6, 26 °C) of **5**.
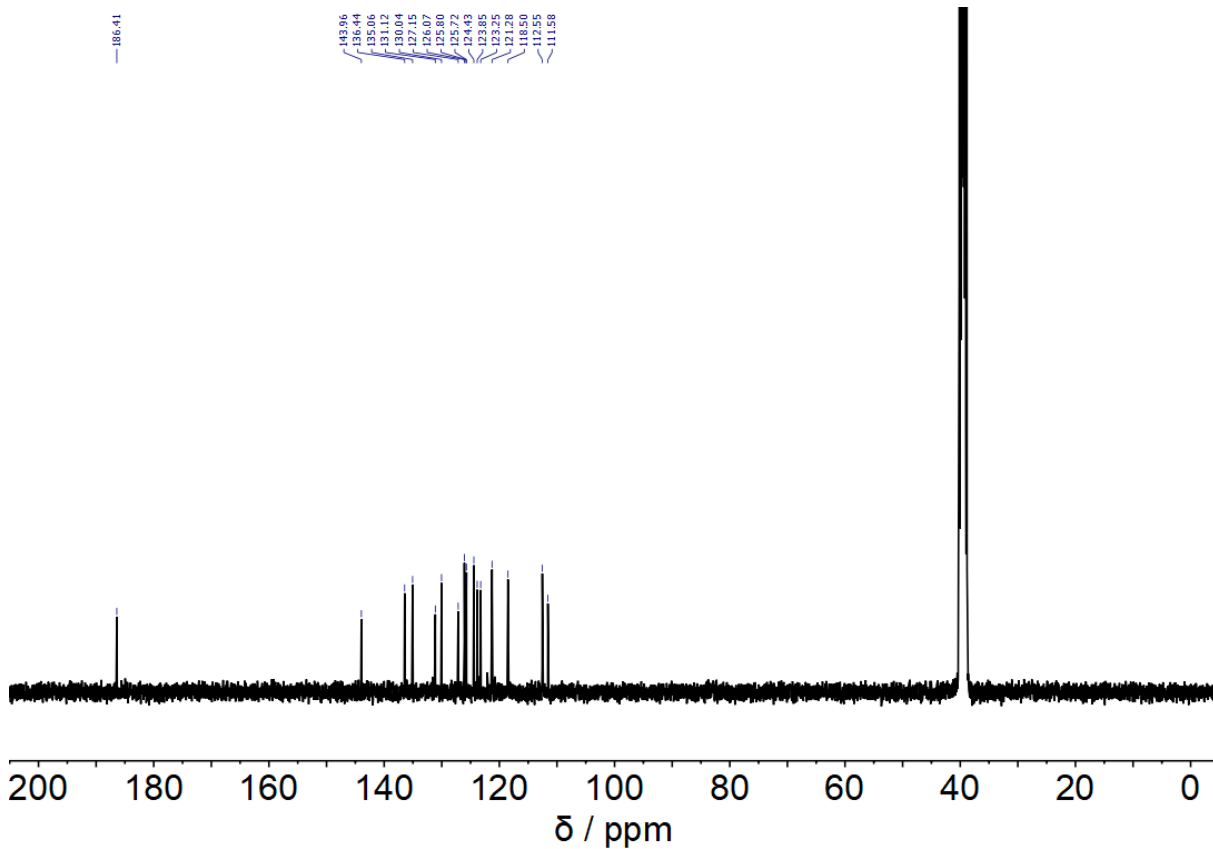
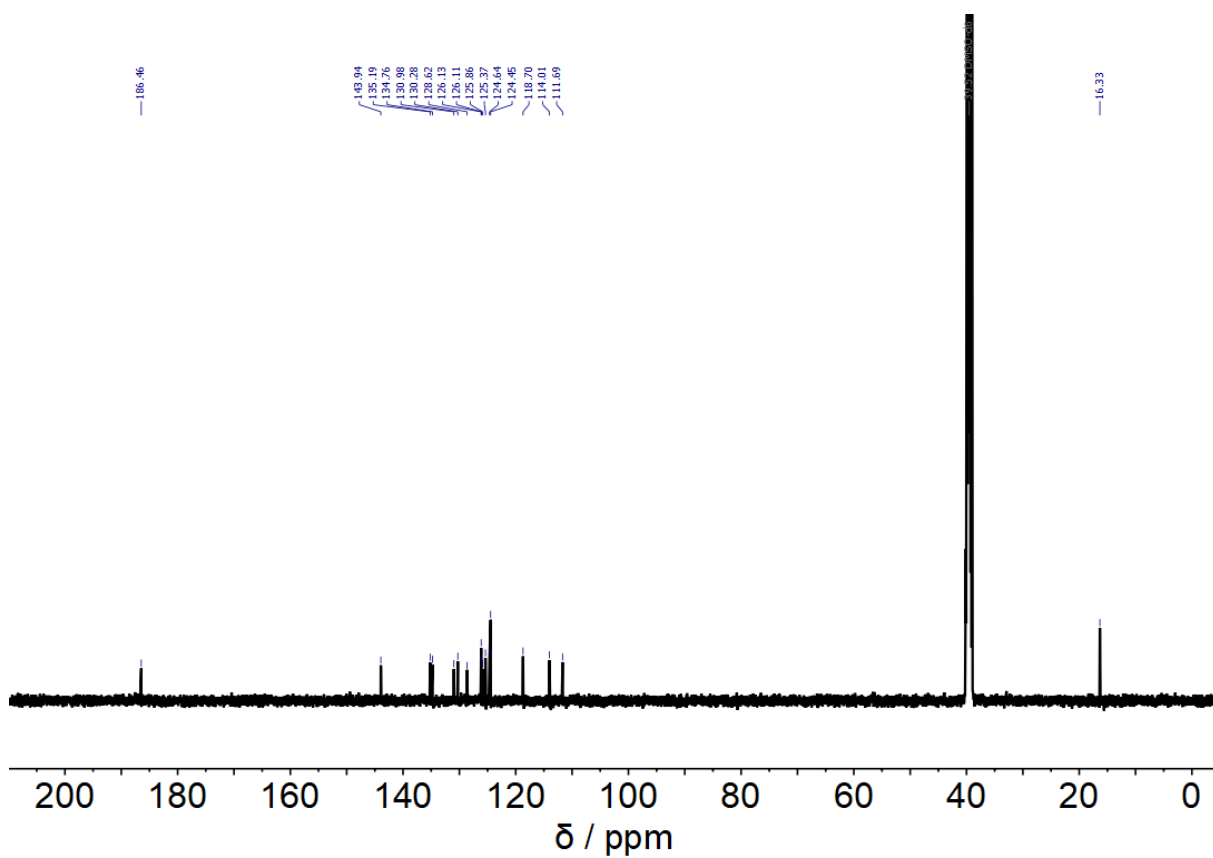**Figure S 122:** ^{13}C NMR spectrum (101 MHz, DMSO-d_6, 26 °C) of **5**.

Figure S 123: ^{1}H NMR spectrum (500 MHz, DMSO-d_6, 26 °C) of *E*/*Z* isomer mixture of **6**.
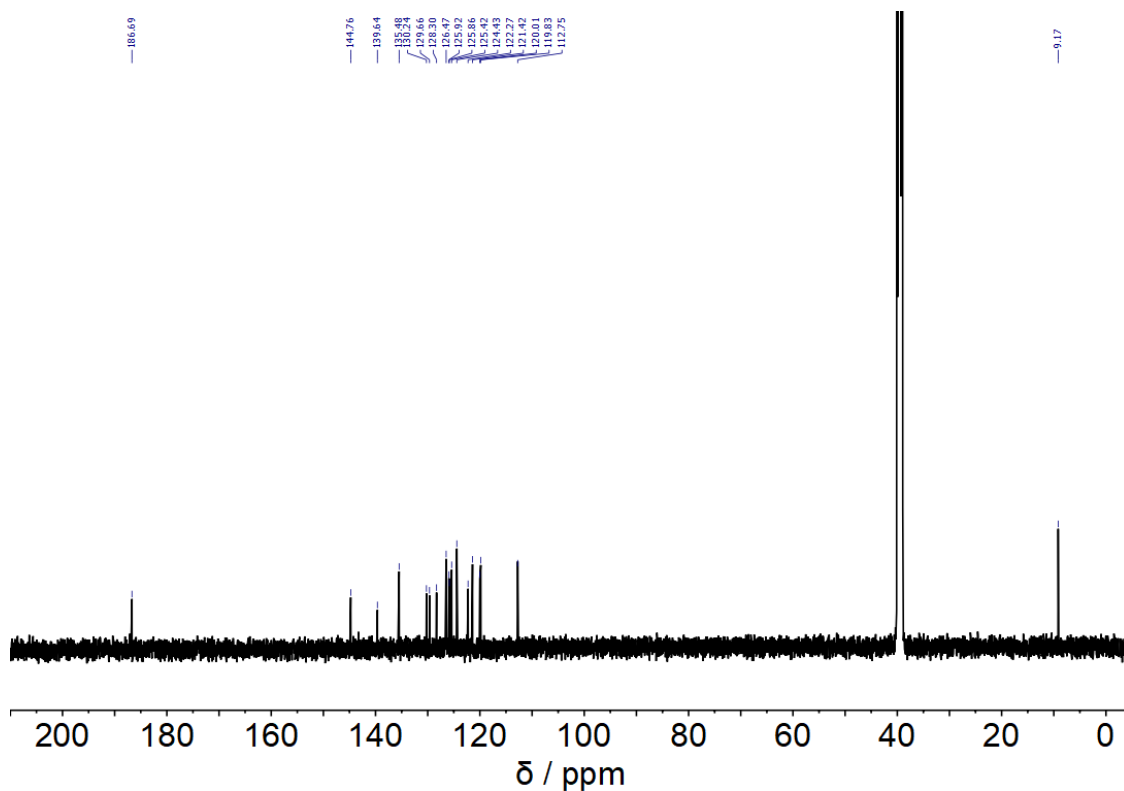
Figure S 124: ^{13}C NMR spectrum (126 MHz, DMSO-d_6, 26 °C) of *E*/*Z* isomer mixture of **6**.
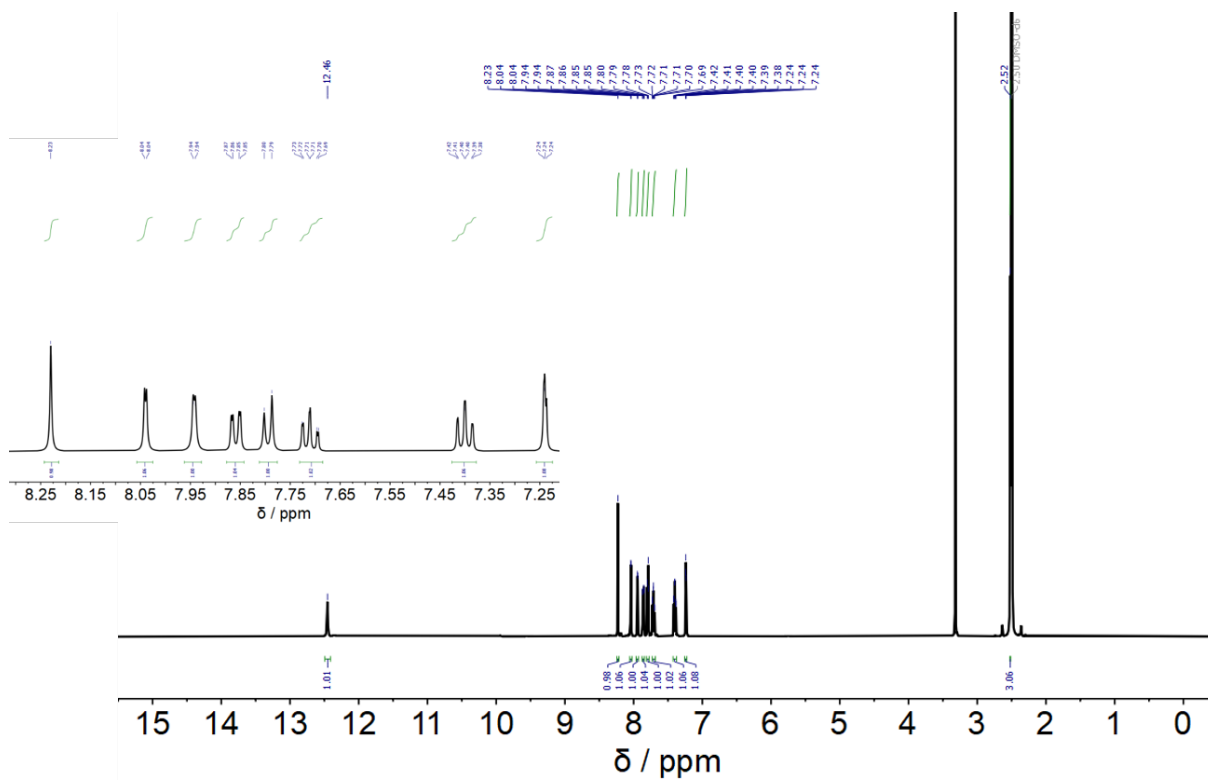
Figure S 125: ^{1}H NMR spectrum (400 MHz, DMSO-d_6, 26 °C) of **7**.
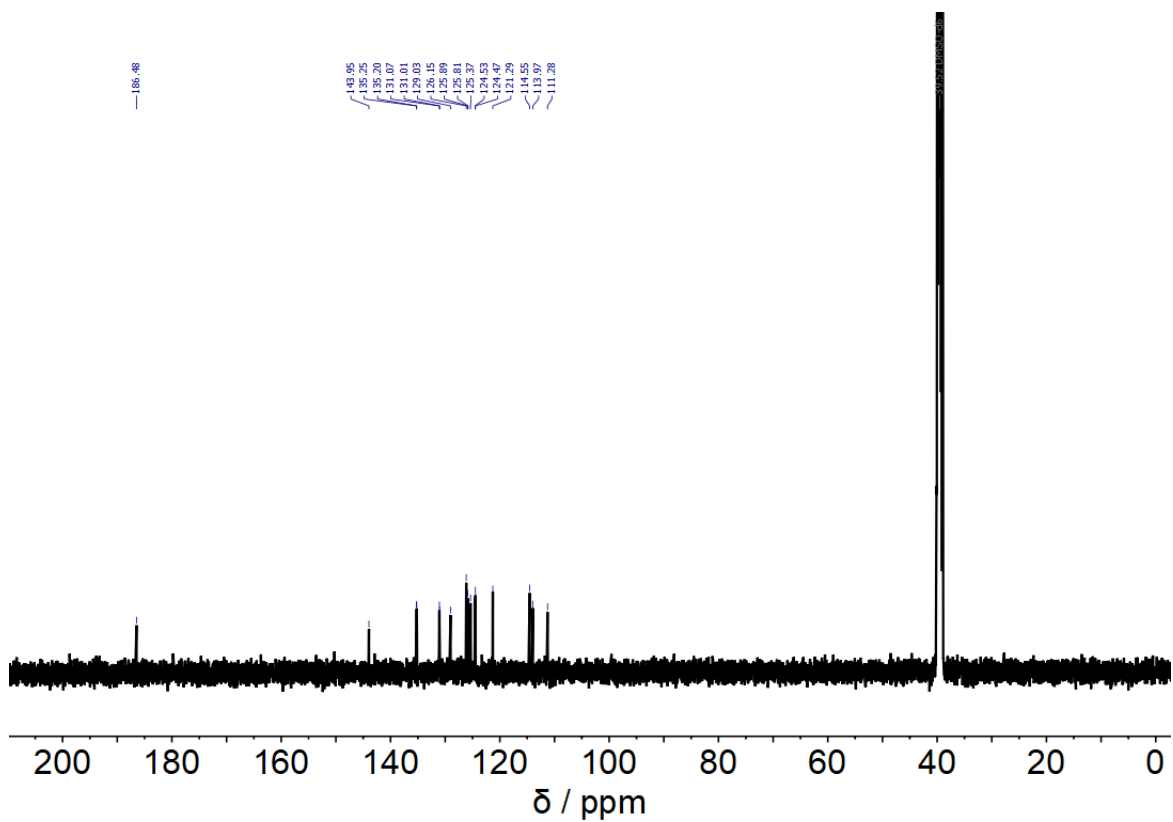
Figure S 126: ^{13}C NMR spectrum (101 MHz, DMSO-d_6, 26 °C) of **7**.

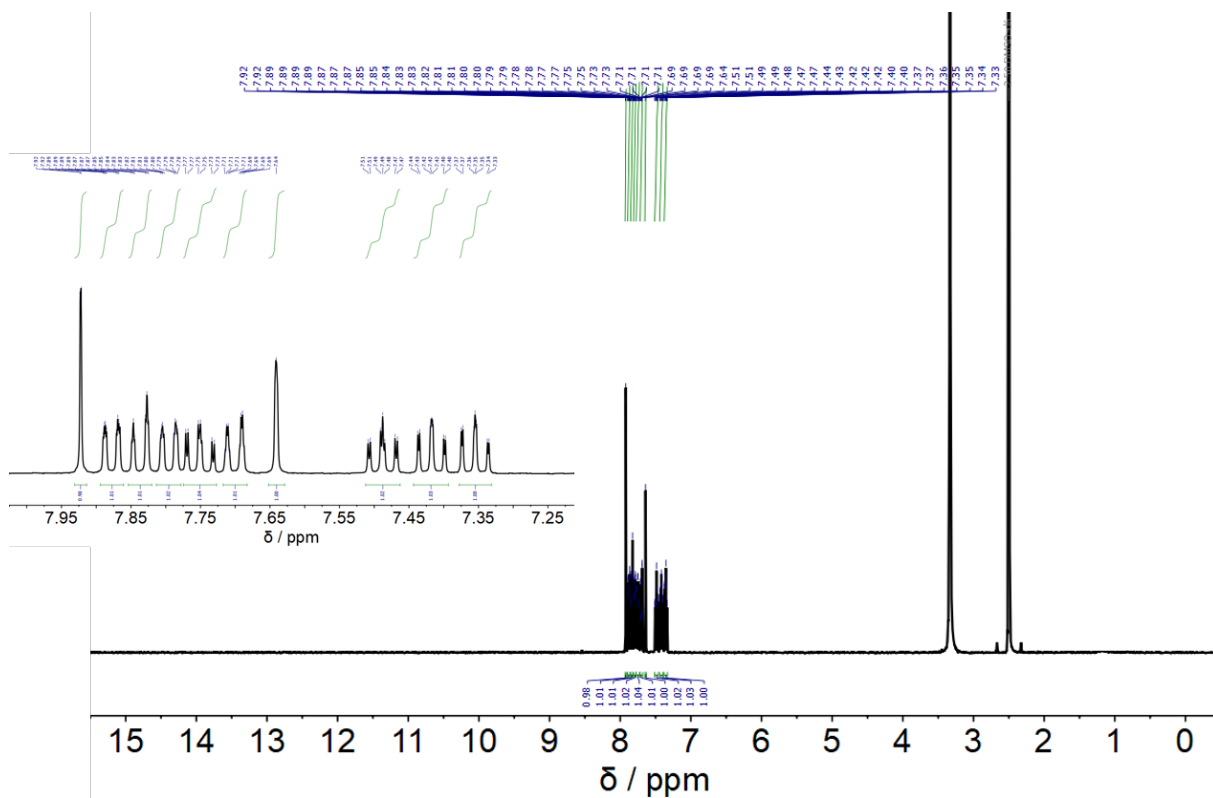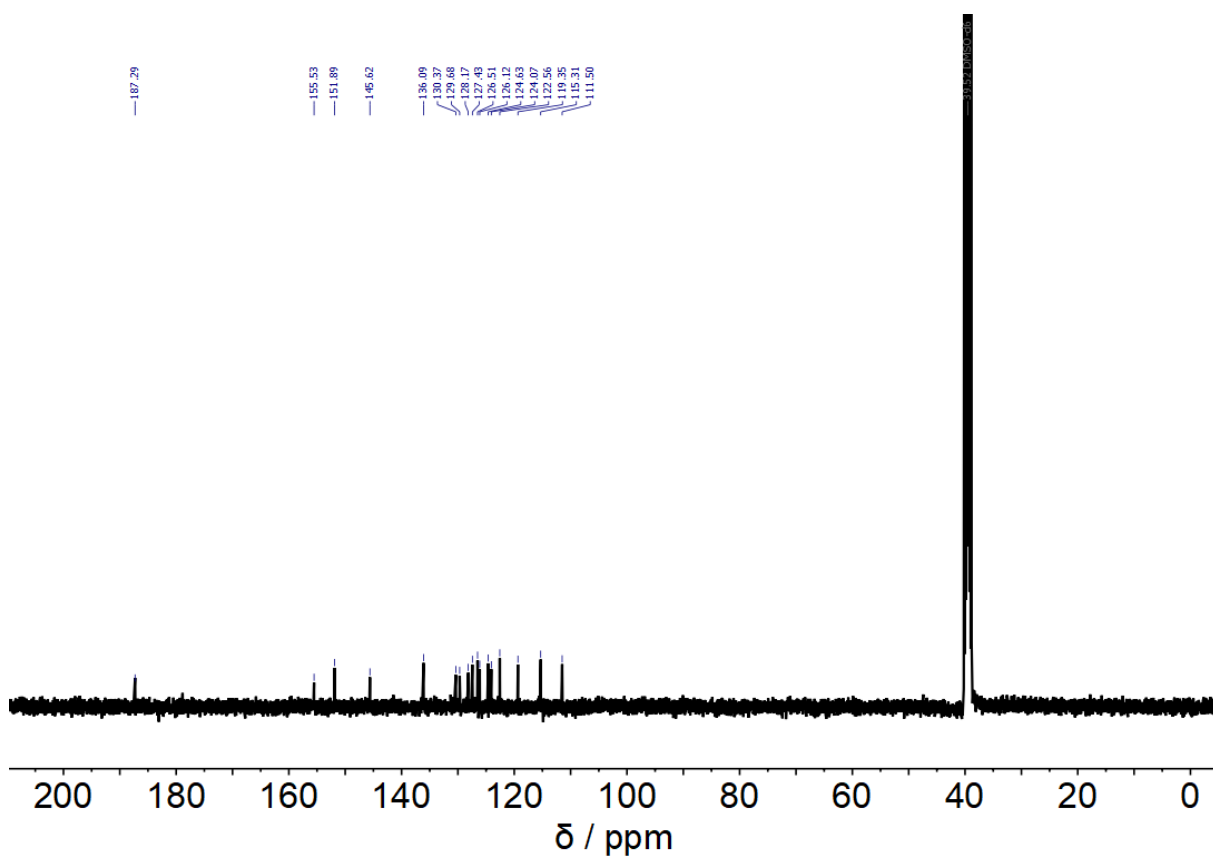**Figure S 127:** ^{1}H NMR spectrum (500 MHz, DMSO-d_6, 26 °C) of **8**.

Figure S 128: ^{13}C NMR spectrum (126 MHz, DMSO-d_6, 26 °C) of **8**.
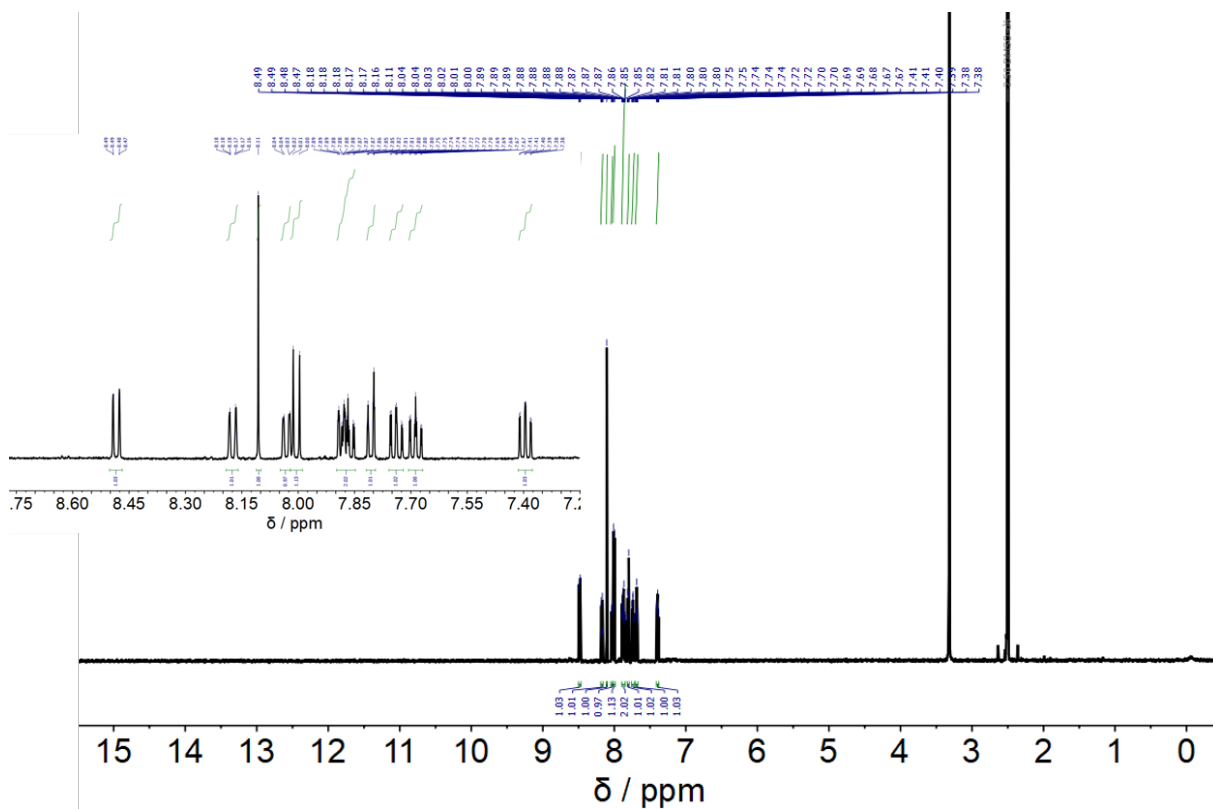
Figure S 129: ^{1}H NMR spectrum (500 MHz, DMSO-d_6, 26 °C) of **9**.
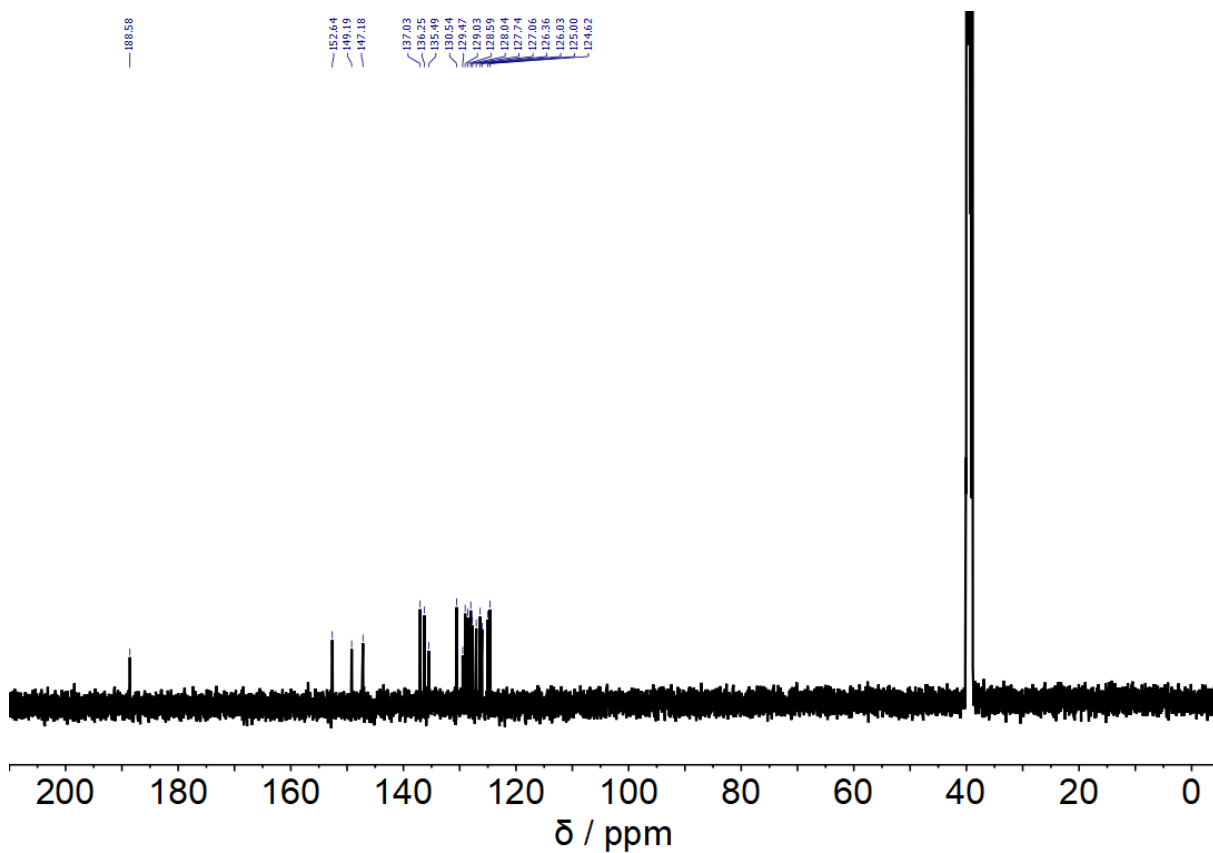
Figure S 130: ^{13}C NMR spectrum (126 MHz, DMSO-d_6, 26 °C) of **9**.

Figure S 131: ^{1}H NMR spectrum (400 MHz, DMSO-d_6, 26 °C) of **10**.

Figure S 132: ^{13}C NMR spectrum (101 MHz, DMSO-d_6, 26 °C) of **10**.

Figure S 133: ^1H NMR spectrum (600 MHz, DMSO-d_6, 26 °C) of **11**.

Figure S 134: ^{13}C NMR spectrum (151 MHz, DMSO-d_6, 26 °C) of **11**.
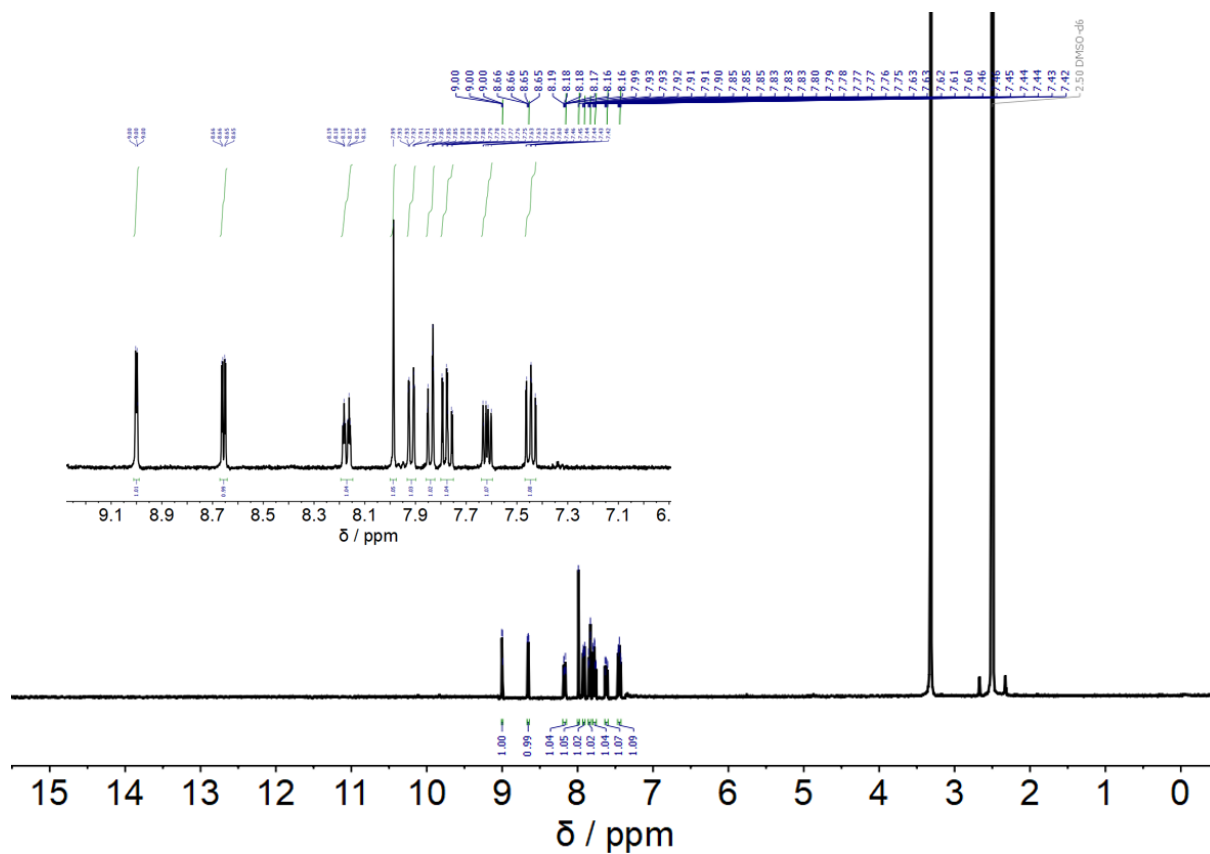
Figure S 135: ^{1}H NMR spectrum (400 MHz, DMSO-d_6, 26 °C) of **12**.
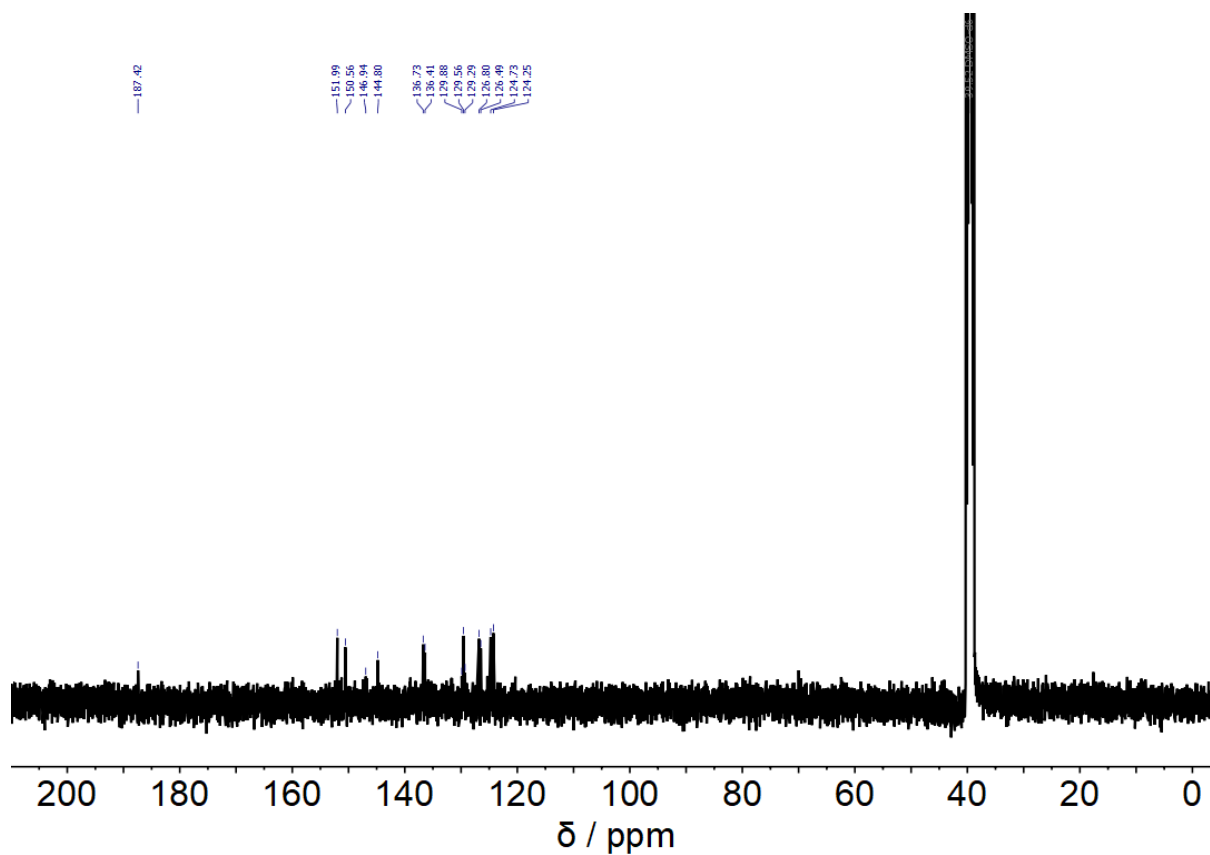
Figure S 136: ^{13}C NMR spectrum (101 MHz, DMSO-d_6, 26 °C) of **12**.

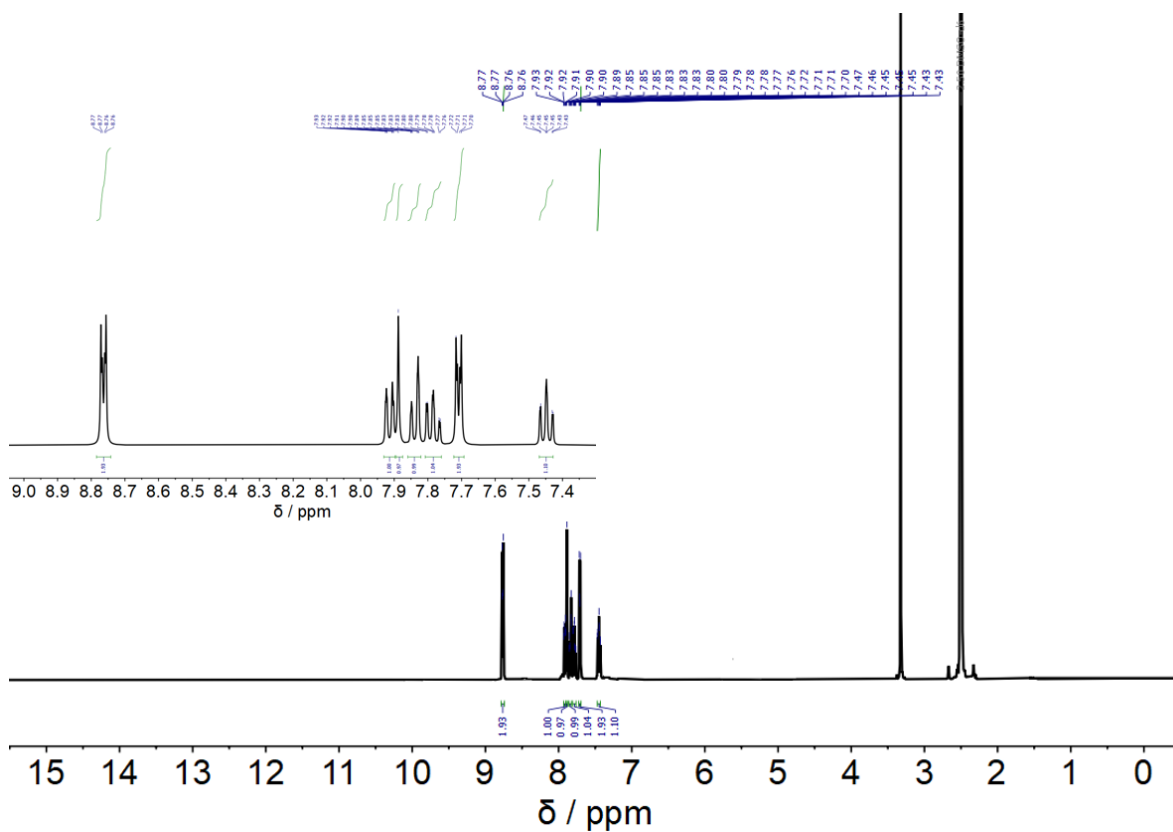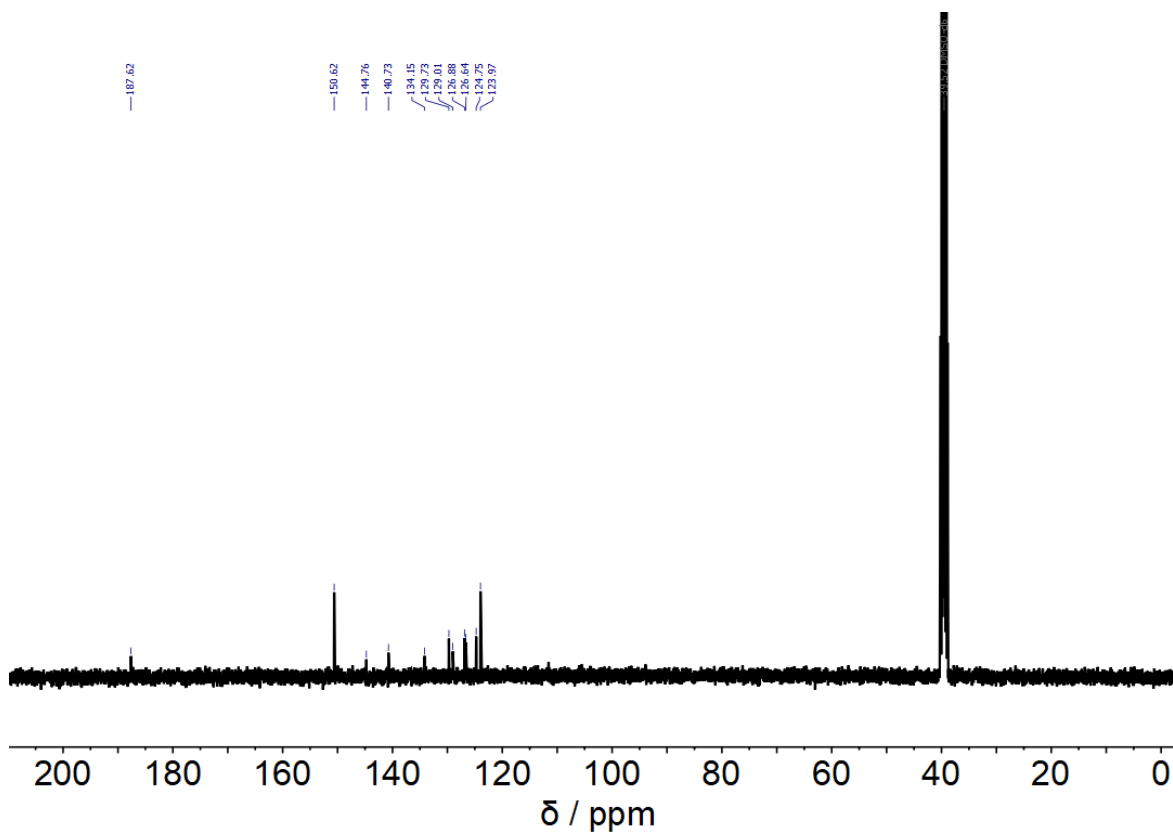**Figure S 137:** ^{1}H NMR spectrum (500 MHz, DMSO-d_6, 26 °C) of **13**.

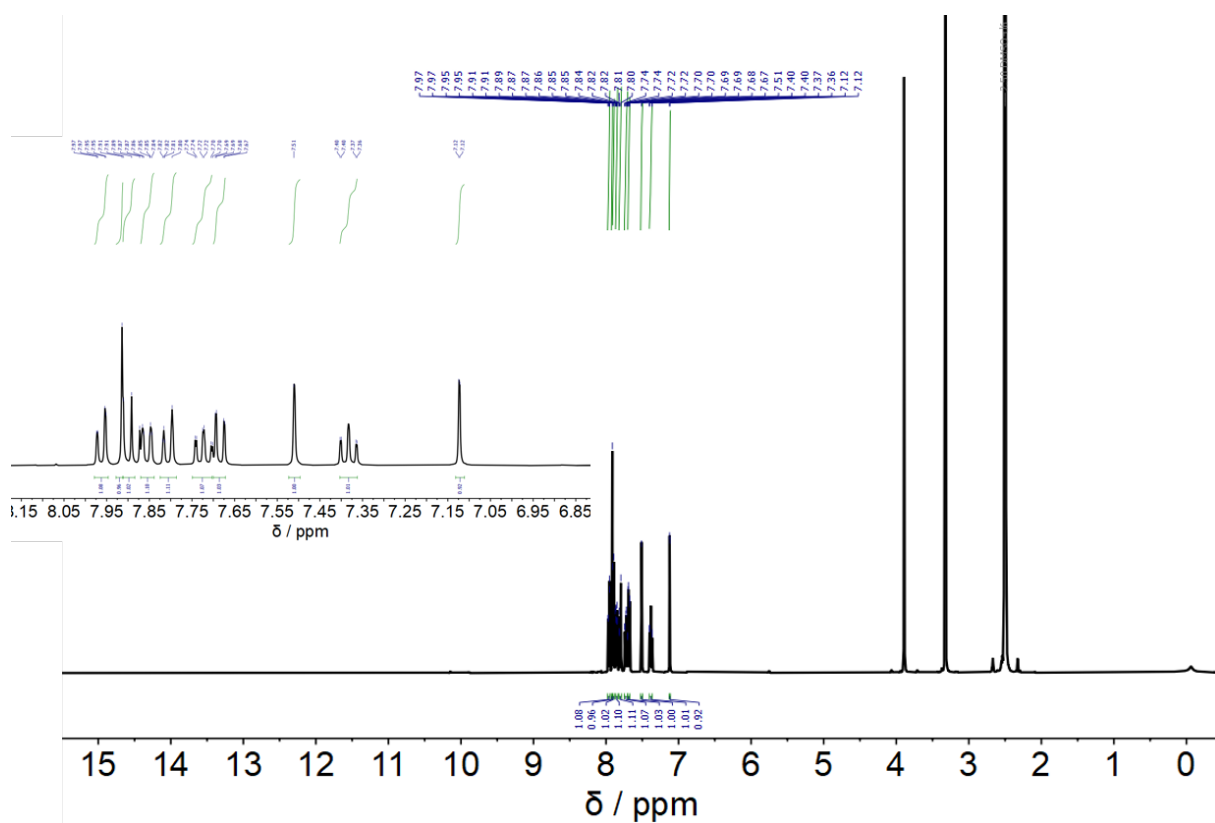**Figure S 138:** ^{13}C NMR spectrum (126 MHz, DMSO-d_6, 26 °C) of **13**.

Figure S 139: ^{1}H NMR spectrum (400 MHz, DMSO-d_6, 26 °C) of **14**.

Figure S 140: ^{13}C NMR spectrum (101 MHz, DMSO-d_6, 26 °C) of **14**.

Figure S 141: ^{1}H NMR spectrum (500 MHz, DMSO-d_6, 26 °C) of **15**.

Figure S 142: ^{13}C NMR spectrum (126 MHz, DMSO-d_6, 26 °C) of **15**.

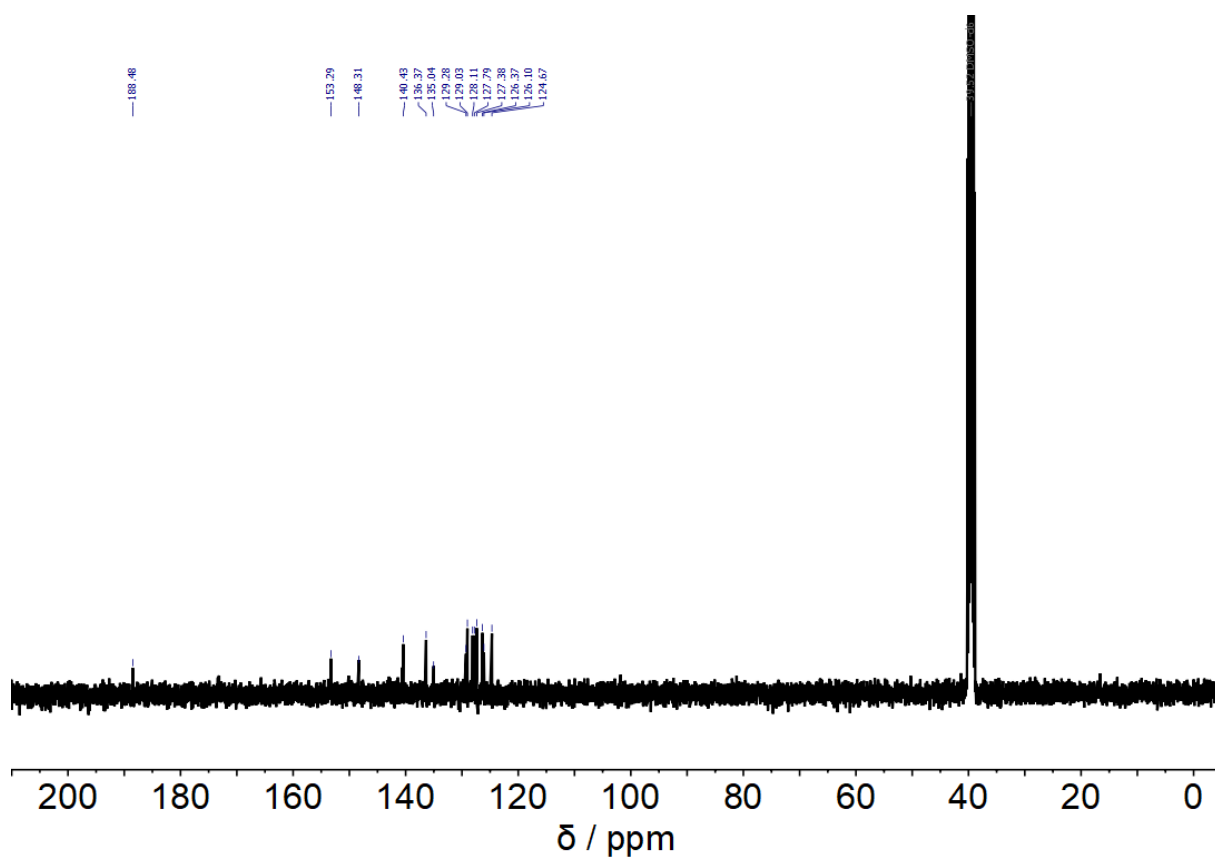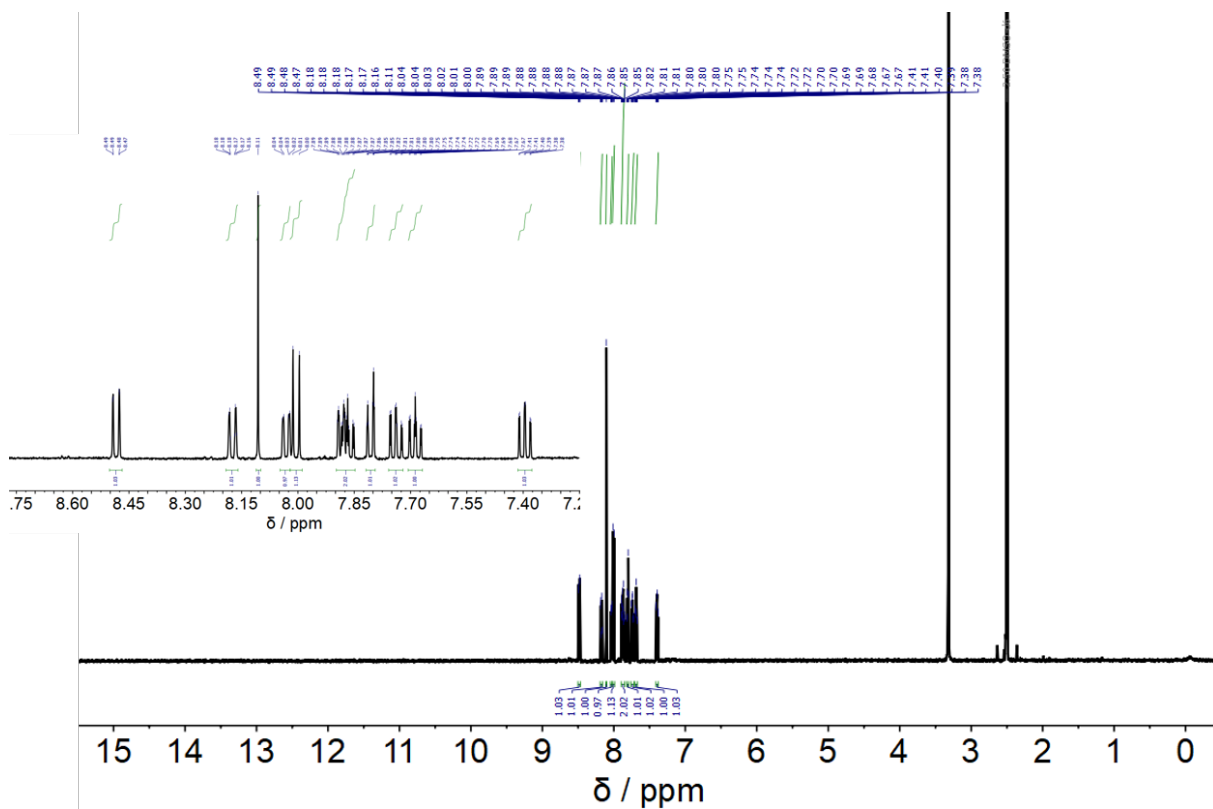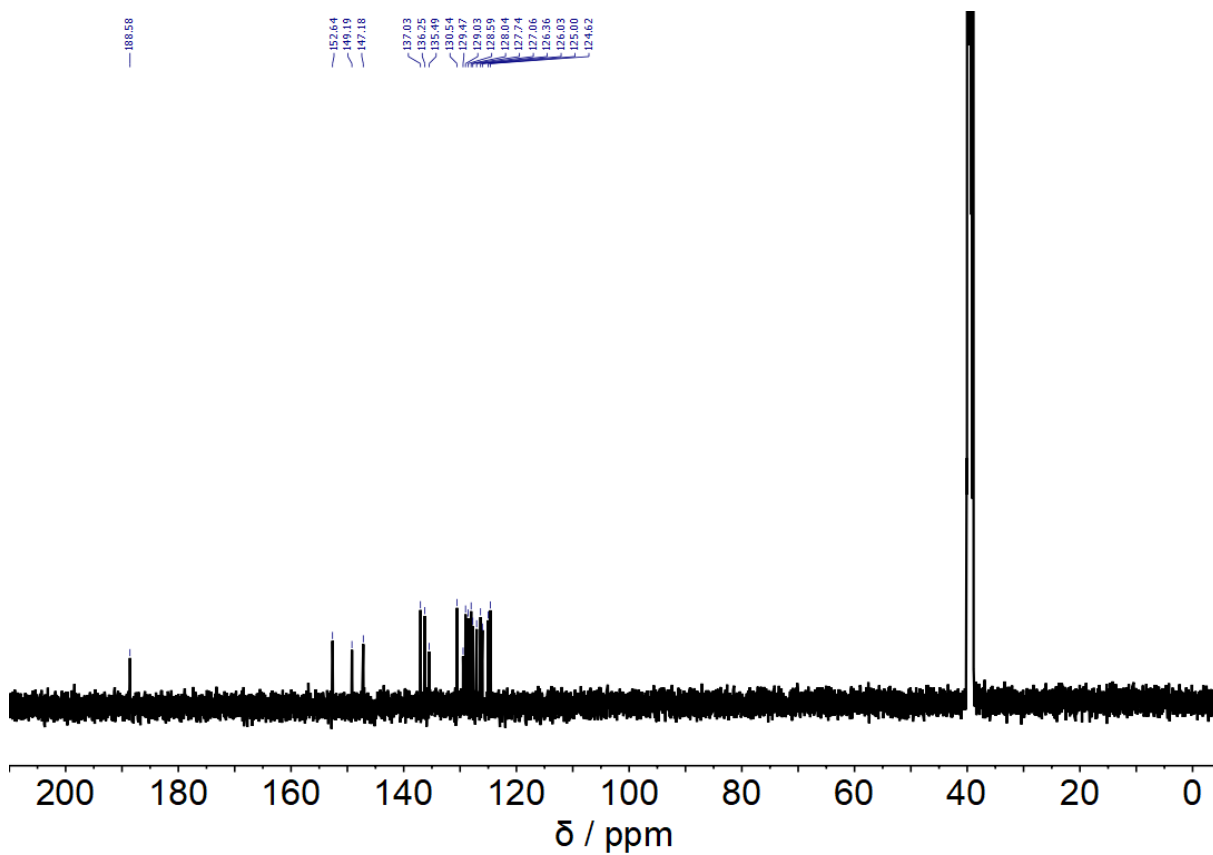**Figure S 143:** ^{1}H NMR spectrum (400 MHz, DMSO-d_6, 26 °C) of **16**.

Figure S 144: ^{13}C NMR spectrum (101 MHz, DMSO-d_6, 26 °C) of **16**.

Literature

1. Zweig, J. E. & Newhouse, T. R. Isomer-Specific Hydrogen Bonding as a Design Principle for Bidirectionally Quantitative and Redshifted Hemithioindigo Photoswitches. *J. Am. Chem. Soc.* **139**, 10956–10959 (2017).

2. Tanaka, K., Kohayakawa, K., Iwata, S. & Irie, T. Application of 2-pyridyl-substituted hemithioindigo as a molecular switch in hydrogen-bonded porphyrins. *J. Org. Chem.* **73**, 3768–3774 (2008).

3. Bursavich, M. G. et. al. Preparation of 3-substituted-1H-indole compounds and their use as mTOR kinase and PI3 kinase inhibitors. US20090311217 (2009).

4. Petermayer, C., Thumser, S., Kink, F., Mayer, P. & Dube, H. Hemiindigo: Highly Bistable Photoswitching at the Biooptical Window. *J. Am. Chem. Soc.* **139**, 15060–15067 (2017).

5. Gerwien, A., Schildhauer, M., Thumser, S., Mayer, P. & Dube, H. Direct evidence for hula twist and single-bond rotation photoproducts. *Nat. Commun.* **9**, 1–9 (2018).

6. Megerle, U., Lechner, R., König, B. & Riedle, E. Laboratory apparatus for the accurate, facile and rapid determination of visible light photoreaction quantum yields. *Photochem. Photobiol. Sci.* **9**, 1400–1406 (2010).

7. Maerz, B. *et al.* Making fast photoswitches faster - Using hammett analysis to understand the limit of donor-acceptor approaches for faster hemithioindigo photoswitches. *Chem. - A Eur. J.* **20**, 13984–13992 (2014).